UNIVERSITEIT VAN PRETORIA
UNIVERSITY OF PRETORIA
YUNIBESITHI YA PRETORIA

ANALYSIS OF SPATIALLY DISTRIBUTED ADAPTIVE ANTENNA ARRAY SYSTEMS IN CELLULAR NETWORKS

by

Marthinus Willem da Silveira

Submitted in partial fulfillment of the requirements for the degree

Philosophiae Doctor

in the

Faculty of

Engineering, Built Environment and Information Technology

UNIVERSITY OF PRETORIA

PRETORIA

2004

© University of Pretoria

SUMMARY

The spatially distributed adaptive array is defined and analyzed. It is applied to both time division multiple access (TDMA) and code division multiple access (CDMA) cellular networks to improve the outage probability at either the base station or mobiles.

In a TDMA network, the distributed array consists of three sub-arrays at alternate corners of a hexagonal cell. It is shown analytically that the SINR of combined beamforming of the distributed sub-arrays is greater than or equal to the SINR of independent beamforming of the sub-arrays. Closed form solutions are derived for estimating the BER performance of Rayleigh fading mobile signals received at a distributed adaptive array with combined beamforming of the sub-arrays. The simulated TDMA uplink outage probability of multiple same-cell co-channel users in a fading environment is compared between conventional, spatially distributed arrays with independent beamforming of the sub-arrays and combined beamforming of the sub-arrays. The effect of the antenna element spacing, number of elements and angular spread is also investigated. Spatially distributed arrays are formed in a CDMA network on the downlink with arrays in multi-way soft handoff with the mobiles. The outage probability performance of combined beamforming of the arrays in handoff is compared to independent beamforming of the arrays as well as to conventional sectorized antennas.

The range between mobiles and distributed sub-arrays in the case of a spatially distributed array can be larger than between conventional center cell arrays and mobiles. Therefore, the effect of interference on the range increase relative to an omni antenna of adaptive and phased arrays in a multipath environment for both narrowband and wideband spread spectrum systems is investigated. An analytical model for predicting the asymptotic range limitation of phased arrays when the angular spread exceeds the array beamwidth is derived.

KEYWORDS: Cellular systems, base stations, spatially distributed adaptive antenna arrays, capacity increase.

SAMEVATTING

'n Ruimtelike verspreide aanpasbare antenne samestelling vir sellulêre toepassings word gedefinieer en geanaliseer. Die konsep word vir beide tyd divisie meervoudige toegang (*TDMA*) asook kode divisie meervoudige toegang (*CDMA*) sellulêre netwerke gebruik ten einde die waarskynlikheid vir 'n seinonderbreking by beide die basisstasie en die selfoon te verminder.

In *TDMA* netwerke word drie sub-antenne samestellings by die alternatiewe hoeke van 'n heksagonale sel geplaas. Die analitiese sein-tot-steuring en ruisverhouding (*SINR*) moontlik met gekombineerde bundelvorming van die sub-antenne samestellings is groter of gelyk aan die *SINR* moontlik met individuele bundelforming van die sub-antenne samestellings. Geslote-vorm uitdrukkings vir die benaderde data fout tempo (*BER*) van die seine wat ontvang word deur so 'n samestelling vanaf 'n selfoon in 'n Rayleigh multipad omgewing word afgelei. 'n Vergelyking deur middel van simulasies word getref van die waarskynlikheid vir 'n seinonderbreking tussen gekombineerde en individuele bundelvorming van die samestelling vir die geval van etlike selfoongebruikers wat deur dieselfde kanaal en in dieselfde sel bedien word. Die invloed van inter-element spasiëring, aantal elemente en multipad hoekverspreiding word ook ondersoek. Die verspreide aanpasbare samestelling word ook in die basisstasie-selfoon skakel van 'n *CDMA* netwerk waar meer as een samestelling in sagte oorhandiging (*soft handoff*) met die selfoon gebruikers is, gebruik. Die waarskynlikheid van 'n seinonderbreking vir gekombineerde bundelvorming, individuele bundelvorming en konvensionele sector-antennes wat in sagte oorhandiging is, word vergelyk.

Die effek van steuringseine op die afstandsbeperking van aanpasbare en fase-gerigte samestellings relatief tot omni-direksionele antennes word vir beide noue- en wye-band stelsels ondersoek. 'n Analitiese model word vir die asimptotiese afstandsbeperking van fase-gerigte samestellings in die geval waar die multipad hoekverspreiding wyer is as die antenne bundelwydte afgelei.

SLEUTELWOORDE: Sellulêre netwerke, basisstasies, ruimtelik verspreide aanpasbare antenne samestellings, kapasiteitsverhoging.

ACKNOWLEDGEMENTS

I would like to express my gratitude to all those who gave me the opportunity to complete this thesis.

First of all, I wish to thank my supervisor Prof. Wimpie Odendaal and co-supervisor Prof. Johan Joubert for taking me on as one of their PhD students and giving me the chance to do this PhD at the University of Pretoria. I wish to thank them for their leadership and advice with the technical content of the thesis, thesis document layout and contents as well technical papers. This thesis was done on a part-time basis in Canada. Thank you for working with me under these unusual circumstances.

I am also grateful to my supervisor for his motivation throughout the duration of this thesis as well as for arranging the NRF bursaries for me to be able to attend the conferences and for the yearly university fees. Thanks for your encouragement and friendship over all these years.

I would like to thank the National Research Foundation for their financial support in the form of bursaries granted to me for several years.

I greatly love and appreciate my parents, brother and sister. My parents supported me through my Bachelors engineering degree at the University of Pretoria, which ultimately allowed me to do this PhD. I will always be thankful to them for laying a solid foundation for my life.

Lastly, and not the least, I would like to thank my wonderful wife Angelika and beautiful son Ethan for their love. Thanks so much for the time you gave to me to do this, for coping with me over this time and for supporting and motivating me to finish this enormous task. I have the deepest love for both of you.

TABLE OF CONTENTS

LIST OF ABBREVIATIONS

Abbreviation	Meaning
1D	One dimensional
1xRTT	CDMA standard for 1x CDMA bandwidth with voice and data
ACF	Autocorrelation function
2D	Two dimensional
BER	Bit error rate
BF	Beamformer or beamforming
BTS	Base station
C/I	Carrier to interference ratio
CDF	Cumulative distribution function
CDMA	Code division multiple access
CIR	Carrier to interference ratio
Comb	Combined
CDVCC	Color code used in TDMA timeslots
dB	Decibel
deg	Degree
DMI	Direct matrix inversion
DOA	Direction of arrival
erfc	Complimentary error function
FFT	Fast Fourier transform
GSM	Global system for mobile communications
Ind	Independent
INR	Interference plus noise ratio
LMS	Least mean squares
MHz	Megahertz
MRC	Maximum ratio combiner
MS	Mobile station
PDF	Probability distribution function
PSK	Phase-shift keying
RAKE	Receiver used in CDMA systems to rack multipath components

Abbreviation	Meaning
RF	Radio frequency
RLS	Recursive least squares
SDMA	Space division multiple access
SINR	Signal to interference plus noise ratio
SIR	Signal to interference ratio
SNR	Signal to noise ratio
TDMA	Time division multiple access
ULA	Uniform linear array
UMTS	Universal standard for mobile telecommunications
Walsh	Orthogonal codes used in CDMA systems
WCDMA	Wideband code division multiple access
wvl	Wavelength

MATHEMATICAL NOTATIONS

The symbols used in the thesis formulations together with their associated meanings are given in Table 1.

Table 1: Symbols that are used the thesis with their associated meaning

Symbol	Meaning
A	Array vector
$\mathbf{A}_{z_d,d}$	Sector z_d array vector transmitting to mobile d
$\ddot{\mathbf{A}}_{(\cap z_d),d}$	Combined beamforming array vector for arrays $(\cap z_d)$ that mobile d is in handoff with
$a(\psi_{z,za,d,k})$	function of angle of arrival relative to array boresight of k-th component of the scattered signal d located in cell z
$\|\|$	Absolute of the value or determinant of matrix
b	User transmit signal bits
c_d	Spreading code of mobile d
CIR_o	Carrier to interference ratio protection ratio
C/I	Carrier to interference ratio
$()^*$	Complex conjugate
$()^H$	Complex conjugate transpose
$()_{\cap(\kappa)}$	Concatenation or combination of sub-array signals
d	User or mobile number
D	Number of users
Δ	Array element spacing
δ	Dirac-delta
ε_d	Difference in amplitude between the array output and reference signal
E{}	Average
F(m,ψ)	Array element m pattern in direction ψ
G	Path gain
$G_{z_d,d}$	Path gain between sector z_d and mobile d
$G_{z_{d_{des}},d_{des}}$	Path gain between sector $z_{d_{des}}$ and mobile d_{des}
$\ddot{G}_{(\cap z_d),d}$	Combined beamforming path loss between the sectors $(\cap z_{d_q})$ and the

Symbol	Meaning
	mobile d_{des}
G_T	Transmit antenna gain
G_R	Receive antenna gain
Γ	Signal to interference plus noise ratio
Γ_n	Interference to noise ratio
γ	Pathloss exponent
$h_{z,za,d}$	RF propagation vector channel transfer function between the d-th mobile in cell z and array in cell za
H	Conjugate transpose
η	Instantaneous SINR
I	Identity matrix
ϑ_d	Voice activity factor of mobile d
$\varphi_{z,za,d,k}$	Phase between mobile d in cell z to array in cell za via scatterer k
k	Scatterer number
K	Number of scatterers
κ	Sub-array number
λ	Carrier wavelength
λ_m	m-th eigenvalue
L	Number of resolvable multipath components (or fingers) in a RAKE receiver
ℓ	Resolvable multipath component or finger in a RAKE receiver
m	Array element number
M	Number of array elements
μ	Convergence constant
μ_w	Constraint on weight vector to have unity response in desired signal direction
N	Number of samples over which average is taken
n_s	Thermal noise vector
n	Symbol number
$n_s(t,m)$	Additive white noise at array element m
$n_{d_{des}}$	Noise power at the desired mobile
p(t)	Transmit pulse shape

Symbol	Meaning
$P_{AOA}(\psi)$	Probability of a signal arriving at an angle ψ
p^{des}	Desired signal power
p^{int}	Interference power
$p^{int+noise}$	Interference plus noise power
P_d	Power of signal d
$p(\ )$	Probability density function
q	Symbol number
Q	Total Number of symbols
R	Cell radius
$\hat{\mathbf{R}}_{nn}$	Interference plus noise covariance matrix averaged over short term (multipath) fading
R_{nn}	Interference plus noise covariance matrix
$\ddot{\hat{\mathbf{R}}}_{nn}$	Interference plus noise covariance matrix of combined distributed array averaged over short term (multipath) fading
$\ddot{\mathbf{R}}_{nn}$	Interference plus noise covariance matrix of combined distributed array
$r^c_{d,z}$	The distance between mobile d in cell z and the boresight of the array
r^s_{max}	Scatterer maximum radius
$r^t_{z,za,d,k}$	Total distance between mobile d in cell z and array in cell za via scatterer k
$r^e_{z,d,k}$	Distance between mobile d in cell z and scatterer k
$r^s_{z,za,d,k}$	Distance between scatterer k and array in cell za for mobile d in cell z
ref_d	Reference signal
ρ	Slow fading amplitude
S	Baseband signal amplitude
σ^2_N	Thermal noise power
σ	Standard deviation
σ_{as}	Angular spread standard deviation
σ_{sf}	Standard deviation of the slow fading PDF
T_c	Chip period

Symbol	Meaning
T	Matrix transpose
t_{HO}	Handoff threshold
$\tau_{z,za,d,k}$	Delay between mobile d in cell z to array in cell za via scatterer k
$\tau_{z_d,d}$	Propagation delay for signals between sector z_d and mobile d
$\ddot{\tau}_{(\cap z_d),d}$	Combined beamforming propagation delay for arrays $(\cap z_d)$ that mobile d is in handoff with
$\mathbf{U}_d$	Propagation vector of signal d at the array elements
$\ddot{\mathbf{U}}_d$	Propagation vector of signal d at the elements of the combined distributed array
$\mathbf{U}_{des}$	Propagation vector of desired signal at the array elements
$\mathbf{U}_{d_{des}}$	Propagation vector of desired signal at the array elements
$\mathbf{U}_{Qd}$	Propagation vector of interference signal d at the array elements
v	Eigenvector
W	Weight vector
$\hat{\mathbf{W}}$	Approximation of the weight vector
$\ddot{\mathbf{W}}_{(\cap z_d),d}$	Combined beamforming weight vector for arrays $(\cap z_d)$ that mobile d is in handoff with
$\xi_{z,d,k}$	Amplitude of k-th component of the scattered signal d in cell z
X(m)	Received signal at each array element
X^{dB}	Received signal in dB
$\aleph$	Power loss of multipath components due to antenna azimuth taper
X	Received signal vector across the array
$\ddot{\mathbf{X}}$	Received signal vector across the combined distributed array
X_κ	Received signal vector across the sub-array κ
X_Q	Interference received signal vector across the array
$Y_{\kappa,d}$	Output of sub-array κ optimized for user d
ψ	Angle between array boresight and mobile
Ψ	Characteristic function
$\Psi_{d,z,k}$	Incidence angle of the k-th scattered component of signal d in cell z

Symbol	Meaning
$\psi_{d,z}^{c}$	Incidence angle between the array boresight and the signal d in cell z
z_d	Sector number that the mobile d is in soft-handoff with
$z_{d_{oc}}$	Handoff sector number of mobile d in a sector not containing the desired mobile
z	Cell Number
Z	Number of cells /Rake receiver output
$\bigcap z_d$	Combination of sectors that the mobile d is in handoff with

1 INTRODUCTION

It is well known that by using the directional properties of adaptive arrays, the interference from multiple users operating on the same channel as the desired user in a time division multiple access (TDMA) cellular network[1], can be reduced significantly [1,2,3]. In these papers the interference from co-channel users in neighboring cells to that of the desired user is considered. It was shown that the reduction in interference results in an increase of the overall system capacity. This is very important, as there is an increasing demand by cellular operators on the capacity of cellular systems.

The capacity of a cellular system can be increased even further by accommodating multiple co-channel users[2] in the same cell [4,5,6], in addition to the co-channel users in the neighboring cells. It was shown in [5] that the capacity of a system can be increased by twelve times (with an array having up to 20 elements) compared to systems with no same cell co-channel users. Three linear arrays in the center of the cell, each covering a 120-degree sector and each sector having a different set of frequencies were proposed. The users in each sector are isolated in angle by reducing the received and transmitted energy towards the co-channel interferers, while maximizing the power towards the desired co-channel users. However, two users with nearly the same angular values relative to the array boresight in a multipath environment with a narrow angular spread[3] and closely spaced antenna elements[4], are difficult to spatially separate from each other and have to be assigned to different channels (different frequency or time slot)[5].

This can be overcome by using an adaptive linear array at every other edge of a hexagonal cell. The concept of placing base stations at the edge of a hexagonal cell is not a new idea [7,8,9]. However, the concept presented in this thesis differs from [7] in that adaptive arrays are used on the base stations instead of 120° overlapping sectorized antennas. It differs from [8,9] in that combined beamforming of the arrays is considered instead of selection diversity. The three arrays form sub-arrays of one large array system (called

[1] Includes North American IS136 systems as well as GSM systems.
[2] Users in a cellular network are called mobiles.
[3] Angle of arrival spread of the multipath signals at the base station array.
[4] Half wavelength spacing between elements is considered small in multi-input multi-output (MIMO) applications for achieving uncorrelated signals across antenna elements [10].

spatially distributed array system), where the steering vector of the array system is optimized to yield the best signal to interference ratio for all co-channel users in the same-cell.

The array system is able to spatially discriminate between co-channel users in a "two-dimensional plane", since each array has a different view angle towards the incoming multipath signals. A desired user in a narrow angular spread environment that is blocked by an interferer as seen from one array can be spatially isolated from the interferer by another array, as the viewing angle is different. The result is that more co-channel users can operate in the same cell compared to the methods proposed up to now with narrow angular spread propagation environment and closely spaced antenna elements.

Beamforming of the distributed sub-arrays can be undertaken in two ways. Firstly, an optimal (in terms of signal to interference plus noise ratio (SINR)) beam can be formed for each sub-array based on the incoming signals towards the individual sub-arrays. The signals at the output of the sub-arrays can then be either optimally combined or the best signal from the sub-arrays can be selected. Apart from the optimum combining of the sub-array output signals, the sub-arrays have no interaction with each other. An alternative beamforming technique is to form an optimum beam based on the signals arriving at all the sub-array elements. This allows the spatially distributed arrays to operate as one large array with reduced outage probability when compared to beamforming on the individual sub-arrays only.

It will be shown analytically (for a specific distributed array geometry and number of signals) in this thesis that the SINR of independent beamforming is equal to or greater than combined beamforming. The performance advantage by means of simulation results of independent vs. combined beamforming will be presented for TDMA systems on the uplink[6] for various array sizes, fading conditions and angular spreads. The bit error rate performance of an adaptive array in a multipath environment was derived analytically in [11]. This formulation will be extended in this thesis to distributed arrays in a multipath environment.

[5] It is assumed that the array element separation is in the order of half of the wavelength.

In order to reduce the probability of a deep fade to and from mobiles in a code division multiple access (CDMA) cellular network, mobiles are connected to (or in handoff[7] with) multiple base stations. The number of base stations that the mobile is in handoff with is based on the measured SINR of the base station pilots[8] received by the mobile. On the downlink[9], all base stations that a particular mobile is in handoff with will transmit the same data. Due to uncorrelated fading between base stations, the probability is low that the signal from multiple base stations will be in a fade. Unfortunately, due to the fact that multiple base stations transmits to a particular mobile in handoff, the interference to mobiles in the surrounding cells is increased[10]. As with TDMA systems, increased interference reduce the network capacity. It is therefore important to apply techniques to reduce the interference to mobiles from multiple base stations in handoff. Adaptive arrays can again be used for this purpose [12,13]. Each of the arrays in handoff will independently form a beam with a maximum signal towards the desired mobile and reduced signal towards the other mobiles in the sector covered by the array.

Similarly to combined uplink beamforming of TDMA distributed sub-arrays (as described above), the beamforming of the CDMA arrays in handoff can also be done as one large combined array. The propagation channel between the combined array and the mobile is critical for the operation of combined beamforming. In [14] a method is proposed for adaptively determining the propagation channel on the downlink based on feedback from the mobile. With the assumption that the downlink propagation channel information is available, it will be shown (by means of simulation results) in this thesis that combined beamforming of the downlink arrays in handoff provides a reduced (relative to independent beamforming) probability of outage at the mobiles.

The range of adaptive and phased arrays is a function of the array geometry, location and number of interferers as well as the propagation environment. In the case of the distributed arrays located at the corner of the cell, the range between the sub-arrays and the mobiles

[6] Uplink is from the mobile to the base station.
[7] Called soft handoff in CDMA systems between cells and softer handoff between sectors of the same base station.
[8] All base stations constantly transmits a signal with a constant power and similar data sequence.
[9] Downlink is from the base station to the mobile.

can be larger than the range between cell center arrays and mobiles. Therefore it is important to investigate the range increase of adaptive and phased arrays relative to an omni antenna. In [2] it was shown that as the array beamwidth becomes narrower than the angular spread, the range increase of a phased array relative to an omni antenna becomes constant as a function of the number of array elements[11]. It was also shown that an adaptive array adapts or matches its beam to the incoming multipath wavefront, and therefore does not have the range limitation of phased arrays. In addition it was shown in [2] that the range limitation of phase arrays disappears in a spread spectrum system if the beam is steered optimally in terms of signal to noise ratio for each RAKE finger[12]. This thesis extends the work of [2] to add the effect of an interfering source in a narrowband system and multiple interferers in a spread spectrum system. An analytical equation is also derived to predict the asymptotic range limitation of phased arrays

1.1 Thesis Outline and Contributions

1.1.1 Thesis Outline

Chapter 2 begins with a general definition of cellular networks with sectorization, frequency reuse patterns of one, three and same cell frequency reuse. This is followed by a description of different beamforming techniques and beamforming configurations. The switched multibeam, phased and adaptive array beamforming is discussed. The uniform linear array and circular array is described. Propagation channel models used in the simulations in later chapters are discussed. The concept of the spatially distributed array is presented. This array geometry is defined and practical implementation considerations for this method are discussed. The signals arriving at the array elements is then defined as well as individual and combined beamforming of the distributed array signals for both narrowband and spread spectrum (CDMA) systems. This is followed by a definition of two methods of estimating the array weight vectors[13]: the direct matrix inversion and least mean squares method. The method of simultaneously estimating the weight vectors for

[10] Interference to mobiles in the same cell as the desired mobile is low due to the use or orthogonal transmit codes.
[11] Limiting the range of a phased array.
[12] The N strongest multipath signals separated by the inverses of the spreading rate is called fingers in a RAKE receiver.
[13] The baseband converted signal of each array element is multiplied by a complex value or weight.

UNIVERSITEIT VAN PRETORIA
UNIVERSITY OF PRETORIA
YUNIBESITHI YA PRETORIA

multiple same-cell co-channel users is described. In the last part of the chapter the methods for estimating the performance of the various systems is presented.

In chapter 3 the range increase of adaptive arrays and phased arrays is compared to an omni antenna in a multipath environment in the presence of interfering sources. Firstly, the range increase of a phased array in a non-multipath environment is formulated. The array geometry, multipath model and array element signals for narrowband and spread spectrum systems are briefly summarized. Simulation results of the range increase of phased and adaptive arrays relative to a reference system are presented. The results are shown as a function of angular spread and angular location of a single dominant interferer in the narrowband case and with multiple interferers in the spread spectrum case. An analytical model is developed that predicts the asymptotic range limitation of a phased array in a multipath environment in the presence of a dominant interferer.

The signal to interference plus noise ratio (SINR) performance of a distributed array in the absence of multipath components is investigated in chapter 4. Analytical expressions for the SINR of a distributed array with independent and combined beamforming of the sub-arrays is developed. It is shown analytically that optimum combining of the individual sub-array signals has a SINR equal to the sum of the SINRs of the individual sub-array signals. Thereafter, it is shown for a single interferer and two element sub-arrays that the SINR of a distributed array with optimum combining of the sub-array signals is greater or equal to the SINR with independent combining of the sub-array signals. This result is also shown numerically to be valid for multiple interferers. Next, the SINR of a distributed array with independent and combined beamforming of the sub-arrays is compared to the SINR of conventional arrays at the cell center. The simulation results are for a single cell as well as seven cell network with and without power control.

In chapter 5 an approximate analytical formulation of the bit error rate[14] (BER) of a distributed array in a multipath environment is developed. The method is based on finding the Laplace transform of the probability density function (PDF) of the array output SINR through a generalized eigenvalue solution. The inverse Laplace transform then yields the

[14] The bit error rate is a function of SINR.

i 17511914
b16427312

required probability density function, which is applied to estimate the BER at the array output. The formulation is first described in detail for a single array and then extended to a distributed array. The BER determined with the analytical model is compared to the BER calculated with a Monte-Carlo[15] simulation for both single and distributed arrays.

The performance of a distributed array with independent and combined beamforming in a multipath environment is compared in chapter 6 by means of Monte-Carlo simulations to the performance of conventional arrays at the cell center. Firstly, the bit error rate (BER) of a single array using the circular vector channel model is compared to the BER with the Rayleigh vector channel model. The BER as a function of the scattering angle[16] and number of elements is presented, followed by the BER of the distributed array as a function of the multipath scattering angle and number of elements. The outage probability[17] of distributed arrays in the presence of fast and slow fading with mobile power control is presented. The outage probability results are shown for a single cell and seven-cell network.

The performance in a CDMA system of combined beamforming of the arrays in sectors experiencing handoff in the downlink is compared to arrays with independent beamforming in chapter 7. The signal model for independent and combined beamforming of the arrays in handoff is defined. This is followed by a description of the mobile power control method used in the simulations. The propagation channel response matrix must be known in order to apply the correct beamforming to the mobiles. Methods that can be used to estimate the propagation channel are described. In order to obtain a first order approximation of the viability of the combined beamforming of the arrays in handoff, simulation results of the SINR of combined vs. independent beamforming with no fading and power control is presented for a single cell followed by a seven cell network. The power control and SINR performance for a single set of mobile locations and fading conditions is presented. This is followed by a comparison of the simulated outage probability of independent and combined beamforming of the arrays in handoff in a nineteen cell network.

[15] Statistical method to estimate the probability density function.
[16] Also referred to as the angular spread.
[17] Probability that the SINR is below a certain threshold.

1.1.2 Thesis Contributions

The main contribution of this thesis is the analysis of spatially distributed adaptive array systems in TDMA and CDMA cellular communication networks. The focus is on arrays operating in a multipath propagation environment with a narrow angular spread and arrays having closely spaced array elements[18]. Secondary contributions were results of an investigation into the range increase of adaptive and phased arrays relative to an omni antenna in the presence of interference and the development of an analytical model for predicting the phased array range limitation. The range increase of adaptive and phased arrays are important to understand, as the range between mobiles in a spatially distributed array configuration can be significantly larger than in a conventional configuration.

A more detailed breakdown of the contributions is as follows:

1) The effect of interference on the range increase (relative to an omni antenna) of adaptive and phased arrays in a multipath environment for both narrowband and wideband spread spectrum systems is investigated. This work was published in [15]. The investigation builds on material presented in [16], where the effect of interference was not considered. The results in this thesis show that the range increase of both adaptive and phased arrays are affected by the angular spread and the angle of the interferer relative to the boresight of the array. A significant reduction in the range increase of a phased array is visible in a narrow angular spread environment when the multipath angular components of the interferer starts to overlap with the array beamwidth. The adaptive array range increase exceeds that of the phased array for the same conditions (number of elements, angular spread and interferer locations) and for both narrowband and spread spectrum systems.
2) An analytical model is derived for predicting the phased array range increase, including the asymptotic range limitation when the angular spread exceeds the array beamwidth. A simplified model is presented for the probability density function of the angle of arrival of multipath signals for the uniform vector channel model.
3) The concept of the spatially distributed array is presented. Adaptive arrays at the center of the cellsite are limited in their ability to separate co-channel users from each other

when they are closely located in angle relative to each other (as seen by the base station antenna) in a small angular spread (low multipath) environment with closely spaced antenna elements (half wavelength). A concept where multiple arrays are located far apart in the cell (spatially distributed array) is introduced. This array consists of three sub-arrays at alternate corners of the cell, and when applied to TDMA[19] type networks has the ability to receive user signals from multiple viewing angles. It is therefore able to obtain an improved rejection of interfering signals relative to the arrays located at the center of the cell. This concept was published in [17,18], where the reduction of the outage probability of a combined distributed array vs. the conventional array at the cell center in a non-multipath environment was presented.

4) An analytical comparison of the SINR of a desired mobile in the presence of an interfering mobile is made between combined beamforming and independent beamforming of two spatially distributed sub-arrays. The comparison shows that combined beamforming of the sub-arrays produce a higher SINR than independent beamforming of the sub-arrays.

5) The simulated bit error rate (BER) performance of a spatially distributed array with combined beamforming of the sub-arrays is compared to the BER performance of independent beamforming of the sub-arrays as well as to conventional arrays at the center of the cell. Power control of the users, fast and slow fading as well as a multi-tiered network interferers are included in the simulations.

6) An analytical model for estimating the BER performance of spatially distributed arrays in a Rayleigh multipath environment is developed. This model is an extension of a model in [11] for determining the bit error rate performance of a single array in a multipath environment. The BER calculated with the derived analytical model is compared to the BER simulated with a Monte-Carlo method. A spatially distributed array with two element sub-arrays and correlated fading between the array elements for each mobile signal is considered.

7) The concept of combined beamforming of the arrays in handoff in the downlink of a CDMA cellular system is presented. Simulation results for the outage probability

[18] Half wavelength spacing between elements is considered small in multi-input multi-output (MIMO). applications for achieving decorrelated signals at the antenna elements [10].
[19] Examples of TDMA networks are IS-136 and GSM.

performance of combined vs. independent beamforming of the arrays is presented. Power control, fast and slow fading, a seven cell network containing the mobile users and nineteen cells as handoff candidates were considered. The results indicate that the combined beamforming concept produces a lower outage probability due to improved signal reduction of out of cell mobile users.

1.2 Literature Review

1.2.1 Array Range Increase

Studies on the range achievable with an adaptive array have been published in [16,19,20]. In [20] different antenna configurations are compared in terms of received SINR for a wideband CDMA system (interference effects not included). The configurations include number of antenna elements, inter-element spacing and a fixed multibeam antenna. In [20], the relative BER performance at the BTS for WCDMA was calculated for dual sectorized diversity sectorized and fixed beam antennas. Interference was modeled as white noise and as colored noise. In [16], the range increase of adaptive vs. phased arrays was studied in a multipath environment for both narrowband and wideband (spread spectrum) systems.

1.2.2 GSM Systems

An eight element adaptive array system for GSM1800 was presented in [21]. The system estimates the direction of arrival (DOA) of the desired and interfering signals using the training sequence in the GSM protocol. The DOAs are then used to determine suitable weight vectors. A beam is steered towards the desired signal multipath components, and all other directions are nulled (thereby placing broad nulls on the interferers).

In [5,22] the capacity increase of GSM systems with multiple co-channel mobiles in the same cell was investigated. Adaptive arrays were used to separate the mobiles signals using spaced division multiple access. In order to reduce interference, mobiles were classified into angular and power groups. Based on this, the frequencies in the cell were allocated to the mobiles. Transmission on the downlink was done using direction of arrival measurements on the uplink. It was shown that between two and twelve times capacity increase is obtainable with up to twenty element arrays.

1.2.3 IS 136/IS54 and PCS Systems

A four element real time adaptive array lab performance is given in [23] for IS136. The Synchronization and CDVCC sequences in the slot are used to determine and update the weights based on an enhanced direct matrix inversion algorithm. A SINR gain of 6dB for a BER[20] of 1e-3 was achieved.

In [24] the dynamic BER performance of adaptive arrays in IS-54 systems is investigated. The least mean squared (LMS) and direct matrix inversion (DMI) methods of weight acquisition and tracking using the synchronization sequence in the slot as desired signal to determine the weight vectors. Various mobile speeds are compared based on the BER performance of the system. It was found that the DMI algorithm gave the best results, with only 0.2dB degradation from ideal SINR performance at a BER of 1e-2 for a mobile with speed up to 60mph.

In [4] a novel approach was described for separating multiple same-cell co-channel signals. The method utilizes the temporal structure of digital signals to determine simultaneously the array response vector and symbol sequence. Two methods were described: The iterative least squares with projection and a method based on the alternating projection combining least squares with enumeration. It was found that signals can be estimated well even if they are located close in angle to each other.

1.2.4 Analytical BER Performance Estimation of Arrays

In [11], analytical expressions were derived for the CDF and BER of adaptive arrays with uncorrelated and correlated fading across the elements in a multipath environment. The closed form expressions were derived in terms of the eigenvalues of the interference co-variance matrix. It was stated that the eigenvalues can be determined analytically for a single interferer, but have to be determined with a Monte-Carlo method for more than one interferer and for correlated fading across the elements. In the case of correlated fading, the eigenvalues have to be determined for each SINR value.

[20] In this thesis BER is the raw BER without coding gain.

Closed form solutions for the CDF and BER of an array with optimum combining with a single interfering signal in a multipath environment is given in [2]. Numerical CDF and BER results determined with Monte-Carlo simulations for two or more interferers were also presented for various array sizes. The correlation between antenna elements of the received multipath components of a single signal as a function of the element spacing and angle spread was described in [25]. It was shown that there is low correlation between elements when either the angular spread is wide (e.g. 30 degrees) or the element spacing is large in terms of wavelengths (e.g. 5 wavelengths or 5λ).

1.2.5 CDMA Systems

It is shown in [13] that the capacity of a CDMA system can be doubled by using an eight element array (spaced half a wavelength apart) at the BTS. On the uplink, the signals from the antenna elements are downconverted, sampled and then a fast Fourier transform (FFT) is applied to the signals. The net effect of that is the same as beamforming with a butler matrix. The FFT essentially forms 8 virtual beams for an eight element array. The strongest virtual beam is then processed by a RAKE receiver. In the downlink, a beam is transmitted in the direction corresponding to the beam in the uplink with the strongest signal.

In [26] the constant modulus algorithm was applied to antenna elements spaced far apart (several wavelength). The SNR performance was compared to switched diversity.

The performance of the uplink and downlink of CDMA systems with adaptive arrays at the base stations and mobiles in a multipath environment was investigated in [12,27,28,29,30,31]. In [12], the uplink outage probability and Erlang capacity was presented. The model included a rake receiver at the output of each array element. Results were obtained with Monte-Carlo simulations for various number of antenna elements. The downlink was described in [30], where an adaptive beam was formed towards each mobile. The required downlink transmit array vector was estimated with the feedback method [14], where training sequences are periodically transmitted from the base station to the mobile on the downlink. From the received signal information, which the mobiles feedback to the base-station, the transmission response vector can be calculated. A Monte-Carlo simulation method was used to determine the outage probability as function of the cell loading. It was

found that for a five element array and an outage probability of 0.01, the capacity increases from 32 mobiles per cell to 123 mobiles.

In [32], various beamforming (or spatial filtering) algorithms applied to CDMA systems were compared in terms of SINR, converging rates, capacity enhancements and computational complexity. The algorithms are conventional (SMI, LMS, RLS and DDLMS) as well as channel estimates (code filtering, autocorrelation matrix, shifted autocorrelation matrix, etc). The 2D SMI algorithm achieved the largest capacity for the 2D RAKE algorithms. However, the 2D RAKE receiver algorithms converged slower than the conventional 1D algorithms.

1.2.6 Macroscopic/Microscopic Diversity

1.2.6.1 Sectorized Antennas

The outage probability of micro-diversity (antennas relatively close together in a typical cellsite) vs. macro-diversity (antennas far apart) was determined in [33] as a function of antenna spacing and two and four port combining. It was shown that macro-diversity is an effective fading countermeasure in micro-cellular environments.

In [34] the capacity increase in a cellular system with macro-diversity applied to the entire cell was studied. A macroscopic diversity architecture was proposed where remote antennas consist of a sectorized 120° antenna and electric-optic converter and the signals are relayed to a central unit (where the demodulation is done) with fiber optic cables. Under specific assumptions, at 90 % area coverage a 9.5dB coverage gain was achieved for selection macro-diversity and 11.3 dB for simulcasting. The selection macro-diversity downlink capacity gain is 6.4 Erlangs per cell at 10% blocking margin.

The uplink bit error probability in a CDMA system with macro diversity is calculated in [35,36] for sectorized antennas. It was shown that macroscopic diversity improves the performance of a CDMA system significantly. In [7] an architecture was introduced with overlapping three sector 120 degree sectorized antennas at every other corner of a hexagonal cell. The signals from each set of three sectorized antennas pointing to the center of the cell, are combined on the uplink. On the downlink all three antennas transmits

simultaneously. It was shown that this configuration can achieve the same downlink C/I for a reuse of three compared to a conventional omni system with a reuse of seven. On the uplink, the C/I ratio is better than 5dB compared to the conventional sectorized system with a reuse of three.

The uplink outage probability for the architecture with overlapping sectorized antennas at the cell edges (macro diversity) are compared to the conventional network architecture with sectorized antennas at the cell center in [37]. Maximum ratio combining vs. selection diversity of the macro diversity antennas (cell edge antennas) was investigated. The analysis included log normal slow fading (but excludes fast fading effects) and power control by the nearest base station in a 37 cell network for a network reuse factor of three. This analysis [37] was extended to the downlink in [38], where simulcast from the edge antennas was considered for networks with reuse factors of 3 as well as 4. Power control in the downlink and uplink of simulcast networks was presented in [39].

1.2.6.2 Arrays

In [8,9] a composite micro and macro diversity system was described. Each array element signals are combined with either selection or maximum ratio combining to combat fast fading (called micro diversity). The maximum output of a number of arrays separated far in distance are then selected (selection macro diversity). Closed form solutions for the average bit error rate vs. SINR were derived. The effect of interference from surrounding cells was not directly considered in the analysis. The conclusion was that composite diversity offers substantial improvement over micro-diversity alone.

Closed form first order expressions for the uplink and downlink capacity increases of a CDMA system with an adaptive array was presented in [40,41]. The effect of multipath (one and three path) and soft-handoff gain was taken into account. The effect of shadowing was taken into consideration by assuming that a certain margin is required for a specific link reliability.

In [42] analytical expressions were derived for a CDMA system for the uplink SINR at antenna diversity elements and in the downlink at the mobile in the presence of Rayleigh fading and log-normal shadowing. The interference from multiple base stations and

multiple same cell and adjacent cell mobiles were included. One of the major assumptions that was made is that the fading across receive antenna elements is uncorrelated, in other words that the angular spread is large and the elements are spaced far apart.

1.2.7 Downlink Propagation Channel Matrix Determination

In order to transmit a maximum signal to the desired mobile while minimizing the interference to the other mobiles, the propagation channel response vector is required. This cannot be determined reliably from the uplink information, as the uplink and downlink do not operate on the same frequency and are therefore not coherent. A method of measuring the propagation channel matrix for all mobiles was given in [14,43]. The method is based on transmitting probing signals from each element of the array and measuring the relative amplitude and phase at each mobile. The measurements are sent back to the BTS array on the uplink. This simulated CDMA capacity improvement of base station arrays in [27] assumed that the propagation channel matrix can be determined according to the above feedback method. However, the method in [14] requires a large amount of feedback data to the BTS. In order to reduce the amount of feedback data, an alternate method was proposed by [44]. This method is well suited for CDMA systems. The received signal at each mobile is correlated with its Walsh code to obtain a signal pertaining to the specific mobile. Nonlinear processing is applied to the signal to extract the hard limited information bits. A scalar error between hard limited signal and a known (or reference) signal is determined. If this error is above a certain value, it will be fed back to the BTS. This error is then used at the BTS to recursively update the transmit weight matrix in order to minimize the errors fed back from the mobiles.

1.2.8 Propagation Channel Models and Measurements

Multibeam, phased and adaptive arrays require propagation models which includes time delay spread and angle of arrival. These types of propagation channel models are referred to as vector channel models. An overview of vector channel models was presented in [45,46].

Several papers gave results of measured angular and delay spread as a function of the propagation environment. In [47] the measured angular and delay spread in a dense urban environment were 8° and 115ns respectively. In suburban environments the measured

angular and delay spread were 3° and 109ns respectively. In [22, p. 204] the measured angular spread in an urban environment was between 3° and 6° and in a sub-urban environment between 1° and 6° for mobile to base station distances between 1km and 2km. The measured path angular spread in an urban environment as reported in [48] was between 5° and 10°.

UNIVERSITEIT VAN PRETORIA
UNIVERSITY OF PRETORIA
YUNIBESITHI YA PRETORIA

2 BACKGROUND AND FORMULATION OF DISTRIBUTED ADAPTIVE ARRAY CONCEPT

2.1 Introduction

This thesis investigates the advantage of combined beamforming vs. independent beamforming for distributed arrays. In addition the range increase relative to an omni antenna of adaptive and phased arrays in the presence of multipath and interferers is investigated. The purpose of this chapter is to set the background for the investigations to follow and to develop a mathematical formulation for the problem. The chapter starts by describing cellular network configurations with different frequency reuse patterns. This is followed by the concept of sectorization to improve the signal to noise ratio at the mobiles. Next, different array systems will be discussed followed by detail of the propagation channel models that will be used in the analysis.

This is followed by the definition of the distributed array system, consisting of arrays at alternate corners of a hexagonal cell. The narrowband (such as in TDMA and GSM systems) and wideband (such as in CDMA and UMTS systems) received signals at the arrays are defined, followed by independent and combined beamforming of these signals to produce an optimum receive signal to noise ratio (for the mobile signals) at the array outputs. Methods of estimating the beamforming weights are presented, followed by performance estimation methods of the array systems in a digital cellular network.

2.2 Cellular Network Definition

The concept of a cellular network is to reuse the same frequency in different cells. The radius (reuse distance) at which the same frequency can be reused is a function of the signal to interference ratio experienced by the mobiles or base stations. The interference from undesired mobiles received by base stations with omni-antennas is much higher than base stations with sectorized antennas. A reuse pattern of seven is typical for base stations with omni antennas, meaning that the same frequency is not used in the six cells surrounding a cell with a particular frequency. Sectorized antennas at the base station allows this reuse distance to be reduced, increasing the network number of mobiles or capacity that can be supported with sufficient signal to noise ratio. Sectorization and reuse distance are described next in more detail.

2.2.1 Sectorization

The number of mobiles that can be supported in each cell is a function of the signal to interference ratio that the mobiles experience. If the signal to noise ratio becomes lower than a certain threshold, the bit error rate will be too high to sustain the call and the call will be dropped or terminated. In order to reduce the interference, sectorization is used in the network. A network has typically three sectors (called tri-sectored in cellular networks). A tri-sectored base station will have three antennas, each with a 3dB beamwidth of 120° and with the boresight directions 120° apart. With sectorization, the reused distance can be reduced and a reuse of three is possible (this will be discussed in section 2.2.2)

A further decrease in interference to mobiles can be achieved with multibeam antennas in each sector with adaptive arrays. Adaptive arrays will tend to maximize the signal to interference ratios of a mobile by steering "nulls" in the directions of the interfering mobiles. The phased array, multibeam and adaptive arrays will be discussed in section 2.3) Adaptive arrays allows a reuse of one as well as same cell co-channel users [22].

2.2.2 Networks with Different Reuse Patterns

The geometry for a network with a frequency reuse pattern of three is shown in Figure 1 [49,50]. The first, second and third tier of interferers are also shown. A reuse pattern of three means that there will be a group of three cells using different frequencies. This pattern group of three repeats in the network in a way that two co-channel cells are not located adjacent to each other.

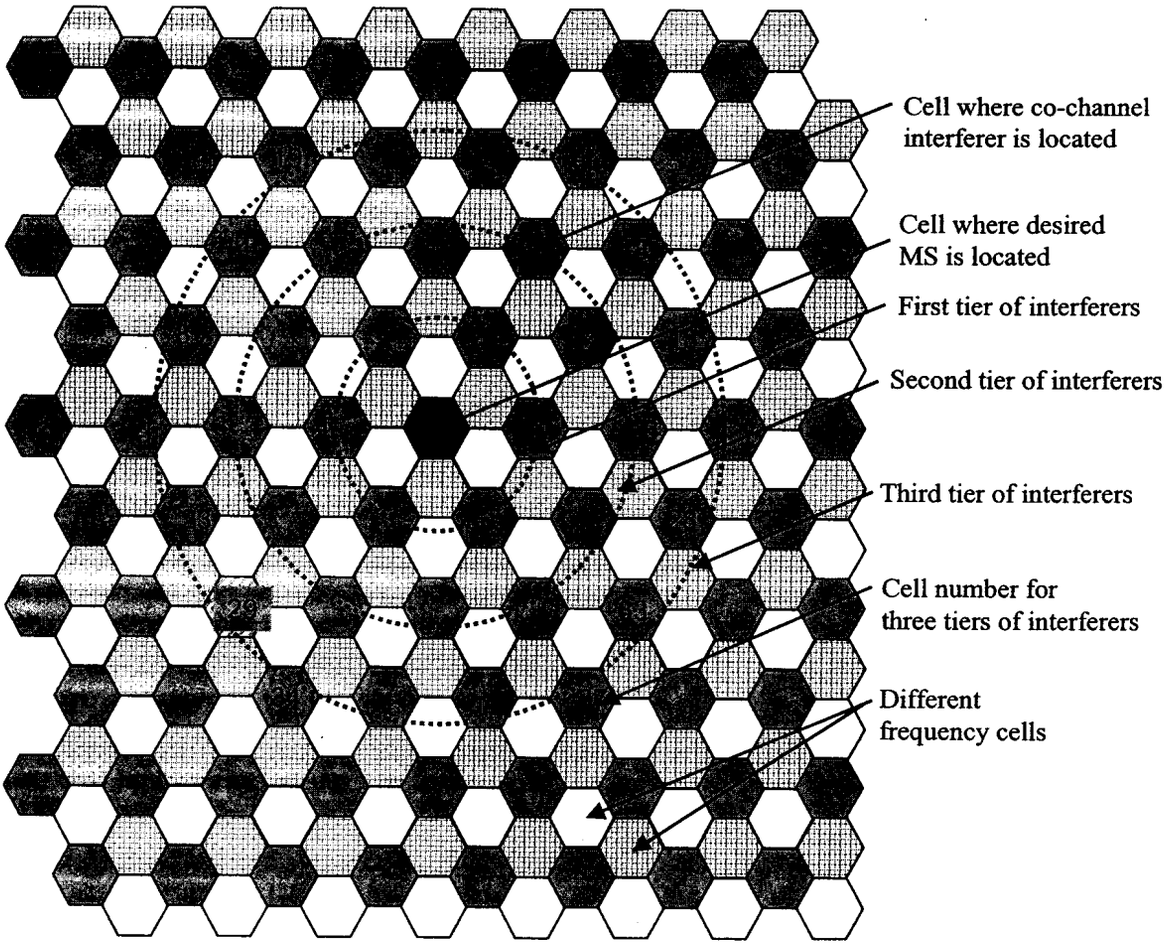

Figure 1: Network geometry with a frequency reuse factor of three.

A network with a frequency reuse pattern of one is shown in Figure 2. The desired user cell is shown in the middle, and the cell numbers are also indicated in the figure. The same frequency is reused in all the cells. This is the tightest reuse pattern with the highest interference and requires sectorization and/or adaptive arrays [50].

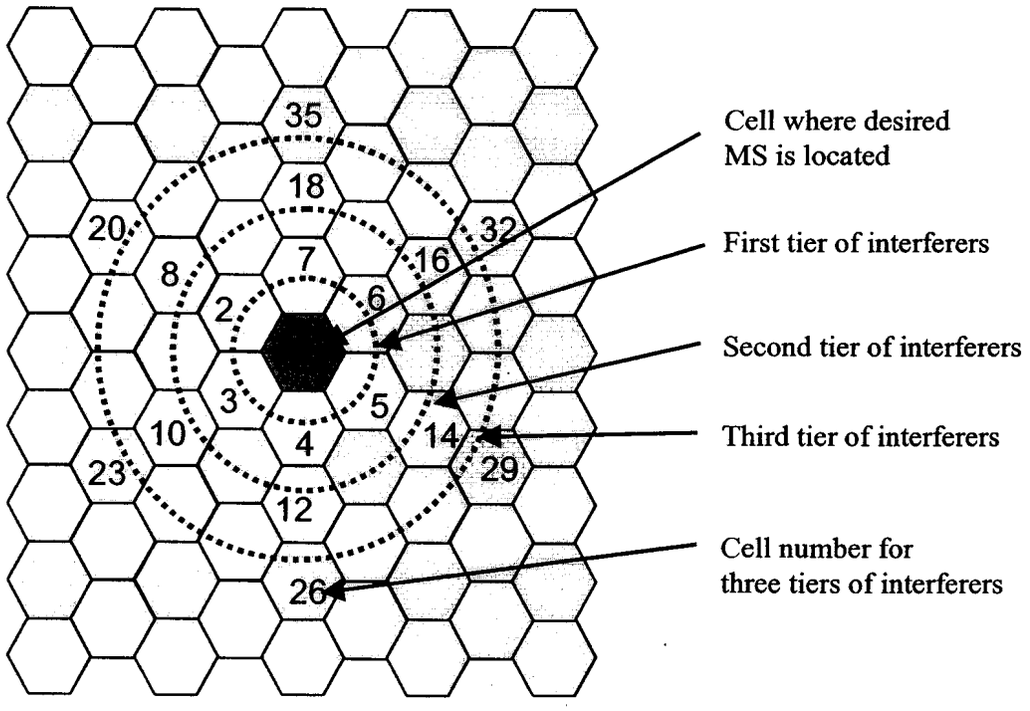

Figure 2: Network geometry with a frequency reuse of one.

One method to further increase the capacity is to have multiple users operating on the same frequency in the same cell [5]. The same cell users are separated from each other by reducing the unwanted interference by means of adaptive pattern shaping. This is called space division multiple access, where user spatial channels are created. This can be in addition to frequency and time channels.

2.3 Array Beamforming Techniques and Configurations

This section discusses different array beamforming techniques as well as array spatial configurations used with the beamforming techniques.

2.3.1 Beamforming Techniques

In this section different array beamforming techniques will be discussed. The beamforming techniques are switched multibeam, phased array beamforming and adaptive array beamforming.

2.3.1.1 Switched Multibeam

A number of fixed beams can be formed by adding a Butler matrix to the output ports of an antenna array [51]. An NxN Butler matrix will form N beams. For example, a 4x4 Butler matrix will form four beams in directions -45°, -15°, 15° and 45°. A four element

beamforming system is shown in Figure 3. In the multibeam system, the beam giving the best signal at the mobile on the downlink and best signal from the mobile on the uplink is selected. The higher directivity of a multibeam antenna compared to a sectorized antenna results in a lower level of interference received at the base station from undesired mobiles. The interference to mobiles on the downlink is also reduced. This allows for an increase in the number of mobiles that can be supported with a certain signal to interference level compared to a sectorized system [52,53].

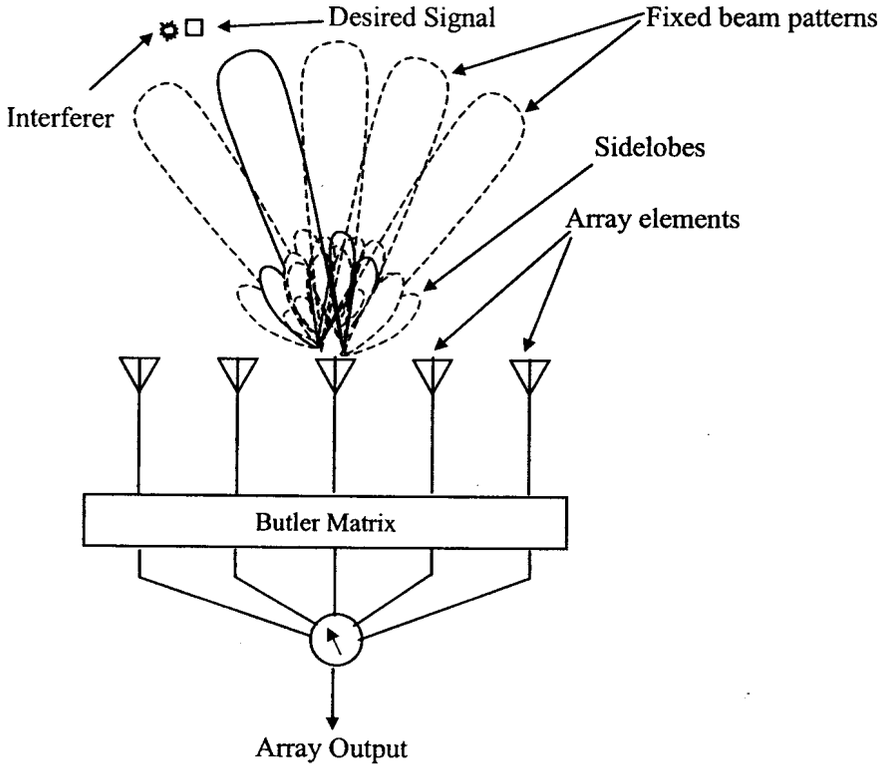

Figure 3: Array forming a number of fixed beams using a Butler matrix beamformer.

2.3.1.2 Phased Array Beamforming

A phased array has more flexibility in beamsteering direction than the multibeam system. The beam is formed by multiplying the signals from each element by a linear phase taper to steer the beam in the direction of the desired signal [51], as shown in Figure 4. An amplitude taper can also be applied to the array elements in order to reduce the sidelobe levels. This will increase the array beamwidth, determined mainly by the number of elements and the spacing between elements. The elements must be spaced close enough to

prevent grating lobes[21], which is a function of the scanning angle. Thus the more the beam is scanned away from boresight, the closer the elements need to be to prevent grating lobes. An element spacing of half a wavelength at the highest frequency is typically used [16].

The ability to separate an interferer from the desired signal depends on the beamwidth of the array. Reduction of the signal of an interferer at an incidence angle less than half a beamwidth away from the desired signal is difficult with a phased array. This is aggravated by the presence of multipath. In addition, if the desired signal multipath angular spread is wider than the array beamwidth, the total received desired signal will be reduced [16]. This will be described in detail in sections to follow.

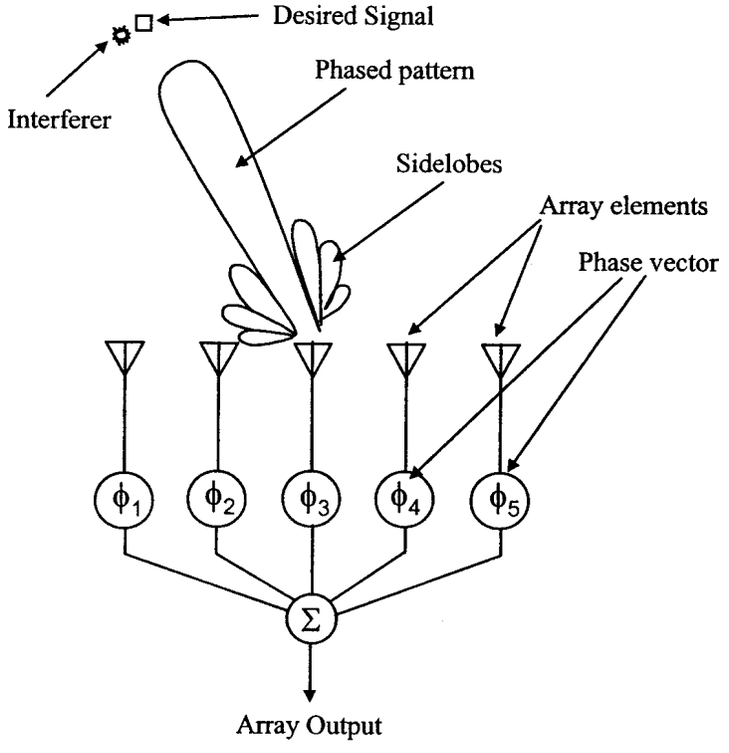

Figure 4: Phased array beam formed in the direction of the desired signal.

[21] Large antenna element spacing can result in multiple main antenna beams (grating lobes) in undesired directions due to phase ambiguities between elements.

2.3.1.3 Adaptive Array Beamforming

Given certain optimization criteria, the adaptive array matches its beamshape to the incoming signal multipath wavefront by multiplying the element signals with a complex weight vector, as shown in Figure 5. The beam is usually formed such that the desired signal to interference plus noise is maximized. The array aims to include all the multipath components of the desired signal, while minimizing all the multipath components from the interferers. The array must track the rapidly fading multipath signal by changing the complex weight vector accordingly with techniques such as least mean squares (LMS) and recursive least squares (RLS) [54].

Since the array adapts the beam to the multipath environment, the elements can be spaced far apart. This will reduce the correlation of signals received at the elements and increase the ability of the array to discriminate between the desired and interfering signals, even if they are in the same direction [2]. The smaller the angular spread, the wider the inter-element spacing needs to be in order to separate the signals. The inclusion of all the multipath signals leads to an M-fold diversity gain, where M is the number of array elements [16].

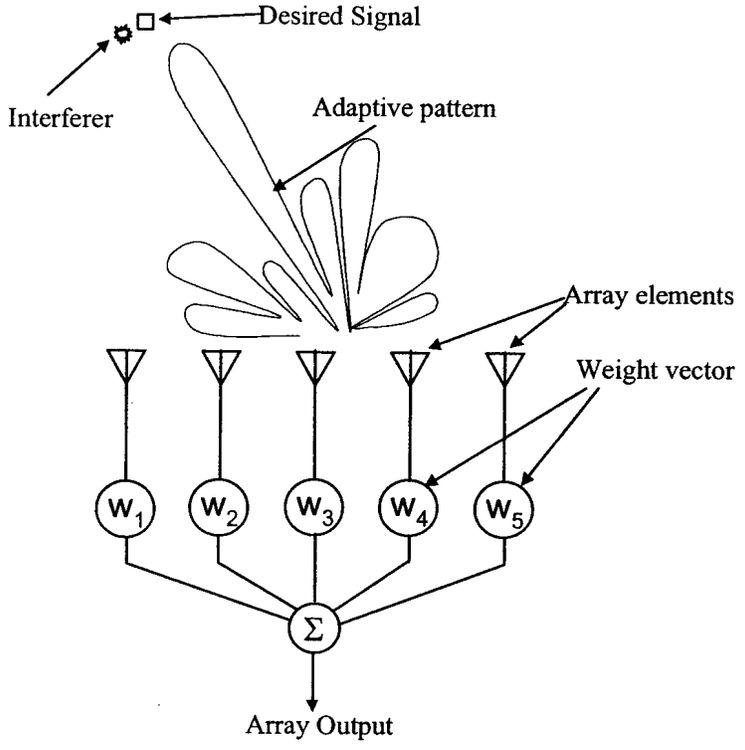

Figure 5: Adaptive array adapting its beam pattern to maximize the signal in the direction of the desired signal, while minimizing it in the direction of the interferer.

2.3.2 Array Geometry and Array Vector

The previous section discussed different beamforming techniques. Each of the beamformers requires an antenna array system. The uniform linear array (ULA) and circular array configurations are used in this thesis and will be discussed next.

The geometry of a uniform linear array is shown in Figure 6. The array consists of M elements orientated in a straight line and spaced a distance Δ apart.

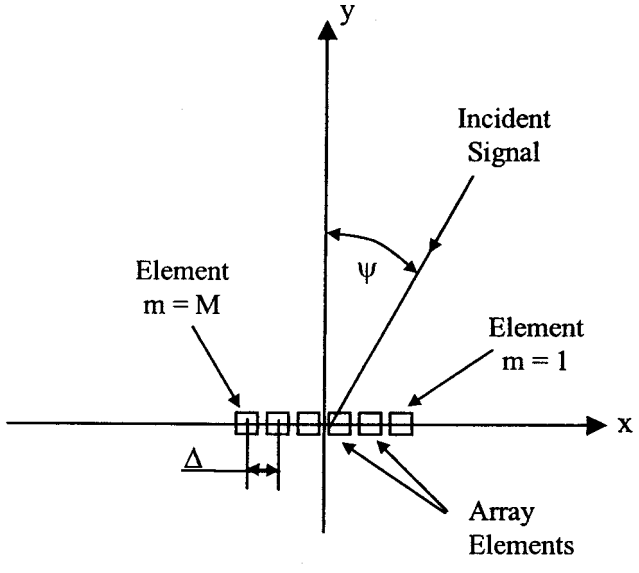

Figure 6: Uniform linear array geometry.

The array vector is [51]:

$$\mathbf{A} = F(\psi)\left\{1, e^{j\frac{2\pi}{\lambda}\Delta\sin\psi}, \ldots, e^{j\frac{2\pi}{\lambda}(M-1)\Delta\sin\psi}\right\}^T \quad (1)$$

where $F(\psi)$ is the element pattern, λ is the carrier wavelength, Δ is the element spacing and T is the transpose. A circular array[22] is shown in Figure 7, with $m \in \{1,\ldots,M\}$ the element number and M the total number of elements.

[22] Also referred to as a cylindrical array.

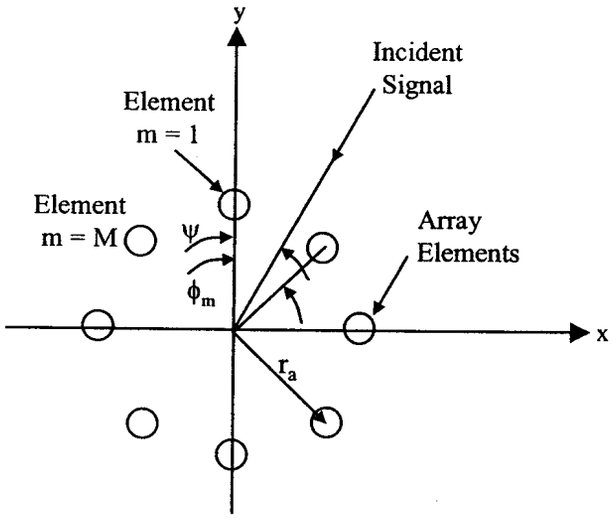

Figure 7: Circular array geometry.

The radius of the array is r_a, given by:

$$r_a = \frac{\Delta}{2\sin\left(\frac{\pi}{M}\right)} \tag{2}$$

where Δ is the spacing between the elements and M is the number of array elements. The angle ϕ_m between the x- axis and each element is given by:

$$\phi_m = \frac{2\pi(m-1)}{M} \tag{3}$$

The array vector for a signal arriving from angle Ψ is given by [16]:

$$\mathbf{A} = \left\{ F(1,\psi)\, e^{-j\frac{2\pi}{\lambda}(r_a \cos[\psi])}, \ldots, F(M,\psi)\, e^{-j\frac{2\pi}{\lambda}\left(r_a \cos\left[\psi - \frac{2\pi(M-1)}{M}\right]\right)} \right\}^T \tag{4}$$

where $F(m,\psi)$ is the element pattern.

2.3.3 Array Element Patterns

The network simulations in later chapters assume a tri-sectored network. The element pattern $F(\psi)$ that will be used in the TDMA reverse link network simulations of chapter 1 is shown in Figure 8.

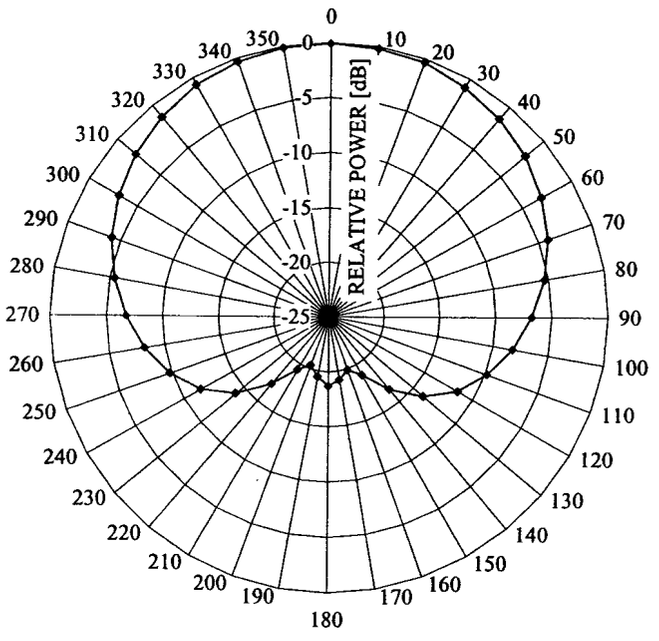

Figure 8: 120 degree element pattern.

In the range increase investigation of adaptive and phased arrays in chapter 1, a cardoid element pattern was used for the circular array elements. The cardoid pattern for the m-th element in the circular array is [16]:

$$F(m,\psi)=\sqrt{2}\cos\left[\frac{\pi}{4}\left(\cos\left\{\psi-\frac{2\pi(m-1)}{M}\right\}-1\right)\right] \qquad (5)$$

The cardoid element pattern is shown in Figure 9. The pattern has a maximum at boresight with no backlobe.

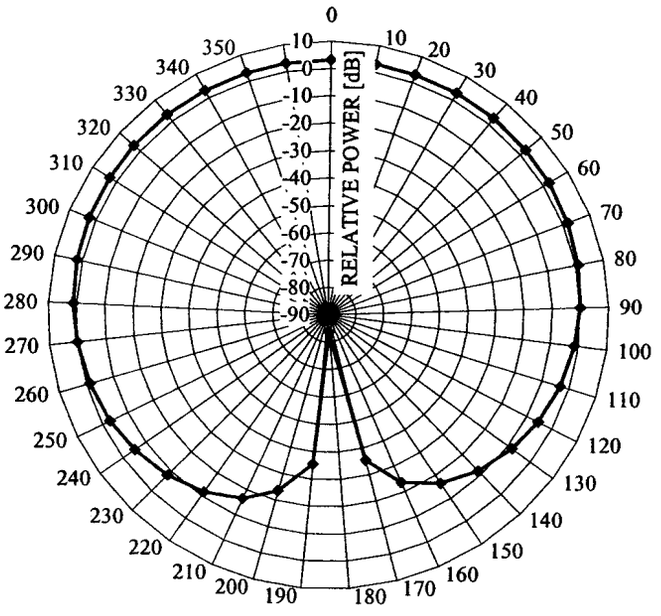

Figure 9: Cardoid element pattern.

2.4 Propagation Channel Models

In this section the propagation channel models that will be used to simulate the fading conditions between the base station and the mobile are discussed. A signal may experience two types of fading, fast and slow fading. Fast fading is due to scattering by a number of objects surrounding the mobile. The signal will add constructively or destructively at the mobile and base station due to the specific phase and amplitude relationship between all these scattered signals. The signal changes rapidly (in and out of fades) as the mobile moves around.

The second type of fading is called slow fading. Slow fading is the long-term variation of the signal due to attenuation by large objects, such as buildings or houses.

2.4.1 Fast Fading

Fast fading will be discussed in this section. Fast fading is the short-term variation of the signal at the mobile or base station due to scattering by objects surrounding the mobile or the base station.

2.4.1.1 Multipath Model

In a typical multipath environment, the mobile is surrounded by a number of scatterers. The signal is reflected, rotated in polarization, scattered and attenuated by these scatterers. The scattered signals will reach the base station with different amplitudes, incidence angles and polarizations[23]. In the case where the base station is taller than the buildings, the incidence angles will fall inside a certain angle sector, called the angular spread, as depicted in Figure 10

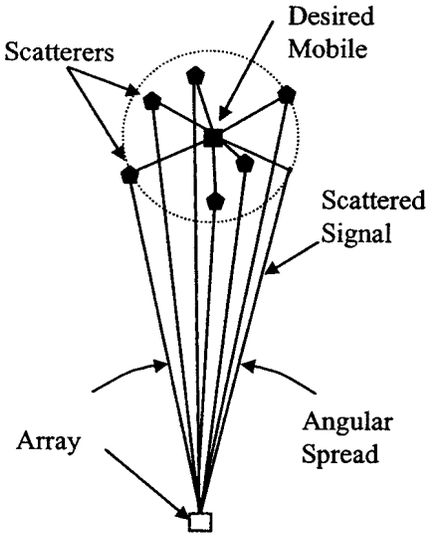

Figure 10: Multipath signals impinging on base station array.

Consider the single scattering multipath geometry[24] as shown in Figure 11. The distance between the mobile and each scatterer is $r^{s}_{d,z,k}$, where d is the mobile number, z is the cell number and k is the scatterer number. The angle between the y-axis and each scatterer is $\phi^{s}_{d,z,k}$ and the range between each scatterer and the center of the array is $r^{e}_{d,z,k}$. The distance between the mobile and the boresight of the array is $r^{c}_{d,z}$. The incidence angle relative to the array boresight of the k^{th} scatterer is $\psi_{d,z,k}$. The total distance $r^{t}_{z,za,d,k}$ between mobile, scatterer and array is a combination of the two distances:

[23] Similar to [4],[24],[32],[46],[56] the effect of polarization was not considered in this thesis.
[24] The single scattering model is not valid for all environments and base station/mobile configurations. It is stated in [22] that it is reasonable to believe that a single scattering model can be used in environments where the base antenna is high in comparison with the surrounding buildings and hills, and where there are relatively few distinct high buildings and hills at longer distances from the base station.

$$r^{t}_{z,za,d,k} = r^{e}_{z,d,k} + r^{s}_{z,za,d,k} \quad (6)$$

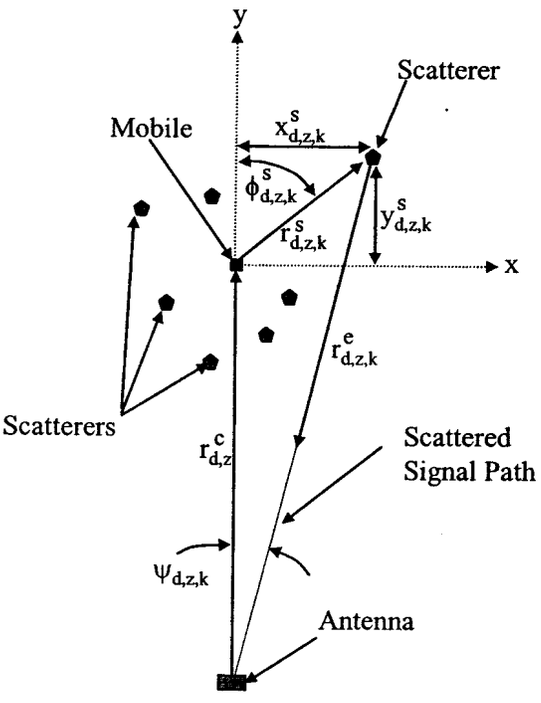

Figure 11: Geometry of multipath environment.

The multipath geometry of the desired signal and an interferer is shown in Figure 12, where the incidence angle between the array boresight and the interferer is $\psi^{c}_{d=2,z}$.

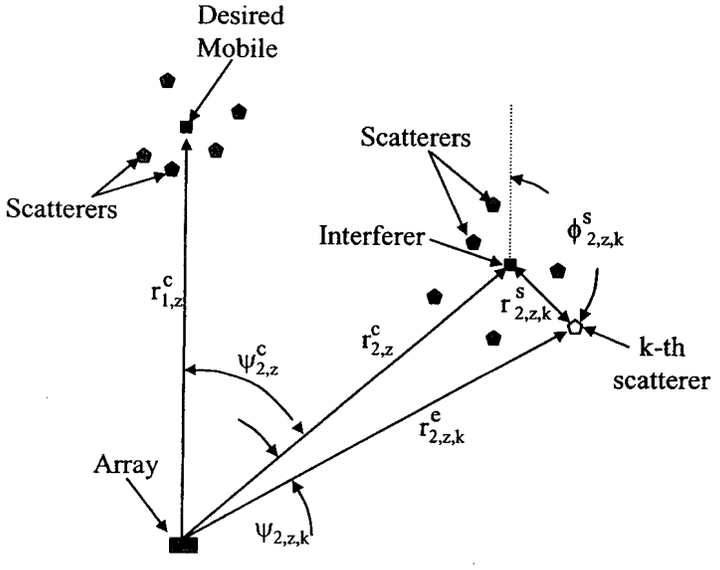

Figure 12: Geometry of desired signal and interferer multipath signals.

The multipath geometry for an interferer in an adjacent cell is shown in Figure 13, with the angle between the array boresight and the interferer in cell z = 2 is $\psi^{c}_{d=2,z=2}$.

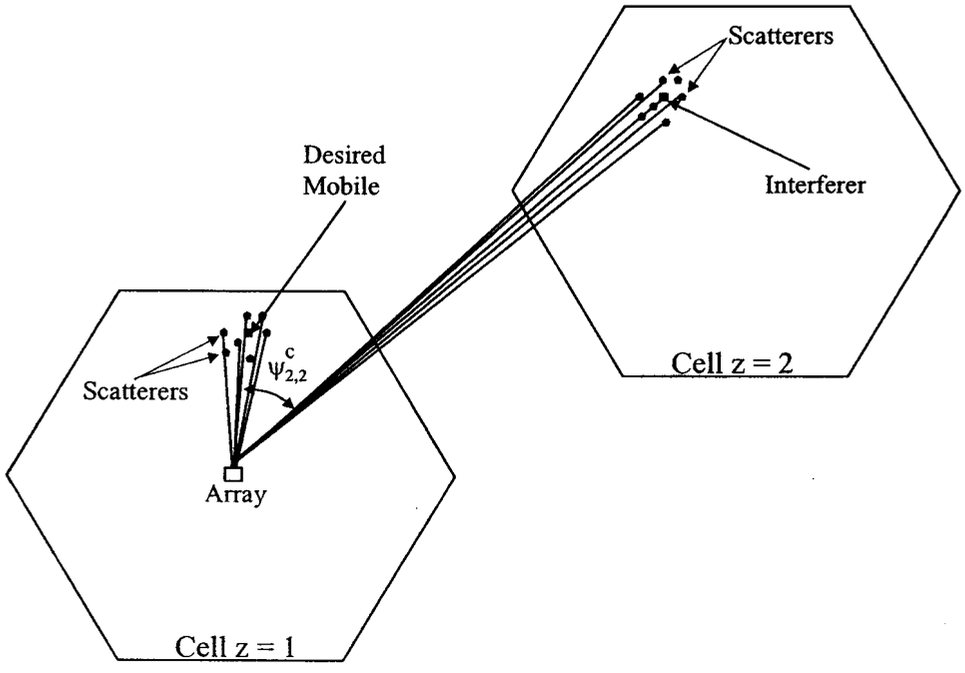

Figure 13: Multipath geometry for an interferer in an adjacent cell.

Each multipath component is considered to be a plane wave, arriving from a discrete direction and with a discrete time delay. The time-variant propagation vector[25] channel impulse response between the d^{th} mobile in cell z and antenna array in cell za [46,55,56], is:

$$\mathbf{h}_{z,za,d}(t) = \sqrt{\frac{1}{\rho_{z,za,d}(t)(4\pi r_0)^2}} \sum_{k=1}^{K} \frac{\xi_{z,za,d,k}(t)\sqrt{F(\psi_{z,za,d,k}(t))}\,\delta(t-\tau_{z,za,d,k}(t))}{\sqrt{\left(\frac{r^{t}_{z,za,d,k}(t)}{r_0}\right)^{\gamma}}} \quad (7)$$

$$e^{j\varphi_{z,za,k,d}(t)}\mathbf{A}(\psi_{z,za,d,k}(t))$$

where, $\rho_{z,za,d}$ is the log-normal[26] shadowing loss, $F(\psi_{z,za,d,k})$ is the array element pattern, $\xi_{z,za,d,k}$ is the amplitude of the signal scattered from the k^{th}-object (or closely located group of objects), $\mathbf{A}(\psi_{z,d,k})$ is the array response vector in the direction of arrival $\psi_{z,za,d,k}$

[25] A vector channel model as defined in [46] includes the angle of arrival. The vector here refers to the array response vector.
[26] Random variable in dB with a zero mean normal distribution.

of the k^{th} -scattered signal , δ is the Dirac-delta function and $r^{t}_{z,za,d,k}$ is the total distance between the mobile, scatterer and array. The delay and phase between the mobile and the k^{th}-scatterer plus between the k^{th}-scatterer and the center of the array is $\tau_{z,za,d,k}$ and $\varphi_{z,za,d,k}(t)$ respectively. Equation (7) can be written in a simplified form as:

$$\mathbf{h}_{z,za,d}(t) = \sum_{k=1}^{K} \sqrt{G_{z,za,d,k}(t)}\, \delta(t-\tau_{z,za,d,k}(t))\, e^{j\varphi_{z,za,k,d}(t)}\, \mathbf{A}(\psi_{z,za,d,k}(t)) \qquad (8)$$

where $G_{z,za,d,k}(t)$ is the path gain[27] given by:

$$G_{z,za,d,k}(t) = \frac{F(\psi_{z,za,d,k}(t))\ \xi^{2}_{z,za,d,k}(t)}{\rho_{z,za,d}(t)\ (4\pi r_0)^2 \left(\dfrac{r^{t}_{z,za,d,k}(t)}{r_0}\right)^{\gamma}} \qquad (9)$$

The amplitude $\xi_{z,za,d,k}$ can be modeled as a fixed or Rayleigh distributed random variable [56]. In the case where it is modeled as a Rayleigh distributed random variable, each scatterer actually consists of a group of scatterers located close (relative to the signal bandwidth) to each other. The case of flat Rayleigh fading is obtained when there is only a single scatterer group (K=1) [50].

2.4.1.1.1 Circular Vector Channel Model

The circular vector channel model is described in this section [25,46]. The geometry of this model for a single mobile is shown in Figure 14. It consists of K scatterers uniformly (with respect to area) distributed in a circular area with radius r^{s}_{max}.

[27] The same terminology as in [22] is used for this term, i.e. path gain.

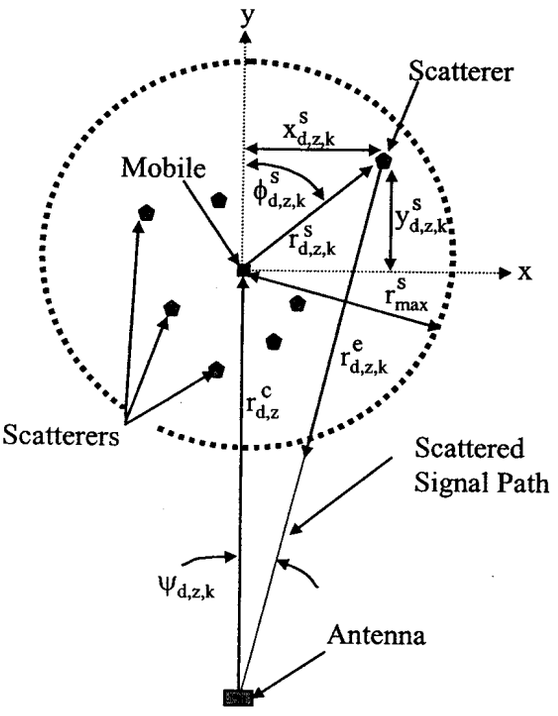

Figure 14: Geometry of the circular vector channel model.

Once the scatter locations have been determined, the propagation channel transfer function given in section 2.4.1.1 can be calculated. In [16] it was assumed that the signal is scattered equally in power by all the scatterers. This amplitude $\xi_{z,za,d,k}$ is then given by:

$$\xi_{z,za,d,k} = \frac{1}{\sqrt{K}} \tag{10}$$

where r_0 is a reference distance [56]. This model was used in the simulations of Chapter 3. The phase shift $\varphi_{z,d,k}$ is uniformly distributed between 0 and 2π [16]. Using the above assumptions, the path gain becomes:

$$G_{z,za,d,k}(t) = \frac{F(\psi_{z,za,d,k}(t))}{K\,\rho_{z,za,d}(t)\,(4\pi r_0)^2 \left(\frac{r^t_{z,za,d,k}(t)}{r_0}\right)^{\gamma}} \tag{11}$$

2.4.1.1.2 Angular Incident Power Distribution

The scattered signal from each of the K objects can either have a constant amplitude or a Gaussian amplitude distribution given by:

$$p(\xi) = \frac{1}{\sqrt{2\pi}\sigma} e^{\left(\frac{-\xi^2}{2\sigma^2}\right)} \tag{12}$$

with a standard deviation of:

$$\sigma = \sqrt{\frac{1}{K}} \tag{13}$$

and with a transmit signal power of 1. This Gaussian amplitude distribution was used in the simulations of section 5.1.2. The phase from each scatterer is $e^{j2\pi\varphi}$, with φ a uniform random variable between 0 and 1. The total signal received at the base station is the sum of all the complex signals from the scatterers and has real and imaginary components that are Gaussian distributed with an envelope that is Rayleigh distributed [11]. The incidence angle ψ is Gaussian distributed with zero mean and with a PDF given by [50]:

$$p(\psi) = \frac{1}{\sqrt{2\pi}\sigma_{as}} e^{\left(\frac{-\psi^2}{2\sigma_{as}^2}\right)} \tag{14}$$

where σ_{as} is the standard deviation of the angular spread or half of the angular spread.

2.4.2 Slow Fading

A mobile signal shadowed from the BTS by a large object, such as a building or bridge, will experience a significant attenuation. This attenuation is typically referred to as slow fading, which is a large scale variation superimposed on the small scale fading or fast fading. The duration of a slow fade is typically the time the mobile moves 10 to 30 m, which corresponds to the typical length of small to medium sized buildings. A typical slow fading variation superimposed on a fast fading pattern is shown in [50].

Slow fading is generally modeled as a log-normal distribution [12]. This means that the slow fading in decibels has a Normal or Gaussian distribution, with probability density function given as [37]:

$$p(\rho_{z,za,d}^{dB}) = \frac{1}{\sqrt{2\pi}\,\sigma_{sf}} e^{\left(-\frac{\left\{\rho_{z,za,d}^{dB}\right\}^2}{2(\sigma_{sf})^2}\right)} \tag{15}$$

where $\rho_{z,za,d}^{dB}$ is the slow fading random variable in dB. The PDF has a zero mean and standard deviation σ_{sf}. A typical slow fading histogram with a standard deviation of 8dB is shown in Figure 15.

Power control normally compensates for slow fading. If the received signal at the mobile is weak due to slow fading, the base station will transmit more power to the specific mobile. In a TDMA system, each user has a particular timeslot. The power for the specific timeslot is increased or decreased depending on the fading attenuation. In CDMA, the power (or forward gain) of a specific traffic channel (Walsh spreading code) is increased or decreased according to the slow fade before all the spreading codes are summed together.

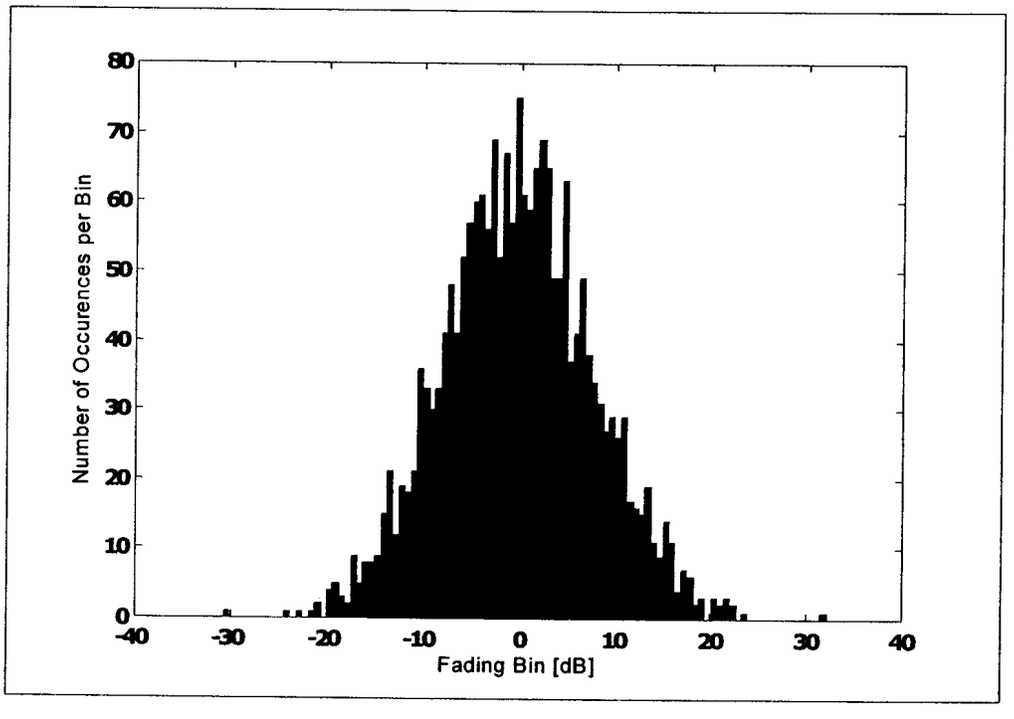

Figure 15: Histogram (PDF) of slow fading loss with a standard deviation of 8dB.

2.5 Spatially Distributed Array Definition

The concept of the spatially distributed array is presented in this section, as well as the practical implementation considerations for this configuration

2.5.1 Distributed Array Concept

A conventional tri-sectored network consists of three 120° sector antennas, with 120° between the boresights of the antennas. In order to reduce (beyond that of sectorization)

the out of cell co-channel interference signals on the uplink (operating on the same frequency and timeslot as the desired mobile in TDMA and GSM systems) and towards mobiles on the downlink, adaptive arrays can be used [1,2,3]. The adaptive arrays are placed at the same locations as the sectorized antennas in the cell (see Figure 16), with element patterns similar to the sectorized antenna pattern.

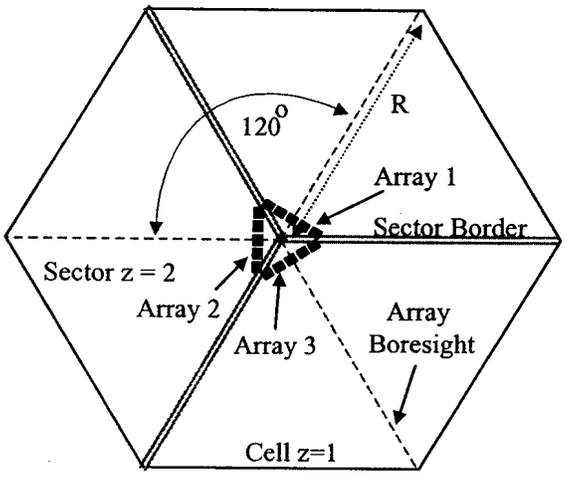

Figure 16: Three arrays at the center of the cell.

With this adaptive array configuration, the capacity can be increased further by allowing multiple co-channel users in the same sector as the desired mobile [4,5,6]. Similar to a tri-sectored configuration, each sector has different frequencies. The users in each sector are isolated from each other in angle with the adaptive array by reducing the received energy from the co-channel interferers, while maximizing the signal of the desired co-channel users. This creates spatial channels for the users, called space division multiple access (SDMA). However two users that have nearly the same incidence angle in an environment with a small angular spread are difficult to be spatially isolated from each other and have to be assigned to different channels (frequency or time) [5].

The spatial resolution required to discriminate between users with a small difference in incidence angle in a narrow angular spread environment can be improved by employing an adaptive array at every other corner of a hexagonal cell. The concept of placing base stations at the edge of a hexagonal cell was first proposed in [7,8,9]. However, the technique presented in this thesis differs from [7] in that adaptive arrays are used on the base stations instead of 120° overlapping sectorized antennas. It differs from [8,9] in that

combined beamforming of the arrays is considered instead of selection diversity. The three arrays on every other edge of a hexagonal cell form sub-arrays of one large array system, where the steering vector of the array system is optimized to yield the best signal to interference ratio for all co-channel users in the same-cell.

The array system is able to spatially discriminate between co-channel users in a two-dimensional plane, as each array has a different viewing angle towards the users. A desired user may be closely located in angle to an interferer as seen from one array, while from a different viewing angle, another array might be able to spatially separate the user from the interferer. The result is that even more co-channel users can operate in the same cell compared to conventional methods in a narrow angular spread environment with closely spaced antenna elements.

2.5.2 Conventional Array Geometry

The performance of the distributed array will be compared to the conventional array, and therefore the conventional array geometry must be defined. The geometry of the conventional arrays at the center of the cell is shown in Figure 17. There are three antenna arrays, each with M antenna elements and with an element pattern covering a nominal angle of ± 60°. The angle between the boresight of each array $\kappa \in \{1,2,3\}$ and scatterer $k \in \{1,2,...,K\}$ is $\psi_{z,za,\kappa,d,k}$, where z is the cell number in which mobile d is located and za is the cell number where the array is located.

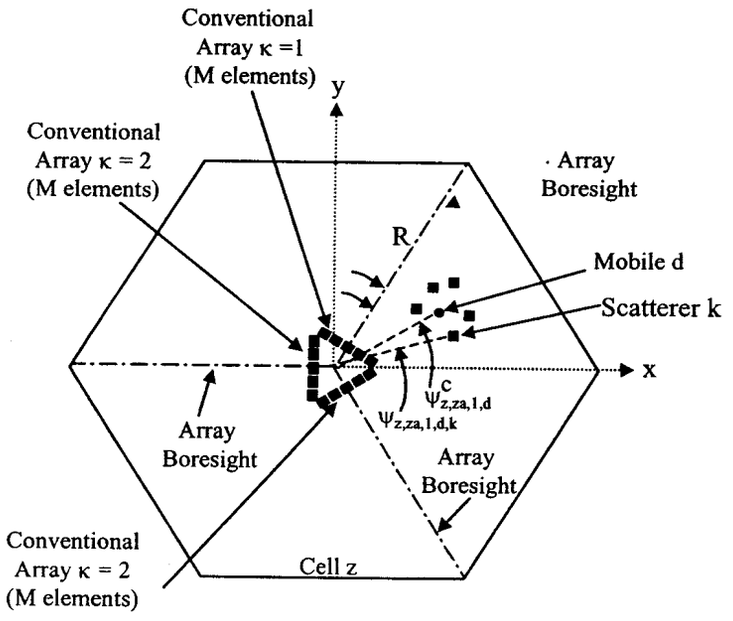

Figure 17: Geometry of the conventional antenna arrays at the center of a hexagonal cell.

R is the cell radius, which is the distance between the center of the cell and the furthest point of the hexagonal cell.

2.5.3 Distributed Array Geometry

The geometry of three sub-arrays at alternate corners of a hexagonal cell is shown in Figure 18. Each of these antenna sub-arrays has M antenna elements. Each antenna sub-array pattern covers a nominal angle of $\pm 60°$. The angle between the boresight of each sub-array $\kappa \in \{1,2,3\}$ and scatterer $k \in \{1,2,...,K\}$ is $\psi_{z,za,\kappa,d,k}$, where z is the cell number in which the mobile d is located and za is the cell number where the distributed array is located.

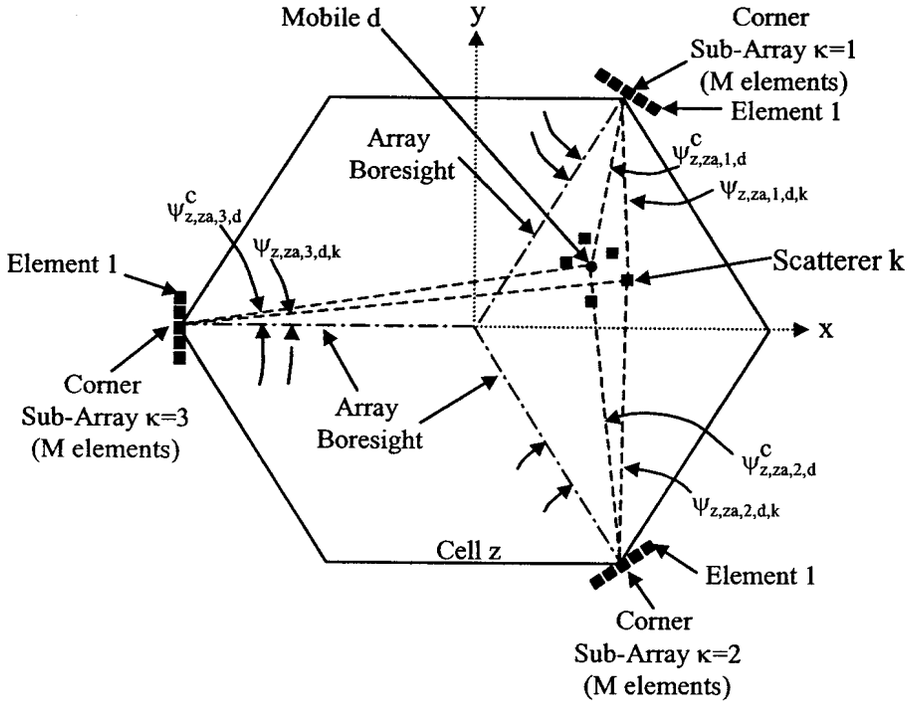

Figure 18: Distributed array geometry.

2.5.4 Practical Implementation Considerations

The fact that the sub-arrays are located at the edges of the cell and thus separated far apart, as well as the fact that they have to function as part of a larger array, results in practical limitations and implementation factors which must be taken into consideration. The following factors: 1) cell size limitation, 2) effective processing of the signals arriving at all the antenna elements, and 3) power control are discussed in sections 2.5.4.1 to 2.5.4.3.

2.5.4.1 Cell Radius of Distributed Array versus Array at the Cell Center

The distributed sub-arrays are located at the edges of the cell. A mobile at the edge of the cell will have a mobile to sub-array separation distance that can be up to twice the separation distance for a standard sectorized cellsite configuration. With a propagation path-loss coefficient of 3.5 (typical for an urban environment [5]) and twice the distance, an additional pathloss of 10.5dB can be encountered between the mobiles and the sub-arrays .

On the other hand, the directivity of the sub-arrays is higher than the directivity of a standard tri-sector antenna. The directivity of distributed sub-arrays varies as a function of the distribution of the mobiles. The mean and standard deviation of the difference in azimuth directivity between each of the sub-arrays and a sector antenna with a 105° half-power beamwidth, were calculated as 5.04dB and 1.26dB for sub-array 1, 4.75dB and 1.22dB for sub-array 2 and 4.77dB and 1.13dB for sub-array 3, respectively. This was calculated with a total of 500 iterations using different mobile positions for each iteration, nine element arrays and seven mobiles uniformly distributed over the whole cell area. The minimum (mean minus standard deviation) difference in azimuth directivity between the adaptive sub-arrays and the sector antenna is approximately 3.5 dB. This gain difference allows the adaptive sub-array range to be 1.26 times the range of the sectorized antenna, with a pathloss exponent of 3.5. Now, without increasing the mobile maximum transmit power or base station sensitivity on the uplink (or mobile sensitivity and base station power on the downlink), the maximum noise limited cell radius of the distributed array can only be 0.63 times (1.26 divided by 2) the maximum noise limited radius of the centrally located sectorized cellsite.

Therefore, due to the fact that the distributed sub-arrays are located at the edges of the cell, the cell radius of the adaptive distributed array will be less than the cell radius of a traditional tri-sector cellsite. This radius difference is a function of the pathloss exponent.

2.5.4.2 Joint Adaptive Beamforming with Spatially Removed Arrays

The optimum steering vector is determined from signals present at all the sub-array elements. In order to determine the steering vector, the baseband signals of all the antenna elements (all the sub-arrays) are added together after being weighted. Using the least mean squares method, this output signal is then compared to a known signal and a cost function is determined as described in section 2.7.1.1.1. The baseband signals can be transmitted to a central processing unit where the optimum weight vector can be determined. However, this will result in a huge amount of data that has to be transmitted to the processing unit.

This can be overcome by first multiplying the baseband signals of each sub-array with an optimum weight vector for each desired user (determined in the previous iteration), adding the result together for each desired user and thus forming the vector at each sub-array:

$$Y_{\kappa}(nT_s) = \mathbf{W}_{\kappa}^{H}\,\mathbf{X}_{\kappa}(nT_s) \qquad (16)$$

where $\kappa \in [1,2,3]$ is the sub-array number, **W** is the weight vector and **X** is the array signals downconverted to baseband at each array. The resultant output for each desired user must then be transmitted to a central processing unit, where the output signal from each base station for each desired user is coherently summed. The total resultant output for each user is compared to the known sequence of each desired user and a complex cost function (complex value) is determined for each desired user. The cost functions are then transmitted to all three base stations. At each base station, the updated steering vector for each user is determined. The resultant steering vector is identical to the steering vector that can be obtained when all the antenna element data is transmitted to and processed in one central location.

The three array output signals must be coherently combined in time and phase, otherwise the desired SINR will decrease. The delay between the three signals must be accurately aligned using for example delay lines at the central receiver. The phase can be aligned by using for example a pilot signal transmitted (via a cable or oprical fibre) from each sub-array (together with the traffic signal) and then changing the phase of the three signals (from the three sub-arrays) with complex digital multipliers until a maximum signal is observed from the combined signals

2.5.4.3 Power Control Implementation

In this section a practical method implementing power control for the distributed array system is presented. Three timeslots are required for power control. During timeslot 1 only sub-array 1 is receiving. The power of all mobiles are adjusted for sub-array 1, based on the received up-link signal, which is a function of distance and fading between the mobiles and sub-array 1. Power control in timeslots 2 and 3 is done for sub-arrays 2 and 3 respectively. The same information is transmitted by all mobiles during all three timeslots.

2.5.5 Distributed Array Power Control in Simulations

In the simulations of chapters 1 and 2, the following two power control methods are used:

1. The power is controlled by the nearest sub-array, as described in 2.5.5.1

2. The power is controlled by the sub-array receiving the strongest signal, including distance and slow fading, as described in 2.5.5.2.

2.5.5.1 Range Power Control

In the absence of slow fading, it is assumed that the power for the co-channel users is controlled by the closest sub-array [37]. If the power control distance for mobile d in cell z and array in cell za is denoted by $r^{c,pc}_{z,za,d}$, the path gain can be written as (see Figure 14):

$$G_{z,za,\kappa,d,k}(t) = \frac{\lambda^2 \xi^2_{z,za,\kappa,d,k}(t)}{(4\pi r_0)^2 \left(\frac{r_{z,za,\kappa,d,k}(t)}{r_0 r^{c,pc}_{z,za,d}(t)} \right)^{\gamma}} F(\psi_{z,za,\kappa,d,k}(t)) \qquad (17)$$

where κ is the sub-array number, $F(\psi_{z,za,\kappa,d,k})$ is the antenna element normalized power pattern (see section 2.3.3), ψ is the angle of the mobile relative to the antenna boresight, γ is the pathloss exponent and r_0 is the free space pathloss reference distance. In the presence of slow fading, power can either be controlled by the closest sub-array or by the sub-array receiving the strongest signal. In the case where the power is controlled (for mobile d in cell z) by the closest base station, the path gain is (see Figure 14):

$$G_{z,za,\kappa,d,k}(t) = \frac{\lambda^2 \xi^2_{z,za,\kappa,d,k}(t)}{(4\pi r_0)^2 \left(\frac{r_{z,za,\kappa,d,k}(t)}{r_0 r^{c,pc}_{z,za,\kappa,d,k}(t)} \right)^{\gamma} \rho_{z,za,\kappa,d}(t)} F(\psi_{z,za,\kappa,d,k}(t)) \qquad (18)$$

where k is the scatter number, $\rho_{z,za,\kappa,d}$ is slow fading path loss between mobile d in cell z and array κ in cell za, $F(\psi_{z,za,\kappa,d,k})$ is the antenna element normalized power pattern (see section 2.3.3), κ is the sub-array number and r_0 is the free space path loss reference distance.

2.5.5.2 Signal Strength Power Control

In the case of power control by the array receiving the strongest signal in the presence of slow fading, the path gain is given by:

$$G_{z,za,\kappa,d,k}(t) = \frac{\lambda^2 \ \xi^2_{z,za,\kappa,d,k}(t)}{(4\pi r_0)^2 \left(\frac{r_{z,za,\kappa,d,k}(t)}{r_0 \, r^{c,pc}_{z,za,d}(t)}\right)^{\gamma} \left(\frac{\rho_{z,za,\kappa,d}(t)}{\rho^{pc}_{z,za,d}(t)}\right)} F(\psi_{z,za,\kappa,d,k}(t)) \qquad (19)$$

where $\rho^{pc}_{z,za,d}$ is the slow fading loss between mobile d in cell z and the sub-array of the controlling base station za where the received signal is a maximum, $r^{c,pc}_{z,za,d}$ is the associated range between the mobile d in cell z and array in cell za and r_0 is the free space pathloss reference distance.

2.6 Array Output Signals and Array Combining

The signals received at the array elements are presented in this section, for both narrowband and wideband (spread spectrum) systems. The multiplication of the signals by a complex weight vector is described as well as combining of all the weight multiplied signals to form one output signal for all the array elements. The extraction of the desired signal component from the wideband array signals will be described, as well as detection and combining of the strongest multipath signals. Methods of combining of the conventional array signals and distributed sub-array signals, will then be presented.

2.6.1 Narrowband Individual Array Output Signals

Assume that the base stations and arrays are synchronized. The output of each array is obtained by multiplying each of the m antenna element signals with a complex weight, and then summing the resultant signal. The sampled output of array κ ($\kappa \in [1,2,3]$) optimized for user d (d is co-channel users with $d \in [1,2,...,D]$) is [1,51,57]:

$$Y_{\kappa,d}(nT_s) = \mathbf{W}^H_{\kappa,d} \, \mathbf{X}_{\kappa}(nT_s) \qquad (20)$$

where n is the sample number, T_s is the sampling period. $\mathbf{W}^H_{\kappa,d}$ is the complex conjugate transpose of the weight vector of array κ optimized for used d, given by:

$$\mathbf{W}_{\kappa,d} = [W_{\kappa,d,1} \ W_{\kappa,d,2} \ \ldots \ W_{\kappa,d,M}]^T \qquad (21)$$

The weight vector estimation procedure is described in section 2.7. $\mathbf{X}_{\kappa}$ are the complex baseband signals (combination of the signals of all D users) at array κ, given by:

$$\mathbf{X}_{\kappa,d} = [X_{\kappa,1}\ X_{\kappa,2} \ldots X_{\kappa,M}]^T \tag{22}$$

Using a far-field approximation, the received signal at the base station antenna is a convolution of the transmit signal and the channel impulse response function in (7). The received signal at element m of array κ (or sub array κ in the case of the distributed array) in cell za is given by [56]:

$$\mathbf{X}_{za,\kappa}(t) = \sum_{z=1}^{Z}\sum_{d=1}^{D} S_{z,d}(t) \otimes \mathbf{h}_{z,za,\kappa,d}(t) + \mathbf{n}_s(t,\kappa) \tag{23}$$

where $\kappa \in [1,2,3]$ is the array number in cell za. $S_{z,d}(t)$ is the complex signal transmitted by the d^{th} co-channel in cell z user convolved with the impulse response of the base station receive filter and $\mathbf{n}_s(t,\kappa)$ is the additive white noise at the array κ elements, which is assumed to be Gaussian distributed with zero mean and variance σ_N^2. Using the propagation channel transfer function in (7), (23) can be written as:

$$X_{za,\kappa,m}(t) = \sum_{z=1}^{Z}\sum_{d=1}^{D}\sum_{k=1}^{K} \{S_{z,d}(t-\tau_{z,za,\kappa,d,k}) \sqrt{G_{z,za,\kappa,d,k}(t)}\ e^{j\varphi_{z,za,\kappa,d,k}(t)} A(m, \psi_{z,za,\kappa,d,k}(t))\} + n_s(t,\kappa,m) \tag{24}$$

where λ is the wavelength. $G_{z,za,\kappa,d,k}$ is the path gain between mobile d in cell z, base station array κ in cell za and multipath component k, given in (17),(18) and (19). Assuming an ideal receive filter and down converting the signal to baseband, the signal amplitude $S_{z,d}(t)$ in equation 24 is:

$$S_{z,d}(t) = \sum_{n=1}^{\infty} b_{z,d}(nT_b)\ p(t-nT_b) \tag{25}$$

where n is the symbol number, $b_{z,d}$ is the d^{th} user complex sequence of transmitted data symbols with period T_b and p(t) is the transmitted pulse shape.

2.6.2 Wideband (Spread Spectrum) Individual Array Output Signals

Spread spectrum systems include e.g. CDMA IS-95 and IS-2000[28] configurations with a spreading bandwidth of 1.2288 MHz. The baseband signal transmitted from the d^{th} mobile in cell z can be written as [12]:

$$S^{t}_{z,d}(t) = \vartheta_{z,d}\sqrt{P_{z,d}}\, b_{z,d}(t) c_{z,d}(t) \tag{26}$$

where $\upsilon_{z,d}$ is the voice activity factor (binary random variable with success $p_{z,d}$), $P_{z,d}$ is the controlled mobile transmit power, b is the differentially encoded information data bits of duration T_b and $c_{z,d}$ is the spreading code (1.2288 MHz bandwidth in IS-95 and IS-2000). The spreading code of user d in cell z can be written as [12]:

$$c_{z,d}(t) = \sum_{n=-\infty}^{\infty} c_{z,d}(nT_c)\, p(t - nT_c) \tag{27}$$

where p(t) is the chip pulse shape (which is assumed rectangular in the simulations to follow) and $c_{z,d}(nT_c)$ are assumed to be independent random variables with values ± 1 and with equal probability. The spread spectrum adaptive array system is shown in Figure 19.

[28] Also referred to as 1xRTT.

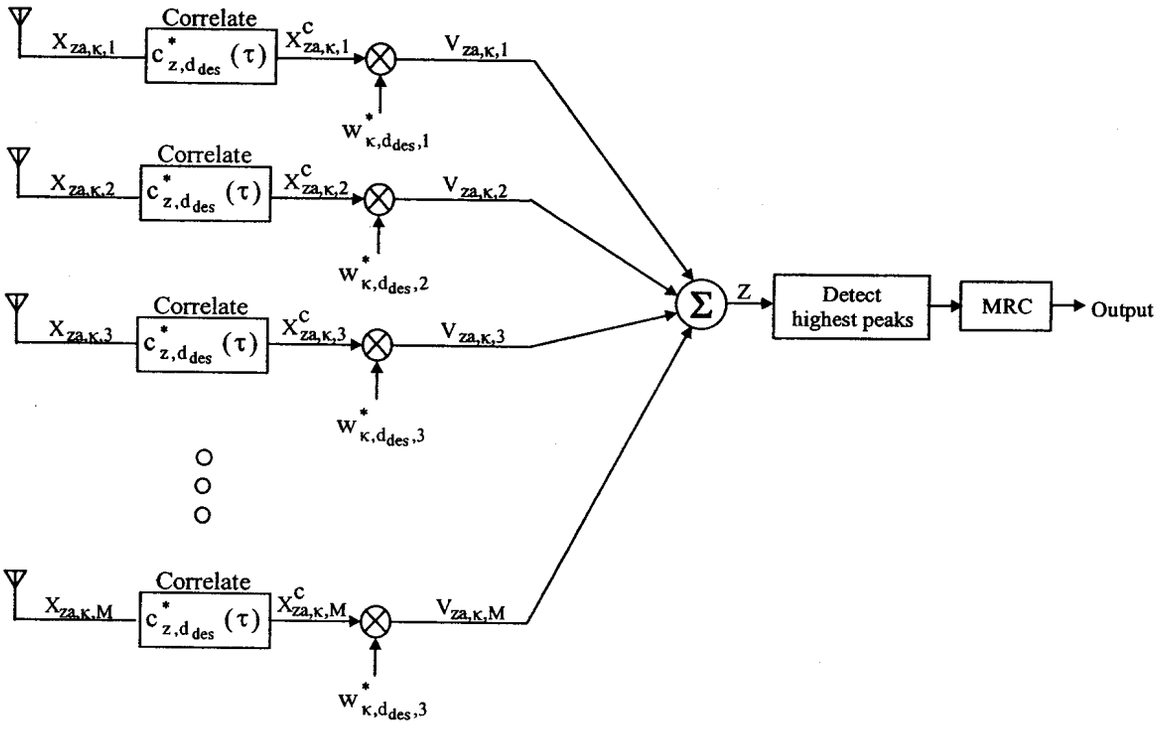

Figure 19: Spread spectrum adaptive array system.

The output of each branch m of array κ is sampled with period T_s and then downconverted to baseband to form the complex baseband signals (combination of the signals of all D users) $\mathbf{X}_\kappa$, where:

$$\mathbf{X}_\kappa(nT_s)=\left[X_{\kappa,1}(nT_s)\quad X_{\kappa,2}(nT_s)\quad \ldots\quad X_{\kappa,M}(nT_s)\right]^T \tag{28}$$

Inserting (26) in (24), the baseband received signal vector from mobile d at element m of array κ in cell za can be written as [12]:

$$X_{za,\kappa,m}(nT_s)=\sum_{z}^{Z}\sum_{d=1}^{D}\sum_{k=1}^{K}\{\vartheta_{z,d}\sqrt{P_{z,d}}\;b_{z,d}(nT_s-\tau_{z,za,\kappa,d,k})\;c_{z,d}(nT_s-\tau_{z,za,\kappa,d,k})$$

$$\sqrt{G_{z,za,\kappa,d,k}(nT_s)}\;e^{j\left\{\frac{2\pi}{\lambda}r^{t}_{z,\kappa,d,k}(nT_s)\right\}}A(m,\psi_{z,za,\kappa,d,k})\}\;+\;n_s(nT_s,\kappa,m) \tag{29}$$

Each antenna element is followed by a RAKE receiver[29], where the first processing stage is to despread the signal with the desired signal d_{des} spreading code $c_{z,d_{des}}$, i.e.

[29] Coherent combining of L multipath signals spaced integer periods apart, with n ≥ 1.

$$X^{c}_{za,\kappa,m}(nT_s, d_{des}) = \int_{-\infty}^{\infty} X_{za,\kappa,m}(nT_s - \tau)\, c^{*}_{z,d_{des}}(\tau)\, d\tau \qquad (30)$$

where X^c is the despreaded signal and z is is the cell containing the desired signal. The autocorrelation function of spreading code $c_{z,d}$ at sample time n T_s is given by (see Figure 20) [16]:

$$ACF[\tau, nT_s] = g_p\left\{1 - \frac{|\tau - nT_s|}{T_c}\right\} \qquad (31)$$

where g_p is the processing gain (ratio between the spreading code rate and the bit rate).

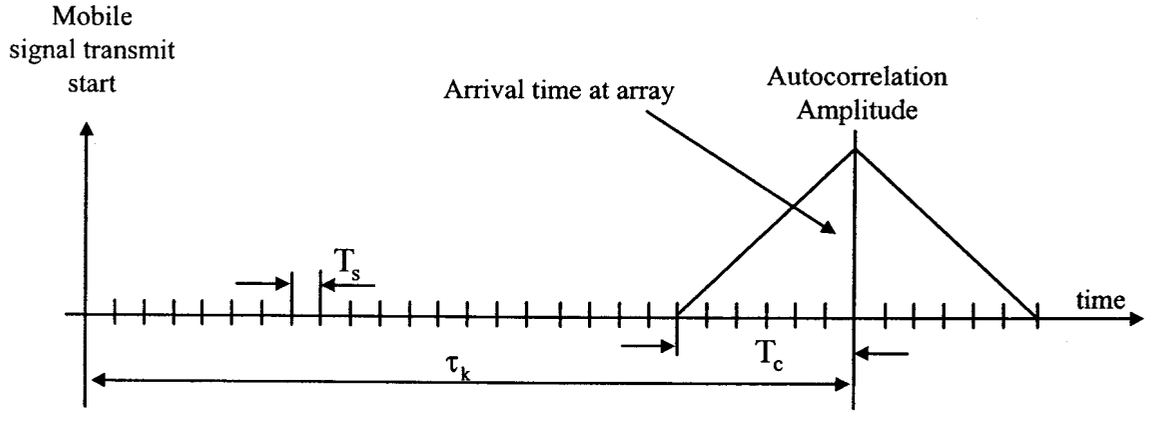

Figure 20: Autocorrelation function of k^{th} multipath component.

Using (30) and (31), the desired signal portion (portion correlating with desired signal spreading code) of (29) at time sample n T_s in cell z_{des} is:

$$X^{c,des}_{z_{des},za,\kappa,m}(n\,T_s, d_{des}) = g_p \sum_{k=1}^{K} \{\vartheta_{z_{des},d_{des}} \sqrt{P_{z_{des},d_{des}}}\; b_{z_{des},d_{des}}(n\,T_s - \tau_{z_{des},za,\kappa,d_{des},k})$$

$$\left[1 - \frac{|\tau_{z_{des},za,\kappa,d_{des},k} - n\,T_s|}{T_c}\right] \sqrt{G_{z_{des},za,\kappa,d_{des},k}(nT_s)}\; e^{j\left\{\frac{2\pi}{\lambda} r^{t}_{z_{des},\kappa,d_{des},k}(nT_s)\right\}}$$

$$A(m, \psi_{z_{des},za,\kappa,d_{des},k})\} \qquad (32)$$

The total received interference plus noise signal after despreading at time sample nT_s is:

$$X^{c,int}_{za,\kappa,m}(nT_s,d_{des}) = \sum_{\substack{d=1\\ d\neq d_{des}}}^{D}\sum_{k=1}^{K}\{\vartheta_{z,d}\sqrt{P_{z,d}}\sqrt{G_{z,za,\kappa,d,k}(nT_s)}\; e^{j\left\{\frac{2\pi}{\lambda}r^{t}_{z,\kappa,d,k}(nT_s)\right\}} A(m,\psi_{z,za,\kappa,d,k}(nT_s))\} + n_s(nT_s,\kappa,m) \quad (33)$$

The signals in (32) and (33) are then multiplied by the conjugate of a complex weight vector $\mathbf{W}_{\kappa,d_{des}}$ for optimization to the desired user d_{des}, to yield the signal vectors $\mathbf{V}^{des}_{za,\kappa,m,d_{des}}(nT_s,d_{des})$ and $\mathbf{V}^{int}_{za,\kappa,m,d_{des}}(nT_s,d_{des})$ optimized for user d_{des}. Weight estimation procedures are described in section 2.7. The components of the vectors $\mathbf{V}^{des}_{za,\kappa,m,d_{des}}(nT_s,d_{des})$ and $\mathbf{V}^{int}_{za,\kappa,m,d_{des}}(nT_s,d_{des})$ is then summed to yield the corresponding signals $Z^{des}_{za,\kappa.d_{des}}(nT_s,d_{des})$ and $Z^{int}_{za,\kappa,d_{des}}(nT_s,d_{des})$. The next step is to detect the L largest peaks (called fingers in a RAKE receiver) separated by integer multiples of the spreading code period in the desired signal $Z^{des}_{za,\kappa}(nT_s,d_{des})$. The resultant desired signal at the time of arrival of each of the fingers ($n_\ell T_s$) of the RAKE receiver is:

$$Z^{des}_{za,\kappa}(n_\ell T_s,d_{des}) = g_p\sum_{m=1}^{M}\sum_{k=1}^{K}\{\sqrt{P_{z,d_{des}}}\; b_{z,d_{des}}(n_\ell T_s-\tau_{z,za,\kappa,d_{des},k})\left[1-\frac{\left|\tau_{z,za,\kappa,d_{des},k}-n_\ell T_s\right|}{T_c}\right]\sqrt{G_{z,za,\kappa,d_{des},k}(n_\ell T_s)}\; e^{j\left\{\frac{2\pi}{\lambda}r^{t}_{z,\kappa,d_{des},k}(n_\ell T_s)\right\}} A(m,\psi_{z,za,\kappa,d_{des},k}(n_\ell T_s))\}\, W^{*}_{\kappa,d_{des}}(\ell,m) \quad (34)$$

where $W_{\kappa,d_{des}}(\ell,m)$ is the ℓ^{th} component of the weight vector and n_ℓ is the time sample number of the ℓ^{th} finger. The interference plus noise signal after weight multiplication is:

$$Z_{za,\kappa}^{int}(n_\ell T_s, d_{des}) = \sum_{m=1}^{M} \sum_{\substack{d=1 \\ d \neq d_{des}}}^{D} \sum_{k=1}^{K} \{\vartheta_{z,d} \sqrt{P_{z,d}} \sqrt{G_{z,za,\kappa,d,k}(n_\ell T_s)}\, e^{j\left\{\frac{2\pi}{\lambda} r^t_{z,\kappa,d,k}(n_\ell T_s)\right\}}$$

$$A(m, \psi_{z,za,\kappa,d,k}(n_\ell T_s))\} + n_s(n_\ell T_s, \kappa, m)] W^*_{\kappa,d_{des}}(\ell, m) \quad (35)$$

The L fingers of the desired signal are then coherently combined[30] to form the array desired signal output:

$$Y_\kappa^{des}(d_{des}) = \sum_{\ell=1}^{L} \left\{ \left| Z_{za,\kappa}^{des}(n_{\ell=1} T_s) \right| + \ldots + \left| Z_{za,\kappa}^{des}(n_{\ell=L} T_s) \right| \right\} \quad (36)$$

The interference plus noise components $Z_{za,\kappa}^{int}(n_\ell T_s, d_{des})$ at the time of arrival of the fingers are incoherently added together to form the total array interference plus noise output signal:

$$Y_\kappa^{int}(d_{des}) = \sum_{\ell=1}^{L} \left\{ Z_{za,\kappa}^{int}(n_{\ell=1} T_s) + \ldots + Z_{za,\kappa}^{int}(n_{\ell=L} T_s) \right\} \quad (37)$$

2.6.3 Conventional and Distributed Array Combining

The conventional array weight vector in (21) and (34) for each of the three arrays (in the three sectors) in each cell is determined only from the signals lying in the (± 60° relative to the array boresight) sector covered by each array. Combining of the desired signals of the three arrays can be done with either selection combining or maximum ratio combining [8, 9]. In the case of selection combining, the largest desired signal of the three array output signals are selected. In the case of maximum ratio combining, the desired signal components of the three array signals are added coherently for each sample.

The desired signal d is received by all three the distributed arrays in each cell. The beamforming of the three arrays can be done in two ways, 1) independent beamforming or 2) combined beamforming.

The weight vector in (21) and (34) for independent beamforming is determined seperately for each of the three arrays, which will be discussed in more detail in section 2.7. Selection

combining or maximum ratio combining can then be applied to combine the three signals [8, 9]. In the case of selection combining, the largest desired signal of the three array output signals are selected. In the case of maximum ratio combining, the desired signal components of the three array signals are added in phase.

The weight vector in (21) and (34) for combined beamforming is determined for all three sub-arrays together, i.e. the three sub-arrays form one large array. This will be discussed in more detail on section 2.7. The output of all three sub-arrays are then summed to obtain the output of the total combined array optimized for user d_{des} as:

$$Y_{TOT,d_{des}} = \sum_{\kappa=1}^{3} Y_{\kappa,d_{des}} \tag{38}$$

2.7 Weight Vector Estimation

Each of the signals at the antenna elements (after downconversion) is multiplied by a different complex value, or weight. The set of weight values are called a weight vector. The weight vector steer a phased array beam in a specific direction or form a beam matched to the incoming wavefront which maximizes the signal to noise ratio for the adaptive array.

Two different techniques to estimate the weight vector of an adaptive array are discussed in this section. They are the least mean squares method and the direct matrix inversion method. In addition, the required weight vector to steer a phased array in a specific direction is also given.

2.7.1 Adaptive Arrays

The weight vector of an adaptive array is usually determined with optimum combining [2,54,56]. The least mean squares and direct matrix inversion techniques are subsets of optimum combining.

[30] Using a maximum ratio combiner.

2.7.1.1 Optimum Combining

Optimum combining is equivalent to maximum ratio combining (MRC) in the absence of interferers or when both the interferers and noise are white[31] [2]. Optimum combining yields the maximum signal to interference plus noise ratio [54] and is used throughout this thesis. An eigenvalue solution for the weight vector maximizing the SINR is given in [60] and is repeated in Appendix D for completeness. The result is presented in this section. The array output signal is [54]:

$$Y = \mathbf{W}^H \mathbf{X} = \mathbf{W}^H (S_{des}\mathbf{U}_{des} + S_{int}\mathbf{U}_{int} + \mathbf{n}_s) \tag{39}$$

where $\mathbf{U}_{des}$ and $\mathbf{U}_{int}$ are the normalized (with respect to data sequences) desired and interfering signals, S_{des} and S_{int} are the data sequences of the desired and interfering signals and $\mathbf{n}_s$ is the noise vector. The desired signal portion of the output signal is:

$$Y_{des} = \mathbf{W}^H \mathbf{U}_{des} S_{des} \tag{40}$$

and the interference portion of the output signal is:

$$Y_{int+noise} = \mathbf{W}^H (S_{int}\mathbf{U}_{int} + \mathbf{n}_s) \tag{41}$$

Using (40) and (41), the average output signal to interference plus noise power ratio (SINR) is then given by:

$$SINR = E\left\{\frac{|Y_{des}|^2}{|Y_{int+noise}|^2}\right\} = E\left\{\frac{(\mathbf{W}^H S_{des}\mathbf{U}_{des})(S_{des}\mathbf{U}_{des})^H \mathbf{W}}{\mathbf{W}^H (S_{int}\mathbf{U}_{int} + \mathbf{n}_s)(S_{int}\mathbf{U}_{int} + \mathbf{n}_s)^H \mathbf{W}}\right\} \tag{42}$$

which is equal to:

$$SINR = \frac{P_{des}\mathbf{W}^H \mathbf{U}_{des}\mathbf{U}_{des}^H \mathbf{W}}{\mathbf{W}^H (P_{int}\mathbf{U}_{int}\mathbf{U}_{int}^H + \sigma_N^2)\mathbf{W}} \tag{43}$$

where σ_N^2 is the noise power and E{ } is the average taken over several symbols of the baseband data. Assuming without loss of generality that the power of the desired and interference signals is equal to one, (43) can be written as:

[31] Random with a Gaussian distribution.

$$SINR = \Gamma = \frac{\mathbf{W}^H \mathbf{U}_{des} \mathbf{U}_{des}^H \mathbf{W}}{\mathbf{W}^H \mathbf{R}_{nn} \mathbf{W}} \quad (44)$$

where $\mathbf{R}_{nn}$ is the interference plus noise co-variance matrix, equal to [54]:

$$\mathbf{R}_{nn} = \mathbf{U}_{int} \mathbf{U}_{int}^H + \sigma_N^2 \quad (45)$$

The optimum weight vector, $\mathbf{W}_{opt}$, which maximizes the SINR (45) is (see Appendix D and Appendix E):

$$\mathbf{W}_{opt} = \mathbf{R}_{nn}^{-1} \mathbf{U}_{des} \quad (46)$$

2.7.1.1.1 Least Mean Squares

A least mean squares (LMS) algorithm is an iterative solution of the optimum weight vector for an adaptive antenna array. The LMS algorithm minimizes the gradient of the mean square of a cost function, which is the error between a reference signal[32] and the output signal. In the limit, the weight vector will tend towards the optimum weight vector as given in (46). The cost function for the desired user d_{des} is given by the difference between the output of the array and a reference signal [2]:

$$\varepsilon_{d_{des}}(nT_s) = ref^*_{d_{des}}(nT_s) - Y_{TOT,d_{des}}(nT_s) \quad (47)$$

where * denotes the complex conjugate, $ref^*_{d_{des}}$ is a reference signal of mobile d_{des}, n is the optimization iteration number, T_s is sampling period and $Y_{TOT,d_{des}}$ is the total array output (all three sub-arrays) for user d_{des}. The approximate weight vector $\hat{\mathbf{W}}_{\kappa,d_{des}}(nT_s)$ of array κ can be updated using the algorithm, which is [2]:

$$\hat{\mathbf{W}}_{\kappa,d_{des}}[(n+1)T_s)] = \hat{\mathbf{W}}_{\kappa,d_{des}}(nT_s) + \mu \mathbf{X}_{za,\kappa}(nT_s) \varepsilon_{d_{des}}(nT_s) \quad (48)$$

where $\mathbf{X}(nT_s)$ is the array received baseband vector, given in (24) for the narrowband system and (29) for the wideband case. $\hat{\mathbf{W}}_{\kappa,d_{des}}[(n+1)T_s]$ is a new estimate of the weight vector at iteration (n+1), and μ is the convergence constant. The convergence constant is

[32] The reference signal is a sequence correlated with the transmitted desired signal, which is typically known at the receiver.

greater than zero and usually less than one. The speed (or rate) of the LMS convergence is a function of the convergence constant. The larger the constant, the faster the algorithm will converge with a larger variation in the final converged result. A value of 0.08 was used in the simulations in [24]. The elements of the initial weight vector are taken as:

$$\begin{aligned} W_{\kappa,d_{des},m}(0)&=1 \quad \text{for} \quad m=1 \\ W_{\kappa,d_{des},m}(0)&=0 \quad \text{for} \quad m\in[2,3,...,M] \end{aligned} \tag{49}$$

where m is the element number, and M is the number of array elements. This means that for the initial condition, only the first element of each sub-array is receiving. The LMS algorithm will maximize the ratio of the desired signal d_{des} power to the sum of the co-channel interference plus noise signal powers, given by:

$$SINR_{d_{des}}=\frac{Y_{TOT,d_{des}}\,Y^{*}_{TOT,d_{des}}}{\left[\sum_{d=2}^{D} Y_{TOT,d_{des}}\,Y^{*}_{TOT,d_{des}}\right]} \tag{50}$$

where $Y_{TOT,d_{des}}$ is the array output optimized for the desired signal. The maximum ratio of SINR that can be obtained with the LMS algorithm will be constrained by the distance between the mobiles. The iteration process in (48) optimizing the steering vector is continued until a certain acceptable minimum SINR for all the co-channel users is obtained, or until a maximum allowable number of iterations has been reached.

In order to maximize the SINR, a large correlation between the desired signal and the reference signal are required and small correlation between the reference signal and the interference signals. There should also be minimum correlation between the interference signals to obtain the maximum SINR. The training sequence in a GSM system used for channel equalization has this property and has been used as a reference signal in [22]. There are eight training sequences in GSM with a length of 26 bits each. The method described here is able to spatially isolate more than eight users at a time in the same-cell, and therefore the number of sequences in a GSM system is inadequate. Instead, Gold sequences with the same correlation properties as the GSM training sequences, but with a larger number of sequences can also be used [17].

2.7.1.1.2 Direct Matrix Inversion

To evaluate the performance of an adaptive array, the least mean squares estimation method (see section 2.7.1.1.1) can be used to obtain the weight vector. However, this method has a slow convergence. In order to improve the weight convergence time, the direct matrix inversion method was used for most of the simulations in this thesis. The optimum weight vector estimation using the direct matrix inversion method is [51]:

$$\mathbf{W} = \mu \mathbf{R}^{-1} \mathbf{U}_{d_{des}} = \mu_{nn} \mathbf{R}_{nn}^{-1} \mathbf{U}_{d_{des}} \tag{51}$$

where $\mathbf{U}_{d_{des}}$ is the desired signal propagation vector and $\mathbf{R}^{-1}$ is the inverse of the full covariance matrix and μ is a constant given by:

$$\mu = \frac{1}{\mathbf{U}_{des}^{H} \mathbf{R}^{-1} \mathbf{U}_{des}} \tag{52}$$

The desired signal angle of arrival have to be estimated with subspace methods such as MUSIC or ESPRIT. Using the derivation in Appendix E, the optimum weight vector can be written in terms of the inverse of the interference covariance matrix $\mathbf{R}_{nn}^{-1}$ as:

$$\mathbf{W} = \mu_{nn} \mathbf{R}_{nn}^{-1} \mathbf{U}_{d_{des}} \tag{53}$$

where μ_{nn} is also a constant given:

$$\mu_{nn} = \frac{1}{\mathbf{U}_{des}^{H} \mathbf{R}_{nn}^{-1} \mathbf{U}_{des}} \tag{54}$$

It is also shown in Appendix E that the contant μ_{nn} cancels out when estimating the SINR. Assuming that the noise is not correlated with the signals at the antenna elements, the co-variance matrix can be written as [51]:

$$\mathbf{R}_{nn} = E\left\{\mathbf{X}^{int}(nT_s)\left(\mathbf{X}^{int}(nT_s)\right)^{H}\right\} + \sigma_N^2 \mathbf{I} \tag{55}$$

where E{} is the average. If the average in (55) is taken over N samples of the baseband data, the co-variance matrix becomes

$$\mathbf{R}_{nn} = \frac{1}{N} \sum_{n=1}^{N} \mathbf{X}^{int}(nT_s)\left(\mathbf{X}^{int}(nT_s)\right)^{H} + \sigma_N^2 \mathbf{I} \tag{56}$$

where $\mathbf{X}^{int}(nT_s)$ is vector at sample time n, containing the interference (excluding noise) received signals at the array elements after downconversion to baseband (see section 2.6 for more detail about array received signal vector), T_s is the sample period, $\mathbf{I}$ is the unity matrix and σ_N^2 is the noise power. If 1) the average in (56) is much less than the fading rate (or time between fades[33]), the propagation vector (or channel) is assumed to be stationary (or constant) over the period N*Ts and 2) the interfering signals arriving at the array are uncorrelated over the same averaging period (N*Ts), the co-variance matrix can be written as (see Appendix A)

$$\mathbf{R}_{nn} = \sum_{\substack{d=1 \\ d \neq d_{des}}}^{D} P_d \, G_{\kappa,d} \left\{ \mathbf{U}_d(nT_s) \mathbf{U}_d^H(nT_s) \right\} + \sigma_N^2 \mathbf{I} \tag{57}$$

where $\mathbf{U}_d$ is the array vector in the direction of the d^{th} interferer, P_d is the power of the d^{th} interferer and G is the pathloss defined in section 2.4. For independent array beamforming (see section 2.6.3), the weight vector for each sub-array is obtained, or

$$\mathbf{W}_{\kappa,d_{des}} = \mathbf{R}_{nn,k}^{-1} \mathbf{U}_{d_{des},\kappa} \tag{58}$$

where $\mathbf{R}_{nn,\kappa}^{-1}$ is the inverse of the covariance matrix of the independent arrays. Using equation (56) in (58), the weight vector for independent arrays beamforming is:

$$\mathbf{W}_{\kappa,d_{des}} = \left\{ \frac{1}{N} \sum_{n=1}^{N} \mathbf{X}_\kappa(nT_s) \, \mathbf{X}_\kappa^H(nT_s) + \sigma_n^2 \mathbf{I} \right\}^{-1} \mathbf{U}_{d_{des}} \tag{59}$$

For combined array beamforming (see section 2.6.3), $\mathbf{R}_{nn}^{-1}$ and $\mathbf{U}_{d_{des}}$ are the covariance matrix and desired propagation vector of all three combined sub-arrays. Using equations (51) and (56), the combined array weight vector is:

$$\mathbf{W} = \left\{ \frac{1}{N} \sum_{n=1}^{N} \mathbf{X}_{\cap(\kappa)}(nT_s) \, \mathbf{X}_{\cap(\kappa)}^H(nT_s) + \sigma_n^2 \mathbf{I} \right\}^{-1} \mathbf{U}_{d_{des},\cap(\kappa)} \tag{60}$$

[33] This is the channel coherence time or time that the channel remains constant. This time is the speed of the mobile divided by the wavelength.

where $\mathbf{X}_{\cap(\kappa)}$ is the concatenated vector of the 3 distributed sub-array receive signal vectors and $\mathbf{U}_{desired,\cap(\kappa)}$ is the concatenated vector of the 3 distributed sub-array desired signal steering vectors

2.7.1.1.3 Simultaneous Co-channel Weight Estimation

In the case of a reuse factor of one (see section 2.2.2) and multiple users operating on the same channel (for TDMA and GSM type systems) in the same cell, the users can be isolated[34] from each other with adaptive beamforming. This is done by creating spatial channels between the users, called space division multiple access or SDMA [22]. In the case where there are D co-channel users in the same cell, the number of co-channel interferers is D-1 for every desired user. An adaptive beam is formed for each user from the sampled and downconverted signals at the antenna elements. The adaptive beam is formed by determining an optimum set of weights for each user. There are thus D sets of weights, with the length of each set equal to the number of elements per array multiplied by the number of arrays, as shown in Figure 21.

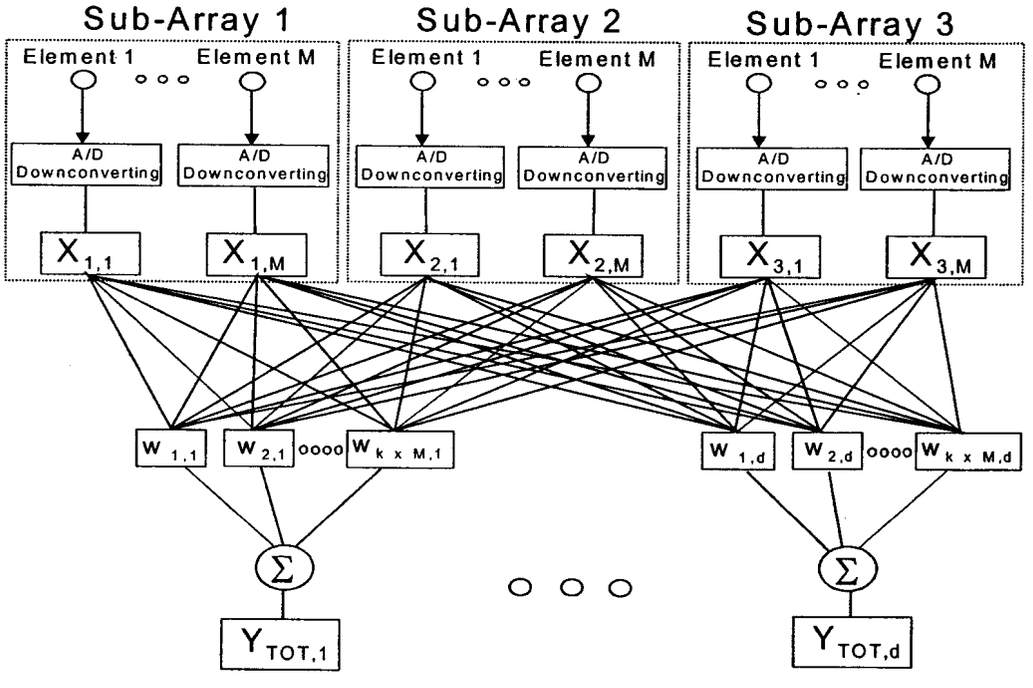

Figure 21: Simultaneous co-channel up-link adaptive beamforming estimation diagram.

[34] In order to extract the data transmitted by each user.

2.7.2 Phased Arrays

A phased array steers a beam in the direction of the desired signal by generating a linear phase across all the array elements [51]. The phased array weight **W** for the desired signal d_{des} is given by:

$$\mathbf{W}_{\kappa,d_{des}} = \mathbf{U}_{d_{des}}(\psi^{c}_{z,za,\kappa,d_{des}}) \tag{61}$$

where $\psi^{c}_{z,za,\kappa,d_{des}}$ is the angle towards the desired mobile in cell z and boresight angle of sub-array κ in cell za and $\mathbf{U}_{d_{des}}$ is the array propagation vector of the desired mobile.

2.8 Distribution of mobiles

In this thesis it is assumed that mobile positions are distributed uniform with respect to area. The histogram for a hexagonal cell structure of the mobile to BTS radius is shown in Figure 22. The figure shows that the probability increases linearly with radius up to 0.866 times the radius, after which it decreases non-linear with radius up to the cell radius (cell radius is 1000m in the figure).

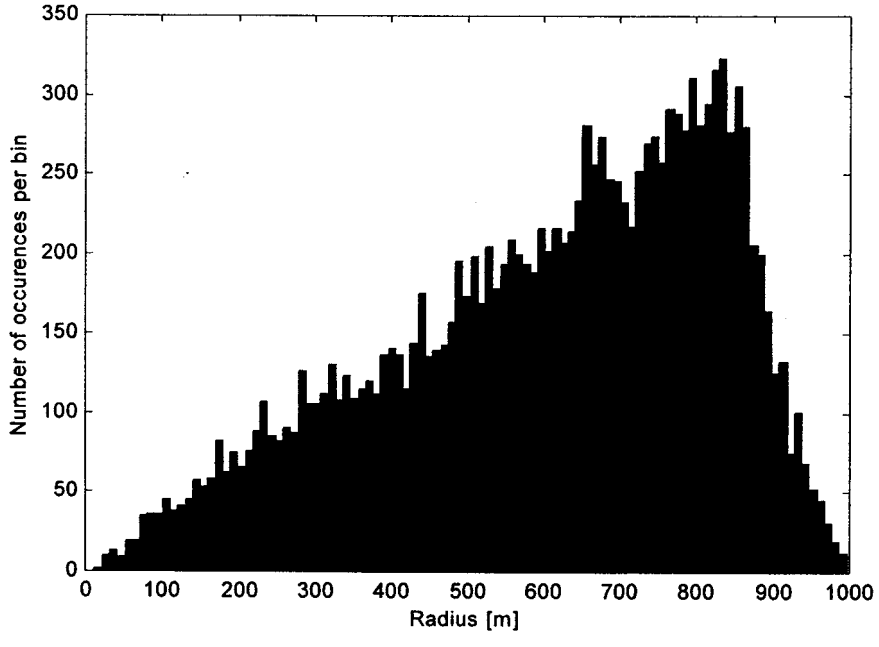

Figure 22: Histogram of mobile to BTS radius with a cell radius of 1000m.

2.9 Performance Evaluation

2.9.1 Monte-Carlo Simulations

Closed form solutions are difficult to obtain when the signals at the array elements are correlated [11]. Since the aim of this thesis is to investigate the performance of the combined array with closely spaced elements in a narrow angular spread propagation environment, the signals between the array elements are correlated. Closed form solutions are therefore difficult to derive [11]. In order to estimate the performance of these arrays, a Monte-Carlo simulation method will be used in this thesis.

The Monte-Carlo method is a statistical technique. If the system under consideration has a random behavior, a Monte-Carlo simulation will produce an approximation of the distribution (probability density function or cumulative distribution function) of the random process. The signal from a mobile will be scattered by a number of obstacles surrounding the mobile.

The scattered signal reaching the base station will have Rayleigh and Log-normal fading. These fading processes are random processes and therefore ideal candidates for the Monte-Carlo method. In the case of closed form solutions, a number of approximations have to be made in order to find the solution. Depending on the specific problem, Monte-Carlo simulations (apart from simulation time constraints) do not have these closed form constraints (or fewer constraints).

2.9.2 Bit Error Rate

It is assumed in this thesis that the signal is phase-shift keyed modulated. If both the noise and received complex interference signals have a Gaussian distribution, the average bit error rate (BER) for coherent detection of phase-shifted PSK signals is given by [11]

$$BER_{average} = \frac{1}{2}\int_{-\infty}^{\infty} p(\eta)\ \mathrm{erfc}(\sqrt{\eta})\,d\eta \qquad (62)$$

where η is the instantaneous signal to interference plus noise ratio (SINR), p( ) is the probablity density function and erfc is the complimentary error function. In this case the

probability density function can be determined with a Monte-Carlo method. Instead of first determining the PDF, the average bit error rate can be determined directly with a Monte-Carlo method (see section 2.9.1). In this case, the BER for each Monte-Carlo sample (i) is given by:

$$\mathrm{BER}(i) = \frac{1}{2}\mathrm{erfc}\{\mathrm{SINR}(i)\} \tag{63}$$

where SINR(i) is the signal to interference plus noise ratio for sample i. The average BER is then the average of all the Monte-Carlo samples.

2.10 Conclusions

In this chapter the reuse distance of a cellular network was described as well as the effect of sectorization and beamforming on the reuse distance. Different array beamforming techniques, geometries and element patterns were discussed. A detailed formulation of the propagation channel models that will be used in this thesis were presented, including fast and slow fading models. The spatially distributed array concept was introduced and practical implementation issues were discussed. This was followed by a detailed definition of the received signals at the distributed sub-array elements. Methods of combining the sub-array output signals for both narrow and wideband systems were discribed. Estimation techniques of the weight vector for phased and adaptive arrays were discussed, followed by a description of the mobile distributions as well as statistical methods that will be used in the simulations.

UNIVERSITEIT VAN PRETORIA
UNIVERSITY OF PRETORIA
YUNIBESITHI YA PRETORIA

3 RANGE INCREASE OF ADAPTIVE AND PHASED ARRAYS IN THE PRESENCE OF INTERFERERS

3.1 Introduction

A higher directive gain at the base station will result in an increased signal level at the mobile receiver, allowing longer range operation or increased coverage. This increased range in a non-multipath environment is described in [45] for narrowband adaptive arrays and in [56] for a CDMA adaptive array. A comparison of the range increase of phased and adaptive arrays in a multipath environment for both narrow-band and spread-spectrum systems is given in [16].

In a phased array the signals received at the individual elements of the array are multiplied by a weight vector and then combined to form a beam in the direction of the desired mobile. The gain of the array (and associated range) will increase and beamwidth will decrease as the number of antenna elements at the base station is increased. The above statement will be valid until the beamwidth becomes comparable with the angular spread of the multipath signals. A further increase in the number of antenna elements will not necessarily result in a significant range increase, due to the loss in power from the scattering signal components arriving outside the array beamwidth. An adaptive array on the other hand optimizes the array pattern to maximize the array signal to interference plus noise ration (SINR) for the desired mobile. The result is that the adaptive array does not present the range limitation found in phased arrays.

In a wideband system, a RAKE receiver can be used to exploit the temporal characteristics of the propagation signal. The signal is combined coherently in time to give an increase in the signal strength through temporal diversity. By forming a different beam for each RAKE finger based on optimal signal to noise ratio, the range limitation of phased arrays can be reduced.

The purpose of this chapter is to present results of a comparative study of the range increase of adaptive versus phased arrays in a multipath environment. This study is an extension of the work presented in [16], with the effect of the presence of interference included in the present study. One of the major advantages of an adaptive array is the

ability to suppress interference, and one would expect the inclusion of the interference in the study would have a significant effect on the results. An approximation for the angle of arrival probability density function (PDF) for the circular vector channel model is also presented. A theoretical model using this PDF, which approximates the range increase of phased arrays in a multipath environment, is proposed.

The focus of this thesis is the performance of spatially distributed adaptive arrays in cellular networks. In TDMA systems, the spatially distributed array consists of sub-arrays located at alternate corners of a typical hexagonal cell structure. As a result of this geometry, the range between the arrays and mobiles can be larger than that of a conventional cell geometry, where the arrays (or sectorized antennas) are located at the center of the cell. Adaptive arrays offer a range increase relative to sectorized and phased arrays. However, this range increase is a function of the number and location of interferers as well as the propagation environment. This range increase is important to the distributed array operation. Although not directly applied to the spatially distributed array performance investigation in the rest of the thesis, it forms an important contribution to the overall spatially distributed array study. In addition, the results can be valuable to future studies on phased arrays applied to spatially distributed arrays systems.

The phased array range increase without multipath is presented in section 3.2. The array geometry and multipath model will be described in section 3.3, and the desired signal, interference and noise power at the output of the phased and adaptive arrays will be given. This is followed by the simulation procedure and simulation results for the narrow-band and spread-spectrum systems in section 3.4. An analytical model is derived for the range increase of phased arrays in a multipath environment in section 3.5, followed by conclusions in section 3.6.

3.2 Phased Array Range Increase without Multipath

In this section the range increase of a phased array relative to an omni (reference) antenna due to the increased gain of the array is described [16,32]. The power received at the omni antenna is:

$$P_{R,Omni} = \frac{P_T G_T G_R \lambda^2}{(4\pi r_0)^2 \left(\frac{r_{omni}}{r_0}\right)^{\gamma}} \tag{64}$$

where P_T is the mobile transmit power, G_R is the omni antenna gain, G_T is the mobile antenna gain, λ is the carrier wavelength, r_{omni}^{γ} is the range between the mobile and the omni antenna and γ is the power pathloss exponent and r_0 is the close in free space reference distance. The gain of an M-element array antenna is [16]:

$$G_{R,array} = M G_R \tag{65}$$

Inserting (65) in (64), the received signal of the array is:

$$P_{R,array} = \frac{M P_T G_T G_R \lambda^2}{(4\pi r_0)^2 \left(\frac{r_{array}}{r_0}\right)^{\gamma}} \tag{66}$$

The objective is now to calculate the range of the array relative to the range of the reference antenna for equal received signal strengths. This can be determined by setting (64) equal to (66):

$$\frac{P_T G_T G_R \lambda^2}{(4\pi r_0)^2 \left(\frac{r_{omni}}{r_0}\right)^{\gamma}} = \frac{M P_T G_T G_R \lambda^2}{(4\pi r_0)^2 \left(\frac{r_{array}}{r_0}\right)^{\gamma}} \tag{67}$$

or

$$\left(\frac{r_{array}}{r_{omni}}\right)^{\gamma} = M \tag{68}$$

Thus the range increase of an array relative to the reference (omni) antenna is:

$$\text{Range Increase} = r_{array} = M^{1/\gamma}\, r_{omni} \tag{69}$$

3.3 Array Geometry and Multipath Model

A circular array with M elements is used with cardoid element pattern as shown in Figure 9. The multipath geometry is shown in Figure 11 and Figure 12. The difference between

the mean angle of arrival of the desired and d^{th} multipath component is β_d^c, with $d \in \{1,2,\ldots,D\}$ and D the total number of signals. The circular vector channel model is used [11,45], consisting of K scatterers uniformly distributed in a circular area with radius r_{max}^s around the desired and interfering signals. Assuming equal power scattered by the K objects, the baseband signal arriving at antenna element m from signal d is:

$$z_{m,d}(nT_s) = S_d(nT_s)\, X_{m,d}(nT_s) \tag{70}$$

where $S_d(t)$ is the baseband signal transmitted by mobile d. Using equation (24), the received signals at the antenna elements are:

$$X_{m,d}(nT_s) = \frac{1}{4\pi r_0} \sum_{k=1}^{K} \{ \frac{F(m,\psi_{d,k})}{\sqrt{K\left(\frac{r_{d,k}^e}{r_0}\right)^{\gamma}}}\, \delta(nT_s - \tau_{d,k}) \tag{71}$$

$$e^{j\left[(2\pi/\lambda)\left\{r_{d,k}^s + r_{d,k}^e\right\} + [\pi\Delta/\lambda \sin(\pi/M)]\cos\{\psi_{d,k} - 2\pi(m-1)/M\}\right]} \} + n_s(nT_s)$$

where λ is the carrier wavelength, Δ is the spacing between elements, T_s is the sample period, n is the sample number, $\tau_{d,k}$ is the delay between source d and array center via scatterer k, $r_{d,k}^s$ is the distance between the source d and scatterer k, $r_{d,k}^e$ is the distance between the scatterer k and the center of the circular array, γ is the pathloss exponent, $n_s(m,nT_s)$ is zero mean Gaussian noise at element m and $F(m,\psi_{d,k})$ is the m^{th} element voltage pattern in direction $\psi_{d,k}$, given by:

$$F(m,\psi_{d,k}) = \sqrt{2}\cos\left[\frac{\pi}{4}\left(\cos\left\{\psi_{d,k} - \frac{2\pi(m-1)}{M}\right\} - 1\right)\right] \tag{72}$$

The phased and adaptive array desired signal, sum of interference and noise power at the output for narrow-band and spread-spectrum systems will be presented next.

3.3.1 Narrow-band Systems

The signal to interference plus noise ratio (SINR) can be written as [45]:

$$SINR = \frac{P_d \mathbf{W}^H \{\mathbf{X}_1 \mathbf{X}_1^H\} \mathbf{W}}{\mathbf{W}^H \mathbf{R}_{nn} \mathbf{W} + \sigma_N^2 \mathbf{W}^H \mathbf{W}} \quad (73)$$

where $\mathbf{W}$ is the array beamforming weight vector, P_d is the desired signal power at the antenna elements, $\mathbf{X}_1^H$ is the complex conjugate transpose of the desired signal receive vector at the antenna elements given in (71), σ_N^2 is the noise power and $\mathbf{R}_{nn}$ is the interference plus noise covariance matrix. Assuming the signals are uncorrelated, $\mathbf{R}_{nn}$ is given by (see Appendix A):

$$\mathbf{R}_{nn} = \sum_{d=2}^{D} P_d \mathbf{X}_d \mathbf{X}_d^H + \sigma_N^2 \mathbf{I} \quad (74)$$

where $\mathbf{I}$ is the identity matrix, $\mathbf{X}_d^H$ is the complex conjugate transpose of the receive vector from the d^{th} interferer receive vector at the antenna elements given in (71) and P_d is the power of the d^{th} interferer. The weight vector $\mathbf{W}$ for the adaptive array is [54]:

$$\mathbf{W} = \mathbf{R}_{nn}^{-1} \mathbf{U}_1 \quad (75)$$

where $\mathbf{U}_1$ is the desired signal array vector. The phased array is steered towards the desired signal, with weight vector $\mathbf{w}$ given by [16]:

$$\mathbf{W} = \mathbf{U}_1(\psi_1^c) \quad (76)$$

where $\mathbf{U}_1(\psi_1^c)$ is the array vector of the desired signal in the direction of ψ_1^c.

3.3.2 Spread Spectrum Systems

In a wideband spread spectrum system, a RAKE receiver can be used to exploit the temporal characteristics of the propagation signal [16]. The signal strength is increased through temporal diversity by coherently combining the multipath signals in time. A three finger (L = 3) RAKE receiver (see section 2.6.2) on each antenna element is assumed in the simulations to follow. The spread spectrum processing (employing a RAKE receiver) is described next. Each source transmits a data sequence that is spreaded by a unique code. The multipath signals received from all the sources at each antenna element $\sum_{d=1}^{D} z_{m,d}(nT_s)$ was first correlated with the spreading code of the desired signal. The signals were then

weighed and summed. The three strongest peaks (or called fingers in CDMA) of the summed signal separated by integer multiples of the of the code rate were then detected with its corresponding time of arrival $n_\ell T_s$, where n_ℓ is the sample number of finger $\ell \in \{1,2,3\}$. The three fingers were then coherently added to yield the following desired array output power P^{des}:

$$P^{des} = P_d \, g_p \sum_{\ell}^{L} \left\{ \left| \sum_{m=1}^{M} W^*(m,\ell) \, v_1(m, n_\ell T_s) \right|^2 \right\} \tag{77}$$

where $v(m, n_\ell T_s)$ is the output signal of correlator m at time sample $n_\ell T_s$, $W^*(m,\ell)$ is the conjugate of complex weight m of finger ℓ and g_p is the processing gain. The processing gain is the same for the reference and array systems and will therefore be ignored in the comparison between systems. The interference power at the array output at time t_ℓ is:

$$P^{int} = \left| \sum_{\ell=1}^{L} \sum_{m=1}^{M} \left\{ W^*(m,\ell) \sum_{d=2}^{D} X_{m,d}(n_\ell T_s) \right\} \right|^2 \tag{78}$$

where $x_{m,d}(n_\ell T_s)$ is the baseband m^{th} element array signal of source d at time sample $n_\ell T_s$, given in (71). The weight vector $\mathbf{W}$ of the adaptive array for finger ℓ is:

$$\mathbf{W}(\ell) = \mathbf{R}_{nn,\ell}^{-1} \, \mathbf{U}_1(n_\ell T_s) \tag{79}$$

and for the phased array:

$$\mathbf{W}(\ell) = \mathbf{U}_1(\psi_1^c) \tag{80}$$

where $\mathbf{U}_1(n_\ell T_s)$ is the desired signal propagation vector in the direction of the multipath component at time sample $n_\ell T_s$, $\mathbf{U}_1(\psi_1^c)$ is the steering vector in the direction ψ_1^c of the desired signal and $\mathbf{R}_{nn,\ell}$ is the interference plus noise covariance matrix at time sample $n_\ell T_s$, given by (see Appendix A):

$$\mathbf{R}_{nn,\ell} = \sum_{d=2}^{D} \left\{ P_d \, \mathbf{X}_d(n_\ell T_s) \, \mathbf{X}_d^H(n_\ell T_s) \right\} + \sigma_N^2 \mathbf{I} \tag{81}$$

An alternative beamforming model alleviating the range limitation of the phased array was proposed in [2]. In this model a RAKE receiver is implemented before weighting and summing of the array signals. The RAKE receiver determines the three multipath fingers, followed by determination of an optimum array pointing direction for each finger. This is done by scanning (or changing the weight vector in (80)) the pointing direction ψ to either side of ψ_l^c for each finger and determining the array pointing direction which gives the maximum output power. This method is applied in the spread spectrum simulations to follow.

3.4 Comparative Study

The procedure that was followed here is similar to the procedure presented in [2]. The average bit error rate (BER) for coherent detection of phase-shift keying signals in a digital system is given in (63). With a specific scattering radius and range between the signal and the reference (omni-antenna) system, the transmitted signal to noise (SNR) and interference to noise ratio (INR) were adjusted until an average BER of 10^{-2} was obtained at the output of the reference system. Using this SNR and INR while the scattering radius is fixed, the range of the array was increased until an average BER of 10^{-2} was achieved. This array range relative to that of the reference system is now the range increase (or extension).

Monte-Carlo simulations (see section 2.9.1) were performed to determine the average BER. The pathloss coefficient γ for the range between each scatterer and the receiver was 4 ($\gamma = 4$) and a total of 20 scatterers were assumed. The effect of shadowing loss (see section 2.4.2) was not taken into account and the spacing between the antenna array elements was a half wavelength.

Narrowband and wideband (spread spectrum) systems with RAKE receivers were considered, as will be discussed next.

3.4.1 Narrow-band Systems

The range extension of adaptive and phased arrays for 10°, 20° and 45° angular spreads with a 16.7dB equal average SNR and SIR are shown in Figure 23, Figure 24 and Figure 25 respectively. Results are shown for both noise only (where the SNR was 13.7dB) and

one interferer cases, with the interferer located at various azimuth angles ψ^c relative to the boresight of the array. A single dominant interferer is typical in TDMA type cellular systems [59]. In order to obtain the same BER for noise only scenario and the scenario with a single interferer, the noise power was decreased when the interferer was added, such that the total SINR is equal to the SNR for the noise only case.

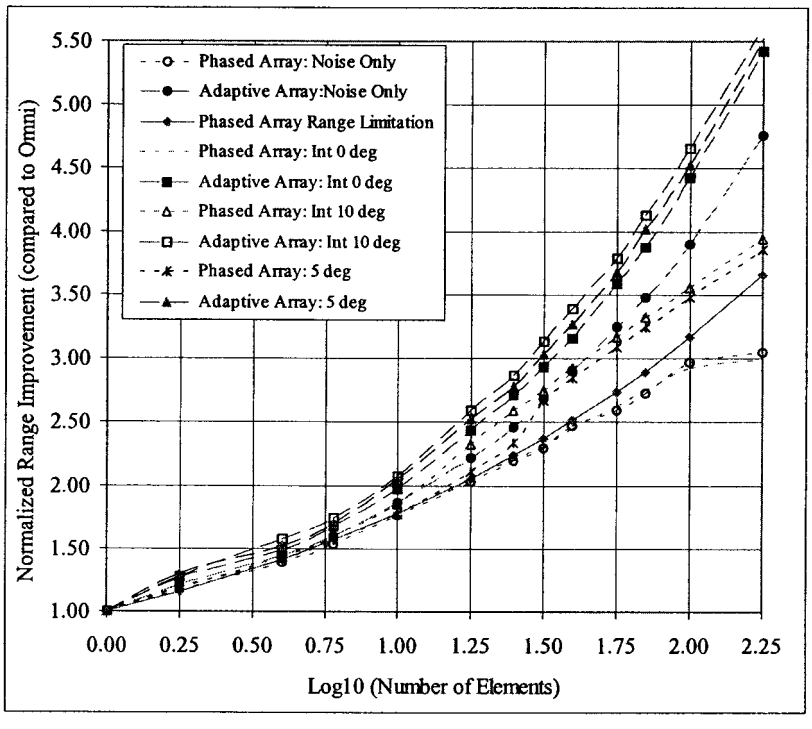

Figure 23: Adaptive and phased array range increase in a narrow-band system for a 10° angular spread, one interferer separated from the user by 0°, 5° and 10°.

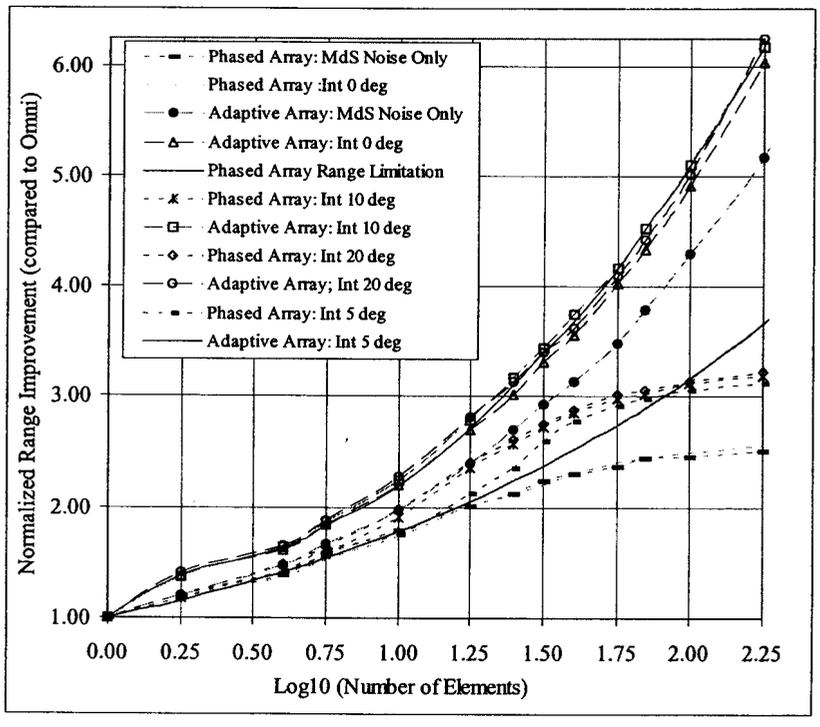

Figure 24 Adaptive and phased array range increase in a narrow-band system for a 20° angular spread, one interferer separated from the user by 0°, 5°, 10° and 20°.

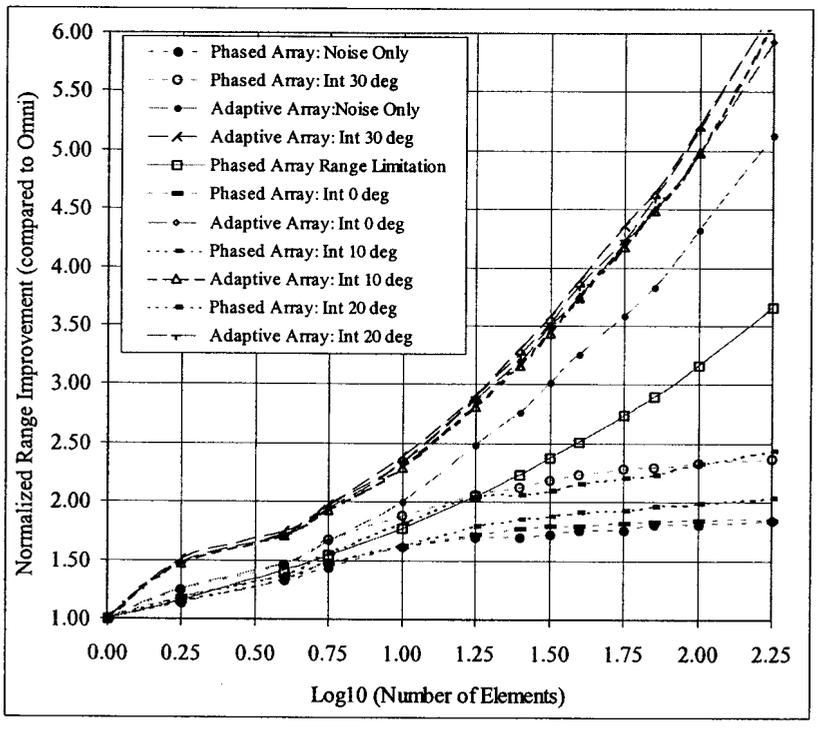

Figure 25: Adaptive vs. phased array range increase in a narrow-band system for a 45° angular spread, one interferer separated from the user by 0°, 10°, 20° and 30°.

In Figure 23 with 10° angular spread, the phased array range extension with an interferer at 0° is the same as the noise only scenario. This is to be expected since the SINR (with an interferer) and SNR (without an interferer) was chosen to be equal, the phased array is not able to distinguish between the desired user and the interferer is contributing to the total system noise. The range increase of the 5° and 10° interferer cases is equal to the phased array noise only range limitation up to the point (approximately 1.5 for 5° case and 1.125 for 10° case) where the interferer angle starts to fall outside the beamwidth of the array. The phased array noise only range limitation is the range at which the array beamwidth becomes smaller than the multipath scattering angle (or angular spread), in which case the array increased gain is offset by the loss of energy falling outside the array beamwidth. When the interferer angle starts to fall outside the array beam, the array is able to cancel a part of the interfering signal, with the result that the range increase exceeds the noise only range increase.

Since the adaptive arrays are able to reduce the interfering signal multipath components (even when the interferer is in the same direction as the desired signal [45]) and constructively add the desired signal multipath components, it can be seen that the range increase exceeds the noise only adaptive array range increase.

3.4.2 Spread Spectrum Systems

In the spread spectrum simulations, it is assumed that there are 12 equal power interferers, randomly located in azimuth angle ψ_q^c. Twelve interferers are assumed, since this is typical for current tri-cellular CDMA systems [56]. The multipath model used for the spread spectrum simulations is similar to the narrowband model. Two signal to noise ratio (SNR) scenarios are investigated. The first is a SNR of 14dB, which comprises 7.5dB required receive energy per bit relative to the noise density Eb/No [12,56] and 6.5dB fading margin. In the second scenario a SNR of 11dB is assumed.

The range increase of adaptive vs. phased arrays for angular spreads of 20° and 45° is shown in Figure 26 and Figure 27 respectively. The phased array weight vector (or beam direction) is optimized for each delay.

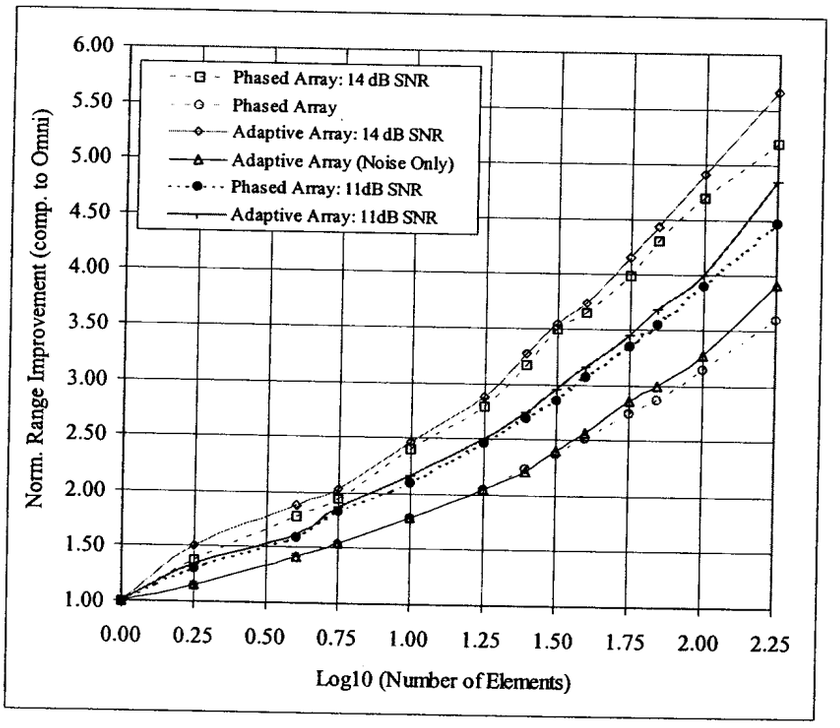

Figure 26: Adaptive vs. phased array range increase for a spread spectrum system with 20° angular spread, twelve randomly positioned interferers for 19.6dB, 11dB and 14dB signal to noise ratio.

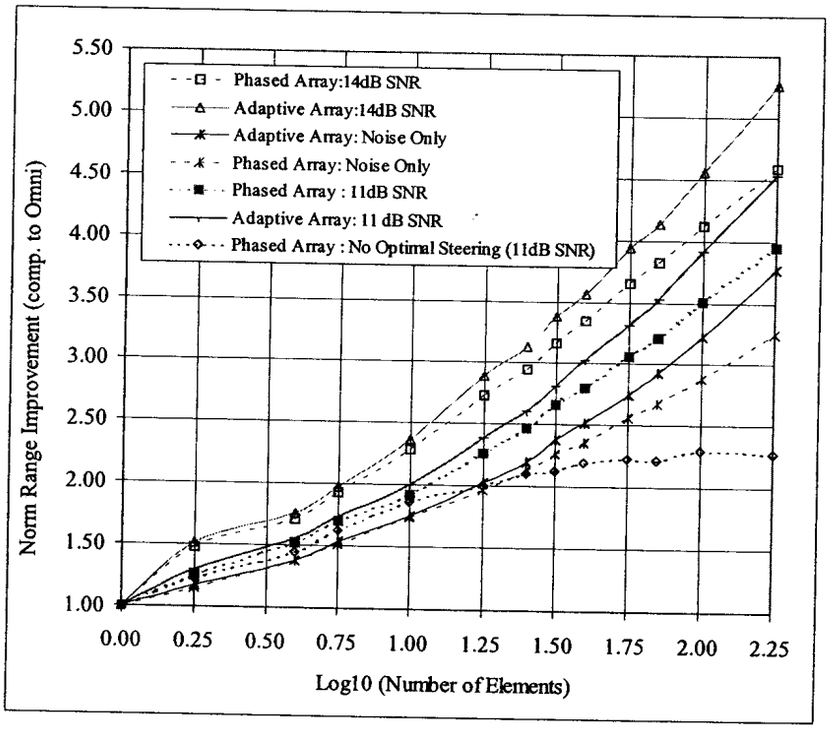

Figure 27 Adaptive vs. phased array range increase for a spread spectrum system with 45° angular spread, twelve randomly positioned interferers for 18.9dB, 11dB and 14dB signal to noise ratio.

In Figure 27 the non-optimized (beam pointing in fixed direction towards desired signal) phased array range increase is also shown. Note that apart from the 6.8dB RAKE diversity gain [16], the same range limitations as in the narrowband case is observed. This phased array range limitation is reduced by optimizing the weight vector for each delay. Since the adaptive array is able reduce the interfering multipath signals and coherently add the desired multipath signals (even if they fall inside the Fresnel beamwidth of the adaptive array), a larger range increase for the adaptive array relative to the phased array is observed (the phased array is unable to cancel interferer multipath signals that falls inside the array Fresnel beamwidth).

3.5 Analytical Model

In this section an analytical model is derived to predict the range improvement of a narrowband phased array in a multipath environment, including the presence of a single interferer. The typical angle of arrival histogram (PDF) of the multipath signal for the circular vector channel model [45] is shown in Figure 28 for an angular spread 40° (ψ_{max} = 20°). The probability of a signal arriving from an angle ψ can be approximated by:

$$P_{AOA}(\psi) = B\cos\left(\frac{\pi\psi}{\psi_{max}}\right)^{0.45} \qquad (82)$$

where B is an arbitrary constant, which cancels in (84). This approximation is shown in Figure 28, with B = 1270 and $\psi_{max} = 20°$. It can be seen that the approximation is a good match to the histogram.

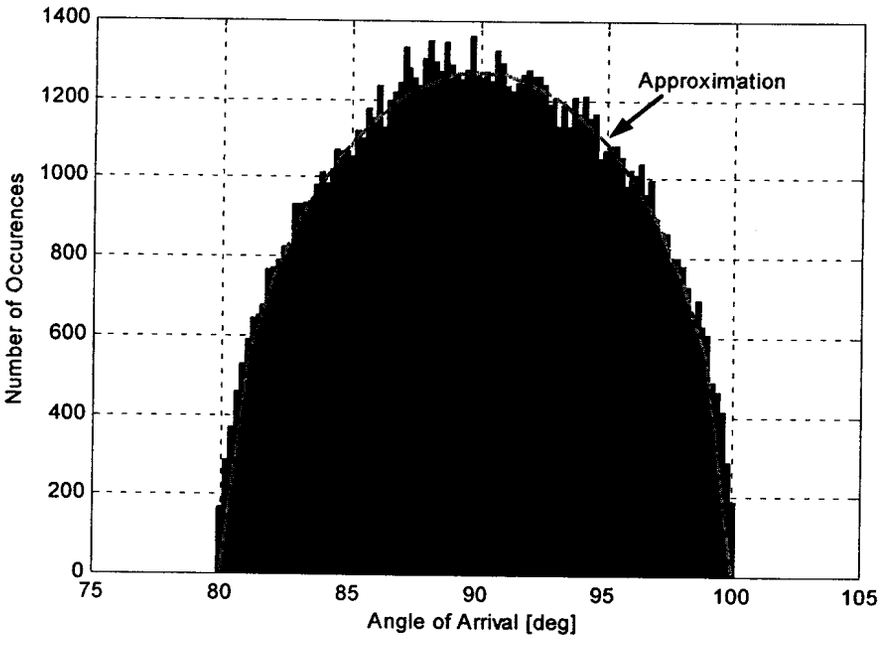

Figure 28: Angle of arrival histogram and approximation.

It was shown in the previous section that the range increase of a phased array in the presence of an interferer is reduced when the angular spread of the desired signal multipath components is wider than the beamwidth of the array. The multipath incident components will be weighted by the beam taper of the phased array. Components falling outside the 10dB beamwidth of the beam will contribute very little energy towards the total energy received by the array. However, the probability of signals arriving at these large angles is also lower as indicated by the PDF in Figure 28. Taking all these factors into account the SINR of a phased array can be approximated by the following equation:

$$SINR_{approx} = \frac{P_d M(1-\aleph)/r_{incr}^{\gamma}}{(P_q M(1-\aleph)/r_{incr}^{\gamma}) + \sigma_N^2} \qquad (83)$$

where P_d and P_q are the average power per element received from the desired and interference signals, respectively. These average powers are calculated for the omni antenna at a specific range as described earlier. r_{incr} is the ratio of the array to omni range, that is the range increase. This ratio is increased to the point where the SINR of the array equals that of the omni antenna. $\aleph$ is the power loss of the multipath components due to the antenna array azimuth pattern taper, r is the range between the center of the array and the mobiles, σ_N^2 is the noise power and γ is the pathloss exponent. The power loss is the

ratio of the maximum of the convolution of the array power pattern and the angle of arrival PDF to the total area of the angle of arrival PDF, given by:

$$\aleph = \frac{\int_{-\infty}^{\infty} P_{AOA}(\psi)\, G(\psi - \xi)\, d\xi}{\int_{-\psi_{max}}^{\psi_{max}} P_{AOA}(\psi)\, d\psi} \tag{84}$$

where $G(\psi)$ is the antenna array power pattern at angle ψ and P_{AOA} is the PDF of the angle of arrival. To find the range increase of the phased array relative to an omni, the distance between the desired user and the array is increased until the $SINR_{approx}$ matches the SINR for the onmi.

A comparison between the range increase possible for a phased array obtained through simulation (similar to section 3) and the analytical model derived (see equation (83)) is shown in Figure 29 for 10°, 20° and 45° angular spreads.

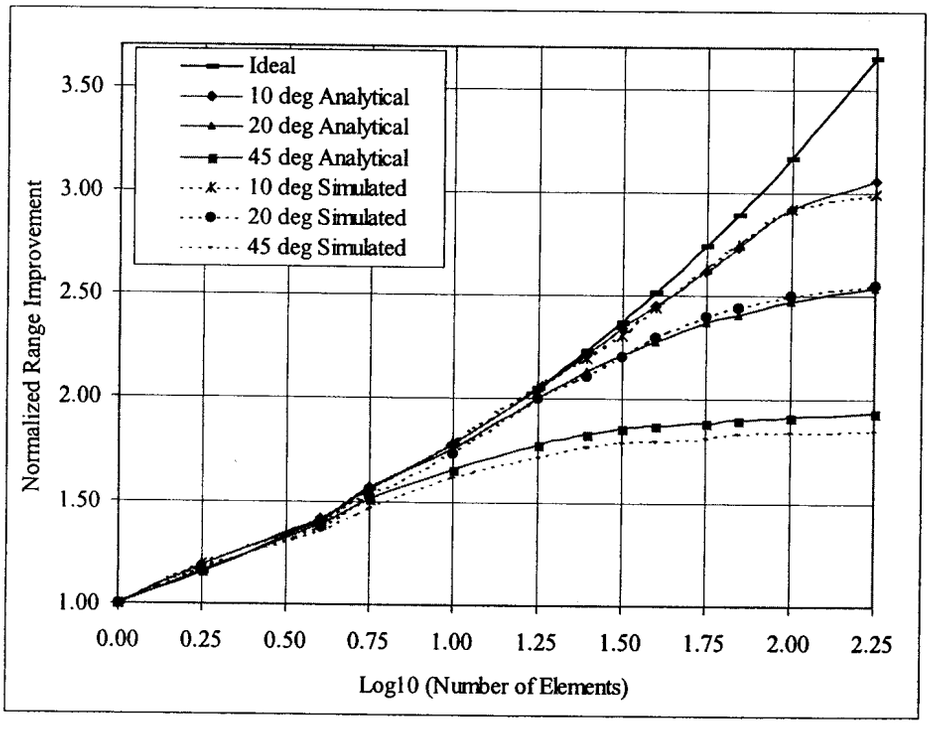

Figure 29: Comparison of simulated and analytical phased array range improvement for 10°, 20° and 45° angular spreads.

Using the approximate equations (82), (83) and (84) presented in this section, it is possible to estimate the range increase of a phased array in a multipath environment in the presence

of interferers using the analytical model derived instead of running time consuming simulations as was done in section 3.4. The results obtained with the analytical model gave accurate approximations for the results obtained through the Monte-Carlo simulations.

3.6 Conclusions

This chapter presented the effect of interference on the range increase (relative to an omni-antenna) of adaptive vs. phased arrays in a multipath environment for both narrowband and spread-spectrum systems.

The range increase of a narrowband cellular system with a single dominant interferer (typical for TDMA cellular systems) at various incidence angles was presented as a function of the number of array elements and scattering angular spread. The adaptive array is able to increase its range by reducing the contributions from the multipath components of the interferer, even when the interferer is in the same direction as the desired signal in low angular spread environment (10 degree angular spread). A phased array on the other hand, achieves a significant range increase when the beamwidth of the array becomes narrow enough that the multipath components of the interferer falls outside the beam of the array.

The range increase of wideband spread spectrums with twelve interferers per sector (typical for CDMA cellular systems) was presented as a function of the number of array elements, scattering angular spread and received signal to noise ratio. Similar to the results in [16], the range increase limitation of phased arrays in the presence of multiple interferers can be improved by using a weight vector optimized for each RAKE receiver finger. The results also showed that the range increase of phased arrays is less than that of adaptive arrays due to the lack of cancellation of interferer multipath components falling inside the beamwidth of the phased array.

An analytical model was derived to predict the range increase of a phased array in a multipath environment in the presence of a dominant interferer. The probability density function of the angle of arrival PDF of a circular vector channel model was approximated and then used in the analytical model to estimated the range increase possible with phased arrays. An asymptotic limit of the range increase possible with a phased array exists when

the array beamwidth becomes narrower than the desired signal angular spread. This limit is a function of the angular spread of the multipath.

4 DISTRIBUTED ARRAYS IN A NON-MULTIPATH ENVIRONMENT

4.1 Introduction

In this chapter the performance of distributed arrays is investigated in a non-multipath environment. Firstly, an analytical expression is derived for the output signal to interference plus noise ratio (SINR) of two distributed arrays with independent beamforming of each array as well as for optimum combining of the two array output signals. A single stationary desired mobile in the presence of stationary interferer is considered. It is then shown that the SINR obtained with optimum combining of the two array output signals is equal to the sum of the SINRs of the individual arrays. Following this, it will be shown analytically that the SINR of the two distributed arrays with combined beamforming is always greater than the SINR with independent beamforming. It will then be demonstrated with simulation results that the analytical results can be extended to multiple interferers. This is followed by simulation results of the signal to noise ratios for distributed arrays with and without power control. The simulations are first done for one of the distributed arrays, followed by all three distributed arrays with mobiles located in a single cell. A seven cell network is then simulated with a reuse factor of three.

4.2 Analytical Investigation of the SINR Performance of Distributed Arrays

4.2.1 SINR of Independent Beamforming of Each Array

Consider two arrays, each with optimum beamforming for the desired signal. It will be shown analytically in this section that the SINR with optimum combining of the output signals of two distributed arrays is the sum of the SINRs of the individual arrays. The geometry under consideration is shown in Figure 30. The system consists of two arrays at the corners of the cell, each having two elements. A desired signal is located at the center of the cell and one interferer is located at an angle of ψ relative to the boresight of arrays 1 and 2. The array elements are spaced a half wavelength apart and fading, pathloss and propagation delays between sub-arrays are ignored for this analysis[35].

[35] The effect of fading and pathloss will be included in later chapters using numerical methods.

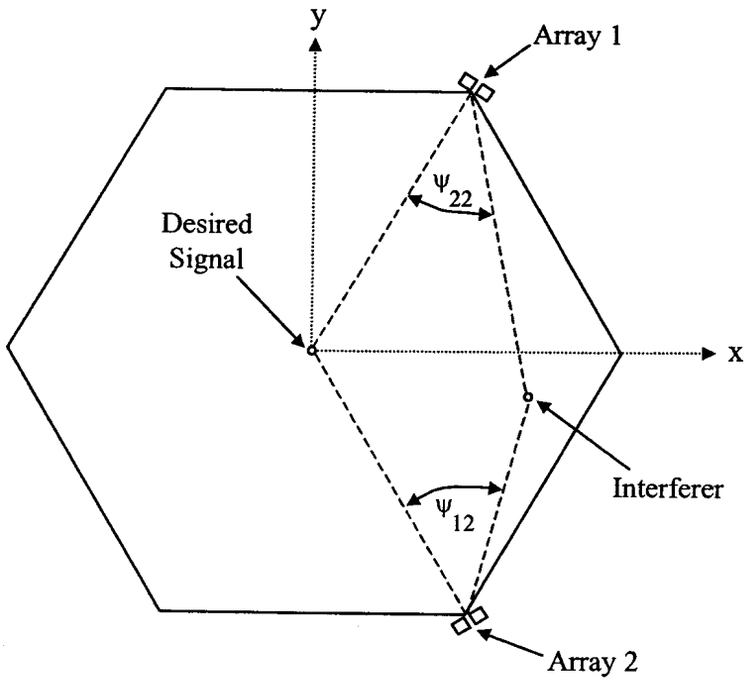

Figure 30: Geometry of two distributed arrays with one interferer.

The received signals at each individual array is combined with optimum beamforming, followed by optimum combining of the two array output signals, as shown in Figure 31. The output of the individual arrays is:

$$\mathbf{Y}_1 = \mathbf{W}_1^H \mathbf{X}_1 = [W_{11}^* \; W_{12}^*] \begin{bmatrix} X_{11} \\ X_{12} \end{bmatrix} \tag{85}$$

and

$$\mathbf{Y}_2 = \mathbf{W}_2^H \mathbf{X}_2 = [W_{21}^* \; W_{22}^*] \begin{bmatrix} X_{21} \\ X_{22} \end{bmatrix} \tag{86}$$

where $\mathbf{W}_1$ is the weight vector and $\mathbf{X}_1$ is the received signal vector of array 1 and $\mathbf{W}_2$ is the weight vector and $\mathbf{X}_2$ is the received signal vector of array 2.

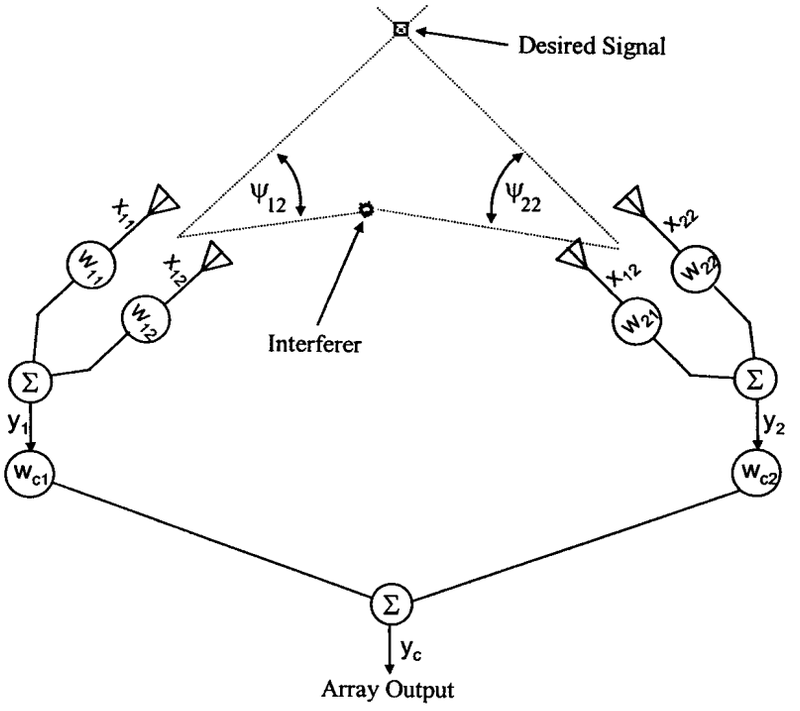

Figure 31: Independent array beamforming geometry.

Optimum combining of the output signals of the two array outputs gives the total array output signal:

$$\mathbf{y}_c = \mathbf{W}_c^H \begin{bmatrix} \mathbf{W}_1^H \mathbf{X}_1 \\ \mathbf{W}_2^H \mathbf{X}_2 \end{bmatrix} \tag{87}$$

where $\mathbf{W}_c$ is the total array weight vector (see Figure 32). The weight vector $\mathbf{W}_c$ for optimum combining of the arrays is [54]:

$$\mathbf{W}_c = \mu_{wc} \mathbf{R}_{nnC}^{-1} \mathbf{U}_d \tag{88}$$

where $\mathbf{R}_{nnC}$ is the total array interference plus noise covariance matrix of the combined array, μ_{wc} is a constant that constraints the array to have a unity response in the direction of the desired signal[36] and $\mathbf{U}_d$ is the desired signal propagation vector, given as:

$$\mathbf{U}_d = [1\,1]^T \tag{89}$$

The constraint μ_{wc} is [54]:

[36] Referred to as the look direction in [54].

$$\mu_{wc} = \frac{1}{\mathbf{U}_d^H \mathbf{R}_{nnC}^{-1} \mathbf{U}_d} \tag{90}$$

The covariance matrix $\mathbf{R}_{nnC}$ is:

$$\mathbf{R}_{nnC} = E\left\{ \begin{bmatrix} \mathbf{W}_1^H \mathbf{X}_{Q1} \\ \mathbf{W}_2^H \mathbf{X}_{Q2} \end{bmatrix} \begin{bmatrix} \mathbf{W}_1^H \mathbf{X}_{Q1} & \mathbf{W}_2^H \mathbf{X}_{Q2} \end{bmatrix}^H \right\} \tag{91}$$

with $\mathbf{X}_{Q1}$ and $\mathbf{X}_{Q2}$ is array 1 and 2 interferer plus noise receive vectors. Multiplying the factors in equation (91), the following is obtained:

$$\mathbf{R}_{nnC} = \begin{bmatrix} \mathbf{W}_1^H E\left(\mathbf{X}_{Q1}\mathbf{X}_{Q1}^H\right)\mathbf{W}_1 & \mathbf{W}_1^H E\left(\mathbf{X}_{Q1}\mathbf{X}_{Q2}^H\right)\mathbf{W}_2 \\ \mathbf{W}_2^H E\left(\mathbf{X}_{Q2}\mathbf{X}_{Q1}^H\right)\mathbf{W}_1 & \mathbf{W}_2^H E\left(\mathbf{X}_{Q2}\mathbf{X}_{Q2}^H\right)\mathbf{W}_2 \end{bmatrix} \tag{92}$$

which can be re-written as:

$$\mathbf{R}_{nnC} = \begin{bmatrix} \mathbf{W}_1^H \mathbf{R}_{nn,11} \mathbf{W}_1 & \mathbf{W}_1^H \mathbf{R}_{nn,12} \mathbf{W}_2 \\ \mathbf{W}_2^H \mathbf{R}_{nn,21} \mathbf{W}_1 & \mathbf{W}_2^H \mathbf{R}_{nn,22} \mathbf{W}_2 \end{bmatrix} = \begin{bmatrix} \mathbf{R}_{nnC,11} & \mathbf{R}_{nnC,12} \\ \mathbf{R}_{nnC,21} & \mathbf{R}_{nnC,22} \end{bmatrix} \tag{93}$$

with $\mathbf{R}_{nn,11}$, $\mathbf{R}_{nn,12}$, $\mathbf{R}_{nn,21}$ and $\mathbf{R}_{nn,22}$ the covariance matrices of the received interference plus noise signals of array 1 and 2. Assuming now that the power levels of the desired and interfering signals are equal to one, the propagation environment is lossless and $\psi_{22} = \psi_{12}$, the signals arriving at the two arrays are:

$$\mathbf{X}_{Q1} = S_Q \mathbf{U}_{Q1} + \mathbf{n}_1 = S_Q \left[e^{j(\pi/2)\sin\psi_{12}} \quad e^{-j(\pi/2)\sin\psi_{12}} \right]^T + [n_{11}\, n_{12}]^T \tag{94}$$

and

$$\mathbf{X}_{Q2} = S_Q \mathbf{U}_{Q2} + \mathbf{n}_2 = S_Q \left[e^{-j(\pi/2)\sin\psi_{22}} \quad e^{j(\pi/2)\sin\psi_{22}} \right]^T + [n_{21}\, n_{22}]^T \tag{95}$$

where S_Q is the amplitude of the interference signal bits, $\mathbf{n}$ is the array element noise vector and $\mathbf{U}_Q$ is the interference signal array vector. It is assumed that the noise is Gaussian and uncorrelated between the array elements. Using (92), the component (1,1) of covariance matrices in (93) becomes:

$$\mathbf{R}_{nn,11} = E\left\{\begin{bmatrix} S_Q e^{j(\pi/2)\sin\psi_{12}} + n_{11} \\ S_Q e^{-j(\pi/2)\sin\psi_{12}} + n_{12} \end{bmatrix}\begin{bmatrix} S_Q^* e^{-j(\pi/2)\sin\psi_{12}} + n_{11}^* & -S_Q^* e^{j(\pi/2)\sin\psi_{12}} + n_{12}^* \end{bmatrix}\right\} \quad (96)$$

$$= \begin{bmatrix} R_{nn,11}(1,1) & R_{nn,11}(1,2) \\ R_{nn,11}(2,1) & R_{nn,11}(2,2) \end{bmatrix} \quad (97)$$

where:

$$\mathbf{R}_{nn,11}(1,1) = E(S_Q S_Q^*) + E(S_Q e^{j(\pi/2)\sin\psi_{12}} n_{11}^*) + E(n_{11} S_Q^* e^{-j(\pi/2)\sin\psi_{12}}) + E(n_{11} n_{11}^*) \quad (98)$$

$$\begin{aligned} \mathbf{R}_{nn,11}(1,2) = {} & E(S_Q S_Q^*) e^{j\pi\sin\psi_{12}} + E(S_Q e^{j(\pi/2)\sin\psi_{12}} n_{12}^*) \\ & + E(n_{11} S_Q^* e^{j(\pi/2)\sin\psi_{12}}) + E(n_{11} n_{12}^*) \end{aligned} \quad (99)$$

$$\begin{aligned} \mathbf{R}_{nn,11}(2,1) = {} & E(S_Q S_Q^*) e^{-j\pi\sin\psi_{22}} + E(S_Q e^{-j(\pi/2)\sin\psi_{22}} n_{11}^*) \\ & + E(n_{12} S_Q^* e^{-j(\pi/2)\sin\psi_{12}}) + E(n_{12} n_{11}^*) \end{aligned} \quad (100)$$

$$\mathbf{R}_{nn,11}(2,2) = E(S_Q S_Q^*) + E(S_Q e^{-j(\pi/2)\sin\psi_{12}} n_{12}^*) + E(n_{12} S_Q^* e^{j(\pi/2)\sin\psi_{12}}) + E(n_{12} n_{12}^*) \quad (101)$$

Using the fact that the signals are uncorrelated with each other as well as with the noise, the matrix $\mathbf{R}_{nn,11}$ becomes:

$$\mathbf{R}_{nn,11} = \begin{bmatrix} 1+\sigma^2 & e^{j\pi\sin\psi_{12}} \\ e^{-j\pi\sin\psi_{12}} & 1+\sigma^2 \end{bmatrix} \quad (102)$$

Similarly, the co-variance matrices $\mathbf{R}_{nn,12}$ $\mathbf{R}_{nn,21}$ $\mathbf{R}_{nn,22}$ are:

$$\mathbf{R}_{nn,12} = \begin{bmatrix} e^{j(\pi/2)(\sin\psi_{12}+\sin\psi_{22})} & e^{j(\pi/2)(\sin\psi_{12}-\sin\psi_{22})} \\ e^{-j(\pi/2)(\sin\psi_{12}-\sin\psi_{22})} & e^{-j(\pi/2)(\sin\psi_{12}+\sin\psi_{22})} \end{bmatrix} \quad (103)$$

$$\mathbf{R}_{nn,21} = \begin{bmatrix} e^{-j(\pi/2)(\sin\psi_{22}+\sin\psi_{12})} & e^{-j(\pi/2)(\sin\psi_{22}-\sin\psi_{12})} \\ e^{j(\pi/2)(\sin\psi_{22}-\sin\psi_{12})} & e^{j(\pi/2)(\sin\psi_{22}+\sin\psi_{12})} \end{bmatrix} \quad (104)$$

and

$$\mathbf{R}_{nn,22} = \begin{bmatrix} 1+\sigma^2 & e^{-j\pi\sin\psi_{12}} \\ e^{j\pi\sin\psi_{12}} & 1+\sigma^2 \end{bmatrix} \quad (105)$$

From (88) and (102), the independent array optimum combining weight vectors after some manipulation become:

$$\mathbf{W}_1 = \mu_{wc1}\mathbf{R}_{nn,11}^{-1}\mathbf{U}_d = \begin{bmatrix} \dfrac{0.5(e^{j\pi\sin\psi_{12}} - \sigma^4 - 1)}{\cos(\pi\sin\psi_{12}) - \sigma^4 - 1} \\ \dfrac{0.5\,(e^{-j\pi\sin\psi_{12}} - \sigma^4 - 1)}{\cos(\pi\sin\psi_{12}) - \sigma^4 - 1} \end{bmatrix} \tag{106}$$

and

$$\mathbf{W}_2 = \mu_{wc1}\mathbf{R}_{Q,22}^{-1}\mathbf{U}_d = \begin{bmatrix} \dfrac{0.5(e^{-j\pi\sin\psi_{22}} - \sigma^4 - 1)}{\cos(\pi\sin\psi_{22}) - \sigma^4 - 1} \\ \dfrac{0.5(e^{j\pi\sin\psi_{22}} - \sigma^4 - 1)}{\cos(\pi\sin\psi_{22}) - \sigma^4 - 1} \end{bmatrix} \tag{107}$$

The SINR of array 1 is given by [54]:

$$SINR_1 = \mathbf{U}_d^H \mathbf{R}_{Q,11}^{-1}\mathbf{U}_d = 2\frac{\sigma^2 + 1 - \cos(\pi\sin\psi_{12})}{(\sigma^2+2)\sigma^2} \tag{108}$$

and array 2:

$$SINR_2 = \mathbf{U}_d^H \mathbf{R}_{Q,22}^{-1}\mathbf{U}_d = 2\frac{\sigma^2 + 1 - \cos(\pi\sin\psi_{22})}{(\sigma^2+2)\sigma^2} \tag{109}$$

Since $\sigma^2 << 1$ and for the case where $\psi_{12} \neq 0$, the SINR of array1 reduces to:

$$SINR_1 = 2\frac{1 - \cos(\pi\sin\psi_{12})}{\sigma^2} \tag{110}$$

and array 2:

$$SINR_2 = 2\frac{1 - \cos(\pi\sin\psi_{22})}{\sigma^2} \tag{111}$$

The cumulative SINR of both arrays is:

$$SINR_1 + SINR_2 = 2\left(\frac{2 - \cos(\pi\sin\psi_{12}) - \cos(\pi\sin\psi_{22})}{\sigma^2}\right) \tag{112}$$

Consider now a simplified case where $\psi_{22} = \psi_{12}$[37]. In this case the SINR of array 1 and array 2 are equal, with the total SINR of (112) simplifying to:

$$SINR_1 + SINR_2 = 2\,\frac{1-\cos(\pi \sin\psi_{12})}{\sigma^2} \tag{113}$$

The combined covariance matrix in (93) in the case where $\psi_{22} = \psi_{12}$ reduces to:

$$\mathbf{R}_{nnC,11} = \mathbf{R}_{nnC,22} = \frac{-0.5\sigma^4(\sigma^4+2)}{\cos(\pi \sin\psi_{12}) - \sigma^4 - 1} \tag{114}$$

and

$$\mathbf{R}_{nnC,12} = \mathbf{R}_{nnC,21} = \frac{0.5\left(\sigma^4[\cos(\pi \sin\psi_{12})+1]\right)}{\cos^2(\pi \sin\psi_{12}) - 2\cos(\pi \sin\psi_{12}) - \sigma^4\cos(\pi \sin\psi_{12}) + \left(\sigma^4+1\right)^2} \tag{115}$$

The SINR of the arrays combined with optimum combining is [54]:

$$SINR_C = \mathbf{U}_{dc}^H\, \mathbf{R}_{nnC}^{-1}\, \mathbf{U}_{dc} \tag{116}$$

where $\mathbf{U}_{dc}$ is the desired signal propagation or steering vector for the combined array, given by:

$$\mathbf{U}_{dc} = [1\ 1]^T \tag{117}$$

Using (93), (114), (115) and (116) and with simplification, the SINR becomes:

$$SINR_C = 4\,\frac{(\sigma^2+1)^2 + \cos^2(\pi \sin\psi_{12}) - 2\cos(\pi \sin\psi_{12}) - 2\sigma^2\cos(\pi \sin\psi_{12})}{(\sigma^4 + 4\sigma^2 - 2\cos(\pi \sin\psi_{12}) + 2)\sigma^2} \tag{118}$$

which reduce to the following when $\sigma^2 << 1$:

$$SINR_C = 2\,\frac{1-\cos(\pi \sin\psi_{12})}{\sigma^2} \tag{119}$$

which is equal to the SINR of the individual arrays in (113). It is shown in Appendix B that the result is valid for the more general case where $\psi_{22} \neq \psi_{12}$.

[37] The general case where $\psi_{22} \neq \psi_{12}$ is given in Appendix B.

4.2.2 SINR of Arrays with Combined Beamforming

Consider the combined beamforming of both arrays as depicted Figure 32. The propagation delays between the sub-arrays are not included here. The desired signal received at the combined array elements is:

$$\mathbf{U}_d = [1\,1\,1\,1]^T \tag{120}$$

and the interference plus noise received at the array elements are:

$$\mathbf{X}_Q = S_Q \mathbf{U}_Q + \mathbf{n} = S_Q \left[e^{j\pi \sin\psi_{12}} \quad e^{-j\pi \sin\psi_{12}} \quad e^{-j\pi \sin\psi_{22}} \quad e^{j\pi \sin\psi_{22}} \right]^T + \mathbf{n} \tag{121}$$

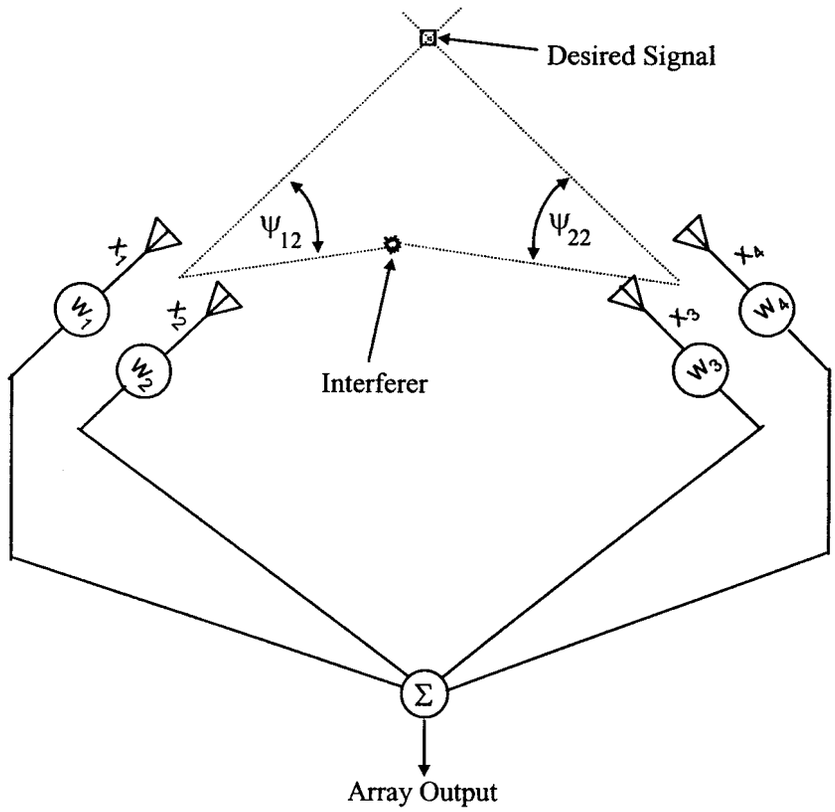

Figure 32: Combined array beamforming geometry.

The received interference plus noise co-variance matrix is [54]:

$$\mathbf{R}_{nn} = E\left\{\mathbf{X}_Q \mathbf{X}_Q^H\right\} \tag{122}$$

Using (121) in (122), the received interference plus noise co-variance matrix is:

$$\mathbf{R}_{nn} = E\left\{S_Q S_Q^*\right\}\begin{bmatrix} e^{j\pi\sin\psi_{12}} \\ e^{-j\pi\sin\psi_{12}} \\ e^{-j\pi\sin\psi_{22}} \\ e^{j\pi\sin\psi_{22}} \end{bmatrix}\begin{bmatrix} e^{-j\pi\sin\psi_{22}} & e^{j\pi\sin\psi_{22}} & e^{j\pi\sin\psi_{22}} & e^{-j\pi\sin\psi_{22}} \end{bmatrix} + \sigma^2\mathbf{I} \quad (123)$$

Since $E\left\{S_Q S_Q^*\right\}$ is unity, the co-variance matrix in (122) becomes:

$$\mathbf{R}_{nn} = \begin{bmatrix} 1+\sigma^2 & e^{j\pi\sin\psi_{12}} & e^{j(\pi/2)(\sin\psi_{12}+\sin\psi_{22})} & e^{j(\pi/2)(\sin\psi_{12}-\sin\psi_{22})} \\ e^{-j\pi\sin\psi_{12}} & 1+\sigma^2 & e^{-j(\pi/2)(\sin\psi_{12}-\sin\psi_{22})} & e^{-j(\pi/2)(\sin\psi_{12}+\sin\psi_{22})} \\ e^{-j(\pi/2)(\sin\psi_{12}+\sin\psi_{22})} & e^{-j(\pi/2)(\sin\psi_{22}-\sin\psi_{21})} & 1+\sigma^2 & e^{-j\pi\sin\psi_{22}} \\ e^{j(\pi/2)(\sin\psi_{22}-\sin\psi_{12})} & e^{j(\pi/2)(\sin\psi_{12}+\sin\psi_{22})} & e^{j\pi\sin\psi_{22}} & 1+\sigma^2 \end{bmatrix} \quad (124)$$

The inverse of the co-variance matrix $\mathbf{R}_{nn}$ is:

$$\mathbf{R}_{nn}^{-1} = \frac{1}{c}\begin{bmatrix} \sigma^2+3 & -e^{j\pi\sin\psi_{12}} & -e^{j(\pi/2)\alpha_1} & -e^{j(\pi/2)\alpha_2} \\ -e^{-j\pi\sin\psi_{12}} & \sigma^2+3 & -e^{-j(\pi/2)\alpha_2} & -e^{j(\pi/2)\alpha_1} \\ -e^{-j(\pi/2)\alpha_1} & -e^{j(\pi/2)\alpha_2} & \sigma^2+3 & -e^{-j\pi\sin\psi_{22}} \\ -e^{-j(\pi/2)\alpha_2} & -e^{j(\pi/2)\alpha_1} & -e^{j\pi\sin\psi_{22}} & \sigma^2+3 \end{bmatrix} \quad (125)$$

where

$$\begin{aligned} c &= \sigma^2(4+\sigma^2) \\ \alpha_1 &= \sin\psi_{12}+\sin\psi_{22} \\ \alpha_2 &= \sin\psi_{12}-\sin\psi_{22} \end{aligned} \quad (126)$$

The SINR of an adaptive array with optimum beamforming is given by [54]:

$$\text{SINR} = \mathbf{U}_d^H \mathbf{R}_{nn}^{-1} \mathbf{U}_d \quad (127)$$

Using (120) and (125) in (127), the SINR for the combined beamforming array after some manipulation becomes:

$$\text{SINR} = -2\frac{\left(\cos(\pi\sin\psi_{12})+\cos(\pi\sin\psi_{22})+2\cos(\pi\alpha_1/2)-2\sigma^2-6+2\cos(\pi\alpha_2/2)\right)}{\sigma^2(4+\sigma^2)} \quad (128)$$

4.2.3 Analytical Evaluation of the SINR of Combined Beamforming vs. Independent Beamforming With a Single Interferer

It has been established in section 4.2.1 that the SINR of the individual array output signals combined with optimum combining is equal to the SINR of the individual arrays. The SINR of the individual arrays with independent beamforming has also been derived. In section 4.2.2, the SINR of the arrays for combined beamforming has been derived. In this section it will be shown that the SINR of combined beamforming is greater or equal to the SINR of independent beamforming.

The ratio Γ of the combined beamforming SINR in (128) and the independent beamforming SINR in (112) is:

$$\Gamma = \frac{\left[\cos(\pi \sin\psi_{12}) + \cos(\pi \sin\psi_{22}) + 2\cos(\pi\alpha_1/2) - 2\sigma^2 - 6 + \cos(\pi\alpha_2/2)\right](\sigma^2+2)}{(\sigma^2+4)(\cos(\pi \sin\psi_{12}) - 2 - 2\sigma^2 + \cos(\pi \sin\psi_{22}))} \quad (129)$$

where

$$\begin{aligned} \alpha_1 &= \sin\psi_{12} + \sin\psi_{22} \\ \alpha_2 &= \sin\psi_{12} - \sin\psi_{22} \end{aligned} \quad (130)$$

Since $\sigma^2 << 1$, equation (129) can be simplified to:

$$\Gamma = \frac{\cos(\pi \sin\psi_{12}) + \cos(\pi \sin\psi_{22}) + 2\cos(\pi\alpha_1/2) - 6 + \cos(\pi\alpha_2/2)}{2\,(\cos(\pi \sin\psi_{12}) - 2 + \cos(\pi \sin\psi_{22}))} \quad (131)$$

The relation between the angles ψ_{12} and ψ_{22} from the geometry in Figure 30 is:

$$\psi_{22} = \arctan\left(\frac{\sin\psi_{12}}{\xi - \cos\psi_{12}}\right) \quad (132)$$

where ξ is the proportion of the range from array 1 to the mobile relative to the distance between the two arrays. Inserting the angle relationship of (132) into (131), the following is achieved:

$$\Gamma = \frac{4\cos(\pi \sin\psi_{12}/2)\,\cos(\pi \sin\psi_{12}/2\varsigma) + \cos(\pi \sin\psi_{12}/\varsigma) + \cos(\pi \sin\psi_{12}) - 6}{2\,(\cos(\pi \sin\psi_{12}) - 2 + \cos(\pi \sin\psi_{12}/\varsigma))} \quad (133)$$

where

$$\varsigma = \sqrt{\xi^2 - 2\xi\cos\psi_{12} + 1} \tag{134}$$

Substituting $\pi\sin\psi_{12} = \omega$ in (133), the following results:

$$\Gamma = \frac{4\cos(\omega/2)\cos(\omega/2\varsigma) + \cos(\omega/\varsigma) + \cos(\omega) - 6}{2\,(\cos(\omega) - 2 + \cos(\omega/\varsigma))} \tag{135}$$

Equation (135) can be simplified further be substituting $\alpha = \frac{\omega}{\varsigma}$:

$$\Gamma = \frac{4\cos(\omega/2)\cos(\alpha/2) + \cos(\alpha) + \cos(\omega) - 6}{2\,(\cos(\omega) - 2 + \cos(\alpha))} \tag{136}$$

Using the trigonometric relationship [60]:

$$\cos(a) = \cos^2(a/2) - 1 \tag{137}$$

equation (136) becomes:

$$\Gamma = \frac{4\cos(\omega/2)\cos(\alpha/2) + \cos^2(\alpha/2) + \cos^2(\omega/2) - 4}{2\,(\cos^2(\omega/2) - 2 + \cos(\alpha))} \tag{138}$$

which can be rewritten as:

$$\Gamma = \frac{(\cos(\alpha/2) + \cos(\omega/2))^2 - 4}{2\,(\cos^2(\omega/2) + \cos^2(\alpha/2) - 2)} \tag{139}$$

by using the property that [58]

$$(\cos(a) + \cos(b))^2 = \cos^2(a) + 2\cos(a)\cos(b) + \cos^2(b) \tag{140}$$

Examining equation (139) it can be seen that Γ becomes equal to one in the limit when $\alpha \to 0$ and $\omega \to 0$ (which is the case when $\psi_{12} \to 0$). This indicates that the combined and independent beamforming is equal when the interfering signal comes close in angle to the desired signal. For all other angles, equation (139) is always greater than one, indicating that that the SINR of the combined beamforming array is greater than the independent beamforming arrays.

4.2.4 Numerical Evaluation of the SINR of Combined Beamforming vs. Independent Beamforming For Two Interferers

It is difficult to extend the analytical formulation of the ratio of the SINR of the combined beamforming arrays to independent beamforming arrays to more than one interferer. The case for two interferers will be illustrated numerically in this section. The geometry under consideration is shown in Figure 33.

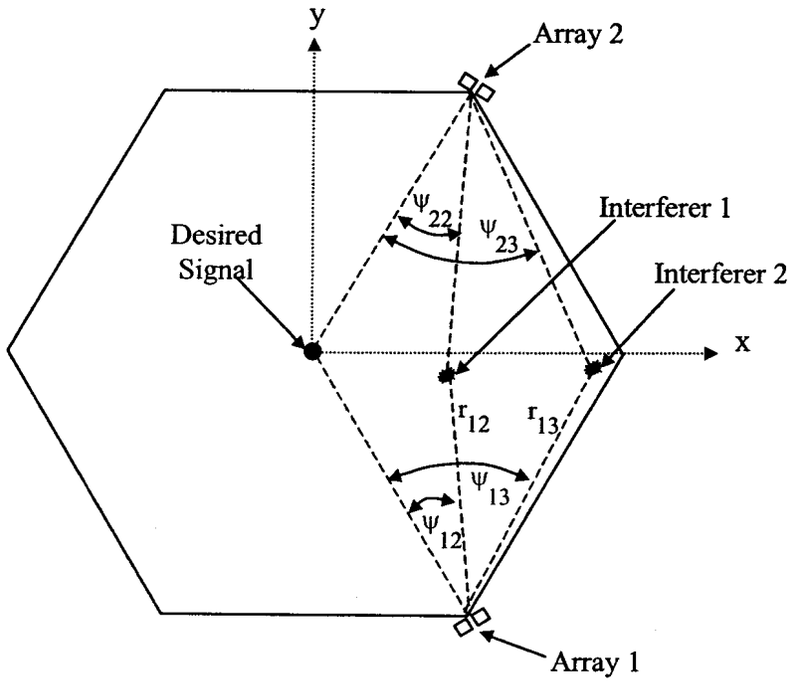

Figure 33: Geometry of two distributed arrays with two interferers.

The SINR is shown in Figure 34 for two fixed angles $\psi_{12} = 20^\circ$ and 40°. In each case the angle ψ_{13} is varied between 0 and 180 degrees. The relationship between the angles is given in (132). The range between array 1 and the two mobiles is equal to 0.4 times the distance between the two arrays, or $\xi = 5/2$ in equation (132). The noise power is 0.001W and the power of the signal and each interferer is equal to 1W.

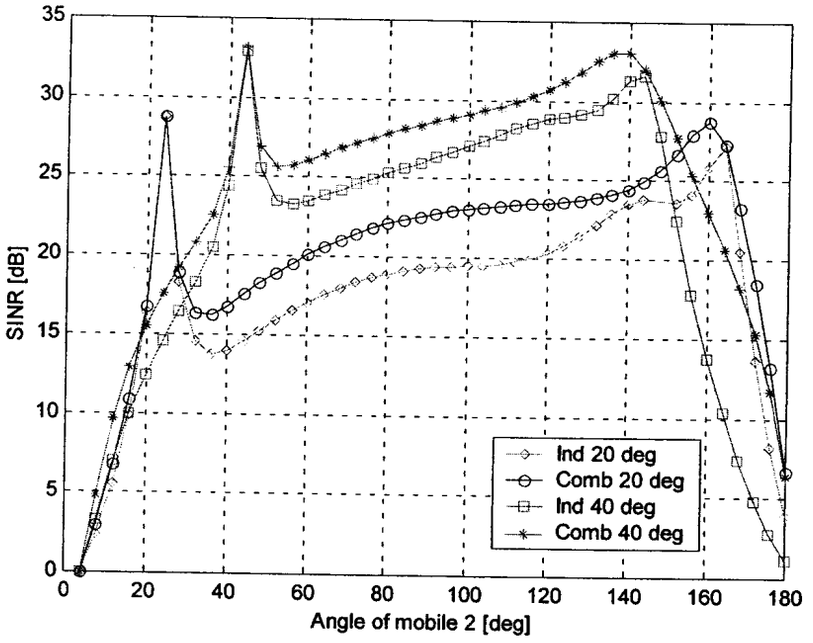

Figure 34: SINR of individual and combined beamforming arrays for ψ_{12} equal to 10° and 20°.

It can be seen in Figure 34 that the SINR of combined beamforming is always greater or equal to the SINR of independent beamforming of the two arrays.

4.2.5 Discussion of the Results of Independent vs. Combined Beamforming

It was shown in the previous sections that the SINR of combined beamforming is always greater or equal to that of independent beamforming for the same number of array elements and for one or two interferers. The fact that the interferer is located on both sides of boresight for the two arrays allowed the combined array to achieve a better cancellation of the interferer. It is an additional "degree of freedom" for the combined array relative to the independent array. It will be shown in later sections that the bit error rate and outage probability of the combined array is significantly better than the arrays combined with independent optimum combining of the arrays.

4.3 Simulated SINR Performance of Distributed Arrays in a Non-Multipath Environment with Three Interferers and Six Elements Per Array

In this section the SINR of distributed arrays will be compared to conventional arrays located at the cell center. In addition the SINR performance of distributed arrays with

combined beamforming of the sub-arrays will be compared to independent sub-array beamforming. The general simulation parameters are as given in Table 2:

Table 2: General simulation parameters

Parameter	Value
Multipath	No
SNR	15 dB
Cell range	1000 m
Reuse factor	3
Number of interferers	3
Signal amplitude (Desired and interferers)	1 (0dB)

The mobile positions are fixed, with the range and angle between the x-axis and the mobiles given in Table 3. The mobiles are all located in the sector covered by array 1 at the cell center, and therefore the SINR of this array only will be compared to the distributed sub-array located at the cell corners.

Table 3: Range and angle of arrival of desired signal and interferers

Array Number	Signal	Range [m]	Angle relative to x-axis [deg]
Center	Desired	500	60
	Interferer 1	500	20
	Interferer 2	500	85
	Interferer 3	100	60
One	Desired	499	240
	Interferer 1	696	267.5
	Interferer 2	586	219
	Interferer 3	900	240
Two	Desired	1322	101
	Interferer 1	1037	92
	Interferer 2	1438	108.5
	Interferer 3	1053	115.3

Array Number	Signal	Range [m]	Angle relative to x-axis [deg]
Three	Desired	1322	19
	Interferer 1	1479	6.6
	Interferer 2	1156	25.5
	Interferer 3	1053	4.72

4.3.1 SINR of Signals In a Single Cell

In this section the SINR performance of conventional center cell arrays and distributed arrays are compared for a single cell with and without power control.

4.3.1.1 SINR Performance Without Power Control

The relative output power as a function of angle for center array one is shown in Figure 35, with six element arrays, three interferers and pathloss exponent of 3.

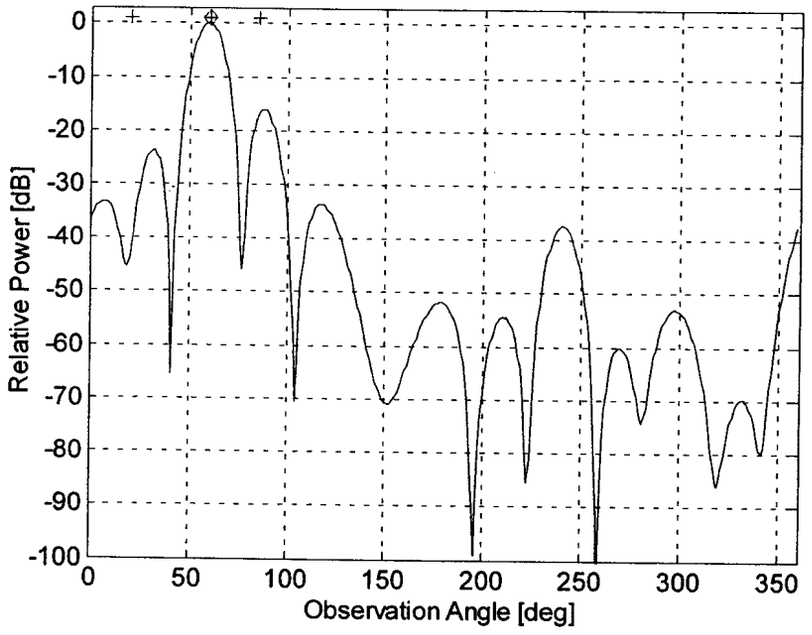

Figure 35: Desired signal received power at center array 1 (Desired Signal indicated with ◊ and interferers with +).

The received signal of the conventional six element arrays at the center of the cell is shown in Figure 36 for pathloss exponent of 3. The figure shows that cancellation of the interferer (interferer 3) in the same direction as the desired signal is difficult to achieve.

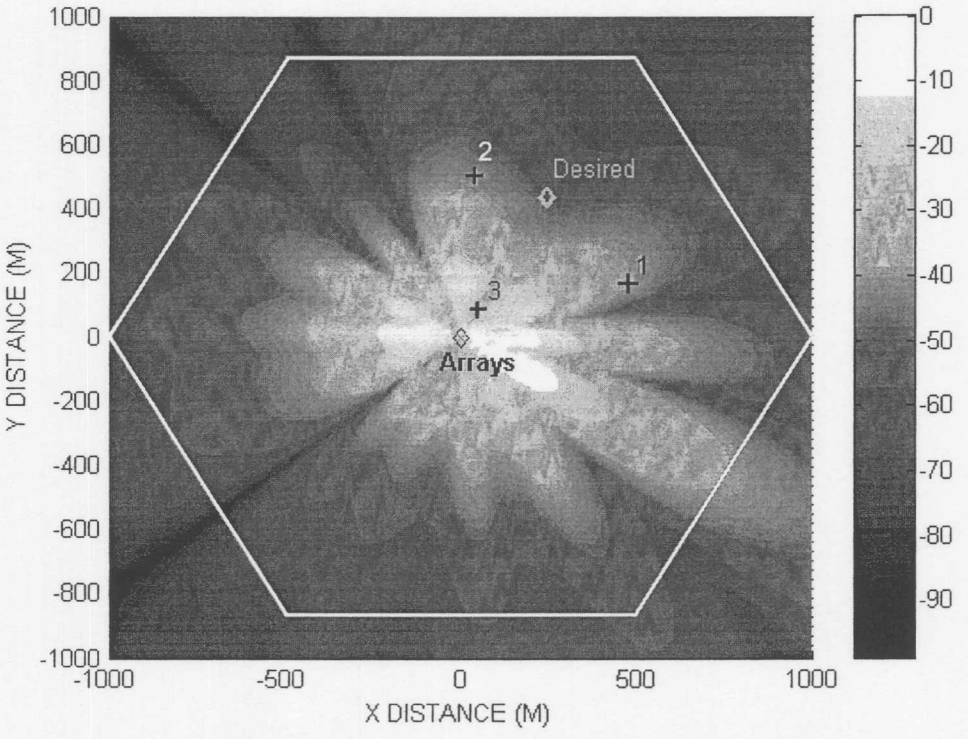

Figure 36: Normalized received power (optimized for the SINR of the desired signal) at the output of the conventional arrays at the cell center in the presence of three interferers (Desired Signal indicated with ◊ and interferers with +) .

The output power as a function of angle for distributed sub-arrays 1, 2 and 3 with independent beamforming and six element arrays is shown in Figure 37, Figure 38 and Figure 39, respectively. In Figure 37, it can be seen that the signals from interferers 1 and 2 was reduced by more than 40dB. However the signal from interferer 3, which is in the same direction as the desired signal) could not be reduced. On the other hand, since all three interferers are seen from different angles by array 2 (see Figure 38) and array 3 (see Figure 39) and the angles are not overlapping (or close to) with the desired signal incidence angle, these arrays are able to separate the signals.

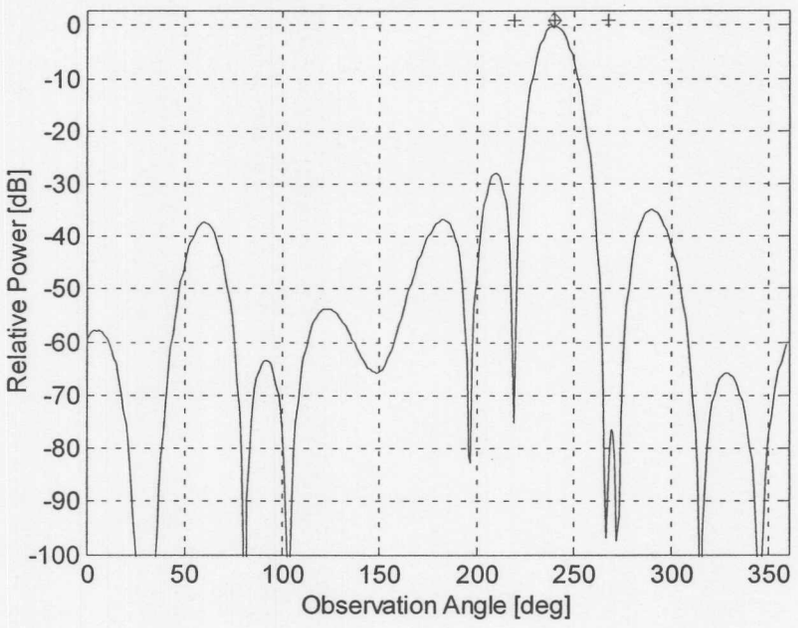

Figure 37: Desired signal received power at array 1 (Desired signal indicated with ◊ and interferers with +).

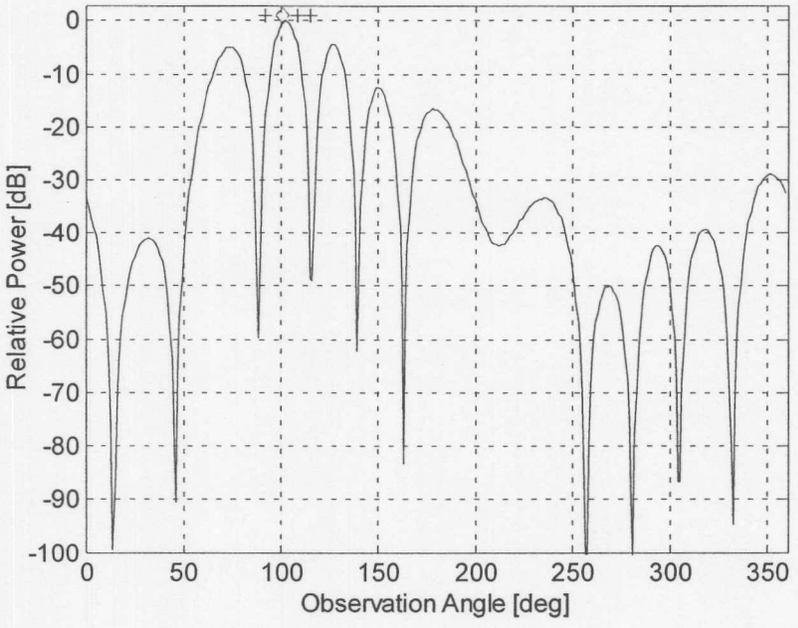

Figure 38: Desired signal received power at array 2 (Desired signal indicated with ◊ and interferers with +).

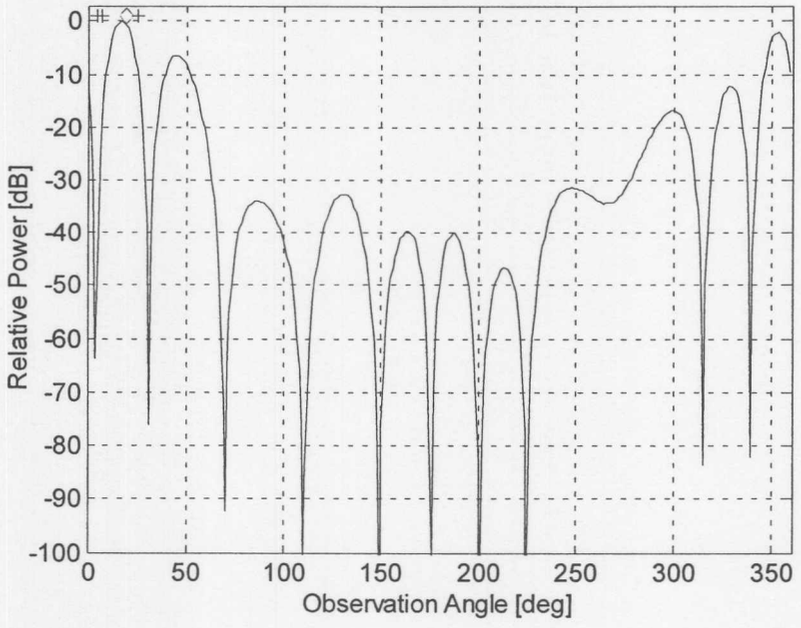

Figure 39: Desired signal received power at array 3 (Desired signal indicated with ◊ and interferers with +).

The received signal at the output of the combined array across the cell area is shown in Figure 40 for six element arrays. It can be seen that the combined array is able to reduce the signals from all three the interferers.

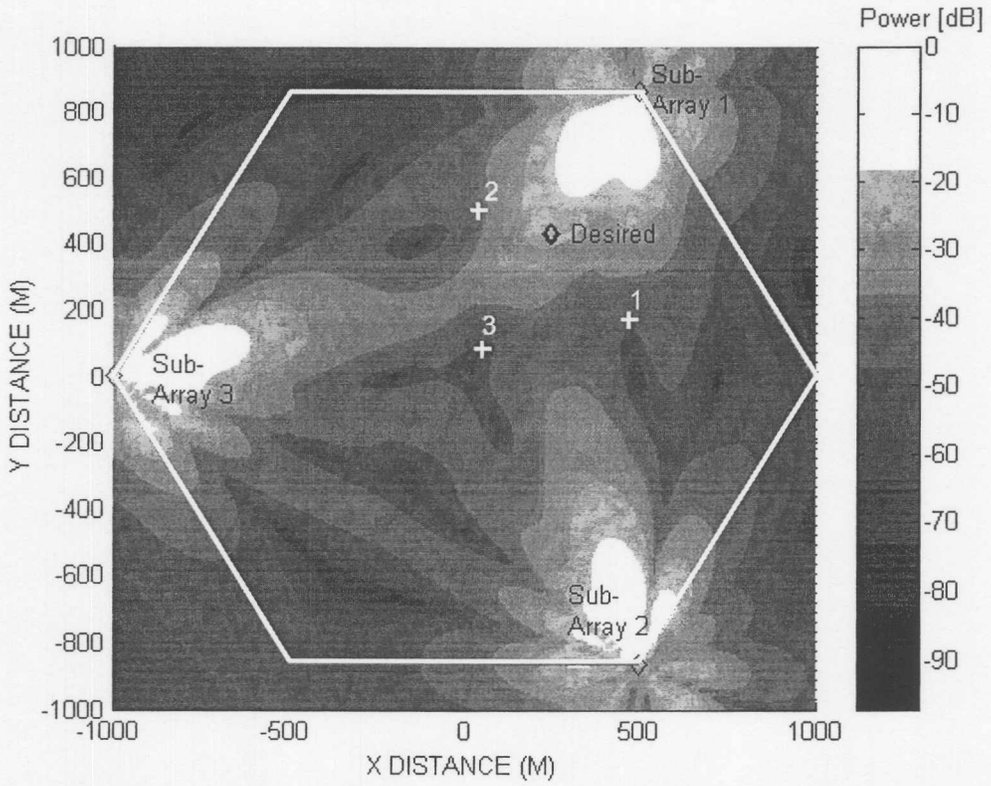

Figure 40: Desired signal normalized received power at the output of the combined distributed array in the presence of three interferers (Desired signal indicated with ◊ and interferers with +).

The SINR of the conventional array at the center of the cell and distributed sub-arrays at the cell corners with independent and combined beamforming is given in Table 4. The independent SINR is the sum of the SINR of all three arrays. The results show that the SINR of the distributed array with combined beamforming is 35dB higher than the conventional center array and 6dB higher than the distributed array with independent beamforming. The SINR of distributed array 1 with independent beamforming is higher than the other two arrays. This is due to the fact that interferer 3 is further in range than that of the desired signal and the other two interferers. The loss to interferers is therefore higher with smaller associated interference than the other two interferers (as seen by sub-array 1).

Table 4: SINR for the distributed array with full sectors, individual arrays and combined array.

Array	SINR [dB]
Distributed full sector	-22.68
Center array	-16.24

Array	SINR [dB]
Array 1	12.02
Array 2	3.68
Array 3	4.03
Independent distributed array beamforming	13.17
Combined distributed array beamforming	19.23

4.3.2 SINR Performance with Power Control

In the following results, power control was applied according to the power control range method described in section 2.5.5.1 for six element arrays with pathloss equal to 3. The power is controlled by the array nearest to the mobile, with the result that a mobile closer to the center of the cell, in case of the distributed array, will transmit the most power. The received power at the center array is shown in Figure 41. Here the angle of arrival of interferer 2 is the same as that of the desired signal. Therefore, the received power from this interferer cannot be reduced by the array. In contrast, the power from the other two interferers has been reduced by more than 30dB.

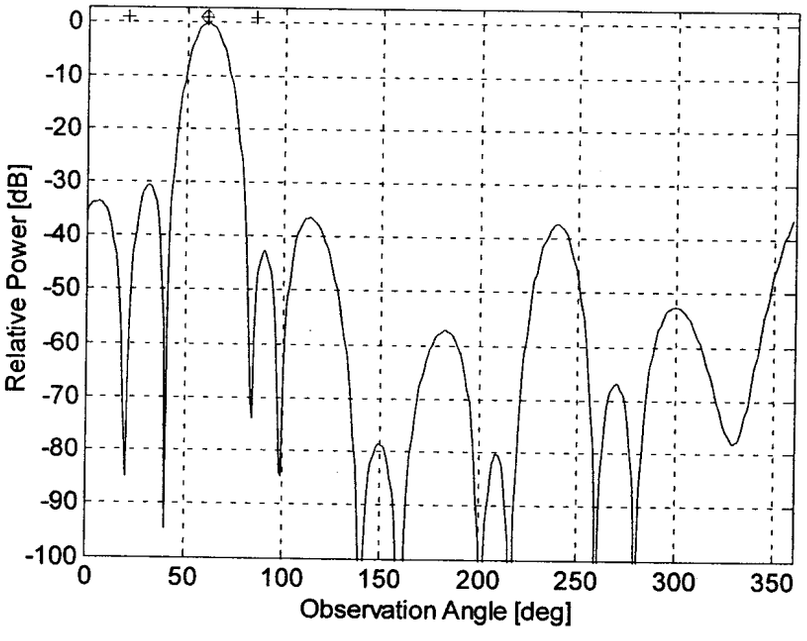

Figure 41: Received power at center array 1 with power control (Desired Signal indicated with ◊ and interferers with +).

The power received by distributed sub-arrays 1,2 and 3 with independent beamforming is given in Figure 42, Figure 43 and Figure 44 respectively. The SINR of the conventional array at the center of the cell and distributed arrays at the cell corners with independent and combined beamforming of the sub-arrays is given in Table 5. The SINR of the combined array is approximately equal for both the power controlled and non-controlled cases. In the case of the center array, the received power of interferer 2 is reduced to be equal to the received power from the other two interferers. The result is that the center array with power control has an improved SINR relative to the non-power controlled case.

Table 5: SINR for the distributed array with full sectors, individual arrays and combined array with power control enabled.

Array	SINR [dB]
Distributed full sector	-7.49
Center array	4.70
Array 1	4.70
Array 2	2.24
Array 3	2.91
Independent distributed array beamforming	8.18
Combined distributed array beamforming	19.15

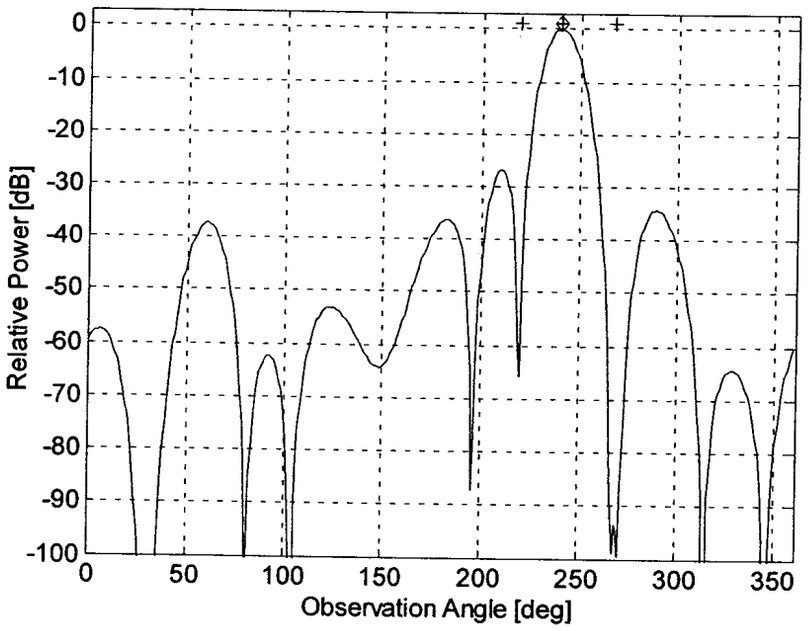

Figure 42: Received power at array 1 with power control enabled (Desired signal indicated with ◊ and interferers with +).

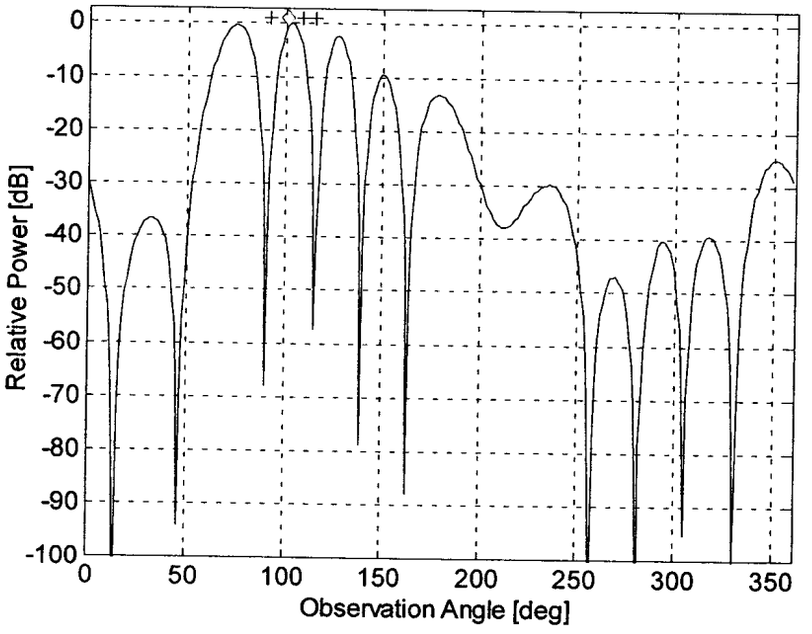

Figure 43: Received power at array 2 with power control enabled (Desired signal indicated with ◊ and interferers with +).

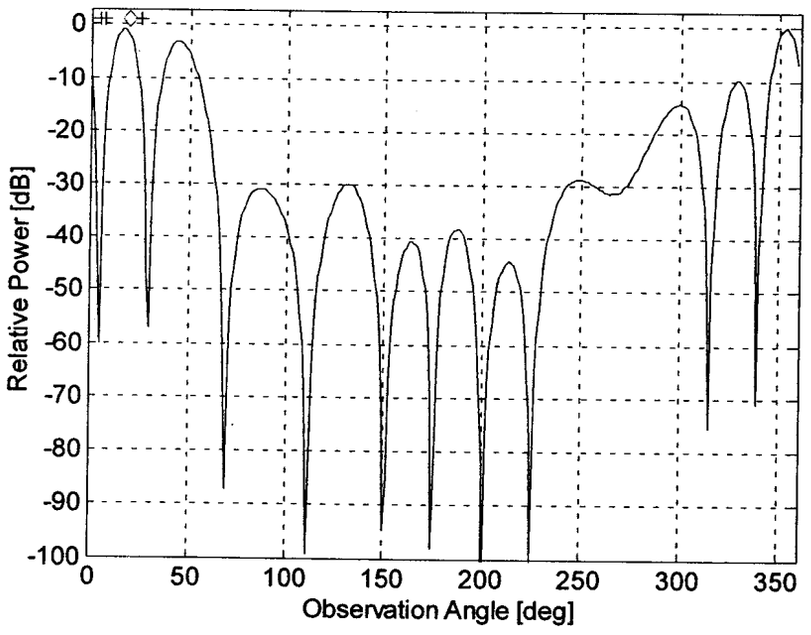

Figure 44: Received power at array 3 with power control enabled (Desired signal indicated with ◊ and interferers with +).

4.3.3 SINR of Signals in a Seven Cell Network (Includes First Tier of Interference)

In this section the SINR performance of conventional center cell arrays and distributed arrays are compared for a seven cell network with and without power control.

4.3.3.1 SINR Performance without Power Control

The received power at the output of distributed six element sub-arrays 1,2 and 3 is shown in Figure 45, Figure 46 and Figure 47 respectively. The pathloss exponent is three.

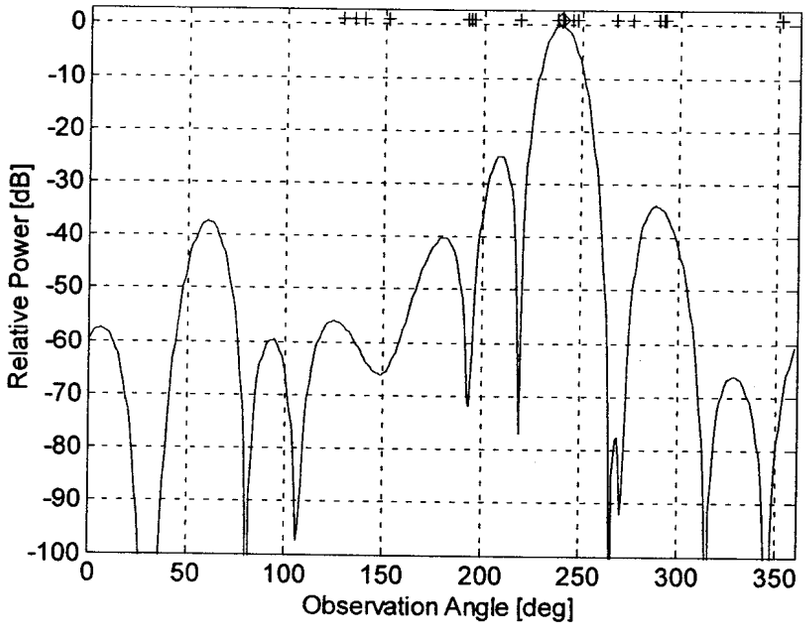

Figure 45: Received power at array 1 without power control in a seven cell configuration (Desired signal indicated with ◊ and interferers with +).

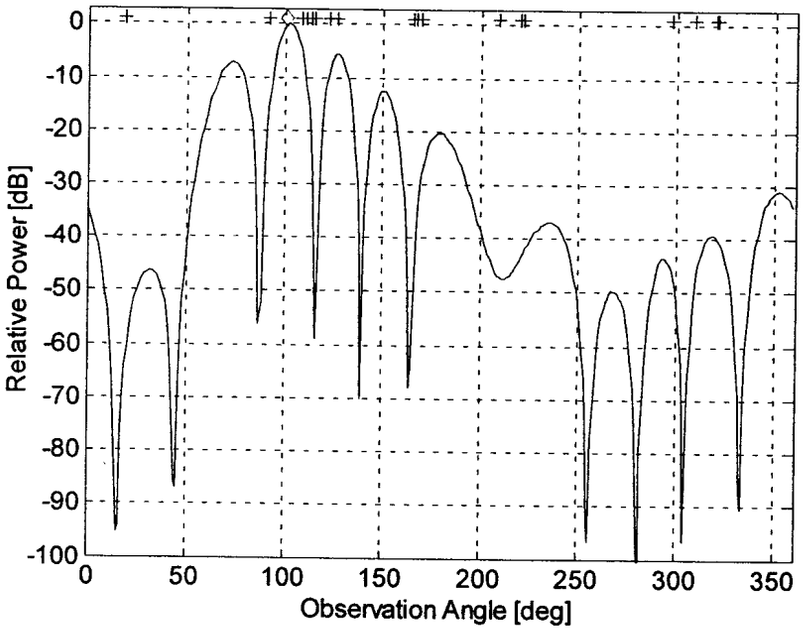

Figure 46: Received power at array 2 without power control in a seven cell configuration (Desired signal indicated with ◊ and interferers with +).

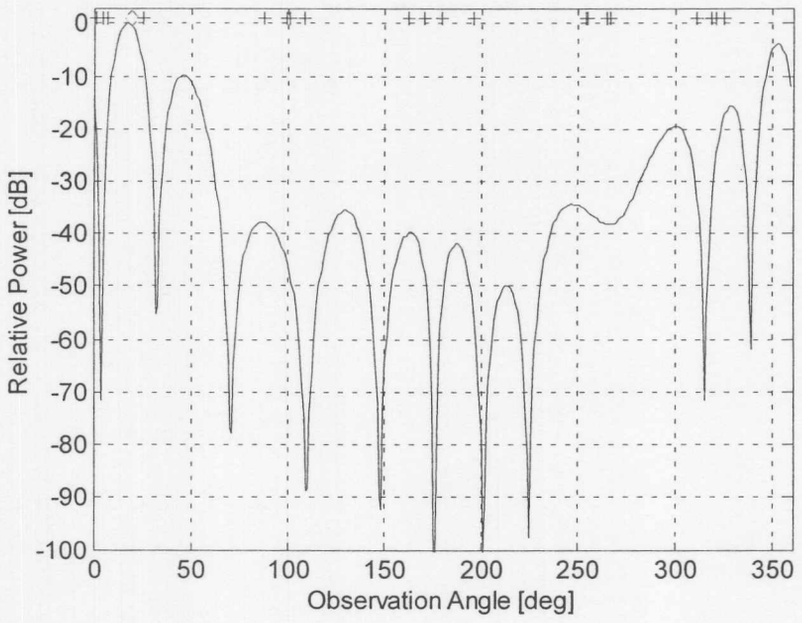

Figure 47: Received power at array 3 without power control in a seven cell configuration (Desired signal indicated with ◊ and interferers with +).

The received power at the output of the combined distributed array is shown in Figure 48 for the seven cell configuration without power control.

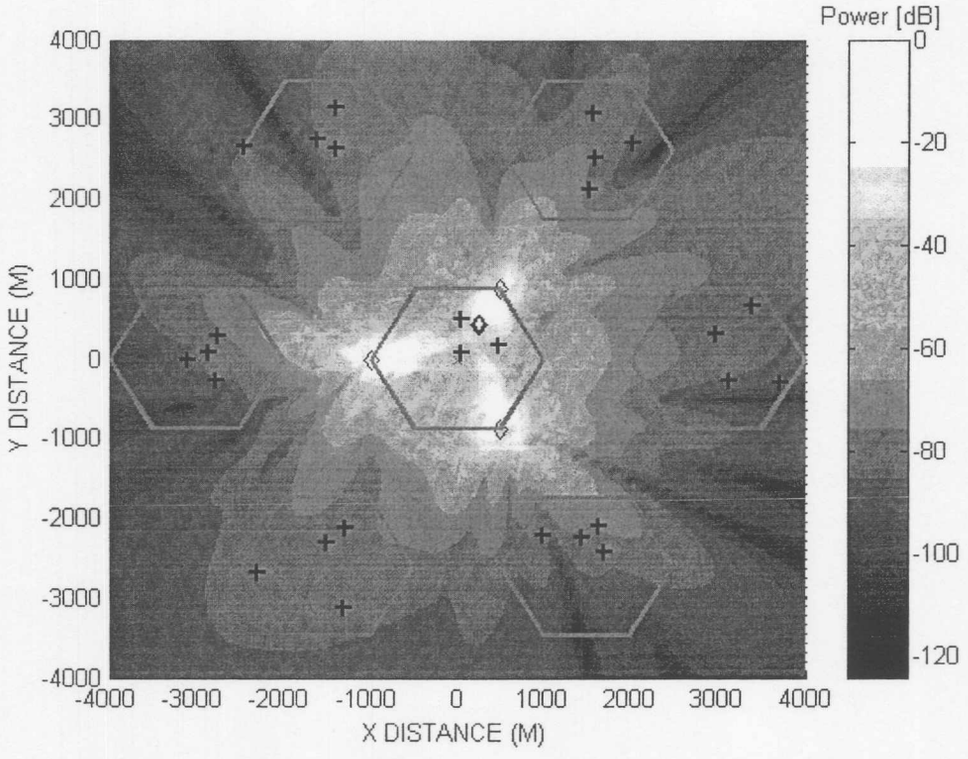

Figure 48: Received signal at combined array without power control in a seven cell configuration (Desired signal indicated with ◊ and interferers with +).

The SINR of the conventional array at the cell center as well as individual and combined beamforming distributed arrays in a seven cell network with power control is given in Table 6. It can be seen that the results are similar to the single cell without power control, but are somewhat lower due to the additional interference from the surrounding cells.

Table 6: SINR without power control of a conventional center cell array and distributed arrays with independent and combined beamforming in a seven cell network.

Array	SINR [dB]
Distributed full sector	-23.66
Center array	-16.19
Array 1	11.91
Array 2	3.23
Array 3	3.59
Independent distributed array beamforming	12.99
Combined distributed array beamforming	18.33

4.3.3.2 SINR Performance with Power Control

The SINR with range power control of the conventional array at the cell center as well as individual and combined beamforming distributed arrays in a seven cell network is given in Table 7. Similar to the SINR of the single cell with and without power contol, the SINR of the center in a seven cell network is higher with power control due to the decrease in the power of the interferer close to the base station. The overall SINR of the combined and independent beamforming arrays in a seven cell network with power control is lower than the single cell SINR with power control due to the additional out of cell interference.

Table 7: SINR with power control of the conventional center cell array and distributed arrays with independent and combined beamforming in a seven cell network.

Array	SINR [dB]
Distributed full sector	-8.99
Center array	4.61
Array 1	4.58
Array 2	0.5
Array 3	1.48
Independent distributed array	13.19

Array	SINR [dB]
beamforming	
Combined distributed array beamforming	16.05

4.4 Conclusions

The signal to interference plus noise ratio (SINR) of the distributed array was investigated in this chapter in the absence of multipath components. Closed form expressions for the SINR of two distributed arrays (each with two elements) with independent and combined beamforming were developed. It was shown analytically that the optimum combined SINR of the individual array output signals (after independent beamforming) is equal to the sum of the individual SINRs of the arrays with independent beamforming. Analytical expressions were derived to show that the SINR of two distributed sub-arrays (each with two elements) with combined beamforming is greater or equal to the SINR of independent beamforming of the arrays for a single interferer. It was also shown numerically that this result can be extended to multiple interferers.

The SINR of independent and combined beamforming of distributed arrays in a non-multipath environment was compared by means of simulation results with conventional arrays at the cell center for one desired signal and three same-cell co-channel interferers. Results indicate that for a seven cell network, mobile range power control, six element arrays and pathloss exponent of three the SINR of the combined beamforming array is approximately 11dB higher the SINR of the conventional center array and 3dB higher the SINR of distributed arrays with independent beamforming.

5 APPROXIMATE ANALYTICAL MODEL FOR PREDICTING THE BIT ERROR RATE PERFORMACE OF DISTRIBUTED ARRAYS IN A MULTIPATH ENVIRONMENT

5.1 Introduction

In this chapter an approximate equation for the bit error rate of a distributed array with combined beamforming in multipath environment will be presented. The model is based on an extension of the analytical model presented in [11] for a single array in a multipath environment. Firstly the detail of the derivation of the single array model by [11] will be given. The correlation between elements of an array in a low angular spread environment as a function of the element spacing will be calculated. This will be followed by a comparison of the bit error rate determined with the analytical model and the bit error rate determined with a Monte-Carlo simulation with high correlation between antenna elements, specifically for an angular spread of 5 degrees and an element spacing of 0.5 wavelengths.

The extension of the single array model to the distributed array will then be presented. This will be followed by a comparison of the bit error rate between the analytical model and a Monte-Carlo simulation for the distributed array with 0.5 wavelength element spacing and 5 degree angular spread.

The objective of the analytical BER calculation method is two fold, (1) to show that the analytical method presented by [11] can be extended to distributed arrays, and (2) to verify the Monte-Carlo simulation method used in this thesis to calculate the BER of the distributed arrays.

5.1 Single Array

5.1.1 Analytical Formulation

Assume that the noise and interference signals are uncorrelated in the short term, all antenna branches have the same noise power and the average of the co-variance matrix is

taken over a period much less than the channel coherence time[38]. A total of D signals are present, with one desired signal and D-1 interferers. It is further assumed that there is Rayleigh fading between each signal and each antenna element. The short term covariance matrix $\mathbf{R}_{nn}$ of the array can then be written as (using (55) and Appendix A):

$$\mathbf{R}_{nn} = \frac{1}{N}\sum_{n=1}^{N}\mathbf{X}(n)\,\mathbf{X}^{H}(n) + \sigma_N^2\,\mathbf{I} \tag{141}$$

where n is the symbol number (or data bit number), N is the total number of symbols over which an average is taken between fades, $\mathbf{I}$ is the identity matrix, $\mathbf{X}(n)$ is the received signal vector at the array element outputs (after sampling and conversion to baseband) and σ_n^2 is the noise power at each element. The vector $\mathbf{X}(n)$ is equal to:

$$\mathbf{X}(n) = S_d(n)\,\mathbf{U}_d(n) \tag{142}$$

where $S_d(n)$ is the transmitted signal amplitude and $\mathbf{U}_d$ is the propagation vector of signal d. Because of Rayleigh fading, U_{dm} (fading of d-th signal at m-th antenna element) is a complex Gaussian random variable. The propagation vector varies at the fading rate, but when averaged over the fading, it has a power equal to P_d, where

$$P_1 = P_{des} \tag{143}$$

and

$$P_d = P_{int} \tag{144}$$

for $d \in \{2,3,....,D\}$. The power of the desired user P_{des} is given by:

$$P_{des} = \Gamma[(D-1)\Gamma_n + 1] \tag{145}$$

where Γ is the SINR and Γ_n is the INR. The power of the interferers P_{int} is given by:

$$P_{int} = \Gamma_n\,\sigma_n^2 \tag{146}$$

Without loss of generality, it is assumed that the baseband transmit power of each signal is unity or:

[38] Channel coherence time is the time that the channel remains constant.

$$E\left\{S_d^2(n)\right\}=1 \tag{147}$$

Assuming that the baseband data of the signals are uncorrelated, using (142) in (141) with (147), equation (141) can be written as (see Appendix A):

$$\mathbf{R}_{nn} = \sum_{d=2}^{D} \mathbf{U}_d \mathbf{U}_d^H + \sigma_n^2 \mathbf{I} \tag{148}$$

With optimum combining, the instantaneous SINR at the output of the array is [2]:

$$\eta=\mathbf{U}_1^H \mathbf{R}_{nn}^{-1} \mathbf{U}_1 \tag{149}$$

where $\mathbf{U}_1$ is the array propagation vector of the desired signal (d = 1). The instantaneous SINR η is a random variable that varies at the fading rate. Since $\mathbf{U}_d$, where $d \in \{1,\ldots,D\}$, is a complex Gaussian variable, the multivariate complex Gaussian probability density function of $\mathbf{U}_d$ can be written as [61].

$$p_d(\mathbf{U}_d) = \frac{1}{\pi^M \left|\hat{\mathbf{R}}_d\right|} e^{\left(-\mathbf{U}_d \hat{\mathbf{R}}_d^{-1} \mathbf{U}_d^H\right)} \tag{150}$$

where $|\,|$ denotes determinant and $\hat{\mathbf{R}}_d$ is the covariance matrix averaged over short term (multipath) fading for user d. It is further assumed that the multipath fading between different mobile signals is independent as they arrive at each antenna element (low correlation at each array element between the received multipath components of two or more different mobile signals). In an environment with narrow angular spread and/or closely spaced antenna elements, the fading between elements for the same signal will be correlated. The probability density function of the output signal to interference plus noise ratio η is a joint function of all the array vectors:

$$p(\eta) = p_\eta(\mathbf{U}_1, \mathbf{U}_2 \ldots, \mathbf{U}_D) \tag{151}$$

where $p_\eta()$ is the joint PDF of η. Due to independent fading between different signals, the joint probability density function can be written as the product of the individual PDF's:

$$p(\eta) = p_\eta(\mathbf{U}_1, \mathbf{U}_2 \ldots, \mathbf{U}_D) = \prod_{d=1}^{D} p_\eta(\mathbf{U}_d) \tag{152}$$

In order to calculate the bit error rate, the PDF of the SINR must be determined. This can be found by first determining the characteristic function of p_η through the Laplace transform:

$$\Psi(z)=\int_0^\infty p(\eta)e^{(-z\eta)}\,d\eta \tag{153}$$

Now, since $p(\eta) = 0$ for $\eta < 0$, (153) may be written as:

$$\Psi(z)=\int_{-\infty}^\infty p(\eta)e^{(-z\eta)}\,d\eta \tag{154}$$

This equation is actually just the expected value of $e^{(-z\eta)}$ [62]. Inserting now (149) and (152) in (154) we get

$$\Psi(z)=\int_{-\infty}^\infty\!\!\ldots\ldots\int_{-\infty}^\infty\left\{p_\eta(\mathbf{U}_1,\mathbf{U}_2\ldots,\mathbf{U}_D)\,e^{(-z\mathbf{U}_1\mathbf{R}_{nn}^{-1}\mathbf{U}_1^H)}\right\}d\mathbf{U}_1\,d\mathbf{U}_2\ldots..\,d\mathbf{U}_D \tag{155}$$

which can be re-written using (152) as:

$$\Psi(z)=\int_{-\infty}^\infty\!\!\ldots\ldots\int_{-\infty}^\infty\left\{p_\eta(\mathbf{U}_1)\;p_\eta(\mathbf{U}_2)\ldots..p_\eta(\mathbf{U}_D)\right\}d\mathbf{U}1\,d\mathbf{U}_2\ldots..\,d\mathbf{U}_D\;G(z,\mathbf{U}_1,\ldots,\mathbf{U}_D) \tag{156}$$

where

$$G(z,\mathbf{U}_1,\ldots,\mathbf{U}_D)=\int_{-\infty}^\infty p_\eta(\mathbf{U}_1)\,e^{(-z\mathbf{U}_1\mathbf{R}_{nn}^{-1}\mathbf{U}_1^H)}d\mathbf{U}_1 \tag{157}$$

Inserting (150) in (157) we have [11]

$$G(z,\mathbf{U}_2,\ldots,\mathbf{U}_D)=\frac{1}{\pi^M\left|\hat{\mathbf{R}}_1\right|}\int_{-\infty}^\infty p_\eta(\mathbf{U}_1)\,e^{[-\mathbf{U}_1(\hat{\mathbf{R}}_1^{-1}+z\mathbf{R}_{nn}^{-1})\mathbf{U}_1^H]}d\mathbf{U}_1 \tag{158}$$

It is shown in [11] that the definite integral in (158) is:

$$\int_{-\infty}^\infty e^{(-\mathbf{x}\mathbf{A}\mathbf{x}^H)}d\mathbf{x}=\frac{\pi^M}{|\mathbf{A}|} \tag{159}$$

Using (159) in (158), the following is obtained:

$$G(z, \mathbf{U}_2, \ldots, \mathbf{U}_D) = \frac{1}{\pi^M \left|\hat{\mathbf{R}}_1\right|} \frac{\pi^M}{\left|\hat{\mathbf{R}}_1^{-1} + z\mathbf{R}_{nn}^{-1}\right|} = \frac{1}{\left|\mathbf{I} + z\hat{\mathbf{R}}_1 \mathbf{R}_{nn}^{-1}\right|} \tag{160}$$

Now $G(z, \mathbf{U}_2, \ldots, \mathbf{U}_D)$ can be re-written as follows:

$$G(z, \mathbf{U}_2, \ldots, \mathbf{U}_D) = G(z, \lambda_1, \ldots, \lambda_M) = \frac{1}{\left|\prod_{m=1}^{M}\left(1+\frac{z}{\lambda_m}\right)\right|} = \prod_{m=1}^{M}\left(\frac{\lambda_m}{z+\lambda_m}\right) \tag{161}$$

where $\lambda_1, \lambda_2, \ldots, \lambda_M$ are the eigenvalues of $\left(\hat{\mathbf{R}}_1 \mathbf{R}_{nn}^{-1}\right)^{-1} = \mathbf{R}_{nn} \hat{\mathbf{R}}_1^{-1}$. The eigenvalues are the solutions to the generalized eigenvalue problem:

$$\mathbf{R}_{nn}\, \mathbf{v} = \lambda \hat{\mathbf{R}}_1\, \mathbf{v} \tag{162}$$

where $\mathbf{v}$ are the eigenvectors. The average of a function g(x) is per definition [62]:

$$E[g(x)] = \int_{-\infty}^{\infty} p(x)\, g(x)\, dx \tag{163}$$

where p(x) is the probability density function of x. Using (163) in (156), the characteristic function $\Psi(z)$ is actually the average of $G(z, \lambda_1, \ldots, \lambda_M)$. It is shown in [11] that the characteristic function can be approximated by:

$$\Psi(z) = \prod_{m=1}^{M}\left(\frac{\langle\lambda_m\rangle}{z+\langle\lambda_m\rangle}\right) \tag{164}$$

where $\langle\lambda\rangle$ is the mean of the eigenvalue. In the case where there is uncorrelated fading between elements for the same signal (large element spacing or wide angular spread), the interference plus noise co-variance matrix simplifies significantly [11]. There are M-1 eigenvalues equal to zero and one non-zero eigenvalue. The BER for this simplified case is given in Appendix C. In the case of all unique eigenvalues (multiplicity equal to one),

which is typically the case when a signal is correlated between antenna branches, a partial fractional expansion of the characteristic function in (164) is given by:

$$\Psi(z)=C\left[\frac{\Omega_1}{(z+\lambda_1)}+\frac{\Omega_2}{(z+\lambda_2)}+....+\frac{\Omega_M}{(z+\lambda_M)}\right] \tag{165}$$

which is equal to:

$$\Psi(z)=C\sum_{m=1}^{M}\left[\frac{\Omega_m}{(z+\lambda_m)}\right] \tag{166}$$

with

$$\Omega_m=\frac{1}{\prod_{i=1,i\neq m}^{M}(\lambda_m-\lambda_i)} \tag{167}$$

and

$$C=\prod_{m=1}^{M}\lambda_m \tag{168}$$

Now, the probability density function $p(\eta)$ is the inverse Laplace transform of the characteristic function in (166), given by:

$$p(\eta)=L^{-1}\{\Psi(z)\}=C\sum_{M=1}^{M}\Omega_m e^{-\lambda_m\eta} \tag{169}$$

The average (over Rayleigh fading) bit error rate (BER) of phased shift keyed signals is given by [11]:

$$BER=\tfrac{1}{2}\int_{-\infty}^{\infty}p(\eta)\,\mathrm{erfc}(\sqrt{\eta})\,d\eta \tag{170}$$

Inserting (169) in (170), the following is obtained:

$$BER=\frac{C}{2}\int_{-\infty}^{\infty}\sum_{m=1}^{M}\left(\Omega_m e^{-\lambda_m\eta}\right)\mathrm{erfc}(\sqrt{\eta})\,d\eta \tag{171}$$

The following general integral formula [11] is used to evaluate (171):

$$\frac{1}{2}\int_0^{\infty} e^{(-a\,x)}\ \mathrm{erfc}(\sqrt{bx}\,dx = \frac{\sqrt{1+\frac{a}{b}}-1}{2a\sqrt{1+\frac{a}{b}}} \tag{172}$$

Finally, using (172) in (171), the average bit error rate is:

$$BER = C\sum_{m=1}^{M}\Omega_m\left(\frac{\sqrt{1+\lambda_m}-1}{2\lambda_m\sqrt{1+\lambda_m}}\right) \tag{173}$$

5.1.2 Single Array Result with Correlated Fading

In order to calculate the bit error rate in (173) the eigenvalues must be determined. It was shown in [11] that the average eigenvalues in the case of uncorrelated fading across the elements can be determined with a Monte-Carlo simulation. In the case of correlated fading between elements, the eigenvalues must be calculated for each interference to noise level. An example of the eigenvalues for one interferer and equal INR and SNR of 20dB was presented in [11] for a correlation value of 0.9.

The performance of closely spaced antenna elements (0.5λ[39]) of distributed arrays in low to moderate multipath environments is investigated in this thesis. The correlation between elements is a function of the element spacing, angular spread and mean incidence angle [25]. A low correlation between elements improves the array's ability to discriminate in the spatial domain between various incoming multipath components. Therefore, it is important to quantify the correlation between elements as function of spacing and angular spread.

The average correlation between the elements of a two-element array is:

$$\text{Correlation} = \frac{\hat{\mathbf{R}}_1(1,2)}{\sqrt{\hat{\mathbf{R}}_1(1,1)\,\hat{\mathbf{R}}_1(2,2)}} \tag{174}$$

where $\hat{\mathbf{R}}_1(n,m)$ is the covariance matrix of elements n and m averaged over short term fading. The correlation as a function of the element spacing was calculated for an angular

[39] This is the typical antenna spacing used in scanning arrays to avoid grating lobes.

spread of 5°, zero mean incidence angle and with a SNR = INR = 10dB. The calculated eigenvalues for one interferer is given in Table 8 with averaging over 4000 iterations. The eigenvalues is the solution of the generalized eigenvalue problem given in (162). The Rayleigh fading model in section 2.4.1.1.2 is used with 30 scatterers to generate the signals at the antenna elements, which is then applied to calculate the co-variance matrices. The eigenvalues decrease with an increase in element spacing. The correlation as a function of the element spacing is shown in Figure 49. This figure indicates, for example, that there is a 50% correlation between elements with an interelement spacing of 4.2λ. Furthermore, it can be seen that there is a correlation of more than 98% between elements when the interelement spacing is 0.5λ.

Table 8: Eigenvalues as a function of the interelement spacing.

Element Spacing [wavelengths]	$\langle\lambda_1\rangle$	$\langle\lambda_2\rangle$
0.2	1.040985	68.89308
0.6	0.985893	8.462671
1.0	0.865898	3.984874
1.8	0.589558	2.318541
3.0	0.439151	1.973366
4.2	0.375803	1.885298
5.0	0.36517	1.870526
6.2	0.34629	1.865329
7.0	0.349004	1.852482
7.8	0.35091	1.877462

Using equation (173), the analytical BER is compared in Figure 50 to that calculated with a Monte-Carlo simulation with the signals in a Rayleigh fading environment. The fading environment is generated with 30 scatterers according to the Rayleigh method described in section 2.4.1.1.2. The configuration is a two-element array with two equal power interferers and an INR of 2. The element spacing is 0.5λ, angular spread is 5° and the number of scatterers is 30. The mean eigenvalues over 2000 iterations is given in Table 9. It can be seen from Figure 50 that there is good agreement between the analytical and the Monte-Carlo simulation results.

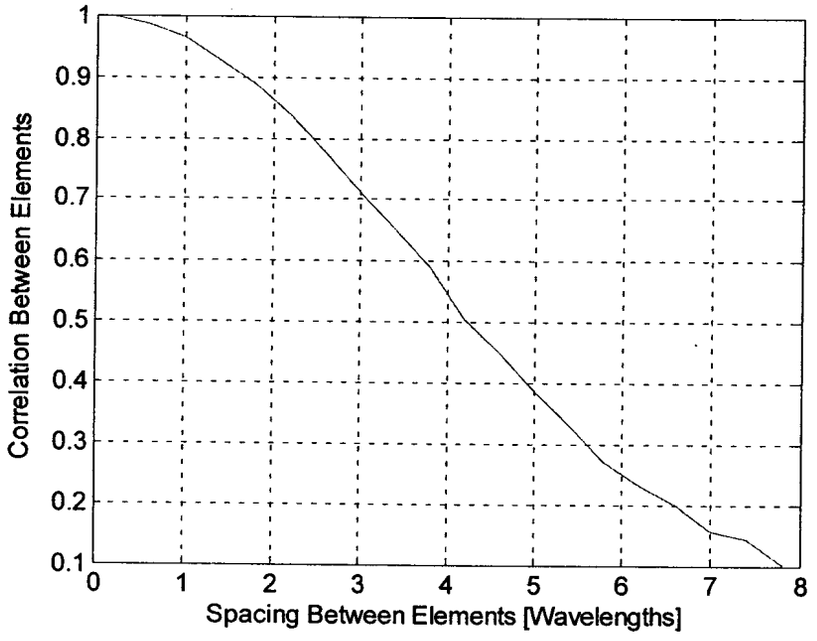

Figure 49: Correlation between two antenna elements as a function of the inter-element spacing for an angular spread of 5°.

Table 9: Mean eigenvalues of a two-element array in the presence of two interferers.

SINR [dB]	$\langle\lambda_1\rangle$	$\langle\lambda_2\rangle$
-10	14.737	375.48
-8	9.094	240.486
-6	6.152	152.195
-4	3.875	92.117
-2	2.492	55.913
0	1.473	37.859
2	0.933	24.089
4	0.604	14.979
6	0.385	9.907
8	0.244	5.815
10	0.147	3.808
12	0.098	2.347
14	0.059	1.424

SINR [dB]	$\langle\lambda_1\rangle$	$\langle\lambda_2\rangle$
16	0.038	0.82
18	0.024	0.628
20	0.014	0.37

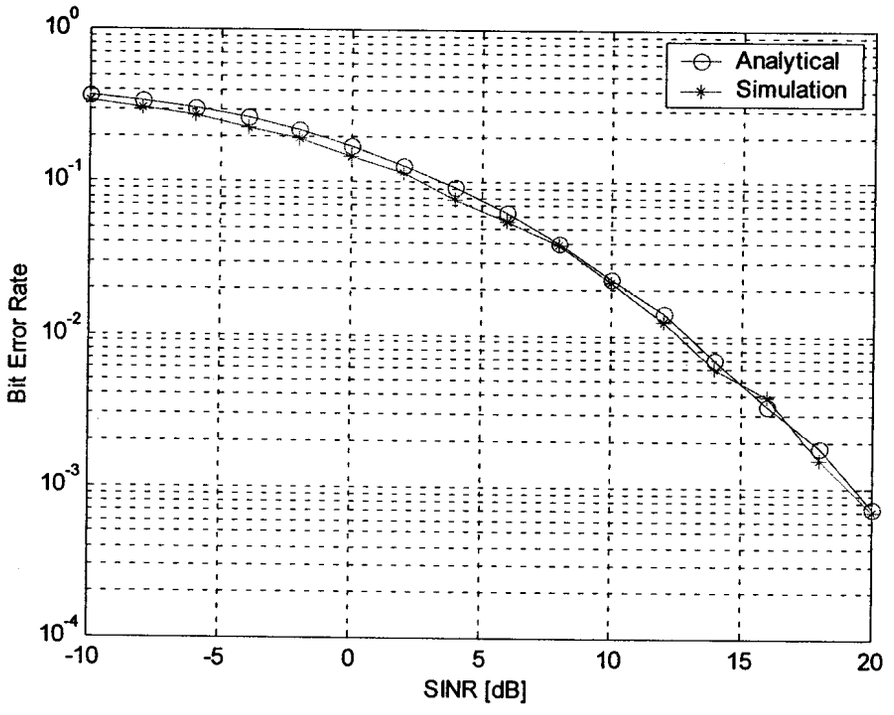

Figure 50: Analytical BER compared to BER calculated with Monte-Carlo simulations with signals in a Rayleigh fading environment for a two-element array with two equal power interferers.

5.2 Distributed Array

In this section an analytical expression will be derived for the bit error rate of a distributed array with combined beamforming in a fast fading environment based on the method of the single array presented in the previous section.

5.2.1 Analytical Formulation

Assume that the noise and interference signals are uncorrelated in the short term, all elements of the three sub-arrays have the same noise power and the average of the interference correlation matrix is taken over a period much less than the channel coherence time. The short term covariance matrix of the interference plus noise of the combined

distributed array (consisting of all three sub-arrays with combined beamforming) $\ddot{\mathbf{R}}_{nn}$ can then be written as:

$$\ddot{\mathbf{R}}_{nn} = \frac{1}{N}\sum_{n=1}^{N}\sum_{d=1}^{D}\ddot{\mathbf{X}}_d(n)\,\ddot{\mathbf{X}}_d^H(n) + \sigma_N^2\,\mathbf{I} \tag{175}$$

where n is the symbol number (or bit number), N is the total number of symbols (or data bits) over which an average is taken, $\mathbf{I}$ is the identity matrix spanning all three sub-arrays, $\ddot{\mathbf{X}}(n)$ is the combined received signal vector of all three sub-arrays and σ_N^2 is the noise power at each element of the combined array. The vector $\ddot{\mathbf{X}}(n)$ is equal:

$$\ddot{\mathbf{X}}(n) = S_d(n)\,\ddot{\mathbf{U}}_d(n) \tag{176}$$

where $S_d(n)$ is the transmitted signal amplitude and $\ddot{\mathbf{U}}_d$ is the propagation vector of signal d at the combined array (given in (1) for the uniform linear array). The propagation vector varies at the fading rate, but when averaged over the fading, it has a power at each element of sub-array $\kappa \in \{1,2,3\}$ equal to $P_{d,\kappa}$, where

$$P_{1,\kappa} = \frac{P_{des}}{\left(\frac{r_{1,\kappa}}{r_{1,\kappa}^{pc}}\right)^{\gamma}} \tag{177}$$

and

$$P_{d,\kappa} = \frac{P_{int}}{\left(\frac{r_{d,\kappa}}{r_{d,\kappa}^{pc}}\right)^{\gamma}} \tag{178}$$

for $d \in \{2,3,....,D\}$. $r_{d,\kappa}$ is the range between the sub-array and mobile d and $r_{d,\kappa}^{pc}$ is the power control radius (see section 2.5.5). The power of the desired user P_{des} is given by:

$$P_{des} = \Gamma\left[(D-1)\Gamma_n + 1\right] \tag{179}$$

where Γ is the SINR and Γ_n is the INR. The power of the interferers P_{int} is given by:

$$P_{int} = \Gamma_n\,\sigma_n^2 \tag{180}$$

Assume without loss of generality that:

$$E\left\{S_d^2(n)\right\}=1 \tag{181}$$

Assuming that the signal data are uncorrelated and using (181), (175) can be written as (see Appendix A):

$$\ddot{\mathbf{R}}_{nn} = \sum_{d=1}^{D} \ddot{\mathbf{U}}_d \, \ddot{\mathbf{U}}_d^H + \sigma_N^2 \mathbf{I} \tag{182}$$

With optimum combining, the instantaneous SINR at the output of the array is [2]:

$$\eta = \ddot{\mathbf{U}}_1 \, \ddot{\mathbf{R}}_{nn}^{-1} \, \ddot{\mathbf{U}}_1^H \tag{183}$$

where $\ddot{\mathbf{U}}_1$ is the combined propagation vector of the desired signal (d = 1) The instantaneous signal to interference plus noise ratio η is a random variable that varies at the fading rate. The multivariate Gaussian density function of $\mathbf{U}_d$, where d $\in$ {1,2,...D}, can be written as [61].

$$p_d(\ddot{\mathbf{U}}_d) = \frac{1}{\pi^M \left|\ddot{\hat{\mathbf{R}}}_d\right|} e^{\left(-\ddot{\mathbf{U}}_d \ddot{\hat{\mathbf{R}}}_d^{-1} \ddot{\mathbf{U}}_d^H\right)} \tag{184}$$

where | | denotes determinant and $\ddot{\hat{\mathbf{R}}}_d$ is the co-variance matrix averaged over short term (multipath) fading. All signals are assumed to have independent scattering, but the fading for each signal may be correlated between the array elements (due to coupling between closely spaced elements, narrow angular spread or mutual coupling). Furthermore, it is assumed that the fading between the sub-arrays are uncorrelated[40]. The rest of the derivation is similar to the single element derivation. Following the same derivation as for the single element case (see section 5.1), the characteristic function $\Psi(z)$ can be approximated by:

$$\Psi(z) = \prod_{m=1}^{M*K} \left(\frac{\langle \lambda_m \rangle}{z + \langle \lambda_m \rangle} \right) \tag{185}$$

[40] This is a valid assumption since the arrays are located far apart.

where $\langle\lambda\rangle$ is the average value of the eigenvalue, determined for the combined array. The total number of eigenvalues is the number of elements multiplied by the number of sub-arrays. With correlation between the elements, the eigenvalues are unique and the BER is given by (using equations (173), (167) and (168)):

$$BER = C\sum_{m=1}^{M*K}\Omega_m\left(\frac{\sqrt{1+\lambda_m}-1}{2\lambda_m\sqrt{1+\lambda_m}}\right) \tag{186}$$

where

$$\Omega_m = \frac{1}{\prod_{i=1,i\neq m}^{M*K}(\lambda_m-\lambda_i)} \tag{187}$$

and

$$C = \prod_{m=1}^{M*K}\lambda_m \tag{188}$$

5.3 Distributed Array Results

In this section the BER calculated with the analytical method is compared to that determined with a Monte-Carlo simulation. A two-element sub-array with two equal strength interferers is considered. The interferers and desired signal are all co-located (worst case) at the following location (see Figure 51):

$$x = 0.5r\cos(30^\circ) = 433\,m \tag{189}$$

and

$$y = 0.5r\sin(30^\circ) = 250\,m \tag{190}$$

The interference to noise ratio is two, angular spread is 5° and the element spacing is 0.5λ. Sub-array 1 is controlling the power (according to the range power control in 2.5.5.1) with a control radius of 620m. The range between mobile and sub-array 2 is 1118m and sub-array 3 is 1454m. The mean eigenvalues calculated with a Monte-Carlo simulation (see section 2.9.1) is given in Table 10. The pathloss exponent is 3.

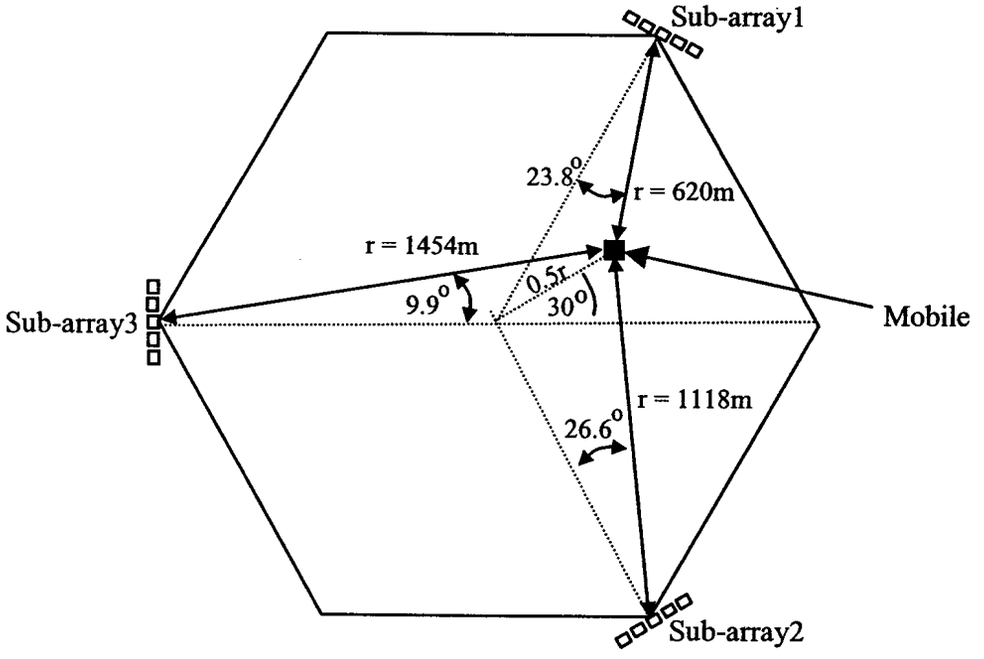

Figure 51: Location of mobiles.

Table 10: Mean Eigenvalues.

SINR [dB]	$\langle\lambda_1\rangle$	$\langle\lambda_2\rangle$	$\langle\lambda_3\rangle$	$\langle\lambda_4\rangle$	$\langle\lambda_5\rangle$	$\langle\lambda_6\rangle$
-10	4.752	15.688	51.227	425.35	3148.572	5228.268
-8	2.84	10.123	33.49	295.658	1798.889	3427.399
-6	1.665	6.537	21.343	169.93	1083.352	1978.911
-4	1.028	3.834	12.88	106.052	692.569	1201.742
-2	0.687	2.168	7.476	69.717	391.569	780.536
0	0.447	1.468	4.858	43.794	295.103	422.912
2	0.289	0.956	3.116	26.505	176.979	353.787
4	0.179	0.623	2.102	16.49	91.783	206.547
6	0.111	0.414	1.367	11.177	69.362	136.821
8	0.082	0.271	0.896	7.322	39.695	79.587
10	0.045	0.148	0.492	4.596	23.218	45.585

A comparison between the BER determined with the analytical method compared to the BER determined with a Monte-Carlo simulation is shown in Figure 52. It can be seen that there is excellent agreement between the two methods.

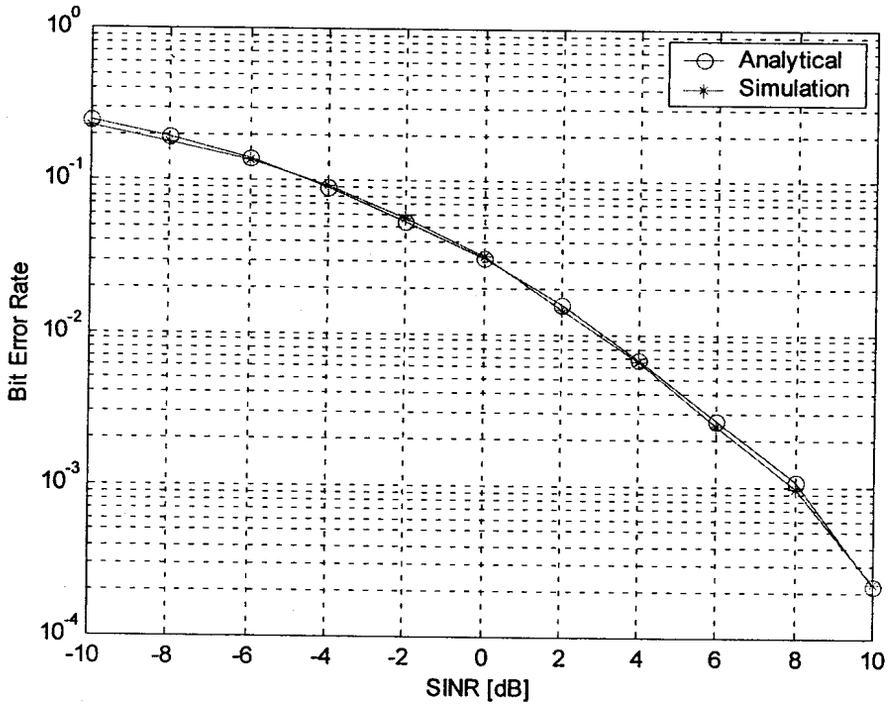

Figure 52: Analytical vs. Monte-Carlo BER comparison for a two-element array with two interferers.

The BER will be lower when the two signals are not co-located. The above result shows the worst case BER as a function of signal to noise ratio.

5.4 Conclusions

An analytical approximation for the bit error rate of a distributed array in a fast fading multipath environment was derived in this chapter. This derivation is based on an extension of a known derivation for the analytical BER of multipath signals received at a single array. The analytical method basically determines a characteristic function as the Laplace transform of the joint multivariate Gaussian probability density function for independent fading between signals. A generalized eigenvalue problem is then solved to determine the eigenvalues of the characteristic function. Once this is known, the characteristic function can be inverted to determine the probability density function. With

this probability function known, the BER can be determined in closed form for phased shift keyed signals.

In order to test the analytical approximation, the bit error rate of a distributed array with half wavelength element spacing was compared to the bit error rate calculated with a Monte-Carlo estimation for two co-located mobiles in a 5° angular spread environment. There are good agreement between the results.

6 DISTRIBUTED ARRAY PERFORMANCE IN A MULTIPATH ENVIRONMENT

6.1 Introduction

The ability of an array to reduce the interference from mobiles with incidence angles close to the desired signal incidence angle, is a function of the angular spread and the distance between array elements. An array with a large element spacing (5λ) and moderate angular spread (5°) or an array with a small element spacing (0.5λ) and wide angular spread (30°) is able to significantly reduce the signal from an interferer closely separated in incidence angle (even equal incidence angles) to that of the desired signal.

Distributed arrays offers an improvement in interference signal rejection relative to conventional arrays at the cell center for signals operating in a moderate multipath environment with closely spaced antenna elements (0.5λ). In the first part of this chapter, the performance (in terms of bit error rate) of a single array will be investigated as a function of the number of elements, the element spacing and the angular spread.

The performance of distributed arrays located at the edges of the cell will then be investigated as a function of the number of elements, element spacing and angular spread. A seven cell network will be considered.

The distributed array performance with combined beamforming (combined weight vector for all sub-arrays) will be compared to arrays with individual beamforming (individual weight vector for all sub-arrays).

The uplink performance of TDMA systems is the focus of the investigation in this chapter. The downlink performance of combined beamforming vs. independent beamforming of adaptive arrays in the CDMA downlink during soft handoff will be investigated in chapter 1.

6.2 Simulation Method and General Parameters

The array element pattern that is used in the simulations is a standard 120° pattern, as shown in Figure 8. The bit error rate for each mean SINR is evaluated with Monte-Carlo simulations over 20 000 iterations (unless stated otherwise), using equation (63). The circular vector channel model with 30 scatterers (K=30) is used and the interferer to noise ratio is 2 [or 3dB]. A diagram of the simulation procedure is shown in Figure 53.

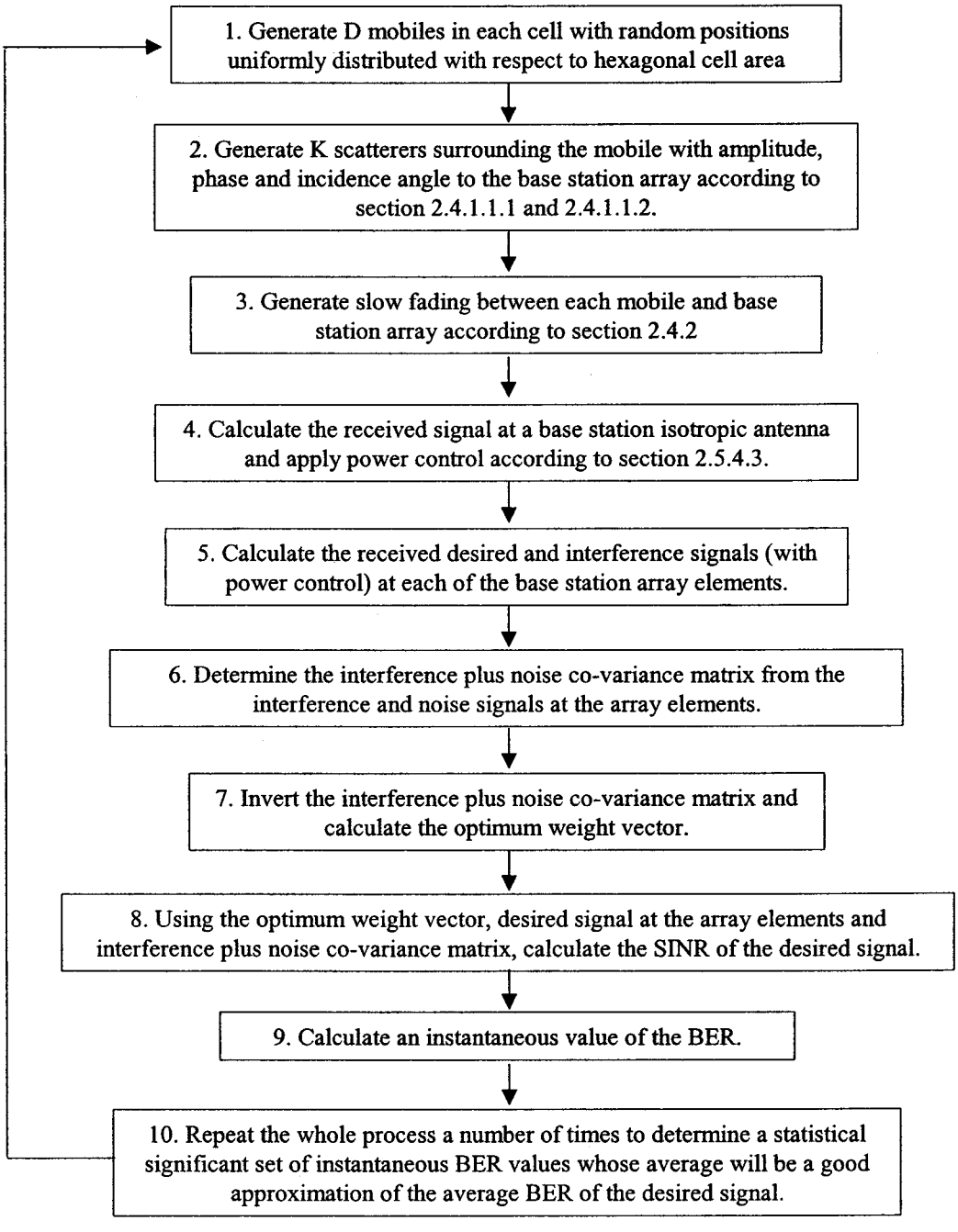

Figure 53: Diagram of the individual simulation steps.

6.2.1 Verification of software code

In this section the accuracy of the implemented simulation program code (based on the formulation in chapter 1) is verified. The calculated BER for two and three element arrays is shown in Figure 54. This is compared to the numerical Monte-Carlo results given in [2] for the case with two equal power interferers. Similar results can be found in [11], where the BER was calculated with an analytical method. The element spacing is 5λ and the multipath scattering angle is 20°. This spacing and angular spread results in uncorrelated or independent fading between antenna elements [25]. The desired signal and interferer are at the same location (therefore the mean incidence angle as seen from the array is the same for both)

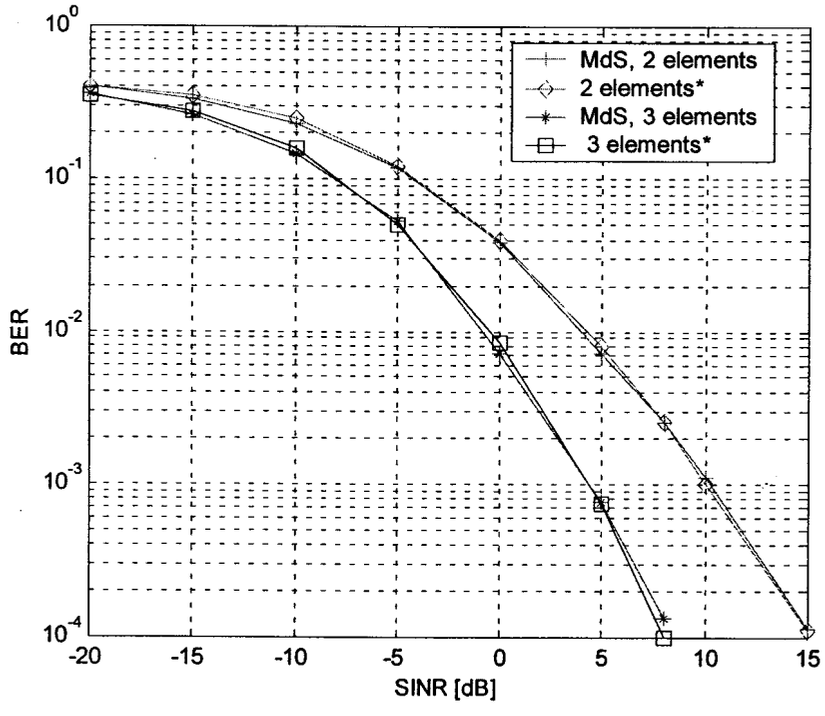

Figure 54: Comparison of results with [2] for a single array with two or three elements and two equal power interferers. * From reference [2].

It can be seen in Figure 54 that there is excellent agreement between the results obtained here and the results in [2], verifying that the software code is accurate.

6.2.2 BER of Circular Vector Channel Model vs. Rayleigh Fading

A comparison between the BER calculated using the circular vector channel model and Rayleigh fading model (see section 2.4.1.1.2) is shown in Figure 55. The configuration is

a two element array with one interferer and interference to noise ratio of 2. An element spacing of 0.5λ and 5λ is considered, and the scattering angle is 5° in both cases. The circular vector channel model gives a higher BER than Rayleigh fading for SINRs above 5dB.

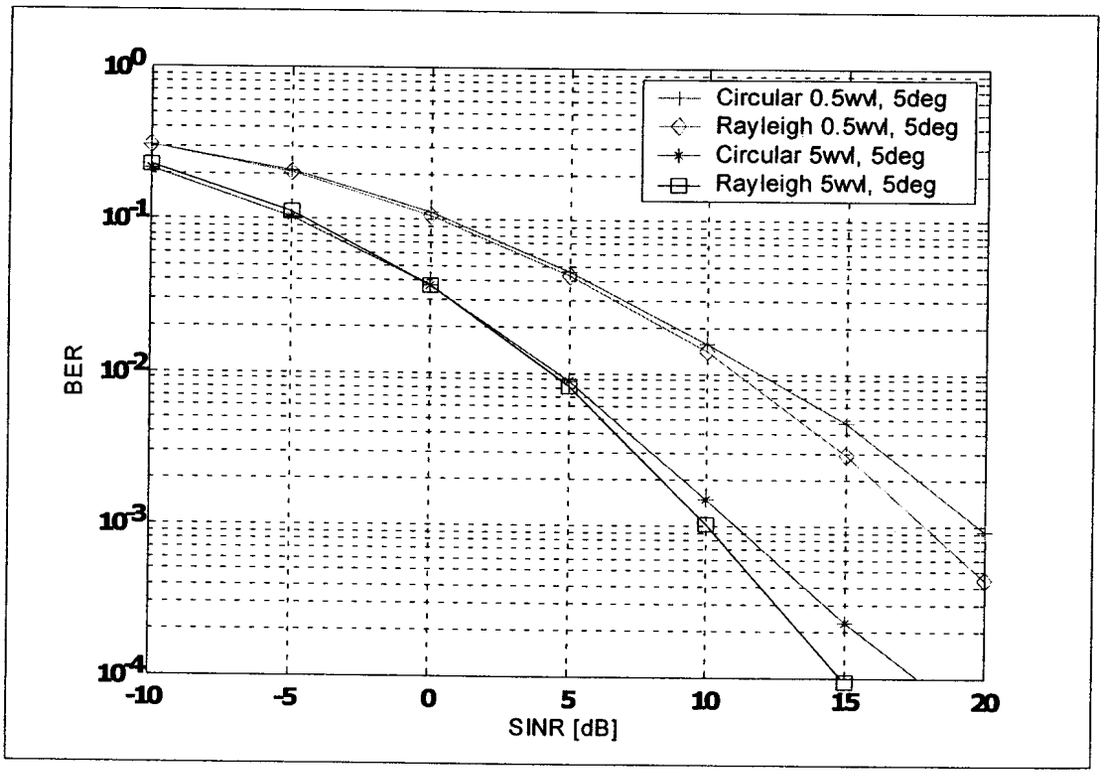

Figure 55: Circular vector channel model vs. Rayleigh fading.

6.2.3 BER vs. Number of Elements (Fixed Element Spacing and Scattering Angle)

The bit error rate versus the number of antenna elements in a rich multipath environment, with large element spacing and one interferer in the same direction as the desired signal, is shown in Figure 56. The array spacing is 5λ and the angular spread is 30°. The figure shows that as the number of elements is increased, the BER is reduced. This is due to improved reduction of the interference multipath components and therefore an increase in the signal to interference plus noise ratio.

6.2.4 BER vs. Scattering Angle

The bit error rate as a function of the SINR and angular spread is shown in Figure 57 for one interferer and in Figure 58 for two interferers in the same direction as the desired signal. The element spacing is 0.5λ and a four element array is considered. The figures

show that as the scattering angle increases, the BER reduces due to improved cancellation of the interference multipath components.

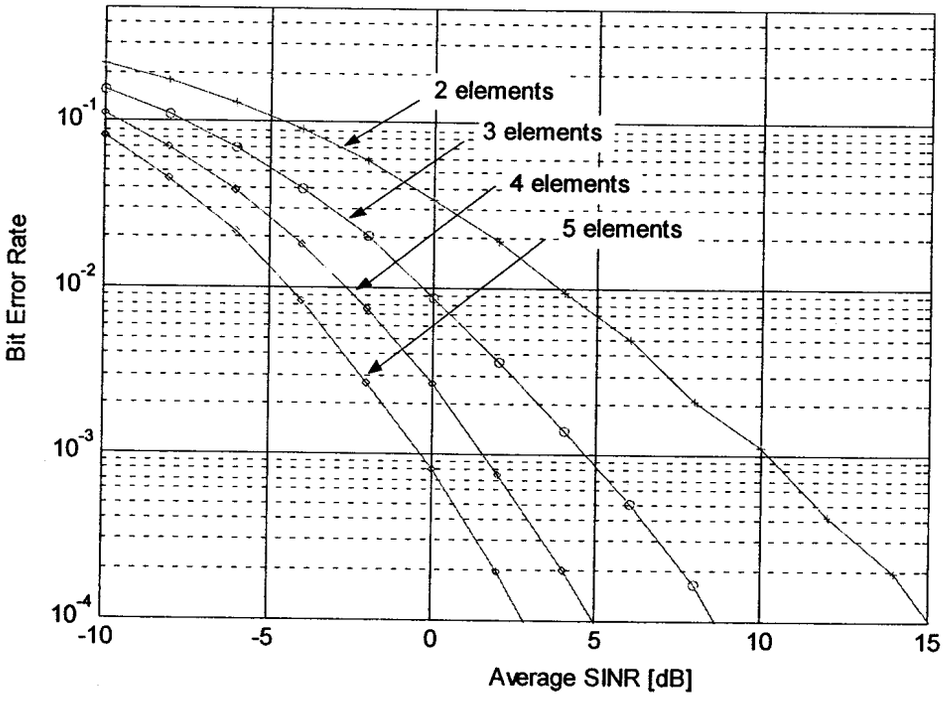

Figure 56: BER as a function of SINR and number of elements with one interferer.

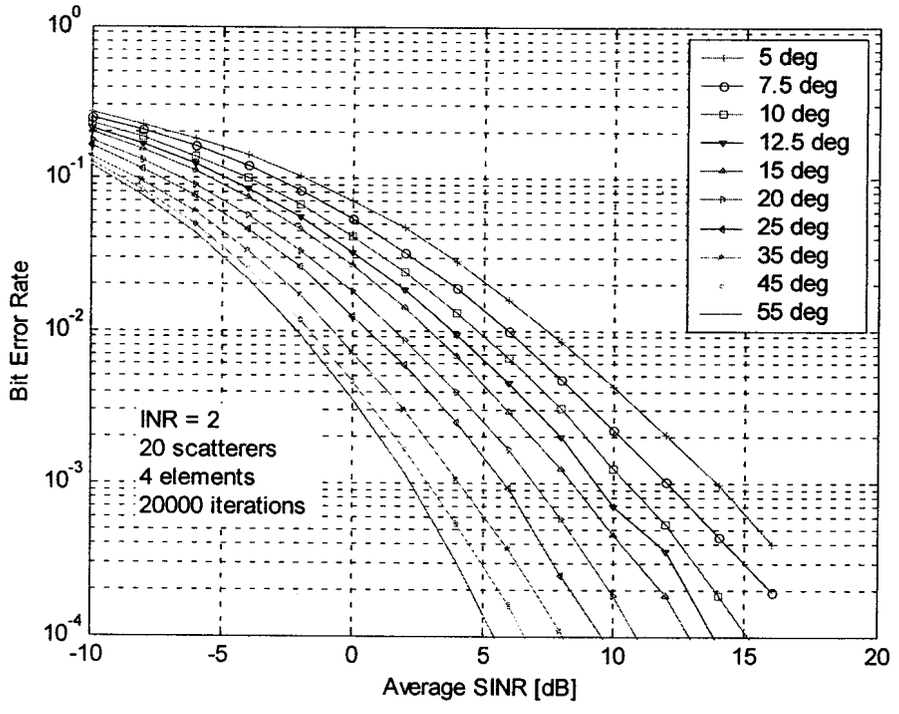

Figure 57: BER as a function of SINR and angular spread with one interferer.

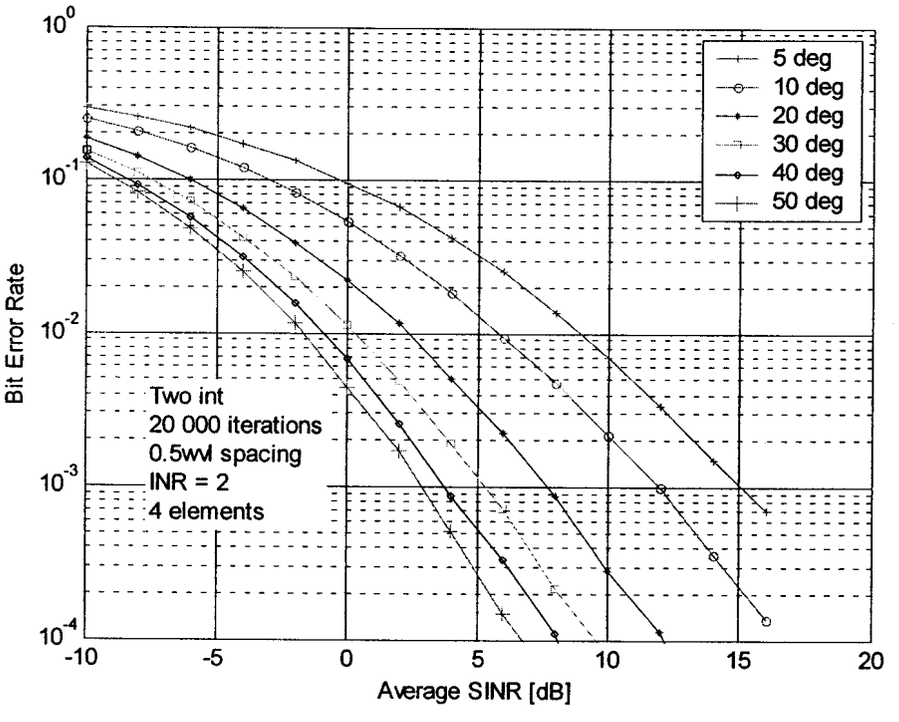

Figure 58: BER as a function of SINR and angular spread with two interferers.

6.3 Distributed Array (Arrays at the Edges of the Cell)

In this section the bit error rate of three distributed arrays at alternate edges of the cell is investigated. The geometry of the distributed array as well as desired and interfering mobiles is shown in Figure 59)

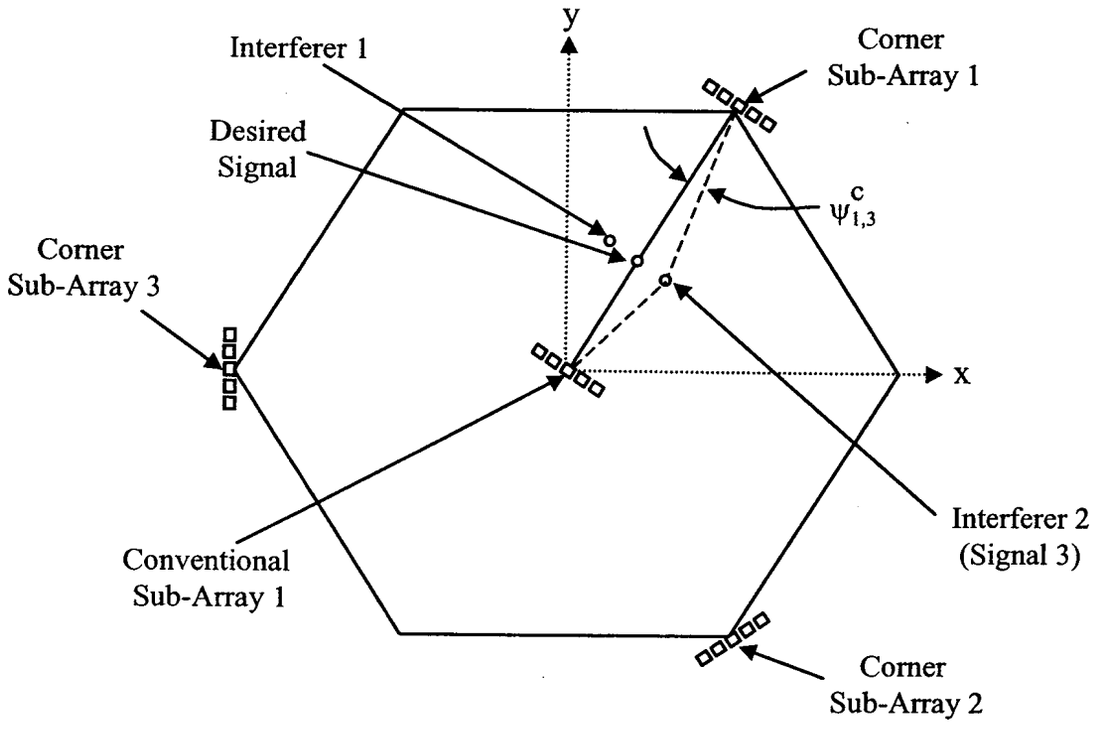

Figure 59: Locations of the desired and interfering signals.

6.3.1 Combined vs. Independent Adaptive Beamforming

The BER of the combined beamforming array vs. the minimum BER of the three independent arrays as a function of the angular spread is shown in Figure 60. The number of array elements is two and two equal power interferers are present. The incidence angles of the desired and interfering signals are all equal and range power control is assumed. It can be seen that the BER of the distributed arrays with independent beamforming is significantly higher than the BER of the combined array. In addition it can be seen that the BER of the independent beamforming arrays decreases as the angular spread increases, as

was also observed for the single four element array in Figure 58. The BER of the combined array on the other hand reduces only slightly as the angular spread increases[41].

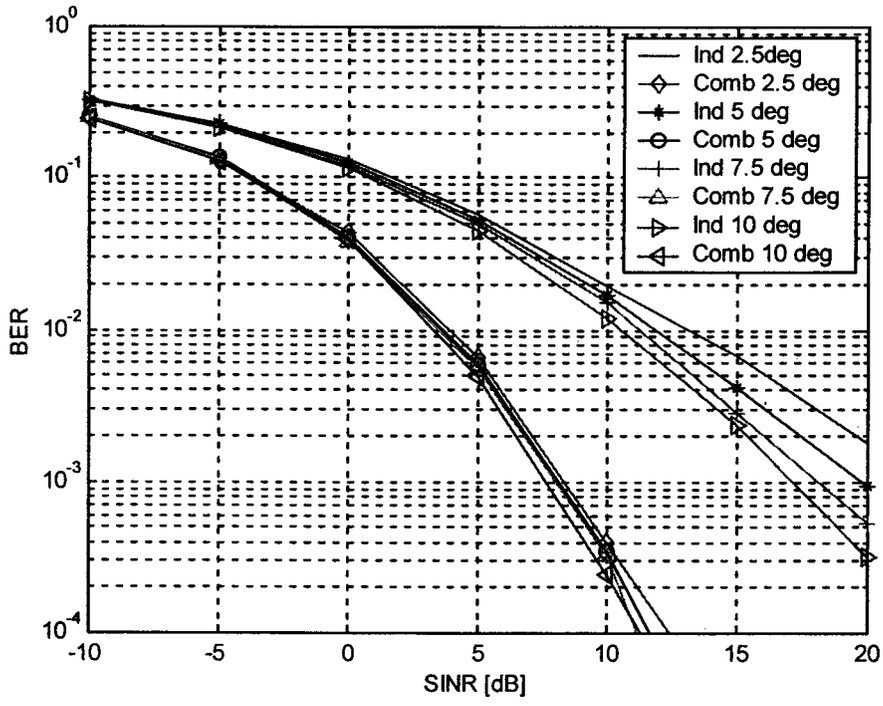

Figure 60: BER of independent vs. combined arrays as a function of angular spread for 2 element arrays.

The BER as a function of the SINR for the desired signal and interferers separated in angle by 5° is shown in Figure 61 for two element arrays with an angular spread of 5° and 10°. Comparing this to Figure 60, it can be seen that the results are very similar. This is to be expected, since the arrays has only two elements with a wide Fresnel beamwidth.

[41] Note that the conventional array BER is the same as the minimum BER of the distributed arrays with independent beamforming.

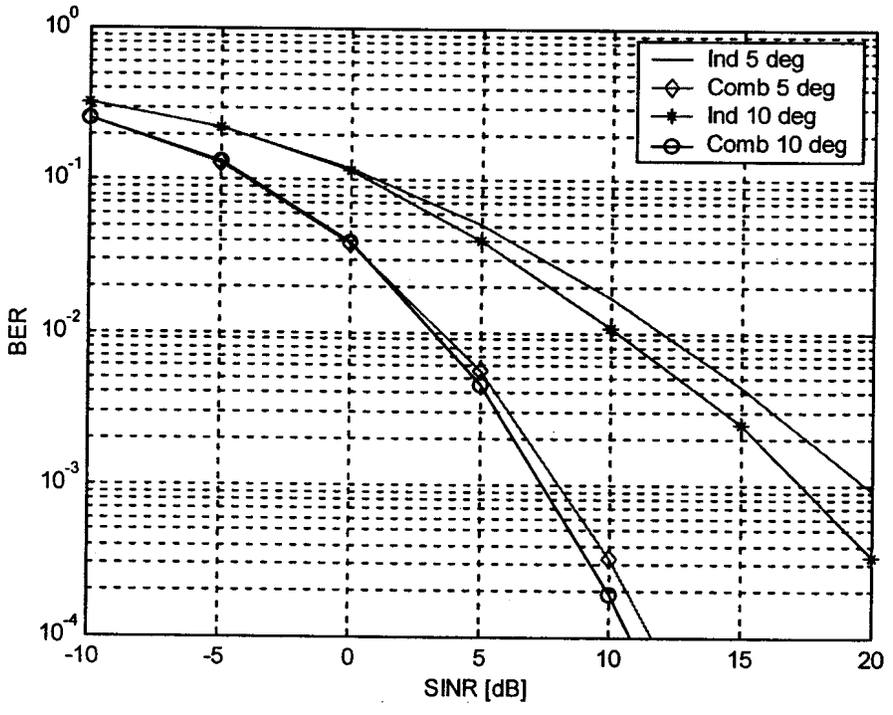

Figure 61: BER as a function of the SINR of independent vs. combined beamforming for two-element arrays with two interferers. The interferers are separated by 5° in angle relative to the desired signal.

The BER as a function of the SINR and angular spread for the center arrays and corner arrays with independent and combined beamforming for a four element array and two equal strength interferers is shown in Figure 62 with the interferers in the same direction as the desired signal. The case where the interfering signals are 5° in angle on both sides of the desired signal (see Figure 59) is shown in Figure 63. Comparing the two cases (Figure 62 and Figure 63), it can be seen that the resolution of the array is only sufficient to achieve a small reduction in the interference and therefore a slight reduction in the BER when the interferers are separated in incidence angle from the desired signal (compared to the same interference and desired signal directions). The results also show that as the angular spread increases, the reduction of the BER between the two cases reduces (the curves moves together), indicating that the angular spread is wide enough so the array is able to separate the interferers from the desired signal. In both cases, the center arrays has the worst performance, followed by the corner arrays with independent beamforming and then the best performance from the corner arrays with combined beamforming.

In Figure 64 and Figure 65 the interferers are offset by 10° and 15° respectively on either side of the incidence angle of the desired signal. There is a significant improvement in the BER when the interferers move from 0° to 10°, but less so when they move between 10° and 15°

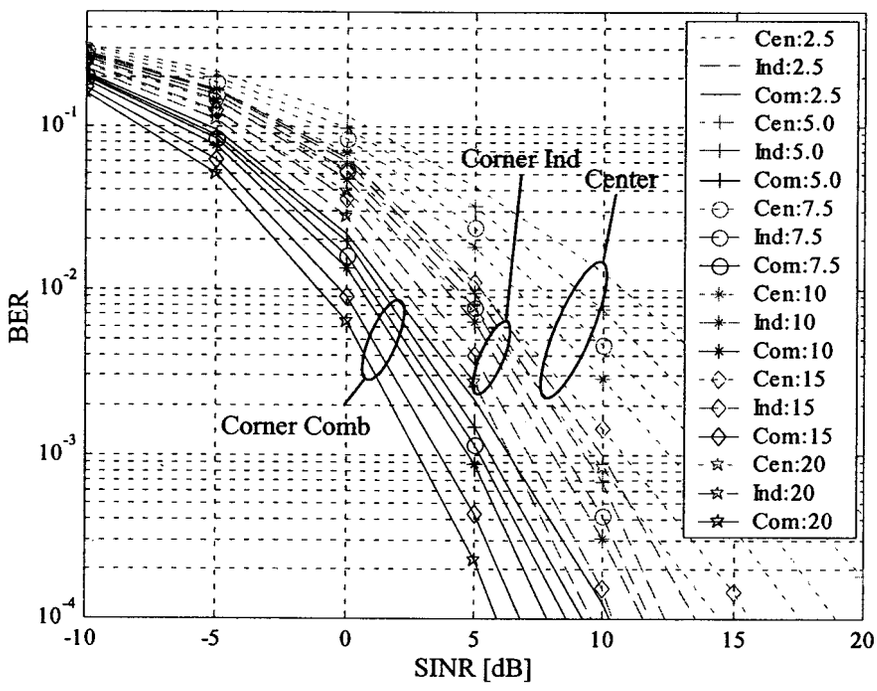

Figure 62: BER as a function of the SINR and angular spread of four element arrays with two equal strength interferers in the same direction as the desired signal.

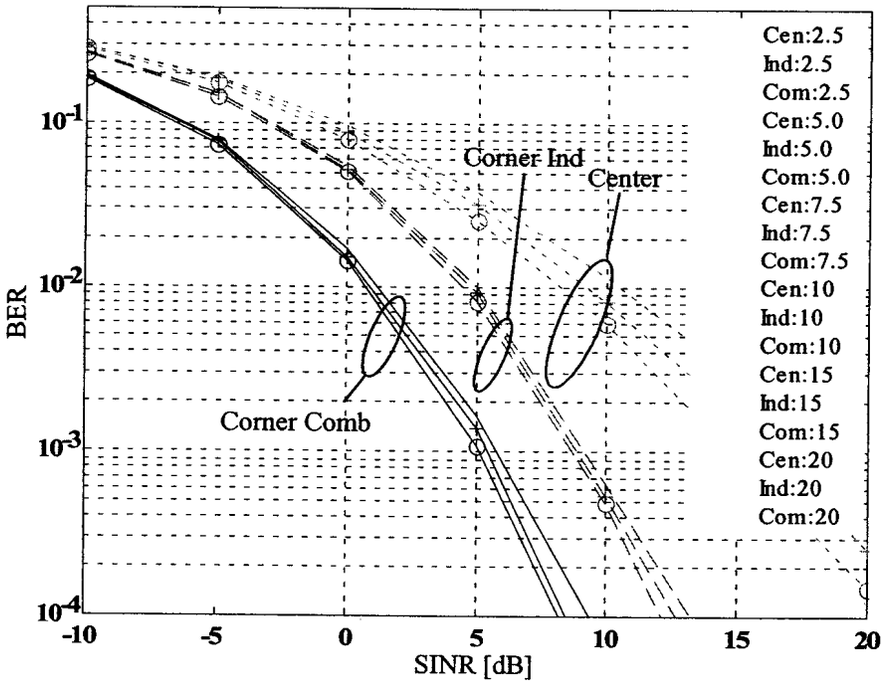

Figure 63: BER as a function of the SINR and angular spread of four element arrays with two equal strength interferers that are 5° offset in angle relative to the desired signal angle.

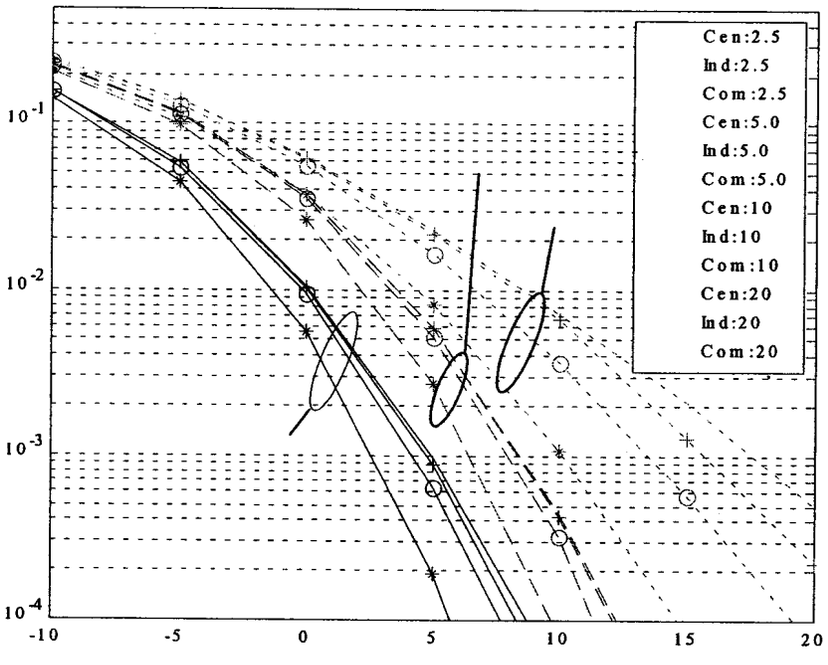

Figure 64: BER as a function of the SINR and angular spread of four element arrays with two equal strength interferers that are 10° offset in angle relative to the desired signal angle.

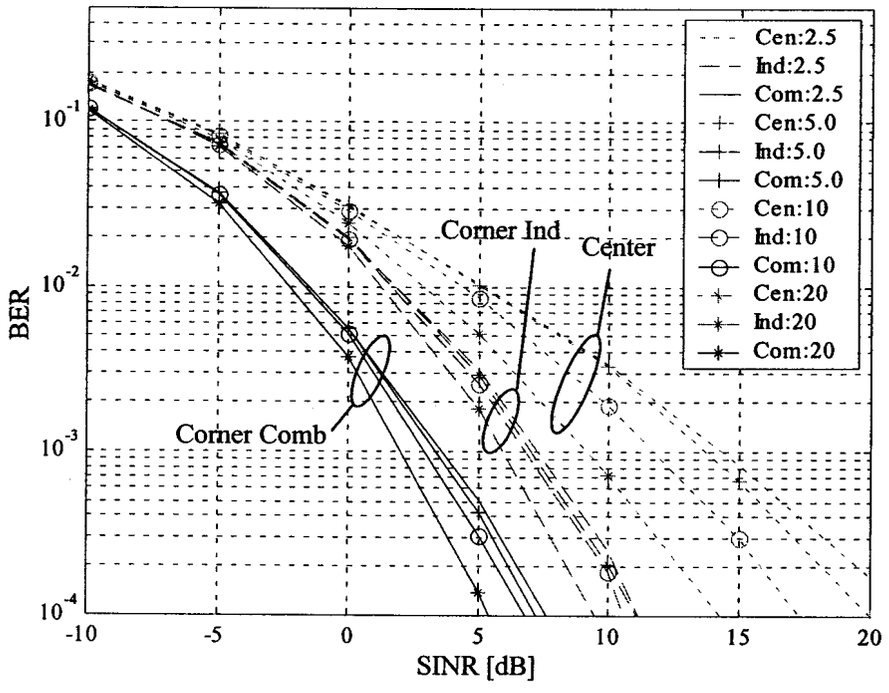

Figure 65: BER as a function of the SINR and angular spread four element arrays with two equal strength interferers that are 15° offset in angle relative to the desired signal angle.

The BER of a single cell with a uniform mobile distribution is shown in Figure 66 for a 2.5° angular spread, and Figure 67 for 5° and 10° angular spreads. The number of array elements is four and two equal strength interferers are present. It can be seen in Figure 66 that the BER is lower for the distributed array with combined beamforming compared to the distributed array with independent beamforming. For example at a SINR of 0dB, the BER of the arrays with combined beamforming is three times lower than the arrays with independent beamforming. The conventional center array has the same BER as the distributed array with independent beamforming, as can be expected. In Figure 67 it is shown that the BER is not significantly affected by angular spread, but it does decrease with larger (5° vs. 10°) angular spreads.

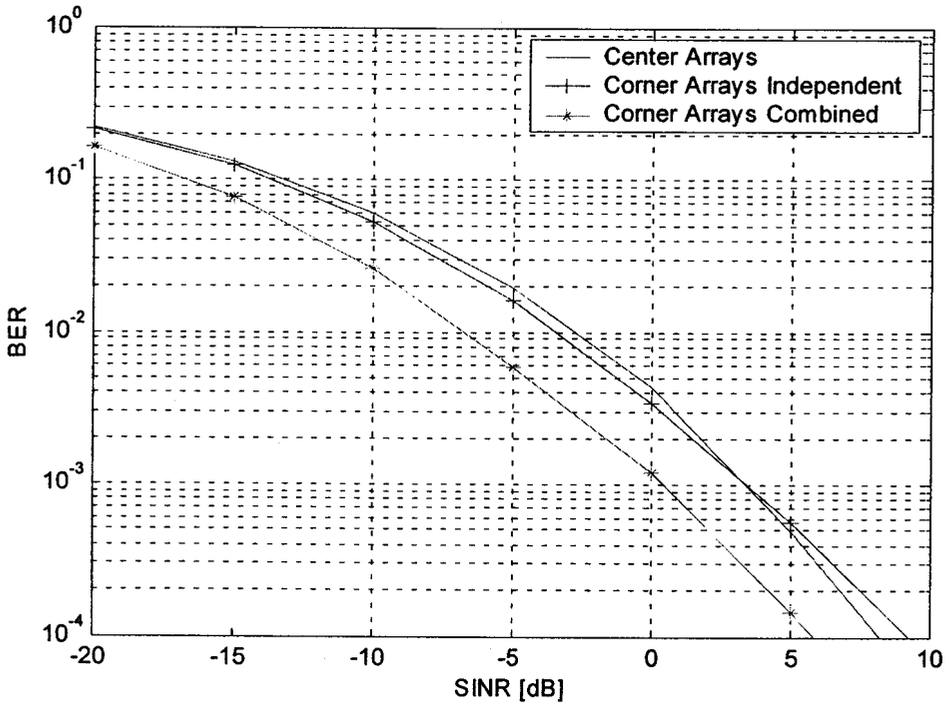

Figure 66: BER as a function of the SINR for conventional center arrays and distributed arrays with independent and combined beamforming with four elements per array and two interferers. The angular spread is 2.5° and the mobile positions is random within the cell.

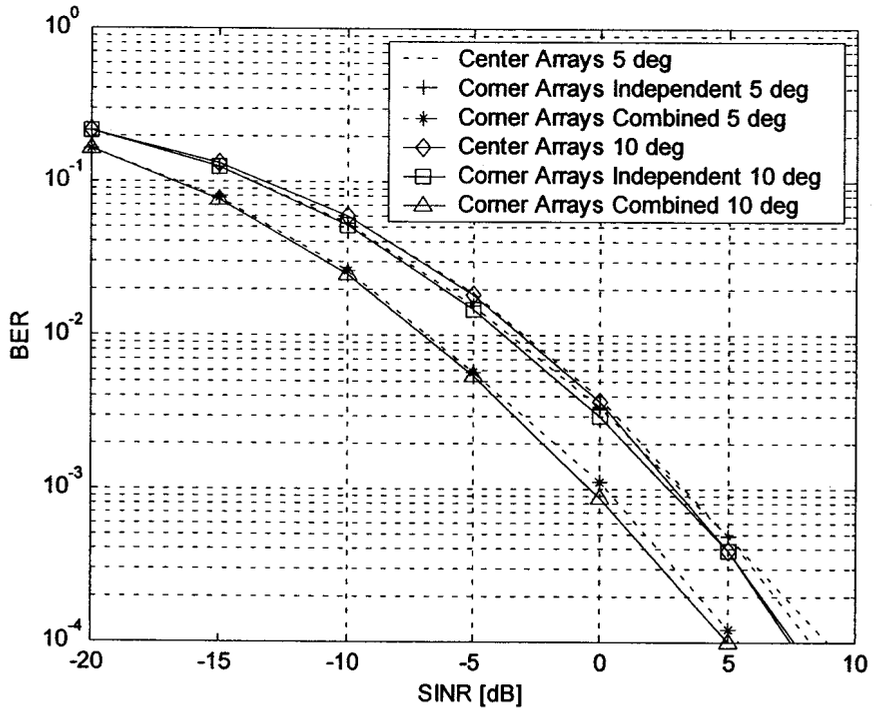

Figure 67: BER as a function of SINR for conventional center arrays and distributed arrays with independent and combined beamforming with four elements per array, two interferers, single cell, 5° and 10° angular spread and mobile positions random within the cell.

6.3.2 Slow Fading

In this section the effect of slow fading on the outage probability of conventional center arrays and corner distributed arrays is examined. The formulation for slow fading is given in section 2.4.2. In order to focus on the effect of slow fading, fast fading will initially be excluded. Slow fading can partially be compensated for by careful control of the basestation and mobile transmit powers. The amount of slow fading compensation in the downlink depends on the maximum available BTS power and mobile sensitivity, and on the uplink on the maximum available mobile transmit power and BTS receiver sensitivity. Slow fading in a multi-basestation configuration (or distributed arrays) can only be compensated for one of the basestations if a single slot in TDMA is used for simultaneous reception by all the basestations. Multi-timeslots can be used to compensate for slow fading to multiple base stations operating in optimum combining mode (see 2.5.4.3).

The effect of fast fading is typically investigated by looking at the bit error rate as was done in the previous section [2,24]. The effect of slow fading is typically investigated by looking at the outage probability [12,38]. The outage probability is the probability that the received SINR is less that a certain protection ratio. The protection ratio is the minimum tolerable carrier to interference ratio for a specific bit error (or frame error) rate performance. The required protection ratio for GSM is 3dB [22].

In order to verify the slow fading method used in this thesis, a Monte-Carlo simulated outage probability result was compared with the outage probability given in [37]. The outage probability for a single element (sectorized) antenna at the center of the cell as well as cell corner distributed sectorized antennas[42] is shown in Figure 68. The slow fading standard deviation is 6dB, the pathloss coefficient is 3.5 and the angular spread is 0°[43]. A network with 37 cells and reuse factor of 3 with one co-channel user per cell was used. In order to compare macro-diversity[44] systems with conventional systems, an interferer

[42] Sectorized antennas located at alternate corners of the cell.
[43] All multipath components have the same incidence angle at the base station antenna.
[44] Macro diversity is a term used for antennas spaced far apart, with uncorrelated (or low correlation) slow fading between then.

activity of 75%[45] was assumed [37]. The outage probability for maximum ratio combing of the corner element signals was calculated based on the approximation given in [37,63]:

$$\mathrm{Prob}_{MRC}(\mathrm{SINR} \le \mathrm{SINR}_o) = \mathrm{Prob}\left(\sum_{\kappa=1}^{3}\mathrm{SINR}_\kappa \le \mathrm{SINR}_o\right) \qquad (191)$$

where SINR_κ is the carrier to interference ratio of corner distributed antenna κ and SINR_o is the protection ratio. The outage probability of combined optimum beamforming of the corner antenna signals (see section 2.7) is also shown in Figure 68. Optimum combining is equivalent to maximum ratio combining in the absence of interferers [2]. Since interferers are present in the calculation, the maximum ratio combining approximation given in [37] is therefore actually an optimum combining approximation.

The calculated results shown in Figure 68 for the center and corner antennas are in close agreement with the results presented in [37], indicating an accurate simulation procedure. In addition, the results indicate a close agreement between the calculated outage probability of optimum combining and maximum ratio combining (which can be expected as described above). It is important to note that the outage probability of a single BTS receiver is higher than that of a multi-BTS optimum combining (or maximum selection) receiver. This is the principle of macro diversity or diversity against shadowing [63]. Macro diversity is used in all CDMA and UMTS systems in handoff (called soft handoff to multi-BTSs as opposed to hard handoff to a single BTS in TDMA systems) [56, page 137, 40]. It is stated in [56, page 137] that the required Eb/No (energy per bit divided by the noise spectral density) is 3dB lower when macro-diversity is applied.

In the next part of this section, the outage probability as a function of the number of antenna elements of conventional center and corner distributed arrays will be investigated. Initially a reuse factor of 3 will be used, with one element per array. Thereafter, the number of users per cell will be increased. This will be followed by an investigation of the outage probability with a cell reuse factor of one and one or more co-channel users per cell.

[45] Means that 25% of the interferers was inactive during each simulation iteration.

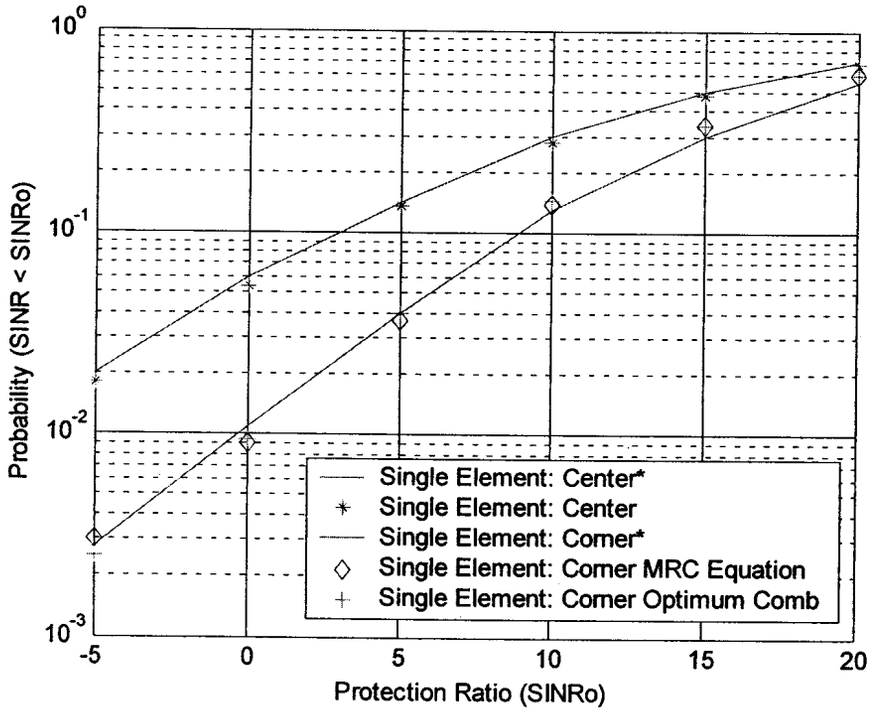

Figure 68: Comparison of simulated outage probability with results in [37] for a single element center antenna as well as corner cell antennas. *From reference [37].

The outage probability for one, two and four element arrays at the center and corners of the cell is shown in Figure 69. The angular spread is 0°, a 37 cell network is used and the reuse factor is 3. The corner array signals are combined in two ways:

1. Optimum beamforming for each corner array followed by approximate optimum combining of all three corner arrays (see equation 191),
2. Full optimum combined beamforming of all three corner arrays,

The results indicate that combined beamforming has a lower outage probability than individual array beamforming. As an example, for an outage probability of 1E-2, combined beamforming requires approximately 2.25dB lower carrier to interference ratio than individual beamforming of the two element arrays and 3.5dB for the four element arrays. In addition, for the same outage probability, the required CIR is approximately 6.5 and 7.0dB lower for the corner arrays with combined beamforming than the conventional array at the cell center, for two and four element arrays respectively.

The outage probability for one same-cell co-channel interferer is shown in Figure 70 for 0° angular spread with 2 and 4 element arrays. Comparing the outage probability in Figure 69 and Figure 70, it can be seen that the outage probability is higher in the case of a co-channel interferer located in the same cell as the desired signal (as can be expected).

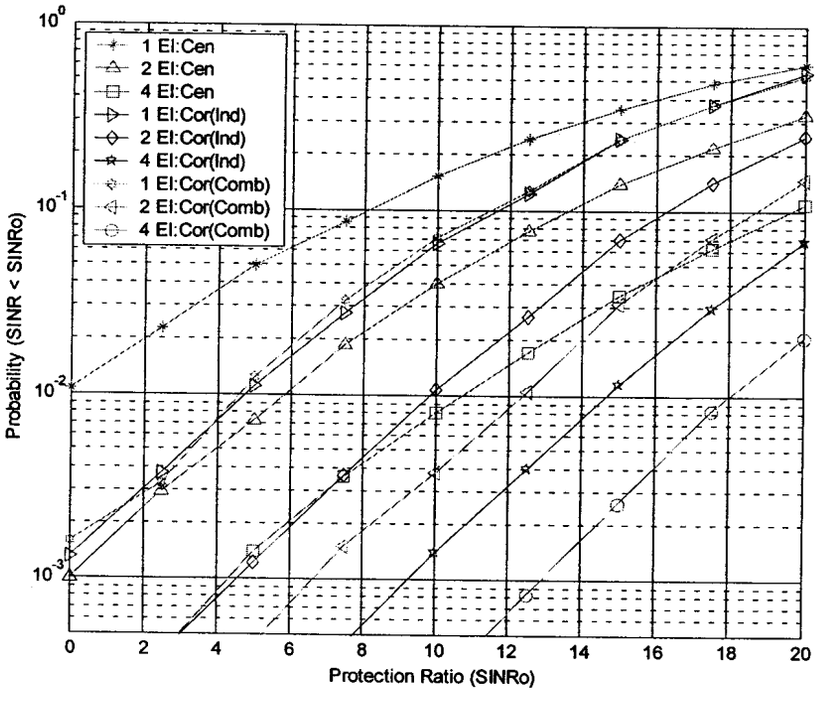

Figure 69: Outage probability as a function of protection ratio for one, two and four element arrays in the center and corners of a cell for a 37 cell network with a reuse factor of three.

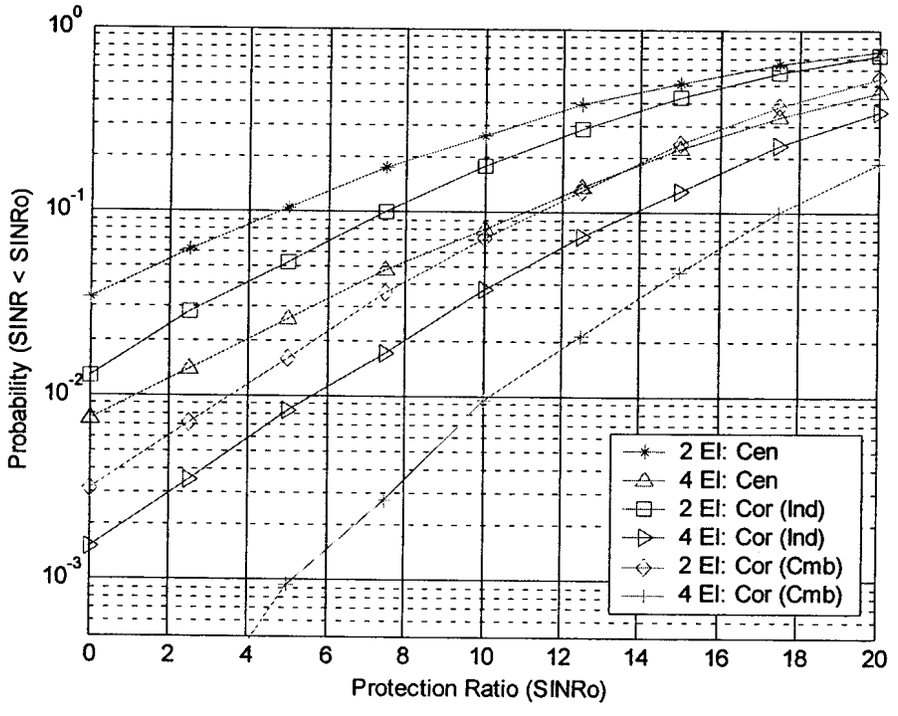

Figure 70: Outage probability as a function of protection ratio and number of elements for center, corner individual and combined beamforming arrays and with one same cell interferer and zero degree angular spread. A 37 cell network with a reuse factor of three is used.

The outage probability for two and four element arrays is shown in Figure 71 for 0° and 5° angular spread and Figure 72 for 5° and 10° angular spread. The figures indicate that there is a slight decrease in the outage probability for 5° angular spread relative to 0°. However the outage probability is similar for the 5° and 10° angular spread cases, indicating that the improvement in outage probability reduces as the angular spread exceeds a certain value (5° in this case).

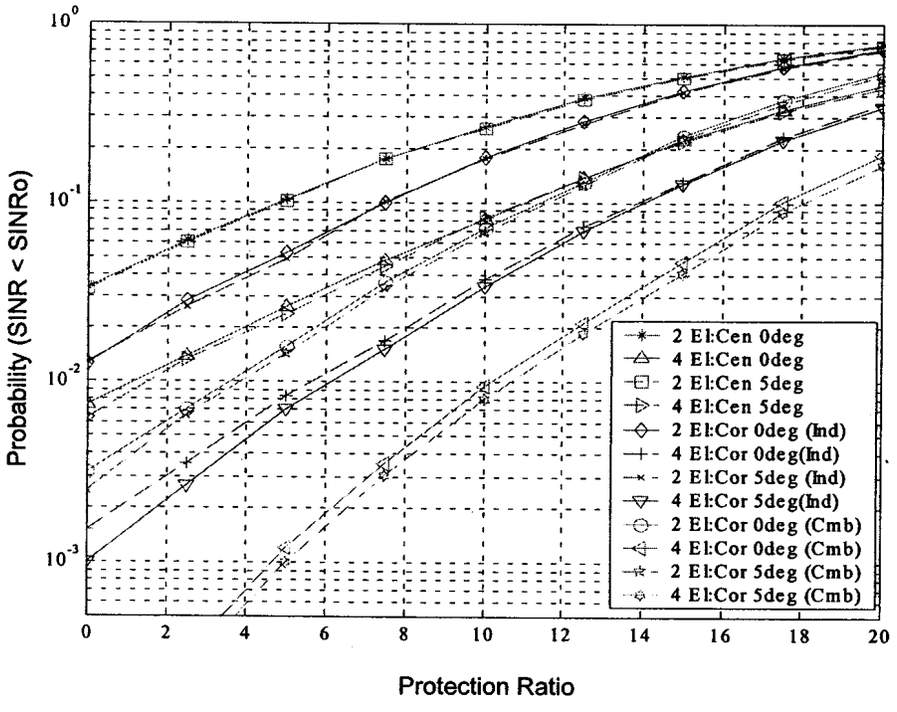

Figure 71: Outage probability as a function of protection ratio, number of elements and angular spread (0° and 5°) for center and corner arrays with independent and combined beamforming with one same-cell interferer. A 37 cell network with a reuse factor of three is used.

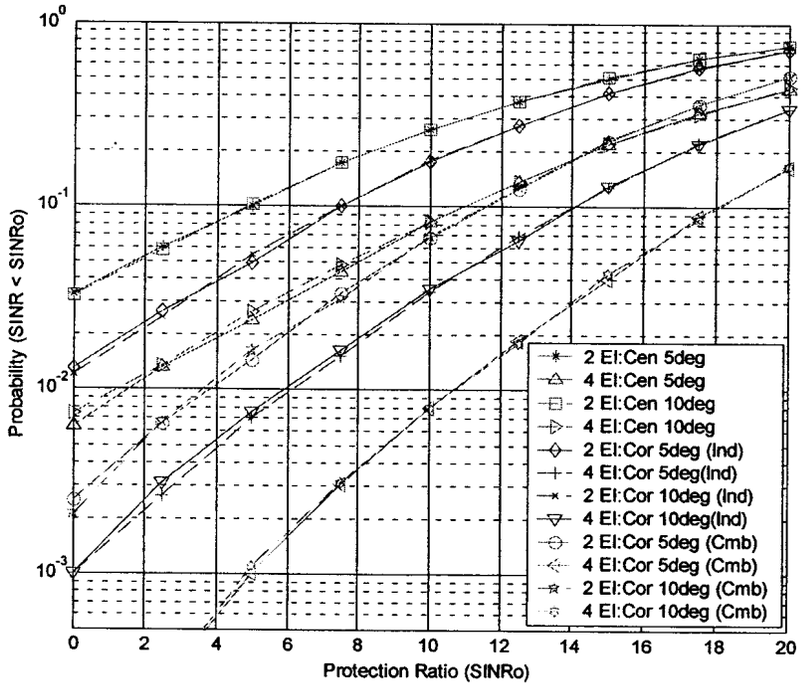

Figure 72: Outage probability as a function of protection ratio, number of elements and angular spread (5° and 10°) for center and corner arrays with independent and combined beamforming with one same cell interferer. A 37 cell network with reuse factor of three is used.

The outage probability as a function of the number of same-cell co-channel interferers (one and two interferers) is shown in Figure 73 for four element arrays and an angular spread of 5°. The figure indicates that the outage probability for the corner arrays with combined beamforming is lower than the outage probability for the center and corner arrays with individual beamforming.

In the case of two interferers and for a 1% outage probability, the combined beamforming array can sustain a protection ratio of 6.5dB vs. 0.8dB for the corner arrays with individual beamforming and –2.5dB for the center arrays.

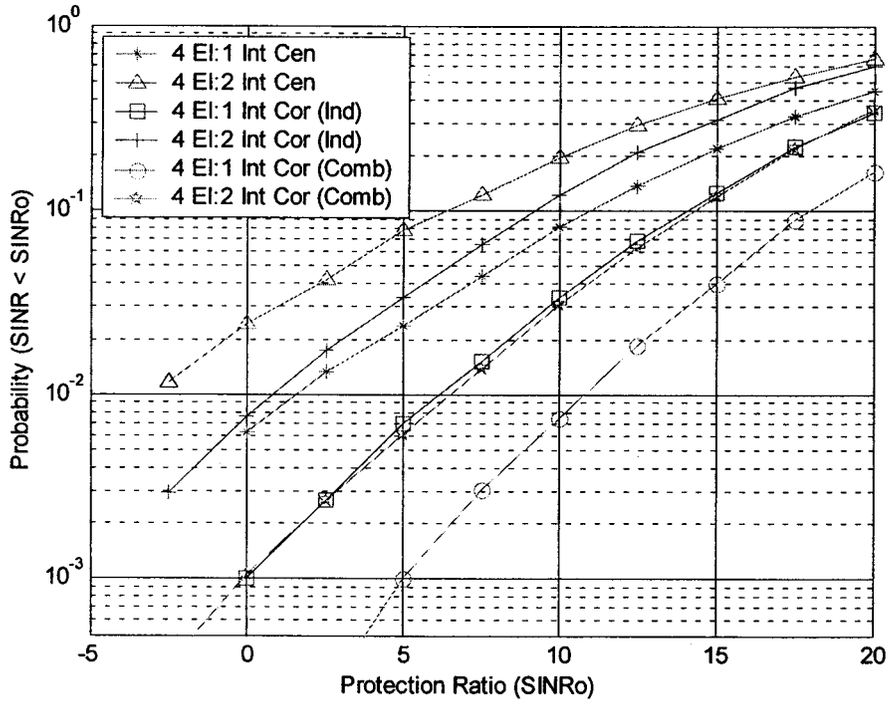

Figure 73: Outage probability as a function of protection ratio, number of same-cell co-channel interferers and array type (center, corner arrays with independent and combined beamforming) with the following conditions: 37 cell network, reuse factor of three, 5° angular spread and four element arrays.

6.3.3 Slow and Fast Fading

In this section the outage probability performance of the array systems in the center (conventional), corner with individual and combined beamforming for both fast and slow fading will be investigated. The loading for the conventional network will be equal to the

networks with arrays at the cell edges[46]. The slow fading standard deviation is 8dB, which is a typical value used in simulations [8,22,42].

According to [22] the average SINR for GSM to provide a reasonable voice quality is 9dB for a Rayleigh fading channel. The required instantaneous SINR of the receiver is 3dB. The simulation results in [22, p.112] show that the outage probability of a conventional three sector GSM system with a reuse of three, slow fading standard deviation of 8dB and pathloss exponent of 3.5 is 2.2%. According to equation 4.4 in [22], the equivalent outage probability (using equation 191) is 20% lower, or approximately 1.83%. A target performance of 2% outage probability is typically required [33, page 1504]. The minimum protection ratio $SINR_0$ that is used in the capacity simulations in [34, p.2057] is 9dB.

The outage probability for one same-cell co-channel interferer is shown in Figure 74 for a four element array and reuse of 3. The shadow fading standard deviation is 8dB and pathloss exponent is 3.5. The power is controlled by the sub-array closest to the mobile (range based power control).

[46] Note that in the previous section the conventional network was loaded 25% lower than the network with base stations at the cell edges [37].

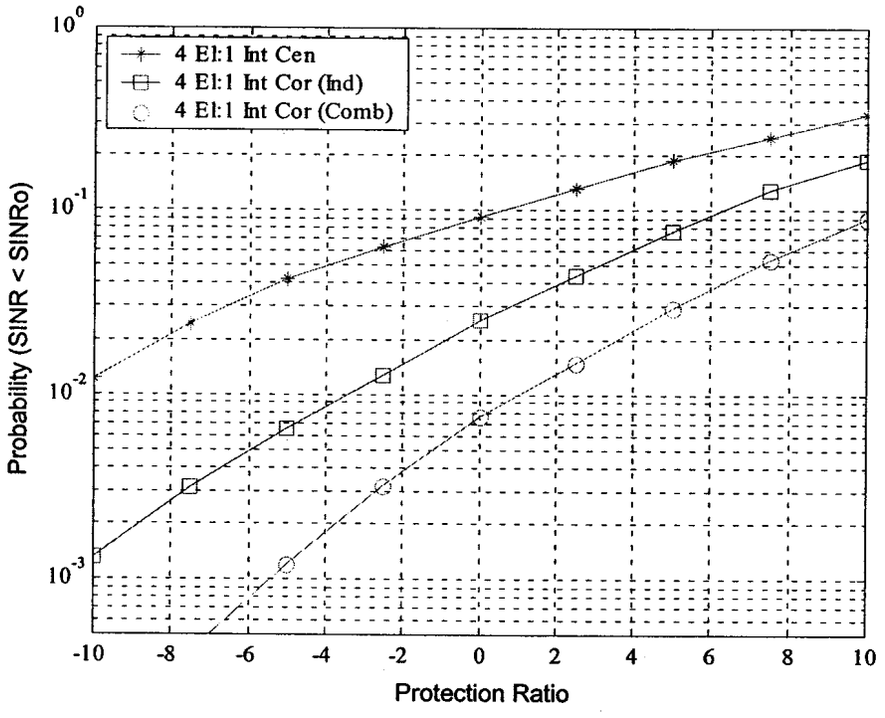

Figure 74: Outage probability as a function of protection ratio and array type (center, corner independent and combined beamforming arrays) with the following conditions: Fast and slow fading, one same-cell co-channel interferer, 4 element arrays, 5° angular spread, 19 cell network, reuse of three and range based power control.

The outage probability as a function of the number of co-channel interferers is shown in Figure 75 for a four element array and reuse of 3. The shadow fading standard deviation is 8dB and pathloss exponent is 3.5. The power is controlled by the sub-array (in the cell containing the desired signal) receiving the maximum signal (receive signal power control). This means that the power of the mobile is adjusted to normalize the slow fading and pathloss between mobile and sub-array receiving the maximum signal. Fast fading power control, such as is used in CDMA, was excluded. Comparing Figure 74 to Figure 75, it can be seen that the outage probability is higher for range based power control. This is because the slow fading is effectively cancelled by increasing the transmit power in received signal based power control.

The results show further that the corner arrays with independent beamforming and two (almost three) same-cell co-channel users (one co-channel interferer) can satisfy the GSM criteria of a protection ratio of 3dB and outage probability of 1.8%. This means that the system capacity is effectively doubled for a reuse of 3. The corner arrays with combined beamforming can support three (almost four) same-cell co-channel users (three co-channel

interferers), thus effectively tripling the capacity for a reuse of 3. The arrays at the cell center is not able to meet the GSM criteria for more than one co-channel same cell user with a four element array.

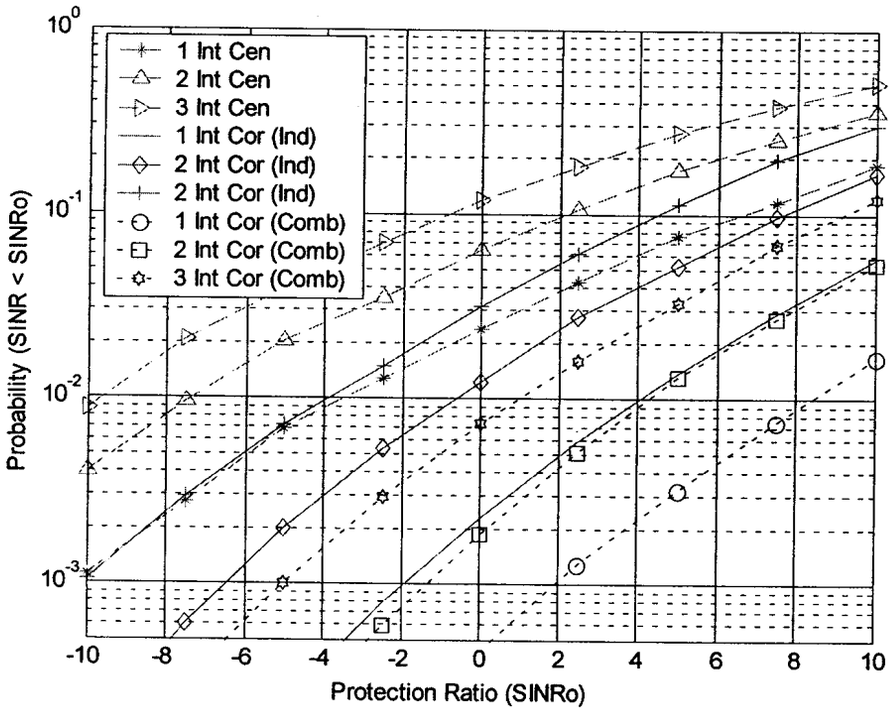

Figure 75: Outage probability as a function of protection ratio and array type (center, corner independent and combined beamforming arrays) with the following conditions: Fast and slow fading, one to three same-cell co-channel interferers, four element arrays, 5 ° angular spread, 19 cell network, reuse of three and received based power control.

The outage probability for a reuse pattern of one and four element arrays for one and two interferers is shown in Figure 76. The same frequency is now reused in all the cells, which leads to an extremely high out of cell interference. This out of cell interference will in turn increase the outage probability (compared to a reuse of 3), which is confirmed by the results in Figure 76. Only the corner array with combined beamforming and one same cell co-channel interferer meets the GSM criteria of outage probability of 1.83% with protection ratio greater than 3dB. This means that with the combined beamforming corner array two same cell co-channel users can be sustained for a four element array, doubling the capacity in a network with a reuse pattern of one.

The outage probability for a reuse pattern of one, six element arrays and one to three interferers is shown in Figure 77. The results indicate that two same cell co-channel users for the corner arrays with independent beamforming and three same cell co-channel users

with the corner arrays with combined beamforming can be supported for the GSM criteria. This is double and triple capacity increases for the corner arrays with independent and combined beamforming, respectively.

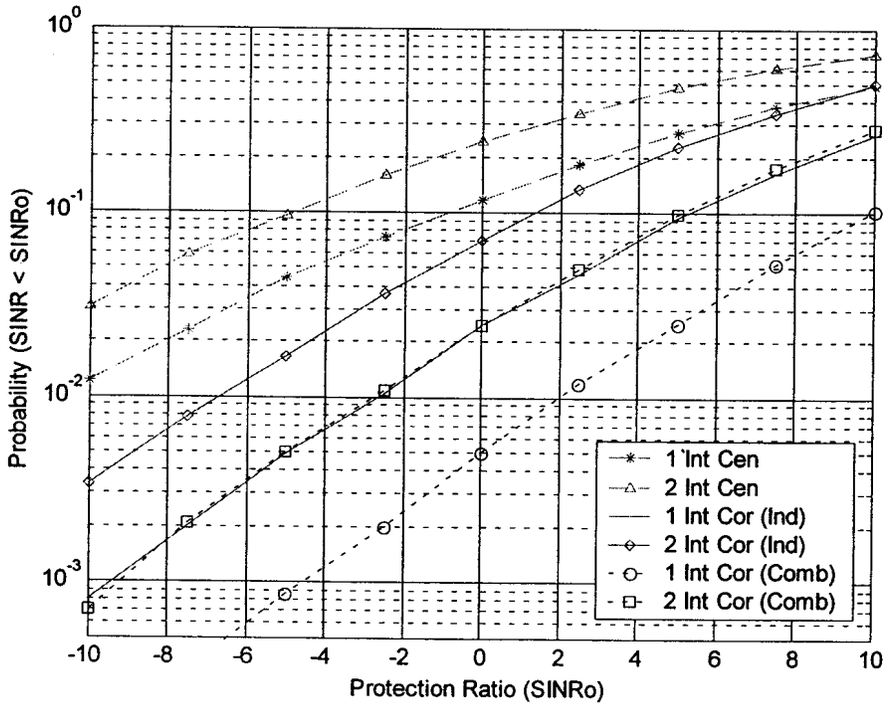

Figure 76: Outage probability as a function of protection ratio and array type (center, corner independent and combined beamforming arrays) with the following conditions: Fast and slow fading, one and two same-cell co-channel interferers, four element arrays, 5° angular spread, 19 cells, reuse factor of one and received based power control.

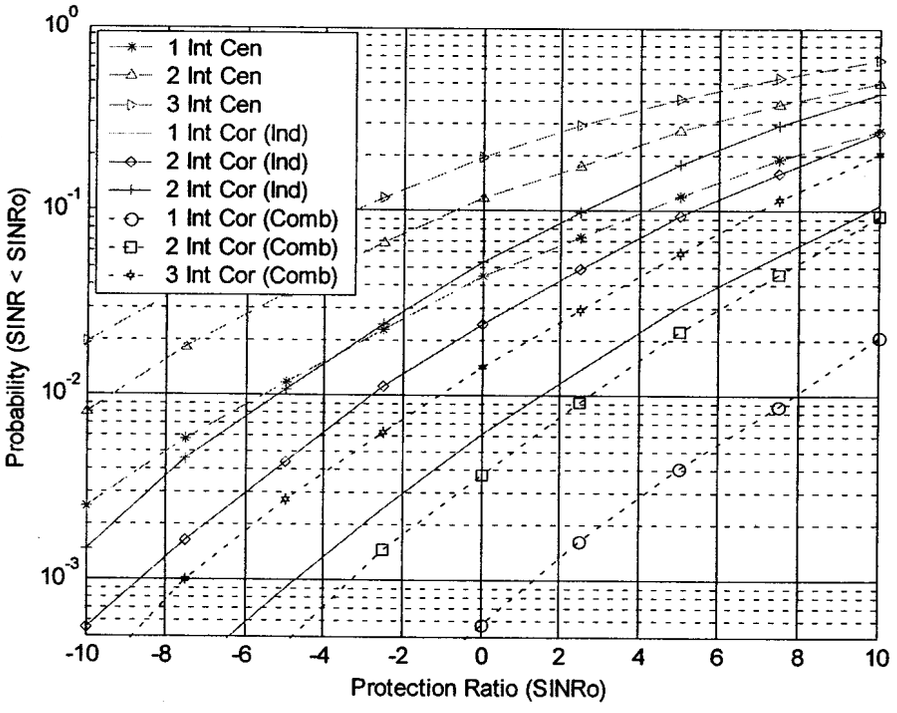

Figure 77: Outage probability as a function of protection ratio and array type (center, corner independent and combined beamforming arrays) with the following conditions: Fast and slow fading, one to three same-cell co-channel interferers, six element arrays, 5° angular spread, 19 cells, reuse factor of one and received based power control).

Thus it is shown how the outage probability is reduced and capacity is increased by increasing the number of array elements. The capacity can be improved further by increasing the number of elements even further. However, practicality limits the maximum array size and thus number of antenna elements. The antenna size is mainly limited by two main factors. Firstly, larger arrays have more wind loading than the single element antennas. Secondly, the antennas are installed on towers and buildings. In order for an operator to get approval to install the antenna, it has to have a minimum visual disturbance. Therefore, operators want to minimize the antenna size. A six element array at 1900MHz is approximately 0.55m wide, which is 3.5 times wider than the standard antenna. This is probably the size limit. Therefore, from a practical point of view the study in this thesis will not cover antenna arrays exceeding 6 elements.

6.4 Conclusions

In this chapter the bit error rate (BER) and outage probability of adaptive arrays was estimated with a Monte-Carlo method as a function of the angular spread, propagation channel model, antenna element spacing, number of interferers and angular separation

between signals. Firstly, it was shown that the BER is reduced significantly in a narrow angular spread environment, if the elements are spaced far apart (5λ vs. 0.5λ), even if the desired signal and the interferers are in the same direction.

The BER (without slow fading) of 0.5λ element spaced conventional arrays and distributed arrays with independent and combined beamforming was compared as a function of the angular spread and separation in angle between the desired signal and the interferers. It was shown that the BER of the distributed array with combined beamforming is lower than the BER of distributed array with independent beamforming, and that the BER reduces as the angular spread increases. The BER of the distributed array with independent beamforming is similar to the BER of the conventional center cell arrays.

The outage probability, including the effect of slow fading, was compared between the distributed array with combined and independent beamforming as well as conventional arrays at the cell center for multiple same-cell co-channel users in a 19 cell network with 0.5λ element spacing. The results indicate that two same cell (frequency reuse of one) co-channel users can be supported by six element distributed arrays with independent beamforming, while three same-cell co-channel users can be supported with a six element distributed array with combined beamforming in a GSM cellular network, where the angular spread is 5°.

7 CDMA DOWNLINK ANALYSIS WITH COMBINED BEAMFORMING ARRAYS

7.1 INTRODUCTION

In chapter 4 corner cell distributed adaptive arrays with combined beamforming of the sub-arrays were compared analytically to independent optimum beamforming of the arrays. It was shown that a higher SINR can be achieved with combined optimum beamforming of all the sub-array signals compared to forming individual optimum beams for each sub-array together with optimum combining of the individual sub-array output signals.

In chapter 1 it was shown that corner cell distributed adaptive arrays with combined beamforming of the sub-arrays can support multiple co-channel interferes in the same cell as the desired user for time division access systems (TDMA) at a lower outage probability than arrays with individual optimum beamforming. The effect of angular spread on the performance of the arrays was also investigated.

A mobile moving between cells in TDMA systems will be given a hard handoff to the cell with the strongest signal[47]. In CDMA systems all users in the network operate on the same frequency channel, but are separated from each other by orthogonal time codes. There is more than one frequency in a CDMA network, but a new frequency will only be used if the capacity of the network on the first frequency is at its maximum. A hard handoff between different frequencies in CDMA is possible, but only in the case where the systems can support it and when the one frequency cannot accept any more calls. In the analysis to follow, handoff to other frequencies is not considered for CDMA systems.

A CDMA mobile constantly monitors the pilots[48] of all cells with a neighbor list supplied to the mobile by the base station. If the signal of one or more base stations is above a certain threshold, the mobile will go into soft handoff with those cells. All base stations

[47] A hard handoff in TDMA systems means that the mobile will retune its receiver to a different frequency channel as directed by the base station handling the call.
[48] Constant power signal transmitted by each base station sector on Walsh code 0, with a unique PN offset for each sector and BTS.

that are in soft/softer handoff[49] with the mobile will transmit equal power (minimum power required to overcome slow fading between mobile and all BTSs in soft handoff) signals to the mobile. The mobile in handoff will then combine all the downlink signals with maximum ratio combining, improving the signal to noise ratio at the mobile compared to the no-handoff case. A mobile experiencing a fade from one of the base stations will most probably not experience a simultaneous fade from the other base stations. This is due to the fact that the base stations are located far apart and therefore the slow fading between BTSs and mobile will be uncorrelated. This gives a diversity gain, called macroscopic diversity [35], allowing the base stations to transmit lower power for a certain signal to noise ratio at the mobile.

In this chapter, it will be investigated whether there is a benefit for the CDMA downlink in combined optimum beamforming of the arrays in soft handoff relative to independent array beamforming of the arrays. The performance will be investigated in terms of the signal to noise ratio as well as outage probability. The basic concept is that the arrays in soft handoff will transmit a reduced signal to the mobiles that are interfered with, since the weights are formed by "looking" at the mobiles from different directions at the same time (see Figure 78). It will be investigated whether this will result in an increase in the overall signal to noise ratio of the mobiles being interfered with when transmitting to a specific mobile.

[49] Term used in CDMA describing mobiles connected to multiple sectors or base stations.

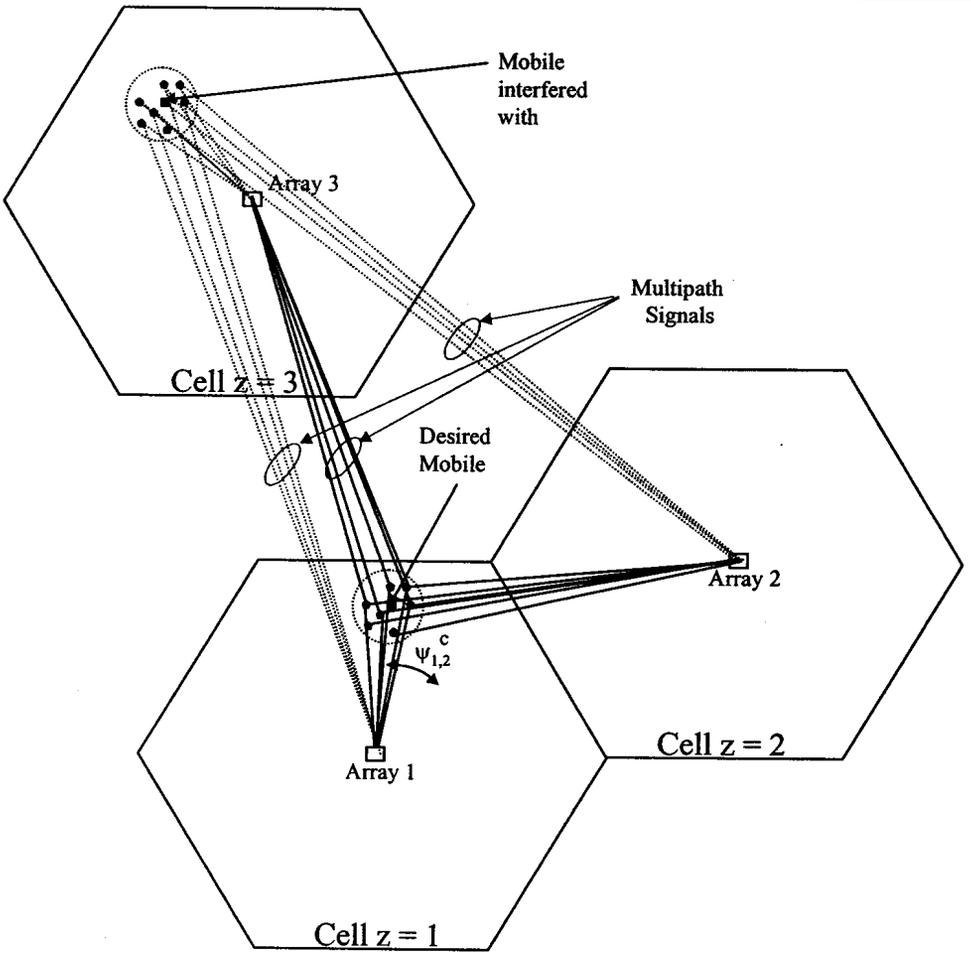

Figure 78: Mobile in soft handoff with three adaptive arrays, showing multipath signals to the desired mobile (solid lines) from the base stations as well as to a mobile being interferer with (dashed lines).

The geometry will be described first in this chapter. This will be followed by formulating the beamforming weight vectors for individual and combined optimum beamforming. The formulation also includes the application of the weight vectors to determine the signal to noise ratio at all the mobiles. This is followed by estimating the SINR of combined and individual beamforming for a three cell network having four mobiles, each in two way handoff, with fixed mobile locations and without fading. Next, the received signal is determined for a seven cell network for both independent and combined beamforming for a mobile in two way soft handoff in a fading environment. This is followed by simulation results for a single iteration as well as outage probability estimation with a Monte-Carlo procedure. Finally, conclusions will be drawn on the performance of independent vs. combined optimum beamforming of the arrays in soft handoff for the CDMA downlink.

7.1 Geometry

It is assumed that the base stations with sectorized or antenna arrays are located at the center of the hexagonal cells[50]. Each base station consists of three 120° sectorized antennas or arrays with a 120° element pattern. The boresight of array in sector 1 is 60°, array in sector 2 is 180° and array in sector 3 is 300° and the radius of each cell is R. The sectors are numbered as shown in Figure 79. The angle relative to the array boresight is ψ and the angle between array (located in cell z_d) boresight and mobile d is $\psi_{z_d,d}$.

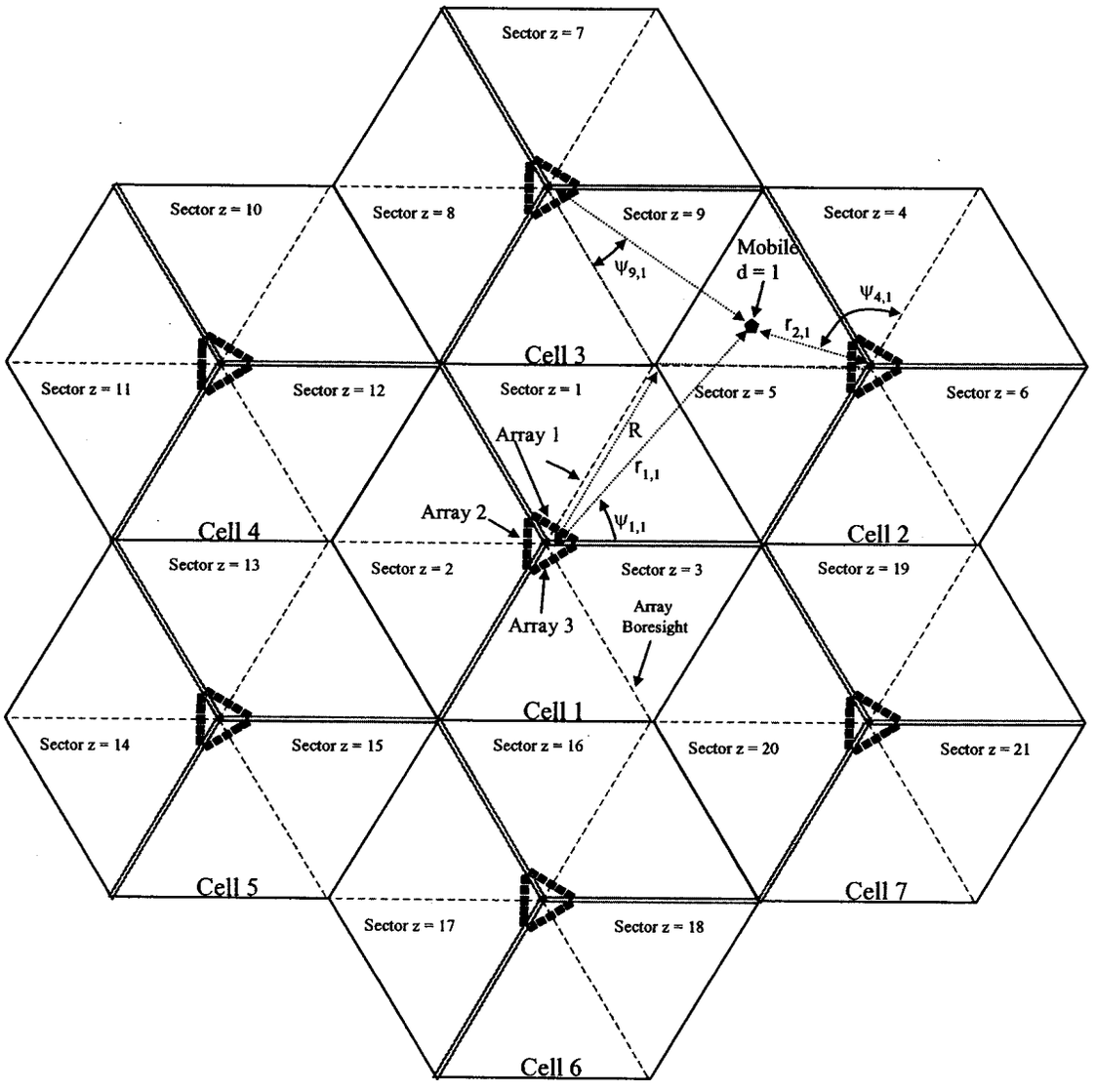

Figure 79: CDMA adaptive array network geometry.

[50] Distributed arrays in the CDMA downlink are located at the cell center, compared to the corner of the cell in the TDMA systems investigated earlier.

7.2 Downlink Formulation

Using the formulation in [30], the received signal $x_{d_{des}}$ at the desired mobile with independent array beamforming is:

$$
\begin{aligned}
x_{d_{des}}(t) = & \sum_{z_{d_{des}}=1}^{Z_{d_{des}}} \Big(\sqrt{P_{d_{des}} G_{z_{d_{des}},d_{des}}}\; b_{d\,des}(t-\tau_{z_{d_{des}},d_{des}})\, c_{d_{des}}(t-\tau_{z_{d_{des}},d_{des}}) \\
& \qquad W^{H}_{z_{d_{des}},d_{des}} U_{z_{d_{des}},d_{des}} \Big) \\
& + \sum_{\substack{d_{ic}=1 \\ d_{ic}\neq d_{des}}}^{D} \sum_{z_{d_{ic}}} \Big(\vartheta_{d_{ic}} \sqrt{P_{d_{ic}} G_{z_{d_{ic}},d_{ic}}}\; b_{d\,ic}(t-\tau_{z_{d_{ic}},d_{ic}})\, c_{d\,ic}(t-\tau_{z_{d_{ic}},d_{ic}}) \\
& \qquad W^{H}_{z_{d_{ic}},d_{ic}} U_{z_{ic},d_{ic}} \Big) \\
& + \sum_{d_{oc}=1}^{D} \sum_{z_{d_{oc}}} \Big(\vartheta_{d_{oc}} \sqrt{P_{d_{oc}} G_{z_{d_{oc}},d_{oc}}}\; b_{d\,oc}(t-\tau_{z_{d_{oc}},d_{oc}})\, c_{d\,oc}(t-\tau_{z_{d_{oc}},d_{oc}}) \\
& \qquad W^{H}_{z_{d_{oc}},d_{oc}} U_{z_{d_{oc}},d_{oc}} \Big) \\
& + n_{d_{des}}(t)
\end{aligned}
\tag{192}
$$

and with combined beamforming is (modification of [30]):

$$
\begin{aligned}
\ddot{x}_{d_{des}}(t) = & \sum_{z_{d_{des}}=1}^{Z_{d_{des}}} \Big(\sqrt{P_{d_{des}} \ddot{G}_{(\cap z_{d_{des}}),d_{des}}}\; b_{d_{des}}(t-\ddot{\tau}_{(\cap z_{d_{des}}),d_{des}})\, \ddot{c}_{d_{des}}(t-\ddot{\tau}_{(\cap z_{d_{des}}),d_{des}}) \\
& \qquad \ddot{W}^{H}_{(\cap z_{d_{des}}),d_{des}} \ddot{U}_{(\cap z_{d_{des}}),d_{des}} \Big) \\
& + \sum_{\substack{d_{ic}=1 \\ d_{ic}\neq d_{des}}}^{D} \Big(\vartheta_{d_{ic}} \sqrt{P_{d_{ic}} \ddot{G}_{(\cap z_{d_{ic}}),d_{ic}}}\; b_{d\,ic}(t-\ddot{\tau}_{(\cap z_{d_{ic}}),d_{ic}})\, c_{d\,ic}(t-\ddot{\tau}_{(\cap z_{d_{ic}}),d_{ic}}) \\
& \qquad \ddot{W}^{H}_{(\cap z_{d_{ic}}),d_{ic}} \ddot{U}_{(\cap z_{ic}),d_{ic}} \Big) \\
& + \sum_{d_{oc}=1}^{D} \Big(\vartheta_{d_{oc}} \sqrt{P_{d_{oc}} \ddot{G}_{(\cap z_{d_{oc}}),d_{oc}}}\; b_{d\,oc}(t-\ddot{\tau}_{(\cap z_{d_{oc}}),d_{oc}})\, c_{d\,oc}(t-\ddot{\tau}_{(\cap z_{d_{oc}}),d_{oc}}) \\
& \qquad \ddot{W}^{H}_{(\cap z_{d_{oc}}),d_{oc}} \ddot{U}_{(\cap z_{oc}),d_{oc}} \Big) \\
& + n_{d_{des}}(t)
\end{aligned}
\tag{193}
$$

where

d_{des} is the desired mobile number,

d_{ic} is the d^{th} mobile in the same sector as the desired mobile,

$Z_{d_{des}}$ is the number of sectors in handoff with the desired mobile,

z_d is the sector number in handoff with mobile d,

$z_{d_{des}}$ is the sector number in handoff with the desired mobile,

$z_{d_{oc}}$ is the handoff sector number of the d^{th} mobile in a sector not containing the desired mobile,

$\bigcap z_d$ is the combination of sectors that the d^{th} mobile is in handoff with,

D is the number of mobiles per sector,

$\vartheta_{d_{ic}}$ is the voice activity factor of mobile d_{ic},

$P_{d_{des}}$ is the desired signal power transmitted from the base stations in handoff,

P_d is the power transmitted from the base station to the d^{th} mobile,

$G_{z_{d_{des}},d_{des}}$ is the path gain between sector $z_{d_{des}}$ and mobile d_{des},

$\ddot{G}_{z_{d_{des}},d_{des}}$ is the combined BF path gain between the sectors $(\bigcap z_{d_q})$ and the mobile d_{des},

$G_{z_d,d}$ is the path gain between sector z_d and mobile d,

$\ddot{G}_{(\bigcap z_d),d}$ is the combined BF path gain between sectors $(\bigcap z_d)$ and mobile d,

b_d is the data bits of mobile d,

c_d is the spreading code of mobile d,

$\tau_{z_d,d}$ is the propagation delay for signals between sector z_d and mobile d,

$\ddot{\tau}_{(\bigcap z_d),d}$ is the combined BF propagation delay for arrays $(\bigcap z_d)$ in handoff with mobile d,

$\mathbf{W}_{z_d,d}$ is the independent array BF weight vector from sector z_d and mobile d,

$\ddot{\mathbf{W}}_{(\bigcap z_d),d}$ is the combined array BF weight vector for arrays $(\bigcap z_d)$ in handoff with mobile d,

$\mathbf{U}_{z_d,d}$ is the array vector in sector z_d transmitting to mobile d,

$\ddot{\mathbf{U}}_{(\cap z_d),d}$ is the combined beamforming array vector for arrays $(\cap z_d)$ in handoff with mobile d,

$n_{d_{des}}$ is the noise power at the desired mobile,

$(\,)^H$ is the complex conjugate transpose.

The received signal at the mobile is now despread with the Walsh code of the desired signal. In the absence of multipath, Walsh codes has the property that signals multiplied by different Walsh codes results in uncorrelated signals in the same sector (where they are completely synchronized) [50]. Multipath causes some correlation between the Walsh codes and thereby increasing the interference to the desired signal from the other users in the same sector. In the simulations to follow, it will be assumed that the Walsh codes remain uncorrelated in the presence of multipath.

After despreading, a RAKE receiver is used at the mobile. The rake receiver will track L multipath signal components separated by multiples of the chip period[51]. The L multipath signal components (called fingers in CDMA) are then coherently combined[52]. A mobile that is in soft handoff with multiple sectors, will receive the same information from all these sectors. The RAKE receiver will search for the L strongest multipath signals from all the sectors in handoff and coherently combine them. The desired component of the received signal (after the RAKE receiver) at the desired mobile with independent array beamforming is:

$$x_{d_{des}}^{des}(t) = g_p\sqrt{P_{d_{des}}}\sum_{\ell=1}^{L}\left|\sqrt{G_{d_{des}}(\ell)}\,b_{d_{des}}\left[t-\tau_{d_{des}}(\ell)\right]\mathbf{W}_{d_{des}}^{H}(\ell)\mathbf{U}_{d_{des}}(\ell)\right| \qquad (194)$$

where g_p is the processing gain and for each multipath component ℓ, $\sqrt{G_{d_{des}}(\ell)}$ is the path gain, $\tau_{d_{des}}(\ell)$ is the delay, $\mathbf{W}_{d_{des}}^{H}(\ell)$ is the weight vector and $\mathbf{U}_{d_{des}}(\ell)$ is the array vector. Without loss of generality, it is assumed that the delays $\tau_{d_{des}}(\ell) = 0$. Equation (194) then becomes:

[51] Walsh codes are spreading codes, and each spreading code bit is called a chip in CDMA.
[52] Added together in phase.

$$x_{d_{des}}^{des}(t) = g_p \sqrt{P_{d_{des}}} \sum_{\ell=1}^{L} \left| \sqrt{G_{d_{des}}(\ell)}\, b_{d_{des}}(t)\, \mathbf{W}_{d_{des}}^{H}(\ell)\, \mathbf{U}_{d_{des}}(\ell) \right| \tag{195}$$

The desired component of the received signal at the desired mobile with combined beamforming is:

$$\ddot{x}_{d_{des}}^{des}(t) = g_p \sqrt{P_{d_{des}}} \sum_{\ell=1}^{L} \left| \sqrt{\ddot{G}_{d_{des}}(\ell)}\, b_{d_{des}}(t)\, \ddot{\mathbf{W}}_{d_{des}}^{H}(\ell)\, \ddot{\mathbf{U}}_{d_{des}}(\ell) \right| \tag{196}$$

The background noise is generally well below the total power received by the mobile and may therefore be ignored [30]. The interference component of the received signal at the desired mobile with independent array beamforming is:

$$x_{d_{des}}^{int} = \sum_{d_{oc}=1}^{D} \sum_{z_{d_{oc}}} \vartheta_{d_{oc}} \sqrt{P_{d_{oc}}\, G_{z_{d_{oc}}, d_{qoc}}}\; \mathbf{W}_{z_{d_{oc}}, d_{oc}}^{H}\, \mathbf{U}_{z_{oc}, d_{oc}} \tag{197}$$

and with combined array beamforming:

$$\ddot{x}_{d_{des}}^{int} = \sum_{d_{oc}=1}^{D} \vartheta_{d_{oc}} \sqrt{P_{d_{oc}}\, \ddot{G}_{(\cap z_{d_{oc}}), d_{oc}}}\; \ddot{\mathbf{W}}_{(\cap z_{d_{oc}}),\, d_{oc}}^{H}\, \ddot{\mathbf{U}}_{(\cap z_{d_{oc}}), d_{oc}} \tag{198}$$

Individual array beamforming weights can be determined with the feedback method from each array in soft handoff separately (see section 7.4). Combined array weights can be determined with the feedback method from all arrays in soft handoff as one large array. The weights of the combined arrays in handoff will be adapted such that the signals from all three base station arrays will add coherently at the mobile. The RAKE fingers are then determined from the multipath signals (separated by more than one chip period) arriving at the mobile from the combined array.

The ℓ^{th} component of the weight vector for the individual array beamforming $\mathbf{W}_{z_d, d}$ (determined with the feedback method as described in section 7.4) is given by:

$$\mathbf{W}_{z_d, d}(\ell) = \frac{M \mathbf{R}_{z_d}^{-1}(\ell)\, \mathbf{U}_d(\ell)}{\mathbf{U}_d^{T}(\ell)\, \mathbf{R}_{z_d}^{-1}(\ell)\, \mathbf{U}_d(\ell)} \tag{199}$$

where $\mathbf{R}_{z_d}^{-1}(\ell)$ is the inverse of the co-variance matrix for each individual array z_d in handoff to the mobile d, and $\mathbf{U}_d(\ell)$ is the array vector towards the signal d for the ℓ^{th}

multipath component. The array is multiplied by the number of elements, in order to compare it to the sectorized case, i.e. the array gain is not part of the normalization. The array vector of signal d for the ℓ^{th} multipath component is:

$$\mathbf{U}_d(\ell) = 1,\ e^{j\pi \sin \psi_{z_d,d}(\ell)},\ e^{j2\pi \sin \psi_{z_d,d}(\ell)},\ldots,e^{j(M-1)\pi \sin \psi^c_{z_d,d}(\ell)} \tag{200}$$

The ℓ^{th} component of the weight vector for the combined array $\ddot{\mathbf{W}}^H_{(\cap z_d),d}$ that mobile d is in handoff with is:

$$\ddot{\mathbf{W}}^H_{(\cap z_d),d}(\ell) = \frac{M N_{z_d} \ddot{\mathbf{R}}^{-1}_{(\cap Z_d)}(\ell)\ \ddot{\mathbf{U}}_d(\ell)}{\ddot{\mathbf{U}}^T_d(\ell) \ddot{\mathbf{R}}^{-1}_{(\cap z_d)}(\ell) \ddot{\mathbf{U}}_d(\ell)} \tag{201}$$

where $\ddot{\mathbf{R}}^{-1}_{(\cap z_d)}$ is the inverse of the co-variance matrix of the combined arrays $(\cap z_d)$ in soft handoff with the mobile. The array weight contains the array gain relative to the sector antenna, where N_{z_d} is the number of arrays in handoff with mobile. The covariance matrix for independent array beamforming is:

$$\mathbf{R}_{z_d,d} = E\left[\mathbf{X}_{z_d}\ \mathbf{X}^H_{z_d}\right] \tag{202}$$

where $\mathbf{X}_{z_d}$ are the signals at elements of array z_d, given by:

$$\mathbf{X}_{z_d}(t) = \sum_{\substack{d=1 \\ d \neq d_{des}}}^{D} \sqrt{G_{z_d}}\left\{b_d(t)\, c_d(t)\right\}\left[1,\ e^{j\pi \sin \psi^c_{z_d,d}},\ e^{j2\pi \sin \psi^c_{z_d,d}},\ldots,e^{j(M-1)\pi \sin \psi^c_{z_d,d}}\right] + \mathbf{n}_{z_d} \tag{203}$$

Inserting (203) in (202) and using the fact that the spreading codes of the mobiles are orthogonal over a certain time period, the covariance matrix can be written as (see Appendix A):

$$\mathbf{R}_{z_d,d} = \sum_{\substack{d=1 \\ d \neq d_{des}}}^{D}\left[\sqrt{G_{z_d}}\left\{\mathbf{U}_d\ \mathbf{U}^H_d\right\}\right] + \sigma^2_N\, \mathbf{I} \tag{204}$$

where σ^2_N is the noise power at the array elements and $\mathbf{I}$ is the unity vector. The covariance matrix for combined array beamforming is:

$$\ddot{\mathbf{R}}_{(\cap z_d),d} = E\left[\ddot{\mathbf{X}}_{z_d}\ \ddot{\mathbf{X}}_{z_d}^{H}\right] \tag{205}$$

where $\ddot{\mathbf{X}}_{(\cap z_d)}$ are the signals at elements of the combined array $\cap z_d$, given by:

$$\ddot{\mathbf{X}}_{(\cap z_d)}(t) = \sum_{\substack{d=1 \\ d\neq d_{des}}}^{D} \sqrt{G_{(\cap z_d),d}}\{b_d(t)\ c_d(t)\}[1,\ e^{j\pi\sin\psi^c_{z_d,d}},\ e^{j2\pi\sin\psi^c_{z_d,d}},\ldots,$$

$$e^{j(M-1)\pi\sin\psi^c_{z_d,d}},\ 1,\ e^{j\pi\sin\psi^c_{z_d,d}},\ e^{j2\pi\sin\psi^c_{z_d,d}},\ldots,\ e^{j(M-1)\pi\sin\psi^c_{z_d,d}},\ldots] \tag{206}$$

$$+\ \mathbf{n}_d$$

which can be written as:

$$\ddot{\mathbf{X}}_{(\cap z_d)}(t) = \sum_{\substack{d=1 \\ d\neq d_{des}}}^{D}\left[\sqrt{G_{(\cap z_d),d}}\{b_d(t)\ c_d(t)\}\ \ddot{\mathbf{U}}_{(\cap z_d)}\right] + \mathbf{n}_d \tag{207}$$

where $\mathbf{U}_{(\cap z_d)}$ is the concatenated vector of all the array vectors $\cap z_d$ that are in soft handoff with the mobile d. Inserting (207) in (205), and using the fact that the spreading codes (Walsh codes) of the mobiles are orthogonal over a certain time period, the covariance matrix for combined beamforming can be written as (see Appendix B):

$$\ddot{\mathbf{R}}_{(\cap z_d),d} = \sum_{\substack{d=1 \\ d\neq d_{des}}}^{D}\left[G_{(\cap z_d),d}\left\{\ddot{\mathbf{U}}_{z_d}\ \ddot{\mathbf{U}}_{z_d}^{H}\right\}\right] + \sigma_N^2\ \mathbf{I} \tag{208}$$

7.3 Power Control of Mobiles

A signal transmitted to mobile d will interfere with all other mobiles located within the angular bounds of the sector in handoff with mobile d. This will reduce the signal to noise ratio of the mobiles interfered by the signal of mobile d. On the other hand, signals are also transmitted at the same time to other mobiles from other sectors, thereby interfering with mobile d and reducing its signal to noise ratio. In order to maintain adequate SINR at all mobile, tight power control is required in a CDMA network.

Power control as implemented in this thesis is based on an iterative procedure. Initially the power for all mobiles is equalized. The mobile with the worst signal to noise ratio is then determined (say mobile d_5). The mobiles interfering with the mobile d_5 is then sorted in

terms of interference power received at mobile d_5. The power of the strongest interferer (say mobile d_8) is then reduced by a certain fixed amount only if the SINR of the interfering mobile d_8 after this power adjustment is above the desired SINR threshold. The power of the other interfering mobiles is then reduced in turn only if the SINR of the mobiles after power adjustment is above the desired SINR threshold. After the power of all the mobiles interfering with d_5 has been appropriately adjusted, the SINRs of all the mobiles are determined using the newly calculated power. The mobile with the lowest SINR is again determined and the power adjustment procedure for all the mobiles interfering with this mobile is repeated. The procedure is repeated a number of times until the SINR of all mobiles are above the threshold or the maximum number of iterations has been reached. If the maximum number of iterations has been reached, it normally means that the power of the interferers can no longer be adjusted without reducing the SINR of the interferers below the SINR threshold. In this case, some mobiles may have a SINR that is below the required SINR, resulting in an outage

7.4 Downlink Propagation Channel Array Signal Matrix Estimation

In order to transmit a maximum signal from the base station to the desired mobile while minimizing the interference to the other mobiles, the downlink propagation channel array signal matrix is required. The channel signal vector of array z to mobile d is $\mathbf{X}_{z_d}$. The complex channel signal matrix of array z is the assembly of all the channel vectors for all the mobiles, given by:

$$\mathbf{X}_z = \left\{\mathbf{X}_{z_1}, \mathbf{X}_{z_2}, ..., \mathbf{X}_{z_D}\right\} \tag{209}$$

The downlink propagation channel array signal matrix cannot be determined from the uplink information, as the uplink and downlink are not reciprocal (scattering behavior is different) due to a relatively large duplex frequency separation[53] [30].

In [14] a method is presented whereby the complex array signal matrix can be measured, providing a complete response to all reflections and scattering in the propagation channel between the base station array and the mobile. The downlink channel signal matrix is measured using feedback from the mobiles. There are two modes of operation. The regular

data mode and the probing mode. During the probing mode, the regular data information to the mobile is temporarily halted while the propagation channel is measured. Each element of the array is excited in turn with a probing signal, agreed on by the transmitter and the mobiles. Each mobile measures the relative amplitude and phase response of the probing signals. The probing signals are orthogonal to each other (signals can be separated in time or transmitted together on different orthogonal codes), so that each probing signal channel response can be measured independently by the mobiles. After measuring the complex channel response at each mobile, the measurements are fed back to the base station on the reverse channel. The channel response matrix can then be used during the regular data mode to transmit to the mobiles. This method requires a large amount of information to be transmitted by the mobile back to the base station on the reverse channel.

An alternative approach, minimizing the feedback data on the reverse link, is presented in [44]. This method is well suited to CDMA systems. The received signal at time sample $i \in \{1,2,\ldots,\infty\}$ at each mobile is correlated with its own Walsh code to obtain signal $v_d(i)$, $d=\{1,2,..,D\}$. Nonlinear processing is applied to $v_d(i)$ to extract the hard limited (+ 1 and –1) transmitted information bits $b_d(i)$. A scalar error between $v_d(i)$ and $b_d(i)$ is then determined. If this error is above a certain threshold value, it will be fed back to the BTS, in order to minimize the error signal information traffic. The base station will then recursively update its adaptive array transmit weight matrix, and thereby achieve the optimum downlink signal to noise ratio at each mobile. Various recursive update methods can be used, such as the least squared or BEACON method proposed in [44]. The propagation channel vector for each mobile at the minimum error is then proportional to the conjugate of the weight vector. Another very important advantage of this method is that the transmit weight matrix is updated while the downlink data is being transmitted, thereby not disturbing the live mobile traffic.

The above methods require that the propagation channel is slow varying with respect to the data rate, i.e. the fading rate is much lower than the data rate. This is applicable to narrowband CDMA systems. It should be noted here that existing mobiles does not contain the functionality to determine the error and transmit it back to the base station. This may be

[53] 60 MHz for 1900 MHz North American cellular systems.

incorporated in a special or dedicated error feedback channel (i.e., Walsh code) required on the reverse link.

7.5 Simulation Results

In this section simulation results for stationary mobiles without fading and power control is presented. This is followed by the received signal at mobiles in a seven cell network with fading included. Finally, Monte-Carlo simulation results for the outage probability of mobiles in a 19 cell network is compared between conventional, independent and combined beamforming of the arrays in handoff.

7.5.1 Stationary Mobiles without Fading and Power Control

In this section the SINR of three downlink adaptive arrays with independent beamforming is compared to three adaptive arrays with combined beamforming under stationary mobile conditions and without fading or power control. The geometry is shown in Figure 80. Four stationary mobiles are assumed with positions as given in Table 11. The signal to noise ratio is 15dB. The element pattern shown in Figure 8 is used. The boresight directions relative to the x-axis are 60°, 180° and 300° for arrays 1-3, respectively.

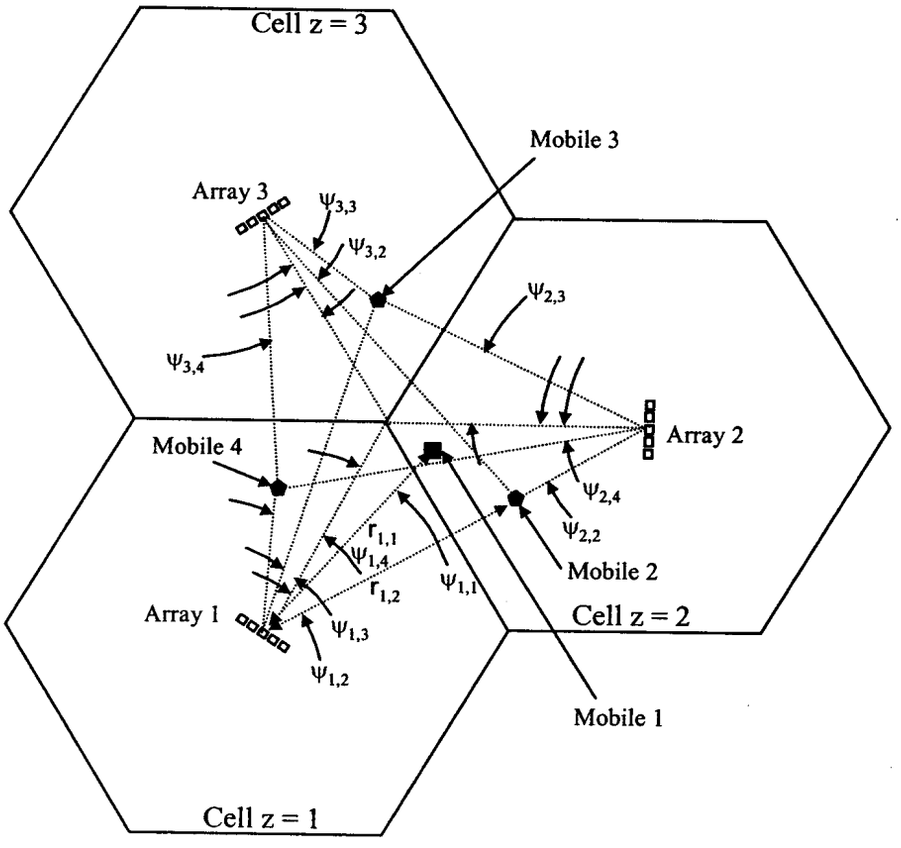

Figure 80: Geometry of three arrays and four stationary mobiles.

Table 11: Locations of the mobiles.

Mobile Number	Angle $\psi_{1,d}$ between array 1 boresight and mobile [degree]	Range $r_{1,d}$ between array 1 and mobile [relative to radius R]
1	15	R
2	40	0.87 R
3	-10	1.50 R
4	-45	0.87 R

7.5.1.1 Three Element Arrays

The received signal across the three cells for the SINR optimization of mobile 1 is shown in Figure 81 with individual array beamforming, and Figure 82 with combined array beamforming. It can be seen that the individual beamforming array is not able to reduce the signal towards all three interferers, while the combined beamforming arrays creates deep nulls in the vicinity of all interferers. The calculated signal to noise ratios for all four mobiles are given in Table 12 for individual and combined beamforming. The SINR is

optimized for each of the four mobiles. The array signals are combined at the mobile with maximum ratio combining.

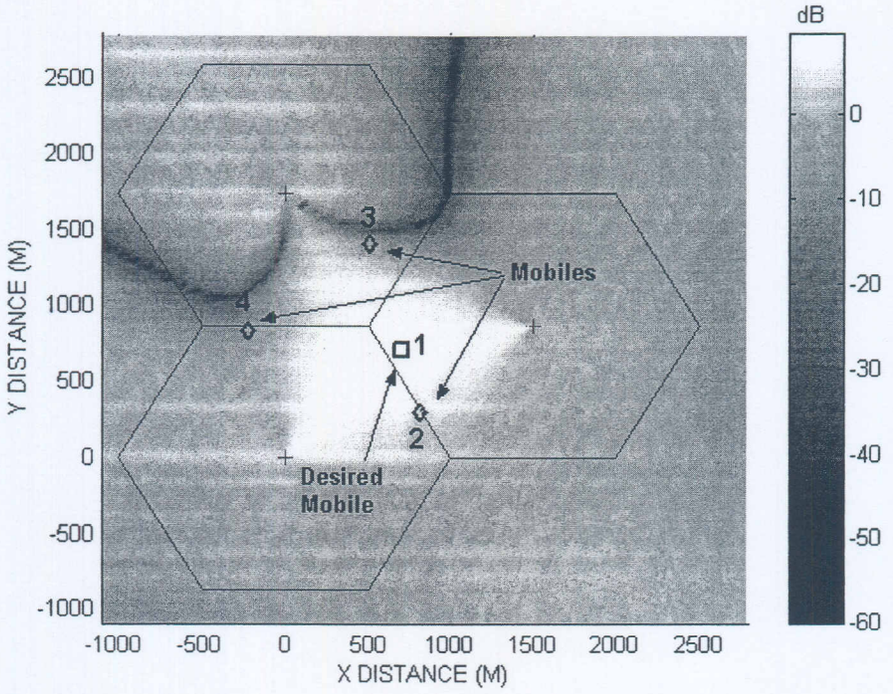

Figure 81: Received signal over three-cell network area for individual beamforming with three element arrays.

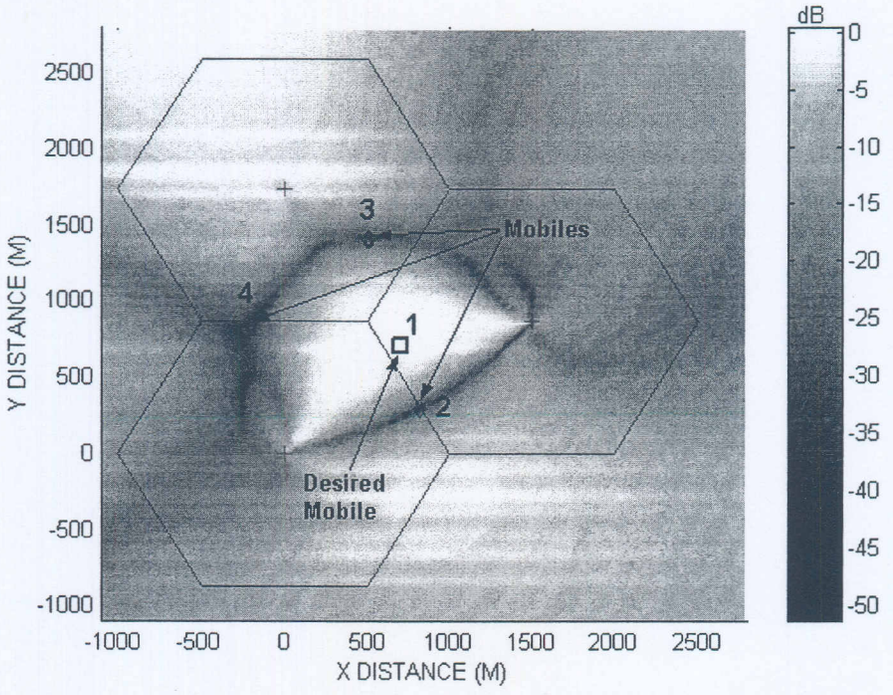

Figure 82: Received signal over three-cell network area for combined beamforming with three element arrays.

Table 12: SINRs at each mobile for independent vs. combined beamforming of three element arrays.

Beamforming method	Mobile 1 SINR [dB]	Mobile 2 SINR [dB]	Mobile 3 SINR [dB]	Mobile 4 SINR [dB]
Independent	-3.56	11.41	20.94	20.59
Combined	30.42	33.5	40.86	36.3

The independent beamforming arrays do not have enough resolution to separate the mobiles in angle, and therefore the SINRs for the independent beamforming arrays is low for mobiles 1 and 2 that are located close in angle. However, the SINRs at the mobiles with combined beamforming arrays are much higher (above 30dB).

7.5.1.2 Five Element Arrays

The received signal across the three cells for SINR optimization of mobile 1 is shown in Figure 83 for individual array beamforming, and Figure 84 for combined array beamforming with five element arrays. It can be seen that the both beamforming schemes creates deep nulls in the vicinity of the interferers. The signal to noise ratios for all four mobiles are shown in Table 13 for individual and combined beamforming.

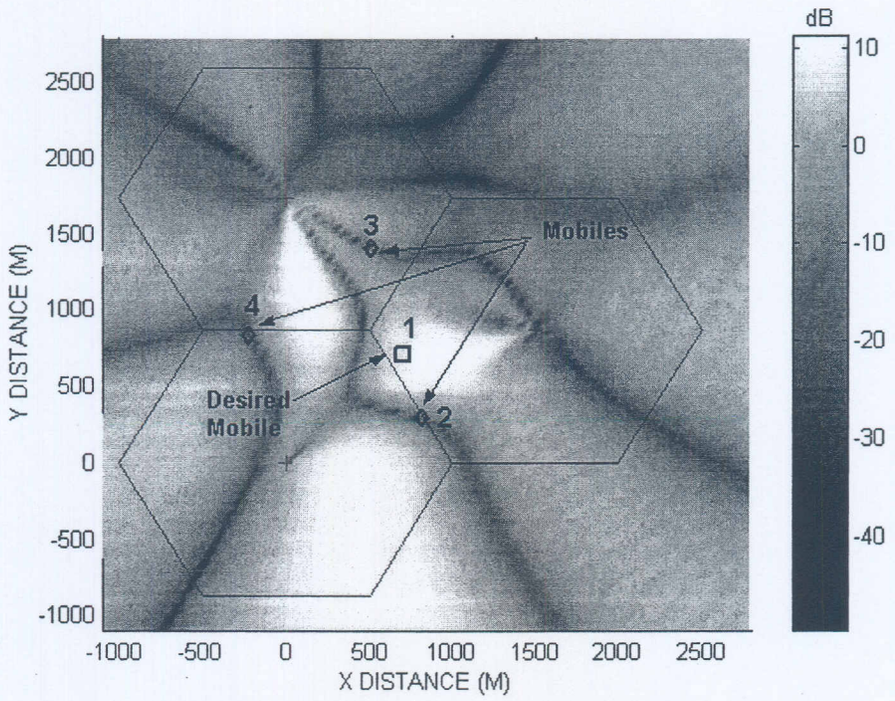

Figure 83: Received signal all over three-cell network area for individual beamforming with five element arrays.

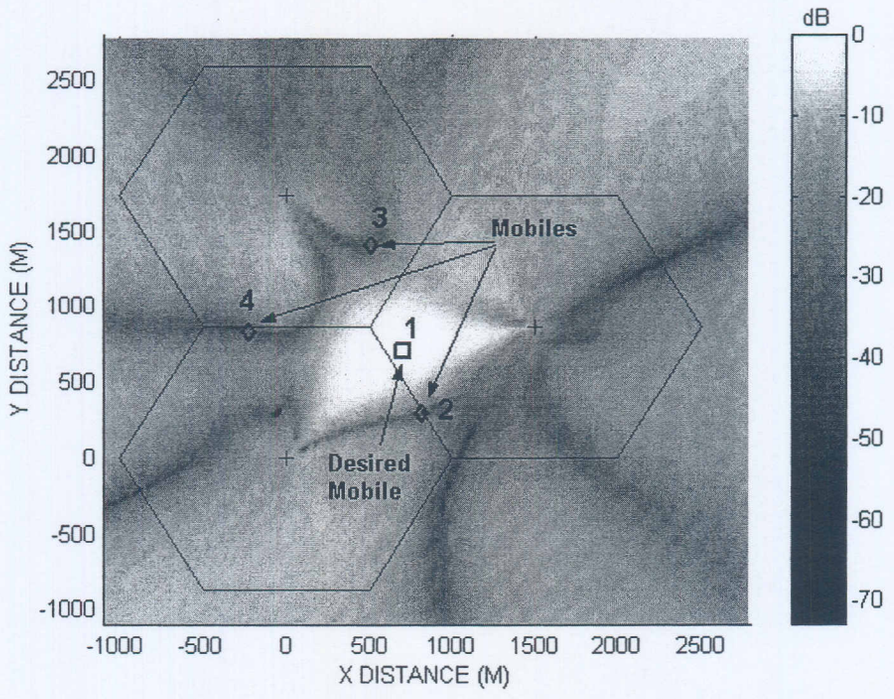

Figure 84: Received signal all over three-cell network area for individual beamforming with five element arrays.

Table 13: SINR at each mobile for independent vs. combined beamforming with five element arrays.

Beamforming method	Mobile 1 SINR [dB]	Mobile 2 SINR [dB]	Mobile 3 SINR [dB]	Mobile 4 SINR [dB]
Independent	37.81	37.9	39.7	41.8
Combined	44.4	37.9	42.5	39.5

In this case (five element arrays) the independent beamforming array resolution is sufficient to separate the mobiles in angle, and thus the SINRs of the independent beamforming arrays are all high. However, the SINRs of the independent beamforming arrays are generally lower (except for one mobile) than the combined beamforming array.

7.5.2 Received Signal Across Seven Cell Network With Fading Included

In this section an example of the received signal at all locations across a seven cell network is presented. The SINR is optimized for mobile 1, which is in a two-way handoff with sectors 1, 5 and 20. Rayleigh fading for each of the L multipath components is assumed

and the incidence angles from the mobiles to all base station sectors are calculated based on the model in section 2.4. The simulation parameters are given in Table 14 and the array element pattern is shown in Figure 85. The received signal is shown in Figure 86 for independent beamforming and Figure 87 for combined beamforming.

There are one mobile per sector in this example, with the locations of the mobiles indicated in the figures. Since the signal at the desired mobile (mobile 1) is optimized, the received signal at this mobile must be high. On the other hand, the signals at the other mobiles must be lower in order to reduce the interference to them. It can be seen that the signal at the desired mobile is high for both independent and combined beamforming in the two figures. However, by visual inspection, it can be seen that the signals at the other mobiles is generally lower for combined beamforming. As an example, the signal at mobile 14 is approximately 10dB lower for combined beamforming relative to independent beamforming.

In the next section, a more quantitative comparison of the performance of the downlink of a CDMA system with independent beamforming versus combined beamforming of the arrays in handoff will be presented.

Table 14: Simulation parameters.

Parameter	Value	Unit
Number of cells	7	-
Number of mobiles per sector	1	-
Number of elements per array	7	-
Signal to noise ratio	25	dB
Angular spread standard deviation	5	degrees
Handoff threshold	-15	dB
Number of multipath components	3	-
Slow fading standard deviation	8	dB
Pathloss exponent	3.2	-
Voice activity factor	1	-

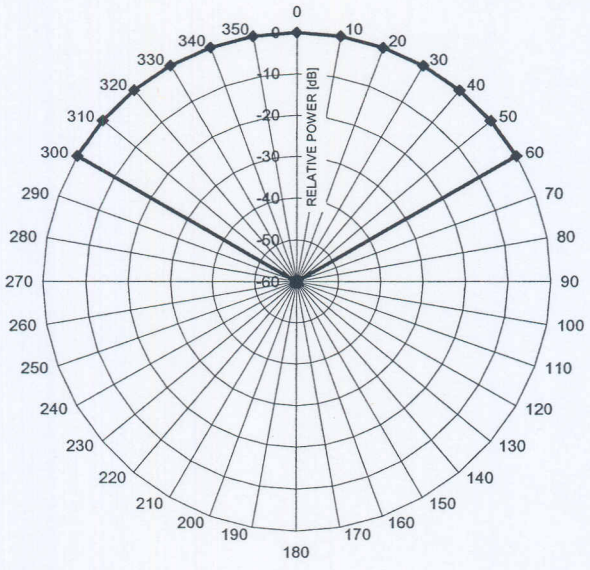

Figure 85: Element pattern that was used in the CDMA downlink simulations.

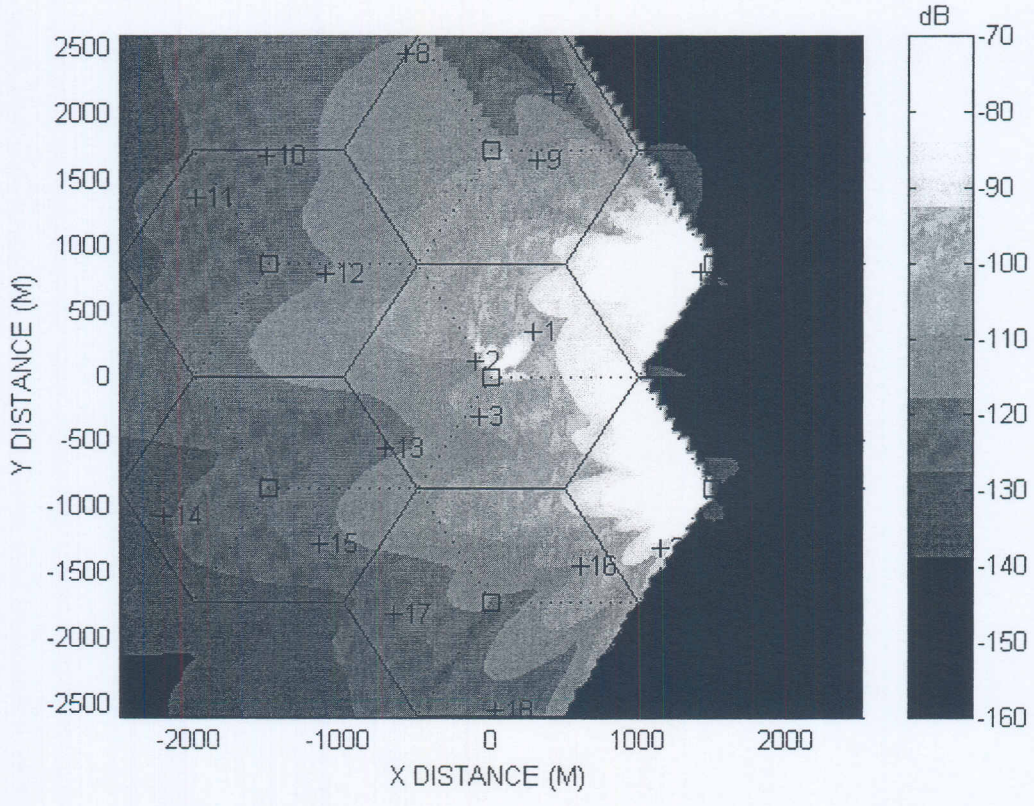

Figure 86: Received signal at all locations in a seven cell network with independent beamforming optimization for desired mobile 1.

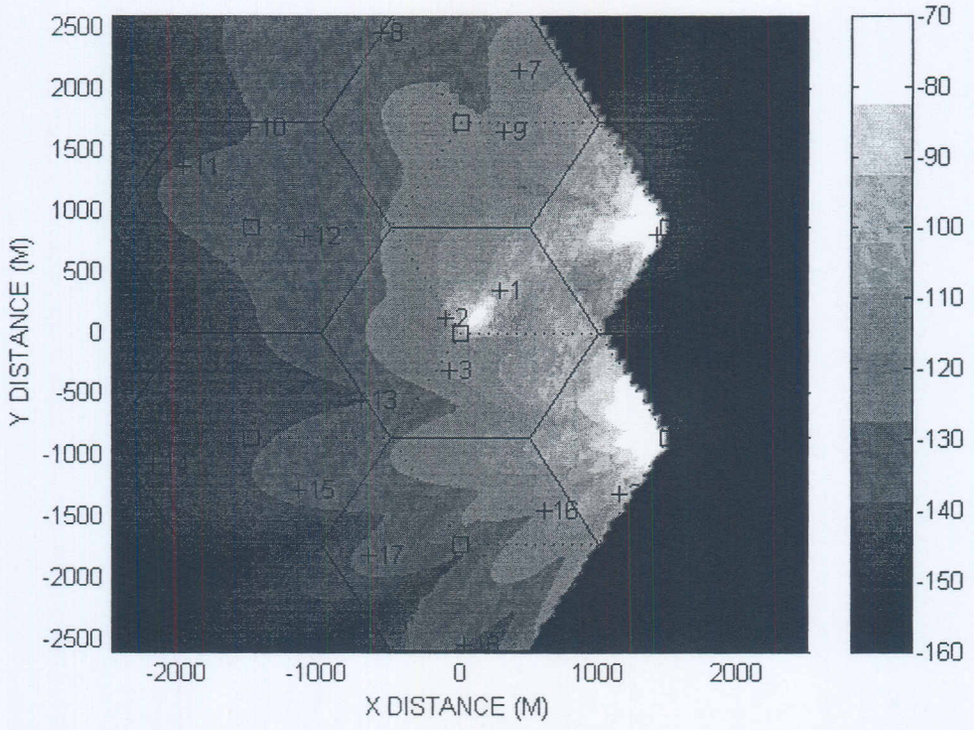

Figure 87: Received signal at all locations in a seven cell network with combined beamforming optimization for desired mobile 1.

7.5.3 Monte-Carlo Simulations

7.5.3.1 Procedure

A Monte-Carlo analysis is applied to estimate the outage probability of the CDMA network. The outage probability of a network with a 120° sector antenna is compared to a network with either independent or combined adaptive beamforming for the sectors in soft/softer[54] handoff. The outage probability is the probability that the signal to noise ratio is below a certain threshold [12,30], or:

$$Outage\ Probability = Probability\left(SNR < SNR_{Threshold}\right) \tag{210}$$

The threshold used in the simulations is 7dB, corresponding to a BER performance of less than 10^{-3} for BPSK (binary phased shifted) modulation [12]. The simulation flow diagram is shown in Figure 88. At each iteration, the mobile positions are randomly generated (with a uniform distribution across the sector), with a certain number of mobiles per sector. The

voice activity factor for each user is determined, based on whether a uniform random number is below a certain threshold, indicating that the mobile is active. All active mobiles are assigned an initial transmit power of one and the inactive mobiles a power of zero. Rayleigh fading for each multipath component is assumed and the incidence angles from the mobiles to all base station sectors are calculated based on the model in section 2.4. Power control for each mobile is applied according to the received signal power level at each mobile (fading included), using the procedure that is described in section 7.3.

The sectors that are in handoff with each mobile are determined next. The sectors where the received pilot power (power before correlation gain is applied) relative to the total interference noise is above a certain handoff threshold, t_{HO}, will be added to the handoff list.

The weight vectors for the combined and independent arrays are determined next (see section 7.2). This is followed by the received signal to noise ratio calculation at each mobile. The power is re-adjusted for the mobiles in the network for both combined or individual array beamforming, again based on the received signal to interference ratios at the mobiles (see section 7.3). After the transmit power of the mobiles has been adjusted with the power control algorithm, the SINRs of all the mobiles are then calculated.

An error will be reported when the SINR of the desired mobile is below the threshold. The total number of errors for the sectorized, individual beamforming and combined beamforming arrays are calculated and divided by the total number of iterations. This ratio is then the outage probability for the specific network, based on the number of mobiles per sector.

[54] Softer handoff is used in CDMA to describe the handoff between sectors of the same base station, while soft handoff refers to handoff between sectors of different base stations.

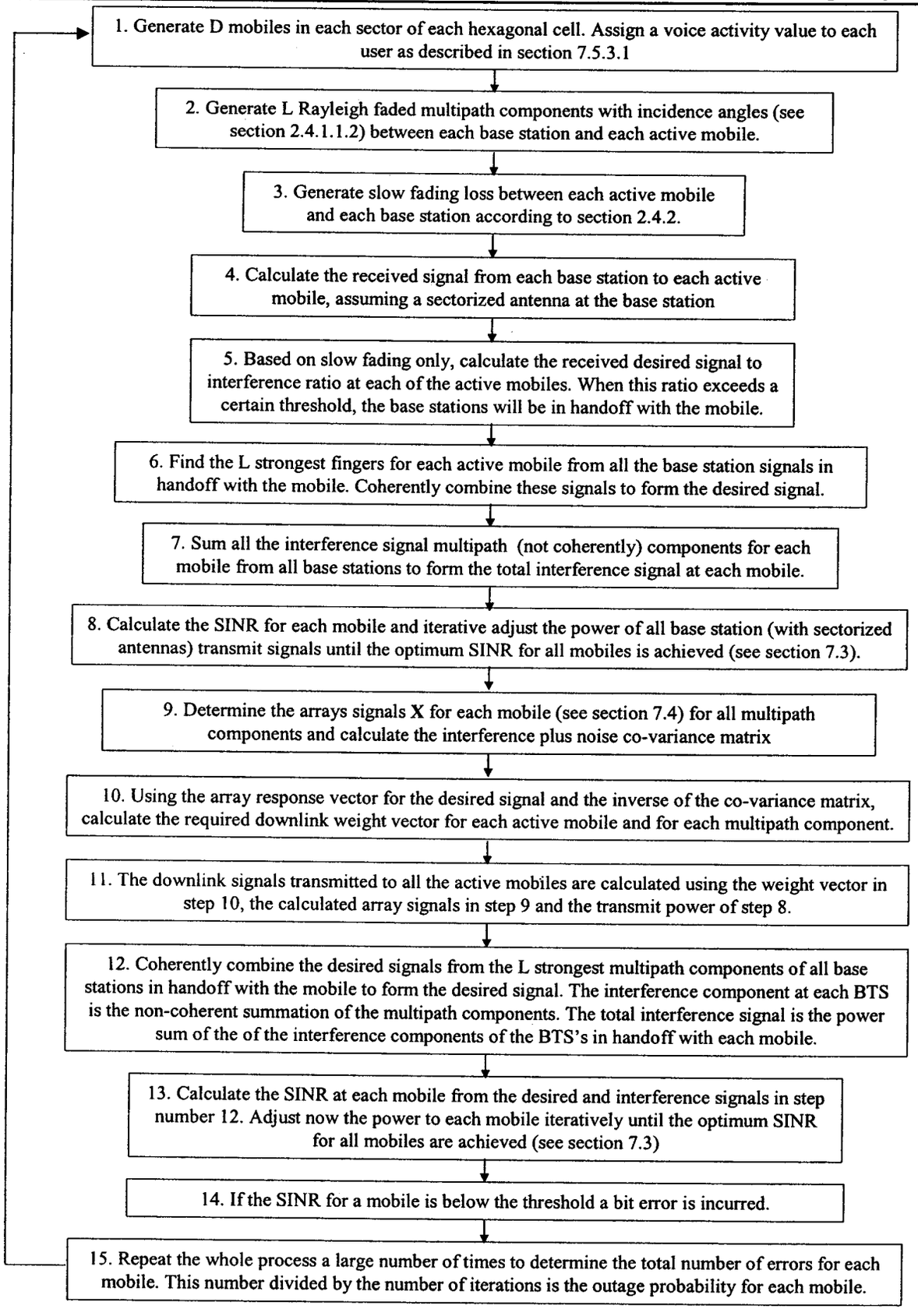

Figure 88: CDMA downlink simulation flow diagram.

7.5.3.2 Simulation Results

The simulation parameters are listed in Table 15, and the antenna element pattern that was used in the downlink simulations is shown in Figure 85.

Table 15: CDMA downlink outage probability simulation parameters.

Parameter	Value	Symbol
Signal to noise ratio	30 dB	SNR
Max number of power control iterations	25	-
Power reduction amount per power control iteration	0.7	-
Cell Radius	1000 m	R
Total number of cells	39	Z
Number of cells containing mobiles	7	-
Pathloss coefficient	3.2	γ
Angular spread standard deviation	2.5°	σ_{as}
Slow fading standard deviation	8 dB	σ_{sf}
Handoff threshold	-15 dB	t_{HO}
Desired signal to noise ratio	7 dB	$SNR_{Threshold}$
Processing gain	21.1 dB	g_p
Number of multipath components	3	L
Voice activity factor	0.375	ϑ

7.5.3.2.1 Results of a Single Run

The SINRs of the sectorized, independent and combined beamforming arrays will be compared for a single snap-shot of the mobile locations and fading conditions in this section. A total of 16 users per sector is considered, the angular spread is 5°, the voice activity factor is 0.375 and the number of elements per array is four. The positions of the mobiles and the number of handoffs of each mobile are shown in Figure 89. It can be seen that the number of handoffs range between no-handoff to two-way handoff[55]. The transmitted power (sectorized, independent beamforming and combined beamforming), SINR of sectorized antenna network before power adjustment and SINR after power

[55] Two-way handoff means that the mobile is combining signals form two base stations (or sectors).

adjustment of the sectorized, independent beamforming and combined beamforming networks are shown in Figure 90.

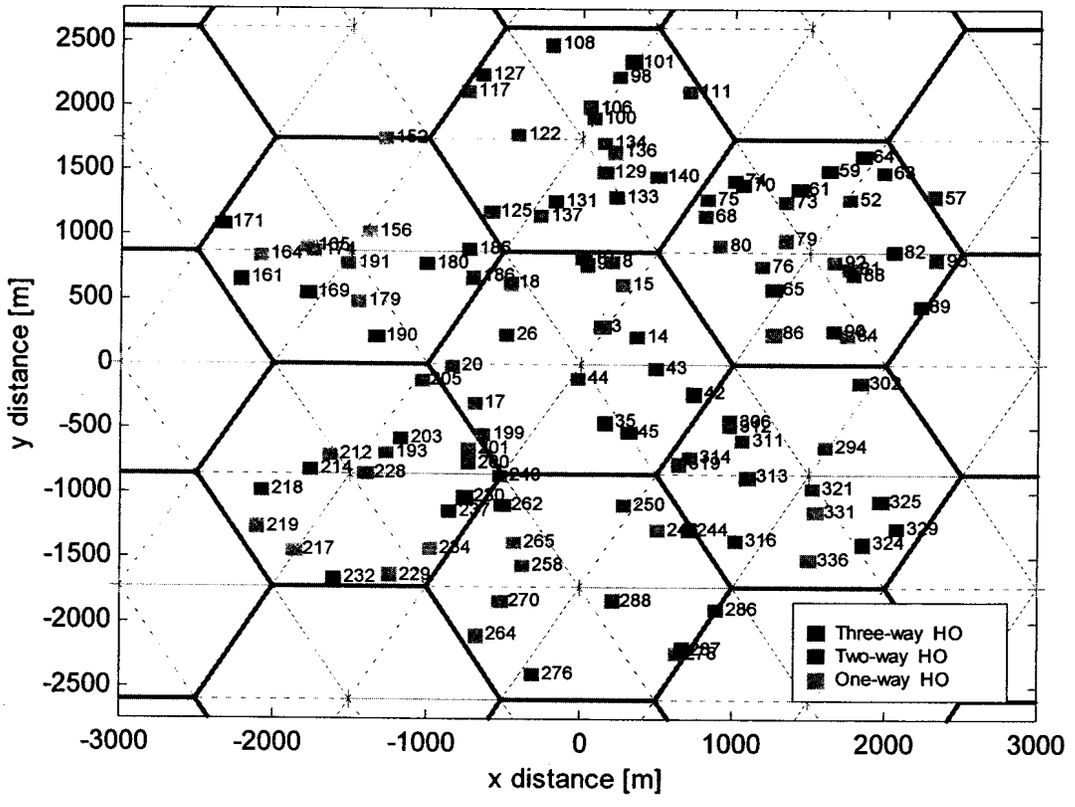

Figure 89: Mobile locations and number of handoffs experienced by each mobile for single iteration.

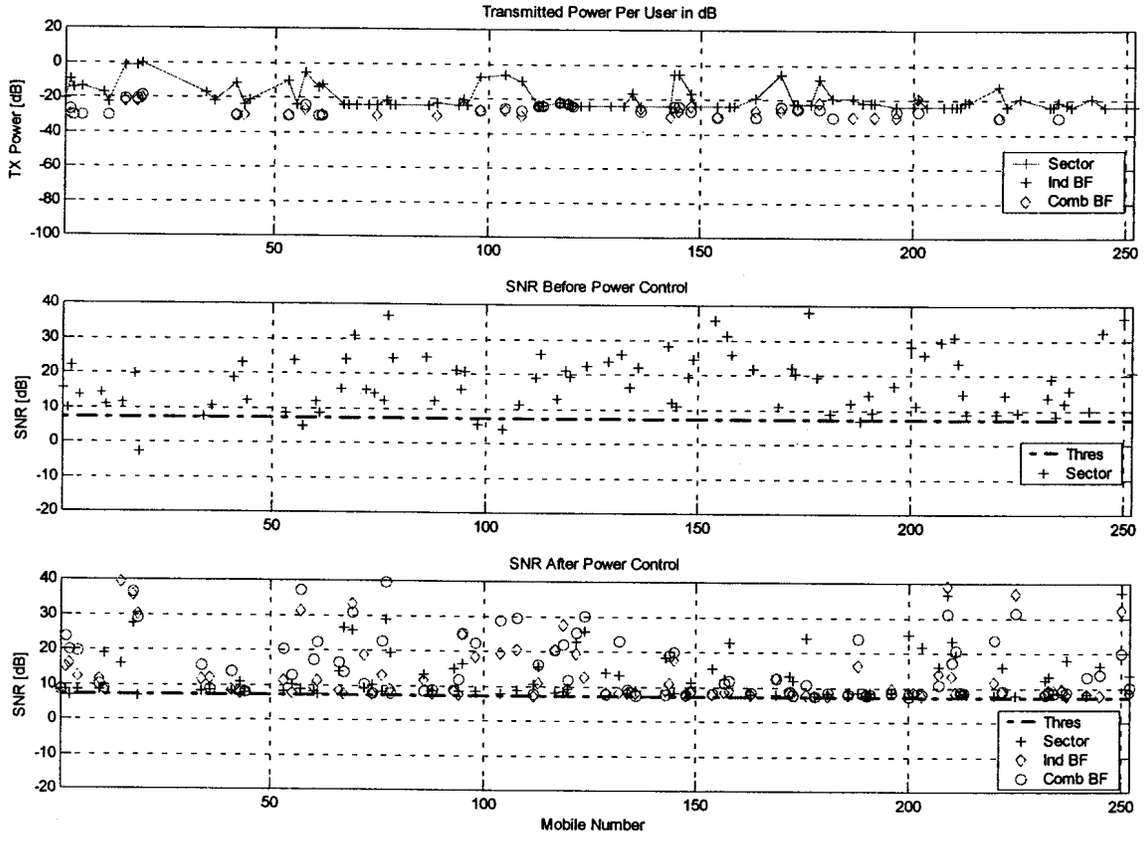

Figure 90: Transmitted power per user, SINR before power control, SINR after power control, SINR of combined beamforming compared to individual beamforming (four elements per array).

In this example the average SINR is 24.3dB for the sectorized antenna, 28.3dB for independent beamforming and 33.9dB for combined beamforming.

7.5.3.2.2 Outage probability estimation

The probability of an outage at the mobile as calculated with Monte-Carlo simulations are presented in this section. The simulation parameters are listed in Table 15. The outage probability as a function of the number of mobiles per sector of a sectorized antenna (reference) network as well as three element distributed arrays with independent and combined beamforming is shown in Figure 91.

The figure shows that the outage probability with the three element arrays is lower than with the sectorized antenna (which can be expected due to the interference reduction of adaptive arrays). In addition it can be seen that with combined array beamforming more

mobiles can be sustained at the same outage probability compared to independent array beamforming. Specifically at a bit error rate of 1E-3 with three element arrays, seven more mobiles per sector can be sustained with the combined beamforming distributed array than with independent beamforming of the arrays.

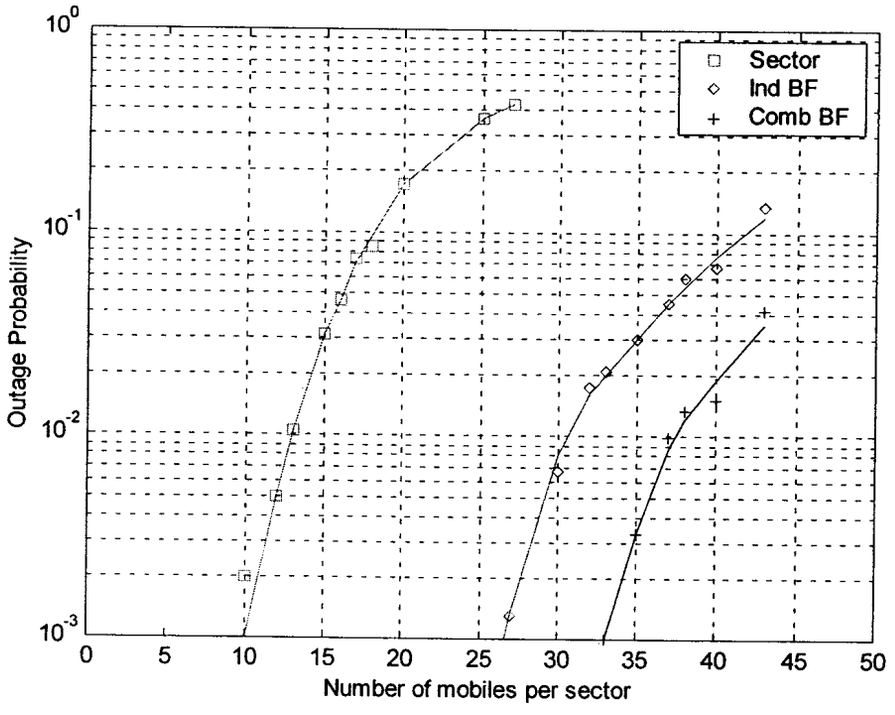

Figure 91: Outage probability as a function of the number of mobiles per sector for the CDMA downlink with sectorized antennas as well as independent and combined beamforming arrays (with three elements). The solid lines are an interpolation of the simulation values.

7.6 Conclusions

The aim of this chapter was to investigate whether there is an advantage in using combined optimum beamforming as opposed to independent beamforming for the arrays in handoff on the downlink of a CDMA system. The results for four stationary mobiles in two way soft handoff in a three cell network gave a minimum SINR improvement of 15dB with combined beamforming of the arrays in soft handoff relative to independent array beamforming (for three element arrays). None of the mobiles with combined beamforming has a SINR below 0dB, while one mobile has a SINR of approximately –5dB with independent beamforming. The five element arrays gave positive SINR for both beamforming schemes.

It was shown with Monte-Carlo simulations that the outage probability with combined beamforming of three element arrays results in a lower outage probability than independent beamforming of the arrays in handoff. The mobiles were randomly located in the cell. It was shown that at a bit error rate of 1E-3, seven more mobiles per sector can be supported with combined beamforming of three element arrays relative to independent beamforming.

8 CONCLUSIONS

8.1 Introduction

Spectral efficiency improvement of cellular networks is becoming an increasingly important means of enhancing network capacity. Spectrum efficiency is improved by increasing the number of mobiles operating on the same frequency channel. Network capacity is mainly limited by the received signal to interference ratio at the mobile and base station. Therefore, interference reduction results in an overall increase in the system capacity.

Adaptive, phased and multibeam arrays are widely studied as a means of significantly reducing this interference. The arrays will form, steer or select a beam that transmits the best signal to the desired mobile on the downlink while minimizing the signal to other users. Similarly, on the uplink the array beam will maximize the signal received from the desired user while minimizing the signals received from interfering mobiles.

In TDMA systems, adaptive array interference reduction allows for a smaller reuse distance up to the point where multiple users can operate on the same frequency and time slot (same cell frequency reuse). An adaptive array is able to reduce the signals to and from interfering mobiles even if they are in the same direction (relative to the array boresight) as the desired signal, provided the array element spacing is large or the propagation environment has a wide angular spread (or both). Large array element spacing is undesirable as it is difficult to install large arrays on towers and buildings due to esthetic, environmental and windloading considerations. Large user densities is typically associated with a wide angular spread environment (urban and dense urban), but there are many cases where the opposite is also true. This case as well as small interelement separations, limits the performance (and thus capacity) of same cell frequency reuse configurations.

The limitation in reduction of interference by center cell arrays with small interelement spacing from mobiles located close in angle to the desired mobile in a narrow angular spread environment can be overcome by moving the arrays to the corners of the cell. Each array can form a beam that will maximize the signal to interference ratio of the desired mobile, whereafter the optimum signal from all the corner arrays can be selected.

Alternatively, all arrays can form a combined beam, which will generally result in the best signal to interference ratio.

Code division multiple access systems (CDMA) on the other hand always has a same cell frequency reuse (with a reuse pattern of one). In soft handoff, signals from multiple base stations are used to reduce the slow fading loss between mobile and base station. Each base station in soft handoff independently forms an optimum beam. However, as with multiple array beamforming in TDMA systems, independent beamforming can produce non-optimum signal to noise ratios, depending on the specific propagation and user locations.

The range of phased arrays is a function of the array beamwidth and the angular spread of the propagation environment. If the phased array beamwidth becomes narrower than the angular spread, the range increase (relative to an omni antenna) is limited. The adaptive array does not have this range limitation, as the array adapts its beam to the incoming multipath components. The presence of interfering mobiles in a multipath environment affects the range increase of phased and adaptive arrays. The array interference reduction ability is affected by the propagation angular spread.

8.2 Relevance

Work in this thesis is an extension of work in the literature on same cell frequency reuse with adaptive arrays as a means of increasing the capacity of FDMA/TDMA cellular networks [4,5,6]. Studies in the past mainly considered antennas at the center of the cell, although some studies investigated the performance of antennas and arrays at alternative locations in the cell [7,8,9,37,38]. None of the studies specifically investigated the combined beamforming of spatially distributed arrays. In this thesis combined beamforming of multiple adaptive arrays at the edges of the cell was investigated.

The soft handoff benefits on the downlink of a CDMA system with sectorized antennas has been studied in [65], and with multiple antenna selection in [30]. The downlink performance of adaptive arrays in CDMA cellular systems is documented in [30]. Studies on the CDMA downlink performance with adaptive arrays in soft handoff is studied in [40,41]. The advantage of combined beamforming of the arrays is soft/softer handoff on

the downlink of a CDMA system was studied in this thesis. Similar studies were not found in the literature.

Past studies investigated the range of phased and adaptive arrays in a multipath environment, excluding the effect of interference [45,56]. A comparison of the range increase of an adaptive array with a phased array in a multipath environment for mobile communication systems was published recently [16]. Work in this thesis elaborated on the study in [16] by adding the effect of interference on the range increase of adaptive and phased arrays relative to an omni antenna.

8.3 Contributions and Conclusions

The effect of interference on the range increase, relative to an omni-antenna, of adaptive and phased arrays in a multipath environment for both narrowband and wideband (spread spectrum) cellular systems was investigated. This work is an extention of the investigation in [16], where the effect of interference was not considered. The range increase of a narrowband cellular system with a single dominant interferer at various incidence angles was presented as a function of the number of array elements and scattering angular spread. The range increase of both adaptive and phased arrays are affected by the angular spread and the angle of the interferer relative to the boresight of the array. A significant reduction in the range increase of a phased array is visible in a narrow angular spread environment when the multipath angular components of the interferer starts to overlap with the array beamwidth. The adaptive array is able to reduce interference multipath components even if the interferer is in the same direction as the desired signal. Therefore, the range increase of the adaptive array exceeds that of the phased array for the same conditions (number of elements, angular spread and interferer locations). The range increase of wideband spread spectrums with twelve interferers per sector (typical for CDMA cellular systems) was presented as a function of the number of array elements, scattering angular spread and received signal to noise ratio. Similar to the results in [16], the range increase limitation of phased arrays in the presence of multiple interferers can be improved by using a weight vector optimized for each RAKE receiver finger. The results also showed that the range increase of phased arrays is less than that of adaptive arrays due to the lack of cancellation of interferer multipath components falling inside the beamwidth of the phased array.

A simplified analytical model for the probability density function of the angle of arrival of multipath signals was presented. Using this probablility density function, an analytical model was derived for predicting the range increase of a phased array in a multipath environment in the presence of a dominant interferer. The model includes the phased array asymptotic range limit when the beamwidth of the array becomes narrower than the angular spread of the desired signal. This limit is a function of the multipath angular spread.

The concept of the spatially distributed array was presented as a means of increasing the same cell frequency reuse capacity of the network beyond that possible with single adaptive array systems located at the center of the cell. Adaptive arrays at the center of the cellsite are limited in their ability to separate co-channel users from each other when they are closely located in angle relative to each other (as seen by the base station antenna) in a narrow angular spread (low multipath) environment with closely spaced antenna elements. A concept with multiple arrays located far apart in the cell (spatially distributed array) was introduced. This array consists of three sub-arrays at alternate corners of the cell and when applied to TDMA type networks has the ability to receive user signals from multiple viewing angles. It is therefore able to obtain an improved rejection of interfering signals relative to the arrays located at the center of the cell. This concept was published in [17, 18], where the reduction of the outage probability of a combined distributed array vs. the conventional array at the cell center in a non-multipath environment was presented.

It was shown analytically that the SINR with optimum combining of the sub-array output signals of a distributed array (after independent optimum beamforming of the sub-arrays) is equal to the sum of the SINRs of the individual sub-arrays with independent beamforming. Analytical expressions were derived to show that the SINR of a distributed array with two sub-arrays is greater or equal to the SINR of independent beamforming of the arrays for a single interferer. The result was extended to multiple interferers through numerical simulations.

The bit error rate and outage probability performance of spatially distributed arrays on the uplink of a TDMA cellular network in the presence of fast fading and shadowing was estimated by means of Monte-Carlo simulations. Combined beamforming of the sub-arrays

was compared to independent beamforming as well as to conventional arrays at the center of the cell. The performance was investigated as a function of the frequency reuse pattern, number of antenna elements, multipath angular spread and power control. Fast and slow fading as well as a multi-tiered network interferers were included in the simulations. It was shown that for a reuse pattern of one with four element arrays, one same-cell co-channel users can be sustained in a GSM network (outage probability less than 1.8% and 3dB protection ratio) with optimum combining of the sub-arrays, while none can be supported with independent array beamforming or conventional arrays. With six element sub-arrays, two same-cell co-channel users can be sustained in a GSM network with independent array beamforming and three users with combined sub-array beamforming.

An analytical model for estimating the BER performance of spatially distributed arrays in a Rayleigh multipath environment was developed. This model is an extension of a model in [11] for determining the bit error rate performance of a single array in a multipath environment. The method is based on finding the Laplace transform of the probability density function (PDF) of the array output SINR through a generalized eigenvalue solution. The inverse Laplace transform then yields a simplified probability density function in terms of eigenvalues, which is applied to estimate the BER at the array output. The BER calculated with the derived analytical model is compared to the BER simulated with a Monte-Carlo method. A spatially distributed array with two-element sub-arrays and correlated fading between the array elements for each mobile signal is considered. It was shown that the analytical and simulated bit error rate results are in close agreement.

The concept of combined beamforming of arrays in handoff for the downlink of a CDMA network was formulated. A formulation for the downlink signals to the mobile from multiple base station arrays were presented. The formulation relies on an accurate estimation of the downlink propagation channel array response matrix. Techniques to etimate this matrix were discussed. Using the downlink formulation, the outage probability at the mobiles was compared by means of Monte-Carlo simulations between combined beamforming of the arrays in multi-way handoff versus independent beamforming of the arrays. The simulations included the effect of fast and slow fading as well as power control for a 19 cell network. It was shown that the outage probability with combined beamforming of three element arrays resulted in a lower outage probability than

independent beamforming. The results specifically showed that for a bit error rate of 1E-3, seven more mobiles per sector can be supported with combined beamforming of three element arrays compared to independent beamforming.

8.4 Future work

The following suggests future work that can flow from this study:

- It was shown analytically that the signal to interference ratio is higher for adaptive arrays with combined beamforming than with individual beamforming in a non-multipath environment for a desired signal and single interferer. This analysis can be extended to multiple interferers.
- Closed form solutions were derived for the bit error rate of distributed arrays in a multipath environment. Although difficult, it may be possible to include the effect of slow fading on the BER of distributed arrays.
- The bit error rate and outage probability of distributed base stations with adaptive arrays was investigated for both TDMA and CDMA systems. The investigation can be extended to include the performance of distributed multibeam and phased arrays.
- It was shown with Monte-Carlo simulations that the outage probability is lower for combined beamforming than independent beamforming of the arrays in handoff in a CDMA network on the downlink. The investigation was done for the case of three element arrays with 2.5 degree angular spread. The investigation can be extended to more antenna elements and wider angular spreads. Multibeam and phased arrays can also be included in the study.
- Instead of Monte-Carlo simulations, closed form solutions for the outage probability of CDMA systems with combined beamforming of adaptive arrays in handoff may be derived when applying some approximation
- In the CDMA downlink simulations it was assumed that the propagation channel between the base station and mobiles can be accurately determined by means of an adaptive method using feedback from the mobile. The effect of errors in this estimation can be investigated.

APPENDIX A

CO-VARIANCE MATRIX OF MULTIPLE UNCORRELATED SOURCES

Consider the signals from D sources impinging on the elements of an array. The received signal of source d at the array elements is:

$$\mathbf{X}_d(t) = S_d(t)\mathbf{U}_d \tag{A1}$$

where $S_d(t)$ is the data transmitted by source d and $\mathbf{U}_d$ is the array vector of source d. The total received signal at the array is the sum of all the signals plus noise received at the array, or:

$$\mathbf{X}(t) = \sum_{d=1}^{D} S_d(t)\mathbf{U}_d + \mathbf{n}(t) \tag{A2}$$

where $\mathbf{n}$ is zero mean Gaussian noise at the antenna elements. The co-variance matrix of the received signals at the array elements is:

$$\mathbf{R} = E\left\{\mathbf{X}(t)\,\mathbf{X}^H(t)\right\} \tag{A3}$$

Inserting now (A2) in (A3) and assuming that the signals and noise are uncorrelated, the co-variance matrix becomes:

$$\mathbf{R} = E\left\{\sum_{d=1}^{D} S_d(t)\mathbf{U}_d \left(\sum_{d=1}^{D} S_d(t)\mathbf{U}_d\right)^H\right\} + \sigma^2\mathbf{I} \tag{A4}$$

where $\mathbf{I}$ is a unity matrix and σ^2 is the noise power. Expanding (A4) the following is obtained:

$$\mathbf{R} = E\begin{Bmatrix} S_1(t)S_1^*(t)\mathbf{U}_1\mathbf{U}_1^H + S_1(t)S_2^*(t)\mathbf{U}_1\mathbf{U}_2^H + \ldots + S_1(t)S_D^*(t)\mathbf{U}_1\mathbf{U}_D^H + \\ S_2(t)S_1^*(t)\mathbf{U}_2\mathbf{U}_1^H + S_2(t)S_2^*(t)\mathbf{U}_2\mathbf{U}_2^H + \ldots + S_2(t)S_D^*(t)\mathbf{U}_2\mathbf{U}_D^H + \\ + \ldots + \\ S_D(t)S_1^*(t)\mathbf{U}_D\mathbf{U}_1^H + S_D(t)S_2^*(t)\mathbf{U}_D\mathbf{U}_2^H + \ldots + S_D(t)S_D^*(t)\mathbf{U}_D\mathbf{U}_D^H + \end{Bmatrix} + \sigma^2\mathbf{I} \tag{A5}$$

Now, if the sources are uncorrelated, then:

Appendix A

$$E\{S_1(t)S_2^*(t)\}=E\{S_1(t)S_2^*(t)\}=.....=E\{S_1(t)S_D^*(t)\}=...=E\{S_D(t)S_1^*(t)\}=...=0 \quad \text{(A6)}$$

Since the power P_d of each signal $d \in \{1,2,...,D\}$ is:

$$P_d = E\{S_d(t)S_d^*(t)\} \quad \text{(A7)}$$

and using (A6) and (A7), equation (A5) becomes:

$$\mathbf{R} = P_1 \mathbf{U}_1 \mathbf{U}_1^H + P_2 \mathbf{U}_2 \mathbf{U}_2^H + ... + P_D \mathbf{U}_D \mathbf{U}_D^H + \sigma^2 \mathbf{I} \quad \text{(A8)}$$

which can be written as:

$$\mathbf{R} = \sum_{d=1}^{D} P_d \mathbf{U}_d \mathbf{U}_d^H + \sigma^2 \mathbf{I} \quad \text{(A9)}$$

APPENDIX B

PROOF THAT THE OPTIMUM COMBINED SINR OF TWO ARRAYS WITH INDIVIDUAL BEAMFORMING IS EQUAL TO THE SUM OF THE SINR OF EACH INDEPENDENT BEAMFORMING ARRAY

It was shown in section 4.2.1 that the signal to interference plus noise ratio after optimum combining of two individual arrays, each with signals combined with independent optimum beamforming, is the sum of the individual array signal to interference ratios. However, it was done for the special case where $\psi_{12}=\psi_{22}$. The derivation will be extended to the general case ($\psi_{12}\neq\psi_{22}$) in this appendix.

The signal to interference plus noise ratio of optimum combining of the individual array signals is given in (116) as

$$\mathrm{SINR}_C = \mathbf{U}_{dc}^H \mathbf{R}_{nnC}^{-1} \mathbf{U}_{dc} \tag{B1}$$

with $\mathbf{R}_{nnC}$ the covariance matrix of the signals from the two arrays, given by:

$$\mathbf{R}_{nnC} = \begin{bmatrix} \mathbf{R}_{nnC,11} & \mathbf{R}_{nnC,12} \\ \mathbf{R}_{nnC,21} & \mathbf{R}_{nnC,22} \end{bmatrix} \tag{B2}$$

and $\mathbf{U}_{dc}$ is the array steering vector in the direction of the desired signal, given by:

$$\mathbf{U}_{dc} = [1\ 1]^T \tag{B3}$$

The inverse of a two by two matrix is [66]:

$$\mathbf{R}_{nnC}^{-1} = \left(R_{nnC,11}R_{nnC,22} - R_{nnC,12}R_{nnC,21}\right)^{-1} \begin{bmatrix} R_{nnC,22} & -R_{nnC,12} \\ -R_{nnC,21} & R_{nnC,11} \end{bmatrix} \tag{B4}$$

Since $R_{nnC,12}=R_{nnC,21}^*$, the inverse in (B4) becomes:

$$\mathbf{R}_{nnC}^{-1} = \left(R_{nnC,11}R_{nnC,22} - R_{nnC,12}R_{nnC,12}^*\right)^{-1} \begin{bmatrix} R_{nnC,22} & -R_{nnC,12} \\ -R_{nnC,12}^* & R_{nnC,11} \end{bmatrix} \tag{B5}$$

Inserting (B5) in (B1), the SINR is:

$$SINR_C = \frac{\left(R_{nnC,11} + R_{nnC,12} + R^*_{nnC,12} + R_{nnC,22}\right)}{R_{nnC,11} R_{nnC,22} - R_{nnC,12} R^*_{nnC,12}} \tag{B6}$$

If it cans now be shown that $R_{nnC,11} R_{nnC,22} >> R_{nnC,12} R^*_{nnC,12}$, then the SINR in (B7) becomes:

$$SINR_C = \left(\frac{1}{R_{nnC,11}} + \frac{1}{R_{nnC,22}} \right) \tag{B8}$$

insert the components of (93) in (B8), the SINR becomes:

$$SINR_C = \left(\frac{1}{\mathbf{W}_1^H \mathbf{R}_{nn11} \mathbf{W}_1} + \frac{1}{\mathbf{W}_2^H \mathbf{R}_{nn22} \mathbf{W}_2} \right) \tag{B9}$$

and using (88) and (89) the following is obtained:

$$SINR_C = \left(\frac{\left(\mathbf{U}_d^H \mathbf{R}_{nn11}^{-1} \mathbf{U}_d\right)^H \left(\mathbf{U}_d^H \mathbf{R}_{nn11}^{-1} \mathbf{U}_d\right)}{\left(\mathbf{R}_{nn11}^{-1} \mathbf{U}_d\right)^H \mathbf{R}_{nn11} \mathbf{R}_{nn11}^{-1} \mathbf{U}_d} + \frac{\left(\mathbf{U}_d^H \mathbf{R}_{nn22}^{-1} \mathbf{U}_d\right)^H \left(\mathbf{U}_d^H \mathbf{R}_{nn22}^{-1} \mathbf{U}_d\right)}{\left(\mathbf{R}_{nn22}^{-1} \mathbf{U}_d\right)^H \mathbf{R}_{nn22} \mathbf{R}_{nn22}^{-1} \mathbf{U}_d} \right) \tag{B10}$$

After cancellation of the components in (B10), the following simplified equation is obtained:

$$SINR_C = \left(\mathbf{U}_d^H \mathbf{R}_{nn11}^{-1} \mathbf{U}_d + \mathbf{U}_d^H \mathbf{R}_{nn22}^{-1} \mathbf{U}_d \right) \tag{B11}$$

comparing this to (108) and (109) it can be seen that:

$$SINR_C = \left(SINR_1 + SINR_2\right) \tag{B12}$$

Using (93), (102) and (105), the product $R_{nnC,11} R_{nnC,22}$ in (B6) is:

$$R_{nnC,11} R_{nnC,22} = \frac{(2+\sigma^2)\sigma^4}{4((\cos(\pi \sin \psi_{12}) - 1 - \sigma^2)(\cos(\pi \sin \psi_{22}) - 1 - \sigma^2))} \tag{B13}$$

The relation between the angles ψ_{12} and ψ_{22} is:

$$\psi_{22} = \arctan\left(\frac{\sin \psi_{12}}{\xi - \cos \psi_{12}} \right) \tag{B14}$$

where ξ is the proportion of the range from array 1 to the mobile relative to the distance between the two arrays. Inserting this angle relationship in (B13) into (B14), the following results:

$$R_{nnC,11}R_{nnC,22} = \frac{\sigma^4}{\cos\left\{\frac{\omega}{\Gamma}\right\}\cos(\omega) - \cos(\omega) - \cos\left\{\frac{\omega}{\Gamma}\right\} + 1} \tag{B15}$$

where

$$\omega = \pi \sin\psi_{12} \tag{B16}$$

and

$$\Gamma = \sqrt{\xi^2 - 2\xi\cos\psi_{12} + 1} \tag{B17}$$

Let $\alpha = \frac{\omega}{\Gamma}$, then (B17) can be written as:

$$R_{nnC,11}R_{nnC,22} = \frac{\sigma^4}{\cos(\alpha)\cos(\omega) - \cos(\omega) - \cos(\alpha) + 1} \tag{B18}$$

Using (93), (103), (104) and (B14) the product $R_{nnC,12}R^{*}_{nnC,12}$ in (B6) becomes:

$$\begin{aligned}
&\frac{1}{4}\sigma^4\left(\cos\left(-\frac{1}{2}\omega+\frac{1}{2}\alpha\right) - \cos(\omega)\cos\left(-\frac{1}{2}\omega+\frac{1}{2}\alpha\right) + \sin(\omega)\sin\left(-\frac{1}{2}\omega+\frac{1}{2}\alpha\right)\right.\\
&\quad + \sigma^2\cos\left(-\frac{1}{2}\omega+\frac{1}{2}\alpha\right) + \cos\left(\frac{1}{2}\omega+\frac{1}{2}\alpha\right) + \cos\left(\frac{1}{2}\omega+\frac{1}{2}\alpha\right)\sigma^2\\
&\quad \left. - \cos\left(\frac{1}{2}\omega+\frac{1}{2}\alpha\right)\cos(\omega) - \sin\left(\frac{1}{2}\omega+\frac{1}{2}\alpha\right)\sin(\omega)\right)^2 \Big/ (1 + 8\cos(\alpha)\sigma^2\cos(\omega)\\
&\quad - 2\cos(\alpha)\cos(\omega)^2\sigma^2 - 2\cos(\alpha)^2\cos(\omega)\sigma^2 + 4\cos(\alpha)\sigma^4\cos(\omega) - 2\cos(\alpha)\\
&\quad + \cos(\alpha)^2 + 4\sigma^2 - 2\cos(\omega) + \cos(\omega)^2 + 6\sigma^4 + \sigma^8 + 4\sigma^6 + 4\cos(\alpha)\cos(\omega)\\
&\quad + \cos(\alpha)^2\cos(\omega)^2 - 2\cos(\alpha)\cos(\omega)^2 - 2\cos(\alpha)^2\cos(\omega) - 6\cos(\alpha)\sigma^4\\
&\quad + \cos(\alpha)^2\sigma^4 - 6\cos(\alpha)\sigma^2 - 2\cos(\alpha)\sigma^6 + 2\cos(\alpha)^2\sigma^2 - 6\sigma^4\cos(\omega)\\
&\quad + \sigma^4\cos(\omega)^2 + 2\sigma^2\cos(\omega)^2 - 6\sigma^2\cos(\omega) - 2\sigma^6\cos(\omega))
\end{aligned} \tag{B19}$$

Using (B18) and (B19), the ration of $R_{nnC,11}R_{nnC,22}$ to $R_{nnC,12}R^{*}_{nnC,12}$ can be calculated. Once (B18) is divided in (B19), the fact that $\sigma^2 << 1$ is used to simplify the result, given by:

$$\frac{R_{nnC,11}R_{nnC,22}}{R_{nnC,12}R^{*}_{nnC,12}} = \frac{A}{BC} \tag{B20}$$

where

$$A = \cos(\alpha)^2\cos(\omega)^2 - 2\cos(\alpha)^2\cos(\omega) - 2\cos(\alpha)\cos(\omega)^2 + 4\cos(\alpha)\cos(\omega) + \cos(\alpha)^2 - 2\cos(\alpha) + \cos(\omega)^2 - 2\cos(\omega) + 1 \tag{B21}$$

$$B = \left(\cos\left(\frac{1}{2}\omega - \frac{1}{2}\alpha\right) - \cos(\omega)\cos\left(\frac{1}{2}\omega - \frac{1}{2}\alpha\right) - \sin(\omega)\sin\left(\frac{1}{2}\omega - \frac{1}{2}\alpha\right) + \cos\left(\frac{1}{2}\omega + \frac{1}{2}\alpha\right) - \cos\left(\frac{1}{2}\omega + \frac{1}{2}\alpha\right)\cos(\omega) - \sin\left(\frac{1}{2}\omega + \frac{1}{2}\alpha\right)\sin(\omega)\right)^2 \tag{B22}$$

$$C = \cos(\alpha)\cos(\omega) - \cos(\alpha) - \cos(\omega) + 1 \tag{B23}$$

Applying the following trigonometry properties to (B23):

$$\cos(a-b) = \cos(a)\cos(b) + \sin(a)\sin(b) \tag{B24}$$

and

$$\cos(a+b) = \cos(a)\cos(b) - \sin(a)\sin(b) \tag{B25}$$

the equation becomes zero (i.e. B = 0), which results in a large value for the ratio $\frac{R_{nnC,11}R_{nnC,22}}{R_{nnC,12}R^{*}_{nnC,12}}$ and thereby proving that the SINR of the arrays combined with optimum combining is equal to the individual array SINRs.

APPENDIX C

BER OF ARRAY WITH MULTIPLE NON-UNIQUE EIGENVALUES (MULTIPLICITY > 1)

In the case of one eigenvalue with multiplicity equal to one and M-1 eigenvalues with multiplicity equal to M-1, the characteristic function of the probability density function can be written as:

$$\Psi(z)=\frac{\langle\lambda_1\rangle^{M-1}\langle\lambda_M\rangle}{(z+\langle\lambda_1\rangle)^{M-1}(z+\langle\lambda_M\rangle)} \tag{C1}$$

A partial fraction expansion of (C1) is:

$$\Psi(z)=\frac{-C}{(z+\lambda_1)^{M-1}(\lambda_1-\lambda_M)}+\frac{-C}{(z+\lambda_1)^{M-2}(\lambda_1-\lambda_M)^2}+\ldots\ldots$$
$$\frac{+C}{(z+\lambda_5)(\lambda_1-\lambda_M)^{M-1}} \tag{C2}$$

where

$$C=\langle\lambda_1\rangle^{M-1}\langle\lambda_M\rangle \tag{C3}$$

Equation (C2) can also be written as:

$$\Psi(z)=C\left\{\frac{\Omega_1}{(z+\lambda_1)^{M-1}}+\frac{\Omega_2}{(z+\lambda_1)^{M-2}}+\ldots\ldots+\frac{\Omega_M}{(z+\lambda_5)}\right\} \tag{C4}$$

where

$$\Omega_1=\frac{-1}{(\lambda_1-\lambda_M)} \tag{C5}$$

$$\Omega_2=\frac{-1}{(\lambda_1-\lambda_M)^2} \tag{C6}$$

and

$$\Omega_M = \frac{1}{(\lambda_1 - \lambda_M)^{M-1}} \tag{C7}$$

The inverse Laplace transform of (C4) is given by:

$$\begin{aligned} p(\eta) &= L^{-1}\{\Psi(z)\} \\ &= C\left\{\Omega_{M-1} e^{-\lambda_1} + \eta\Omega_{M-2} e^{-\lambda_1\eta} + ...+ \eta^{M-2}\Omega_1 e^{-\lambda_1\eta} + \Omega_M e^{-\lambda_M\eta}\right\} \end{aligned} \tag{C8}$$

The average bit error rate (BER) of phased shift keyed signals is given by [11]:

$$BER = \frac{1}{2}\int_{-\infty}^{\infty} p(\eta)\ \mathrm{erfc}(\sqrt{\eta})\,d\eta \tag{C9}$$

Inserting (C8) in (C9) the following is obtained:

$$BER = \frac{C}{2}\int_{-\infty}^{\infty}\left\{\Omega_{M-1} e^{-\lambda_1} + \eta\Omega_{M-2} e^{-\lambda_1\eta} + ...+ \eta^{M-2}\Omega_1 e^{-\lambda_1\eta} + \Omega_M e^{-\lambda_M\eta}\right\}\mathrm{erfc}(\sqrt{\eta})\,d\eta \tag{C10}$$

The following general integral formula [67] is used to solve (C10)

$$\frac{1}{2(K-1)!}\int_0^{\infty} x^{K-1} e^{(-ax)}\ \mathrm{erfc}(\sqrt{bx}\,dx = \left(\frac{\sqrt{1+\frac{a}{b}}-1}{2a\sqrt{1+\frac{a}{b}}}\right)^K \sum_{k=0}^{K-1}\binom{K-1+k}{k}\left(\frac{\sqrt{1+\frac{a}{b}}+1}{2\sqrt{1+\frac{a}{b}}}\right)^k \tag{C11}$$

where

$$\binom{K-1+k}{k} = \frac{(K-1+k)!}{k!(K-1)!} \tag{C12}$$

Using (C11) in (C10) the bit error rate is

$$BER = -C\sum_{m=2}^{M-1}\left\{\Omega^{M-1}\ \zeta_1^m\right\}\sum_{i=0}^{m-1}\left\{\frac{(m-1+i)!\,\mu^i}{i!(m-1)!}\right\} + C\Omega^{M-1}\zeta_M \tag{C13}$$

where

$$\zeta_1 = \frac{\sqrt{1+\lambda_1}-1}{2\lambda_1\sqrt{1+\lambda_1}} \tag{C14}$$

$$\zeta_M = \frac{\sqrt{1+\lambda_M} - 1}{2\lambda_5\sqrt{1+\lambda_5}} \tag{C15}$$

and

$$\mu = \frac{\sqrt{1+\lambda_1} + 1}{2\sqrt{1+\lambda_1}} \tag{C16}$$

APPENDIX D

OPTIMUM COMBINING WEIGHT VECTOR

The average output signal to interference plus noise power ratio (SINR) is given in (44) as:

$$\text{SINR} = \Gamma = \frac{\mathbf{W}^H \mathbf{U}_{des} \mathbf{U}_{des}^H \mathbf{W}}{\mathbf{W}^H \mathbf{R}_{nn} \mathbf{W}} \tag{D1}$$

where $\mathbf{R}_{nn}$ is the interference plus noise co-variance matrix, equal to [54]:

$$\mathbf{R}_{nn} = \mathbf{U}_{int} \mathbf{U}_{int}^H + \sigma_N^2 \tag{D2}$$

The optimum weight vector, $\mathbf{W}_{opt}$, which maximizes the SINR is now required. The derivation given here is from [58]. Since the interference plus noise co-variance matrix $\mathbf{R}_{nn}$ is positive definite, i.e.

$$\mathbf{W}^H \mathbf{R}_{nn} \mathbf{W} > 0 \tag{D3}$$

(positive definiteness is ensured since it has an uncorrelated noise component included) it can be factored into the product of two Hermitian ($\mathbf{G} = \mathbf{G}^H$) matrices:

$$\mathbf{R}_{nn} = \mathbf{G}\mathbf{G} \tag{D4}$$

and

$$\mathbf{R}_{nn}^{-1} = \mathbf{G}^{-1}\mathbf{G}^{-1} \tag{D5}$$

Matrix $\mathbf{G}$ can now be used to transform the weight vector $\mathbf{W}$ into a new vector $\mathbf{V}$ and visa versa:

$$\mathbf{V} = \mathbf{G}\mathbf{W} \tag{D6}$$

and

$$\mathbf{W} = \mathbf{G}^{-1}\mathbf{V} = (\mathbf{G}^{-1})^H \mathbf{V} \tag{D7}$$

Substituting equations (D6) and (D7) in (D1) yields:

$$\Gamma = \frac{\mathbf{V}^H \mathbf{G}^{-1} \mathbf{U}_{des} \mathbf{U}_{des}^H \mathbf{G}^{-1} \mathbf{V}}{\mathbf{V}^H \mathbf{G}^{-1} \mathbf{G} \mathbf{G} \mathbf{G}^{-1} \mathbf{V}} \tag{D8}$$

which is equal to:

$$\Gamma = \frac{\mathbf{V}^H \mathbf{G}^{-1} \mathbf{U}_{des} \mathbf{U}_{des}^H \mathbf{G}^{-1} \mathbf{V}}{\mathbf{V}^H \mathbf{V}} = \frac{\mathbf{V}^H \mathbf{B} \mathbf{V}}{\mathbf{V}^H \mathbf{V}} \tag{D9}$$

where

$$\mathbf{B} = \mathbf{G}^{-1} \mathbf{U}_{des} \mathbf{U}_{des}^H \mathbf{G}^{-1} \tag{D10}$$

The maximization of the SINR has now been reduced to a generalized eigenvalue problem, that of maximization of (D9), whose solution is:

$$\mathbf{V} = \mathbf{E}_{max} \tag{D11}$$

and

$$\mathbf{B}\mathbf{E}_{max} = \lambda_{max} \mathbf{E}_{max} \tag{D12}$$

where λ_{max} is the largest eigenvalue of $\mathbf{B}$ and $\mathbf{E}_{max}$ is the associated eigenvector. Inserting (D11) and (D12) in (D9), the following is obtained:

$$\Gamma_{max} = \frac{\mathbf{E}_{max}^H \lambda_{max} \mathbf{E}_{max}}{\mathbf{E}_{max}^H \mathbf{E}_{max}} = \frac{\lambda_{max} \mathbf{E}_{max}^H \mathbf{E}_{max}}{\mathbf{E}_{max}^H \mathbf{E}_{max}} = \lambda_{max} \tag{D13}$$

Inserting (D11) in (D7), the equivalent weighting vector is:

$$\mathbf{W}_{opt} = \mathbf{G}^{-1} \mathbf{E}_{max} \tag{D14}$$

Let now:

$$\mathbf{C} = \mathbf{G}^{-1} \mathbf{U}_{des} \tag{D15}$$

then equation (D10) becomes:

$$\mathbf{B} = \mathbf{C}\mathbf{C}^H \tag{D16}$$

inserting (D16) in (D12), the following is obtained:

$$\mathbf{B}\mathbf{E}_{max} = \mathbf{C}\mathbf{C}^H \mathbf{E}_{max} = \lambda_{max} \mathbf{E}_{max} \tag{D17}$$

and therefore the maximum eigenvalue is:

$$\lambda_{max} = \mathbf{C}\mathbf{C}^{H} \tag{D18}$$

B is a rank one matrix and $\mathbf{E}_{max}$ is the only eigenvector with non-zero eigenvalue. Substitution of (B17) and (D18) in (D14) and also using (D15) and (D16), the weight vector that will optimize the signal to interference ratio is:

$$\mathbf{W}_{opt} = \mathbf{G}^{-1}\mathbf{G}^{-1}\mathbf{U}_{des} = \mathbf{R}_{nn}^{-1}\mathbf{U}_{des} \tag{D19}$$

APPENDIX E

WEIGHT VECTOR WITH INTERFERENCE CO-VARIANCE MATRIC

In this appendix a derivation will be shown for re-writing the optimum weight vector containing the full co-variance matrix in terms of only the interference plus noise co-variance matrix. It will also be shown how the constant in the optimum weight vector cancels out when estimating the SINR. The optimum weight vector using the received co-variance matrix is given in [54] as:

$$\mathbf{W}_{opt} = \mu \mathbf{R}^{-1} \mathbf{U}_{des} \tag{E1}$$

where μ is a constant give as:

$$\mu = \frac{1}{\mathbf{U}_{des}^{H} \mathbf{R}^{-1} \mathbf{U}_{des}} \tag{E2}$$

and

$$\mathbf{R} = \mathbf{U}_{des} \mathbf{U}_{des}^{H} + \mathbf{R}_{nn} \tag{E3}$$

is the full received signal co-variance matrix. Using the matrix inversion lemma, the inverse of the full received signal co-variance matrix can be written as:

$$\mathbf{R}^{-1} = \mathbf{R}_{nn}^{-1} - \frac{\mathbf{R}_{nn}^{-1} \mathbf{U}_{des} \mathbf{U}_{des}^{H} \mathbf{R}_{nn}^{-1}}{1 + \mathbf{U}_{des}^{H} \mathbf{R}_{nn}^{-1} \mathbf{U}_{des}} = \frac{\Omega \mathbf{R}_{nn}^{-1} - \mathbf{R}_{nn}^{-1} \mathbf{U}_{des} \mathbf{U}_{des}^{H} \mathbf{R}_{nn}^{-1}}{\Omega} \tag{E4}$$

where Ω is a scalar given by:

$$\Omega = 1 + \mathbf{U}_{des}^{H} \mathbf{R}_{nn}^{-1} \mathbf{U}_{des} \tag{E5}$$

Inserting now (E4) in (E1) the following is obtained:

$$\mathbf{W}_{opt} = \frac{\left(\frac{\Omega \mathbf{R}_{nn}^{-1} - \mathbf{R}_{nn}^{-1} \mathbf{U}_{des} \mathbf{U}_{des}^{H} \mathbf{R}_{nn}^{-1}}{\Omega} \right) \mathbf{U}_{des}}{\mathbf{U}_{des}^{H} \left(\frac{\Omega \mathbf{R}_{nn}^{-1} - \mathbf{R}_{nn}^{-1} \mathbf{U}_{des} \mathbf{U}_{des}^{H} \mathbf{R}_{nn}^{-1}}{\Omega} \right) \mathbf{U}_{des}} = \frac{\left(\Omega \mathbf{R}_{nn}^{-1} - \mathbf{R}_{nn}^{-1} \mathbf{U}_{des} \mathbf{U}_{des}^{H} \mathbf{R}_{nn}^{-1} \right) \mathbf{U}_{des}}{\mathbf{U}_{des}^{H} \left(\Omega \mathbf{R}_{nn}^{-1} - \mathbf{R}_{nn}^{-1} \mathbf{U}_{des} \mathbf{U}_{des}^{H} \mathbf{R}_{nn}^{-1} \right) \mathbf{U}_{des}}$$

$$= \frac{\mathbf{R}_{nn}^{-1} \left(\Omega - \mathbf{U}_{des} \mathbf{U}_{des}^{H} \mathbf{R}_{nn}^{-1} \right) \mathbf{U}_{des}}{\mathbf{U}_{des}^{H} \mathbf{R}_{nn}^{-1} \left(\Omega - \mathbf{U}_{des} \mathbf{U}_{des}^{H} \mathbf{R}_{nn}^{-1} \right) \mathbf{U}_{des}} = \frac{\mathbf{R}_{nn}^{-1} \mathbf{U}_{des}}{\mathbf{U}_{des}^{H} \mathbf{R}_{nn}^{-1} \mathbf{U}_{des}}$$

$$= \frac{}{\mathbf{U}_{des}^{H}\mathbf{R}_{nn}^{-1}\mathbf{U}_{des}}\ \mathbf{R}_{nn}^{-1}\ \mathbf{U}_{des} = \mu_{nn}\,\mathbf{R}_{nn}^{-1}\ \mathbf{U}_{des} \qquad \text{(E6)}$$

Equation (E6) gives the weight vector in terms of a constant and co-variance matrix of the interference signals alone (as well as desired signal array vector). Using now (E6) in the average SINR as given in equation (41), the average SINR becomes:

$$\text{SINR} = \frac{P_{des}(\mu_{nn}\mathbf{R}_{nn}^{-1}\mathbf{U}_{des})^{H}\mathbf{U}_{des}\mathbf{U}_{des}^{H}(\mu_{nn}\mathbf{R}_{nn}^{-1}\mathbf{U}_{des})}{(\mu_{nn}\mathbf{R}_{nn}^{-1}\mathbf{U}_{des})^{H}\left(P_{int}\mathbf{U}_{int}\mathbf{U}_{int}^{H}+\sigma_{N}^{2}\right)(\mu_{nn}\mathbf{R}_{nn}^{-1}\mathbf{U}_{des})}$$

$$= \frac{(\mu_{nn})^{2}P_{des}(\mathbf{R}_{nn}^{-1}\mathbf{U}_{des})^{H}\mathbf{U}_{des}\mathbf{U}_{des}^{H}(\mathbf{R}_{nn}^{-1}\mathbf{U}_{des})}{(\mu_{nn})^{2}(\mathbf{R}_{nn}^{-1}\mathbf{U}_{des})^{H}\left(P_{int}\mathbf{U}_{int}\mathbf{U}_{int}^{H}+\sigma_{N}^{2}\right)(\mathbf{R}_{nn}^{-1}\mathbf{U}_{des})}$$

$$= \frac{P_{des}(\mathbf{R}_{nn}^{-1}\mathbf{U}_{des})^{H}\mathbf{U}_{des}\mathbf{U}_{des}^{H}(\mathbf{R}_{nn}^{-1}\mathbf{U}_{des})}{(\mathbf{R}_{nn}^{-1}\mathbf{U}_{des})^{H}\left(P_{int}\mathbf{U}_{int}\mathbf{U}_{int}^{H}+\sigma_{N}^{2}\right)(\mathbf{R}_{nn}^{-1}\mathbf{U}_{des})} \qquad \text{(E7)}$$

It can be seen in (E7) that the constant μ_{nn} cancels out of the SINR

REFERENCES

[1] S.C. Swales, M.A. Beach, D. J. Edwards, J.P. McGeehan, "The Performance Enhancement of Multibeam Adaptive Base Station Antennas for Cellular Land Mobile Radio Systems", IEEE Trans. Veh. Tech., Vol. 39, No. 1, Feb. 1990, pp. 56-67.

[2] J.H. Winters, "Optimum combining in digital mobile radio with co-channel interference", IEEE Journal on Selected Areas in Comm., Vol. SAC-2, 4 July 1984, pp. 528-539.

[3] M.C. Wells, "Increasing the Capacity of GSM Cellular Radio using Adaptive Antennas", IEE Proc. Comm., Vol. 143, No. 5, Oct. 1995, pp. 304-310.

[4] S. Talwar, A Paulraj, M Viberg, "Reception of Multiple Co-Channel Digital Signals using Antenna Arrays with Applications to PCS", IEEE Int. Conf. on Humanity Through Comm., SUPERCOMM/ICC '94, Vol. 2, May 1994, pp. 790-794.

[5] P. Zetterberg, "The Spectrum Efficiency of a Base Station Antenna Array System for Spatially Selective Transmission", IEEE Trans. Veh. Tech., Vol. 44, No. 3, Aug. 1995, pp. 651-660.

[6] J.H. Winters, J. Salz, R.D. Gitlin, "The impact of Antenna Diversity on the Capacity of Wireless Communications Systems", IEEE Trans. on Comm., Vol. 42, No. 2/3/4, Feb./Mar./ Apr. 1994, pp. 1740-1750.

[1] S. Zürbes, W. Papen, W. Schmidth, "A new architecture for mobile radio with macroscopic diversity and overlapping cells", Proc. 5th IEEE Int. Symp. on Pers., Indoor and Mobile Radio Comm. (PIMRC '94), Den Haag, Sept. 1994, pp. 640-644.

[8] A. Turkmani, "Performance evaluation of a composite microscopic plus macroscopic diversity system", IEE Proc.-1, Vol. 138, No. 1, Feb. 1991, pp. 15-20.

[9] A. Turkmani, "Probability of error for m-banch macroscopic selection diversity", IEE Proc. 1, Vol. 139, No. 1, Feb. 1992, pp. 71-78.

[10] S. Loyka, "MIMO Channel Capacity: Electromagnetic Wave Perspective", 27th URSI General Assembly, Maastricht, The Netherlands, Aug. 2002, pp. 1-12.

[11] T.D. Pham, "Multipath performance of adaptive antennas with multiple interferers and correlated fadings", IEEE Trans. Veh. Tech., Vol. 48, No. 2, Mar. 1999, pp. 342-352.

[12] A.F. Naguib, A. Paulraj, "Effects of multipath and base-station antenna arrays on uplink capacity of cellular CDMA", IEEE Global Comm. Conf., GLOBECOM'94, Vol. 1, Nov. 1994, pp. 395-399.

[13] U. Martin, I. Gaspard, "Capacity enhancement of narrowband CDMA by intelligent antennas", The 8th IEEE International Symp. on Personal, Indoor and Mobile Radio Comm. PIMRC '97, Vol. 1 , Sept. 1997, pp. 90-94.

[14] D.G. Gerlach, A.Paulraj, "Base-station transmitting antenna arrays with mobile to base feedback", Proc. 27th asilomar conference on signals, systems and computers, 1993, pp. 1432-1436.

[15] M. da Silveira, J.W. Odendaal, J. Joubert, "The range increase of adaptive vs. phased arrays in mobile radio systems: Interference included", URSI, July 2001, Boston, p. 85.

[16] J.H. Winters, "The range increase of adaptive vs. phased arrays in mobile radio systems", IEEE Trans. Veh. Tech., Vol. 48, No. 2, Mar. 1999.

[17] M. da Silveira, J.W. Odendaal, J. Joubert, "Same cell co-channel interference reduction using multiple spatially distributed adaptive array systems", Signal Processing, Vol. 81, 2001, pp. 2059-2068.

[18] M.da Silveira, J.W. Odendaal, J. Joubert, " Cellular system capacity increase using spatially distributed adaptive array systems", URSI, July 2000, Salt Lake City, p. 137.

[19] J. Ylitalo, E. Tiirola, "Performance evaluation of different antenna array approaches for 3G CDMA uplink", IEEE Veh. Tech. Conf., May 2000, pp. 883-887.

[20] E. Tiirola, J. Ylitalo, "Comparison of beamforming and diversity approaches for coverage extension of WCDMA macro cells", 54th IEEE Veh. Tech. Conf., Vol. 3, Oct. 2001, pp. 1274-1278.

[21] A. Kuchar, M. Tafener, "A robust DOA-based smart antenna processor for GSM base station", IEEE Int. Conf. on Comm., ICC '99, June 1999, pp.11-16.

[22] P. Zetterberg, "Mobile Cellular Communications with Base Station Antenna Arrays: Spectrum Efficiency, Algorithms and Propagation Models", Report Number TRITA-S3-SB-9712, ISSN 1103-8039, Dept. of Signals, Sensors and Systems, Royal Institute of Technology, Stockholm, Sweden, 1997, pp. 24-101.

[23] R. Cupo, G. Golden, "A four element adaptive antenna array for IS-136 PCS base stations", 47th IEEE Veh. Tech. Conf., Vol. 3, May 1997, pp. 1577-1581.

[24] J.H. Winters, "Signal acquisition and tracking with adaptive arrays in the digital mobile radio system IS-54 with flat fading", IEEE Trans. Veh. Tech., Vol. 42, No. 4, Nov. 1993, pp. 377-384.

[25] T.D. Pham, "Statistical behavior and performance of adaptive antennas in multipath environments", IEEE Trans. On Microwave Theory and Tech., Vol. 47, No. 6, June 1999, pp 727-731.

[26] W. Mu, Y. Zhang, S. Park, M. Amin, "On the performance of CMA array in spatial macro-diversity antennas", 1998. Conference Record of the Thirty-Second Asilomar Conf. on Signals, Systems & Computers, Vol. 2 , Nov. 1998, pp. 1505-1509.

[27] A.F. Naguib, A. Paulraj, "Capacity improvement with base-station antenna arrays in cellular CDMA", IEEE Trans. on Veh. Tech., Vol. 43. No.3. Aug. 1994, pp. 691-698.

[28] A.F. Naguib, A. Paulraj, "Performance enhancement and trade-offs of smart antennas in CDMA cellular networks", 45th IEEE Veh. Tech. Conf., Vol. 1, July 1995, pp. 40-44.

[29] A.F. Naguib, B. Suard, "Performance of CDMA mobile communication systems using antenna arrays", IEEE Int. Conf. on Acoustics, Speech, and Signal Processing, ICASSP-93, Vol. 4, Apr. 1993, pp. 153-156.

[30] A.F. Naguib, A. Paulraj, "Performance of CDMA cellular networks with base-station antenna arrays: the downlink", IEEE Int. Conf. on Comm., SUPERCOMM/ICC '94, May 1994, pp. 795 -799.

[31] A.F. Naguib, "Power control in wireless CDMA: Performance with cell site antenna arrays", IEEE Global Telecommunications Conf., GLOBECOM '95, IEEE, Vol. 1 , Nov. 1995 , pp. 225-229.

[32] R.B. Ertel, S.V. Schell, "Comparative study of adaptive antenna arrays in CDMA communication systems", Nov. 1998, pp.1-9.

[33] I. Rivas, L.J. Ibbetson and L. Lopes, "Macro-cellular reception performance investigation in microcellular networks", 47th IEEE Veh. Tech. Conf., Vol. 3, May 1997, pp. 1503–1507.

[34] U. Weiss, "Designing macroscopic diversity cellular systems", 49th IEEE Veh. Tech. Conf., Vol. 3 , July 1999, pp. 2054 – 2058.

[35] M. Juntti, "Performance analysis of linear multi-user receivers for CDMA in fading channels with base station diversity", IEEE Trans. Veh. Tech., Sept. 1999, pp2845-2849

[36] M. Juntti, "Performance analysis of linear multi-sensor multi-user receivers for CDMA fading channels", IEEE Journal on Selected Areas in Comm., Vol. 18. No. 7, Jul. 2000, pp. 1221-1229.

[37] W. Papen, "Uplink performance of a macro-diversity cellular mobile radio architecture", Sixth IEEE Int. Symp. on Pers. Indoor and Mobile Radio Comm., PIMRC'95, Vol. 3 , 27-29, Sept. 1995, pp. 1118-1122.

[38] S. Zurbes, "Outage probabilities and handover characteristics of simulcast cellular mobile radio systems", 46th IEEE Veh. Tech. Conf., Vol. 1 , May 1996, pp. 522-526.

[39] S. Zürbes, "Power control in simulcast digital cellular radio networks", 8th IEEE Int. Symp. on Pers., Indoor and Mobile Radio Comm., PIMRC '97, Vol. 3, Sept. 1997, pp. 887-991.

[40] D.C. Hastings, H. M. Kwon, "Soft Handoffs in code division multiple access systems with smart antenna arrays", IEEE Veh. Tech. Conf., Sept. 2000, pp. 181-188.

[41] D.C. Hastings, H. M. Kwon, "Optimization of sector orientation in CDMA communication architectures based on soft handoff", MILCOM 2000, 21st Century Military Communications Conference Proceedings, Vol. 2 , Oct. 2000, pp. 826- 830.

[42] W. Yung, "Direct sequence spread spectrum code division multiple access cellular systems in Rayleigh fading and log-normal shadowing channel", IEEE Int. Conf. on Comm., ICC 91, June 1991, pp. 871-876.

[43] D.G. Gerlach, A.Paulraj, "Adaptive transmitting antenna arrays with feedback", IEEE Signal Proc. Letters, Vol. 1, No. 10, Oct. 1994, pp. 150-152.

[44] S. Nagaraj, Y. Huang, "Downlink transmit beamforming with selective feedback", Conference Record of the Thirty-Fourth Asilomar Conf. on Signals, Systems and Computers, Vol. 2 , Nov. 2000, pp.1608-1612.

[45] R.B. Ertel, "Antenna array systems: propagation and performance", Preliminary review of initial research and proposal for current and future work towards PhD, Dec. 1998.

[46] R.B. Ertel, "Overview of spatial channel models for antenna array communication systems", IEEE Pers. Comm. Mag., Vol. 5, No.1. Feb. 1998, pp. 10-22.

[47] M. Larsson, "Spatio-temporal channel measurements at 1800 MHz for adaptive antennas", 49th IEEE Veh. Tech. Conf., 1999, Vol. 1 , July 1999, pp. 376-380.

[48] J. Laiho-Steffens, A. Walker, "Experimental evaluation of the two dimensional mobile propagation environment at 2GHz", 47th IEEE Veh. Tech. Conf., 1997 Vol. 3, May 1997, pp. 2070-2074.

[49] W.C.Y. Lee, *Mobile cellular telecommunications: analog and digital systems*, McGraw-Hill, Second Edition, 1995.

[50] T. S. Rappaport, *Wireless Communications: Principles and Practices,* Prentice-Hall, 1996.

[51] J. Ylitalo, M. Katz, "An adaptive antenna method for improving downlink performance of CDMA base stations", IEEE 5th Int. Symp. on Spread Spectrum Tech. and App., Vol. 2, Sept. 1998, pp. 599-603.

[52] A. Lopez, Performance predictions for cellular switched-beam intelligent antenna systems", IEEE Comm. Magazine, Oct. 1996, pp. 152-154.

[53] J. Litva, T. Lo, *Digital Beamforming in Wireless Communications,* Artech House, 1996, Ch. 3, pp. 42 - 43.

[54] L.C. Godara, "Applications of antenna arrays to mobile communications, Part II:, Beamforming and Direction of arrival Considerations", Proc. IEEE , Vol. 85, No. 8, Aug. 1997, pp. 1195-1245.

[55] R. Kohno, "Spatial and temporal communication theory using adaptive antenna array", IEEE Pers. Comm., Vol.5., No. 1, Feb 1998, pp. 28-35.

[56] J.C. Liberti, T. S. Rappaport, *Smart antennas for wireless communications: IS-95 and third generation CDMA principles,* Prentice Hall, New Jersey, 1999.

[57] R. Monzingo, T Miller, *Introduction to Adaptive Arrays,* John Wiley and Sons, 1980, Chapter 4, pp. 166-168.

[58] J.E. Hudson, *Adaptive Array Principles,* Peter Peregrinus, 1981, Chapter 3, pp. 58-75.

[59] P.A. Ranta, A. Lappetelainen, H. Zhi-Chun, "Interference cancellation by joint detection in random frequency hopping TDMA networks", 5th IEEE Int. Conf. on Universal Pers. Comm., Vol. 1 , 1996, pp. 428 -432

[60] M. R. Spiegel, *Mathematical handbook of formulas and tables*, NcGraw-Hill, 1968.

[61] S.M. Kay, Fundamentals of Statistical Signal Processing: Estimation Theory, Englewood Cliffs, NJ: McGraw-Hill, 1991.

[62] F.G. Stremler, *Introduction to communication systems*, Addison-Wesley, 1982, p. 446.

[63] W.C. Jakes, *Microwave mobile communications,* IEEE Press, New York, Jan. 1994.

[64] J. Gorricho, Paradells, J, "Evaluation of the soft handover benefits on CDMA systems", 5th IEEE Int. Conf. on Universal Pers. Comm., Vol. 1, Sept. 1996, pp. 305-309.

[65] W. Jianming, S. Affes, P. Mermelstein, "Forward-link soft-handoff in CDMA with multiple-antenna selection and fast joint power control" IEEE Trans. on Wireless Comm., Vol. 2., Issue 3 , May 2003, pp. 459 –471.

[66] G. Strang, *Linear algebra and its applications,* third addition, Harcourt Brace Javanovich, 1988.

[67] D.H. Johnson and D.E. Dudgeon, *Array signal processing: Concepts and Techniques,* Englewood Cliffs, NJ: Prentice-Hall, 1993.